BORA AYDIN

# HYDRODYNAMICS OF TRICKLE BED REACTORS
## Steady- and Nonsteady-State Operations

Thèse présentée
à la Faculté des études supérieures de l'Université Laval
dans le cadre du programme de doctorat en Génie Chimique
pour l'obtention du grade de Philosophiae Doctor (PhD)

DÉPARTEMENT DE GÉNIE CHIMIQUE
FACULTÉ DES SCIENCES ET DE GÉNIE
UNIVERSITÉ LAVAL
QUÉBEC

2008

# Résumé

Parmi les réacteurs triphasiques gaz-liquide-solide utilisés dans la pratique industrielle, les réacteurs catalytiques à lit fixe arrosé à cocourant de gaz et de liquide vers le bas, i.e., trickle bed reactors (TBR), sont très répandus en particulier dans divers processus de transformation à hautes température et pression. Les travaux expérimentaux se poursuivent depuis plus de quatre décennies sur la quantification des paramètres hydrodynamiques (transition des régimes d'écoulement, perte de pression biphasique, rétention liquide, efficacité de mouillage, etc.) pour cette configuration de réacteurs. Différentes approches ont été mises en œuvre par un grand nombre d'équipes de recherche pour mesurer ces paramètres hydrodynamiques dans le but de construire des outils de prédiction et de description par rapport aux conditions réelles d'opération des processus à l'échelle industrielle. La présente contribution se propose de répondre à la question suivante :

Dans quelle mesure les connaissances accumulées à partir d'observations à l'échelle laboratoire dans les conditions ambiantes sont-elles fiables pour opérer un TBR à pression et température élevées?

Une question sous-jacente à la précédente concerne le comportement hydrodynamique avec la température lorsque le réacteur est alimenté par un liquide non-newtonien.

L'intensification des procédés est une approche en vogue et prometteuse pour continuer à apporter des perfectionnements (gains en économie et en efficacité) au réacteur TBR. Aussi, l'induction artificielle d'impulsions est-elle envisagée dans cette étude en tant que méthode d'intensification de processus pour des températures et pressions non-ambiantes. Le présent travail tentera de démontrer les avantages de plusieurs variantes de l'opération périodique sur l'hydrodynamique des TBR pour des systèmes coalescent, non-newtonien et moussant à des températures et pressions augmentées.

# Abstract

Trickle bed reactor (TBR) is one of the most widely used three-phase reactors in various processes mostly operated at high temperature and high pressure. The ongoing experimental work on the hydrodynamic parameters (flow regime transition, pressure drop, liquid holdup, wetting efficiency etc.) of this packed bed reactor configuration goes to early 1960's. Different techniques were applied by different researchers for the measurement of these hydrodynamic parameters which let the comparison and the decision of more convenient method by means of doing investigations at conditions near to that of industrial processes.

Process intensification is considered to be a leading approach for the ongoing research on the economic reduction and reactor efficiency enhancement. Artificial induction of pulses is pronounced as one of the methods for the process intensification in TBRs.

As trickle bed reactor is also used in biochemical processes, and the initial liquid behaving like a Newtonian fluid could turn into a non-Newtonian fluid after various biochemical processes; it is emphatic to study TBR hydrodynamics with non-Newtonian systems.

Despite large amount of work exists in the literature for steady state hydrodynamics of TBR operating at high pressure; the hydrodynamic behavior of TBR at high temperature has been left as a concealed issue. Additionally none of the experimental work performed to demonstrate the advantages of periodic operation on TBR hydrodynamics dealt with the effects of increased temperature and pressure.

This study illustrates the hydrodynamics of TBR at increased temperature and pressure under constant throughput flow and cyclic operation.

# Foreword

This PhD thesis comprises eight chapters. Each chapter represents an article published, accepted or submitted in the scientific journals. These articles are listed below.

[1] Aydin, B., Larachi, F. Trickle bed hydrodynamics and flow regime transition at elevated temperature for a Newtonian and a non-Newtonian liquid. *Chemical Engineering Science*, 60, 6687-6701, 2005

[2] Aydin, B., Fries, D., Lange, R., Larachi, F. Slow-mode induced pulsing in trickle-bed reactors at elevated temperature. *AIChE Journal*, 52, 3891-3901, 2006

[3] Aydin, B., Fries, D., Lange, R., Larachi, F. Slow-mode induced pulsing in trickle beds at elevated temperature for (non-)Newtonian liquids. *Chemical Engineering Science*, 62, 5554-5557, 2007

[4] Aydin, B., Larachi, F. Flow regime transition and hydrodynamics of slow-mode liquid-induced pulsing at elevated temperature for (non-)Newtonian liquids. *Chemical Engineering Science*, accepted

[5] Aydin, B., Cassanello, M.C., Larachi, F. Influence of temperature on fast-mode cyclic operation hydrodynamics in trickle-bed reactors. *Chemical Engineering Science*, 63, 141-152, 2008

[6] Aydin, B.; Larachi, F. Trickle bed hydrodynamics at elevated temperature for (non-) Newtonian foaming liquids. *Chemical Engineering Journal*, submitted

[7] Aydin, B., Hamidipour, M., Larachi, F. Fast-mode alternating cyclic operation in trickle beds at elevated temperature for foaming systems. *Chemical Engineering Science*, 62, 7539-7547, 2007

[8] Aydin, B., Bilodeau, S., Hamidipour, M., Larachi, F., Kleitz, F. Polymer-filled composite porous catalytic particles for hydrodynamic studies in trickle bed reactors. *Industrial and Engineering Chemistry Research*, submitted

Some results in these studies were presented in the following conferences:

[1] Aydin, B., Larachi, F. *Flow regime transition and pulsing flow properties in trickle beds at elevated temperature for Newtonian and non-Newtonian liquids* (poster presentation), 5th International Symposium on Catalysis in Multiphase Reactors & 4th International Symposium on Multifunctional Reactors, Portorose, Slovenia, June 2005

[2] Aydin, B., Larachi, F. *Hydrodynamics in trickle bed reactor at elevated temperature for non-Newtonian liquids*, 55$^{th}$ Canadian Chemical Engineering Conference, Toronto, Canada, October 2005

[3] Aydin, B., Fries, D., Lange, R., Larachi, F. *Slow-mode induced pulsing in trickle beds at elevated temperature for (non-)Newtonian liquids*, 19$^{th}$ International Symposia on Chemical Reaction Engineering, Potsdam/Berlin, Germany, September 2006

[4] Aydin, B., Cassanello, M.C., Larachi, F. *Fast-mode induced pulsing in trickle bed reactors at elevated temperature and pressure* (poster presentation), 5$^{th}$ International Conference on Unsteady State Processes in Catalysis, Suita City, Japan, November 2006

[5] Aydin, B., Larachi, F. *Hydrodynamics of Trickle Bed Reactors at Elevated Temperature and Pressure for Newtonian/non-Newtonian Liquids – Steady and Unsteady Operation*, 3$^{rd}$ annual conference of the Turkish American Scientists and Scholars Association (TASSA), Yale University, New Haven, USA, March 2007

[6] Aydin, B., Hamidipour, M., Larachi, F. *Fast-mode alternating cyclic operation in trickle beds at elevated temperature for foaming systems* (poster presentation), 8th International Conference on Gas-Liquid and Gas-Liquid-Solid Reactor Engineering, New Delhi, India, December 2007

# Acknowledgements

Primarily I would like to specify my eternal appreciation to my mom, Leyla Aydin, my sibling Sara Berna Aydin and my aunts Gulen, Zehra, Emel Kadioglu for their unceasingly support. I would like to indicate my gratitude to Aysegul Turkucu for her support and apprehension during this long way.

I would like to thank to Prof. Faïçal Larachi for his help in this research by being an admonisher with his interminable ideas and encouragement.

I want to thank to Donata Fries who helped for the experimental work of Chapter 2 during her Diplomarbeit period in summer 2005. My second thank goes to Mohsen Hamidipour for his collaboration in the experimental & theoretical work of Chapters 7 and 8. I am thankful to Prof. Freddy Kleitz for his supervision and Simon Bilodeau for his help in Chapter 8. Pouya Hajiani's help for modeling in Chapter 8 is acknowledged. The help of Lyes Mohammed Essalhi in performing some of the experiments in Chapter 6 is also acknowledged with gratitude.

I appreciate Dr. Ion Iliuta's help with his discussions that conduced better understanding of the steady state trickle bed reactor hydrodynamics.

The help of the chemical engineering department technical staff Adrien Pouliot, Jerome Noel, Marc Lavoie, and Claude Carrier during this research project is also appreciated. I would like to thank my office colleagues for their support. I express my gratitude to Prof. Henri Delmas, Dr. Marzouk Benali, Prof. Freddy Kleitz and Prof. Bernard Grandjean for their approval to be in my defense committee. Finally, I acknowledge the financial support of Natural Sciences and Engineering Research Council of Canada (NSERC).

*In memory of my dad, Ugur Aydin*

*"Life is not about finding our*
*limitations, about finding our infinity."*
*Herbie Hancock*

# Table of contents

# List of tables

# List of figures

# Introduction

Trickle bed reactor (TBR) is the most prevalent fixed bed reactor in industrial applications. Cocurrent flow of gas and liquid phases without any throughput limitation lets this type of reactor used in various processes i.e. petrochemical and chemical industries, waste treatment, biochemical and electrochemical processes. For example in effluent treatment plants trickling filters are used for removal of organic matter from wastewater streams by aerobic bacterial actions. In this process, biological growths are allowed to attach themselves to a bed of stone or other support over which the wastewater is allowed to trickle in contact with air. Table I-1 lists some examples of reactions carried out in TBR. They find widespread use in industry, for example in the Fischer-Tropsch synthesis of hydrocarbons from synthesis gas (Krishna et al., 1996). Trickle-bed reactors (TBR) are used extensively for hydrotreating and hydrodesulfurization applications in the refining industry, and hydrogenation, oxidation and hydrodenitrogenation applications in the chemical, biochemical and waste treatment industries (Al-Dahhan et al., 1997; Saroha and Nigam, 1996).

Kinetics and/or thermodynamics of reactions conducted in trickle bed reactors require high temperatures, which in turn increase gas expansion and impede the gaseous reactant from dissolving sufficiently into the liquid. Therefore, elevated pressures are necessary to improve gas solubility and mass and heat transfer rates, to handle large gas volumes at less capital expense and to slow down the catalyst deactivation (Al-Dahhan et al., 1997).

**Table I-1** Examples of reactions worked in TBR

| | |
|---|---|
| Hydrogenation of α-methylstyrene | Satterfield et al. (1969)<br>Morita and Smith (1978)<br>Herskowitz et al. (1979)<br>El-Hisnawi et al. (1982)<br>Herskowitz and Mosseri (1983)<br>Mc Manus et al. (1993) |
| Oxidation of sulphur dioxide | Hartman and Coughlin (1972)<br>Mata and Smith (1981)<br>Pavko and Levec (1981)<br>Berruti et al. (1984)<br>Haure et al. (1989, 1992) |
| Wet air oxidation of formic acid, acetic acid and ethanol | Goto and Smith (1975)<br>Levec and Smith (1976) |
| Biochemical reactions, fermentations | Bailey and Ollis (1986) |
| Oxidation of benzene, toluene and xylene | Chuang et al. (1992) |
| Hydration of propene to 2-propanol using sulfonic acid ion-exchange resin | Westerterp and Wammes (1992) |
| Synthesis of butynediol from acetylene and aqueous formaldehyde | Gianetto and Speechia (1992) |
| Hydration of 2-methyl-2-butene | Goto et al. (1993) |
| Hydrogenation of naphthalene with $Pt/Al_2O_3$ catalyst | Huang and Kang (1995) |
| Oxidation of Poly (α-olefin) lubricant in the presence of inert (glass) and active (brass, steel) surfaces | Koh and Butt (1995) |
| Hydrocracking for production of high-quality middle-distillate fuels | Meyers (1996) |
| Hydrodenitrification | Meyers (1996) |

In a trickle bed reactor the liquid and gas phases flow cocurrently downwards through a fixed bed of catalyst particles while the reaction takes place (Figure I-1). In certain cases, the two-phases also flow cocurrently upwards. The cocurrent upward flow operation provides better radial and axial mixing than the downward flow operation, thus facilitating better heat transfer between the liquid and solid phases. This is highly useful in exothermic reactions where heat is required to be removed continuously from the reactor. However, due to higher axial mixing in the upward flow operation, the degree of conversion, a crucial factor in the operation is preferred because of lower axial mixing, better mechanical stability and less flooding, thus facilitating processing of higher flow rates and increased reactor capacity (Dudukovic et al., 2002).

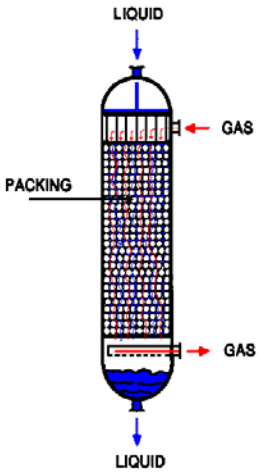


**Figure I-1** Schematic diagram of a trickle bed reactor

The study of the hydrodynamics of trickle bed reactors has received much attention in the past decade. However, the still unclear view on hydrodynamics of trickle bed reactors is mostly due to the lack of reliable experimental data especially under high temperature operation. Approximately all the work done on the hydrodynamics of the TBR was performed at ambient temperature even some addressed the effect of the high pressure. There is a little attempt done to show the effect of temperature on the hydrodynamic parameters of the TBR. The aim of this work was to show the effect of temperature on the hydrodynamic parameters of the TBR operating at moderate pressure. Hydrodynamics at elevated temperature was studied for steady (constant throughput) and unsteady (cyclic) operation with different systems.

# Flow Regimes

Trickle bed reactors operate in a variety of flow regimes ranging from gas-continuous to liquid-continuous patterns. They usually fall into two broad categories referred to as low interaction regime (trickle flow regime) and high interaction regime (pulse, spray, bubble and dispersed bubble flow regimes). The low interaction regime is observed at low gas and liquid flow rates and is characterized by a weak gas-liquid interfacial activity and a gravity-driven liquid flow. High interaction regime is characterized by a moderate to intense gas-liquid shear due to moderate to high flow rate of one or both of the fluids. As a result, various flow patterns arise depending on the gas and liquid flow rates and the physical properties of the liquid. Knowledge of this is essential in understanding the hydrodynamics and mass transfer characteristics (Ramachandran and Chaudhari, 1983).

## *Trickle Flow*

Trickle flow occurs at low liquid and gas flow rates. In the trickle flow regime (Figure I-2) the liquid flows down the reactor on the surface of the packing in the form of rivulets and films while the gas phase travels in the remaining void space. The trickle flow regime can be further divided into two regions. At very low gas and liquid flow rates, the liquid flow is laminar and a fraction of the packing remains unwetted. This regime is called partial wetting regime. If the liquid flow rate is increased, the partial wetting regime changes to complete wetting trickling regime in which the packing is totally covered by a liquid film. The trickle flow regime is also termed as gas continuous regime or homogeneous flow or low interaction regime because very little interaction between gas and liquid exists in this regime (Saroha and Nigam, 1996).

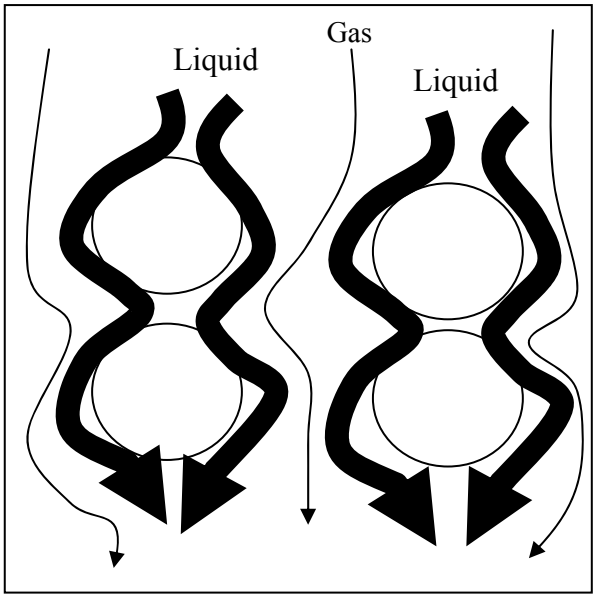


**Figure I-2** Schematic diagram of the trickle flow

### *Pulse Flow*

The pulse flow occurs at relatively high gas and liquid input flow rates. It refers to the formation of slugs that have a higher liquid content than the remainder of the bed. The pulsing behaviour refers to gas and liquid slugs traversing the reactor alternately. It begins when the flow channels between packing are plugged by a slug of liquid, followed by blowing off the slug by the gas flow (Figure I-3). Pulses always begin at the bottom of the bed, as the gas velocity is higher there due to lower pressure. As the gas flow rate is increased, the incipient point of pulsing moves to the upper part of the reactor. The gas pulse is not completely devoid of liquid. A thin film of liquid always exists on the surface of the packing within the gas pulse. Similarly, the liquid pulse also contains some small gas bubbles, particularly at the front end of the liquid phase. As the slug travels down the reactor, liquid is shed behind the slug in the form of liquid films that decelerate to a lower velocity. Thus the average liquid velocity in a slug is higher than that in a pulse. Although the liquid slug loses liquid continuously to the pulse upstream, it overtakes the gas phase downstream and picks up liquid from the pulse at its front so that its length remains constant (Saroha and Nigam, 1996).

The pulsing flow regime may be approached either from the gas-continuous trickle flow or from the liquid-continuous coalesced bubble flow regime. Such a pulsing regime is observed for moderate liquid flow rates and moderate to high gas flow rates and can be depicted as a macroscopic combination of dispersed bubble flow occurring in the liquid-rich slugs and trickle flow in the gas-rich slugs, both propagating along the bed (Al-Dahhan et al., 1997). This particular flow regime is identified by the alternating passage of liquid-rich and gas-rich two-phase flow down the packed column and it is associated with high mass and heat transfer rates (Tsochatzidis and Karabelas, 1995).

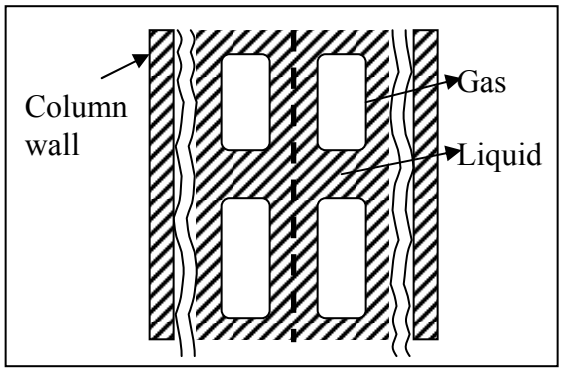


**Figure I-3** Schematic diagram of the pulse flow

At present, trickle flow is the most common flow regime encountered in industrial applications. A more favorable flow, pulsing flow, is well known for its advantages in terms of an increase in mass and heat transfer rates, complete catalyst wetting and a decrease in axial dispersion compared to trickle flow (Lemay et al., 1975; Chou et al., 1979; Tsochatzidis and Karabelas, 1994; Rao and Drinkenburg, 1985; Boelhouwer et al., 2001, 2002). The operation of a trickle bed reactor in the pulsing flow regime is favorable in terms of a capacity increase and the elimination of hot spots. Extending the knowledge on the hydrodynamic nature and characteristics of pulsing flow stands at the basis of further exploitation of the effects of this flow regime on reactor performance. Axial dispersion is less compared to trickle flow due to increased radial mixing and disappearance of stagnant liquid holdup (Lerou et al., 1980; Fukushima and Kusaka, 1977; van Swaaij et al., 1969). Wu et al. (1999) demonstrated that pulsing flow has a positive effect, particularly on selectivity, with respect to trickle flow.

Some data on pulse characteristics are reported in early studies by Weekman and Myers (1964) and Sato et al. (1973). In more recent studies, pulse properties (pulse velocity, pulse frequency etc.) were experimentally determined by conductance techniques and correlations for these properties were developed (Blok and Drinkenburg, 1982b; Rao and Drinkenburg, 1983; Tsochatzidis and Karabelas, 1995; Bartelmus et al., 1998). Blok and Drinkenburg (1982b) examined the effect of superficial gas and liquid velocities on pulse velocity, duration and liquid holdup. They concluded that pulse and base liquid holdup, pulse velocity and pulse height were invariant to the superficial liquid velocity. Tsochatzidis and Karabelas (1995) noticed a small influence of the superficial liquid velocity on pulse velocity at high liquid flow rates.

### *Spray Flow*

Spray flow regime occurs at high gas and low liquid flow rates. The liquid phase moves down the reactor in the form of droplets entrained by the continuous gas phase (Figure I-4) (Saroha and Nigam, 1996).

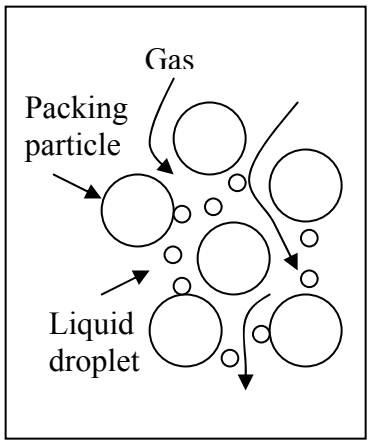


**Figure I-4** Schematic diagram of the spray flow

### *Bubble Flow*

Low gas flow rates and sufficiently high liquid flow rates lead to the bubble flow regime with a continuous liquid phase which contains small spherical bubbles (Figure I-5). At medium gas flow rates but with still high liquid flow rates, the liquid phase remains

continuous but the bubbles coalesce and the gas flows in the form of elongated bubbles. This flow regime is referred to as the dispersed bubble flow.

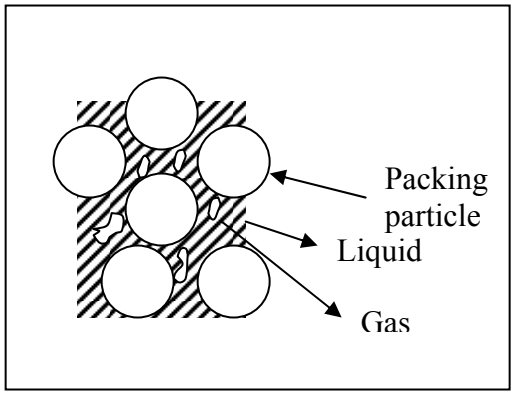


**Figure I-5** Schematic diagram of the bubble flow

In order to properly design trickle bed reactors based on laboratory data, it is important to predict in which flow regime the reactor is operating for a given set of conditions. The transition between the pulse flow and the trickle flow regime is sharp, while the transition to spray flow and dispersed bubble flow is more gradual.

Knowledge of the several transitions is indispensable in the design of trickle bed reactors; several studies show that the pressure drop, liquid saturation, liquid mixing and heat and mass transfer coefficients are affected differently in each regime.

Techniques employed for identifying the flow patterns commonly include simple visual observations (e.g. Charpentier and Favier, 1975), pressure signals (e.g. Chou et al., 1977; Helwick et al., 1992; Holub et al., 1993) and the use of a movie or a video camera (e.g. Sato et al., 1973; Melli et al., 1990). Kolb et al. (1990) recorded signals of pressure fluctuations and identified acoustic signatures of some flow regimes. Latifi et al. (1992) employed a matrix of microelectrodes, mounted flush on the bed wall, in connection with an electrodiffusion technique to identify various flow regimes.

The visual observation through the wall of the reactor is a direct technique provided that all or part of the column is transparent. This method was used by Wammes (1990) to observe

the pulse and dispersed bubble flow regimes up to 6 MPa in a transparent polycarbonate column. Hasseni et al. (1987), Battin (1987) and Larachi (1988) observed the bubble and pulse flow regimes at high pressure up to 10,1 MPa in a stainless steel column equipped with a thick transparent plexiglass. This method was proved to be reliable for small scale installations, but unfortunately for the columns of great dimensions; the observation through the wall does not inform us inevitably about the nature of the flow at the center of the reactor (Sundaresan 1987).

Weekman and Myers (1964) characterized the pulse flow (frequency, velocity of the pulses) by introducing light through the column and acquisition of the signal obtained by means of photoresistances laid out behind the wall contrary to the source of light. Melli et al. (1990) observed flow regimes at microscale (pore) and macroscale (column) by means of a video camera at high speed. Chou et al. (1977) and Christensen et al. (1986) characterized these transitions from the pressure fluctuations at the wall by means of pressure transducer. Sato et al. (1973) used pressure transducers, conductimetric probes and photographs to characterize the the pulse flow, the distribution of the phases and the pulse flow characteristics. Blok and Drinkenburg (1982b), Blok et al. (1983), Rao and Drinkenburg (1983) and Tsochatzidis and Karabelas (1991) used conductimetric probes to detect the appearance of the first pulse in the flow on the one hand and on the other hand to characterize the frequency and the velocity of these pulses.

Several investigators have studied the flow pattern in trickle bed reactor at atmospheric pressure and presented their data in terms of flow maps. Various coordinates have been used by different investigators to present the flow maps. For example, typical for the empirical flow charts is the flow-regime map of Charpentier and Favier (1975) (Figure I-6). It uses the coordinates proposed by Baker (1954) for two-phase flow in horizontal tubes. The abscissa is the superficial mass flow rate of the gas; the ordinate is the ratio of the liquid-to the gas-mass flow rates. The properties of the gas and the liquid are taken into account by the parameters (Bertucco and Vetter, 2001):

$$\lambda = \left( \frac{\rho_G}{\rho_{air}} \frac{\rho_L}{\rho_w} \right)^{0.5} \tag{I-1}$$

$$\psi = \frac{\sigma_w}{\sigma_L} \left[ \frac{\mu_L}{\mu_w} \left( \frac{\rho_w}{\rho_L} \right)^2 \right]^{0.33} \tag{I-2}$$

where $\rho_{air}$, $\rho_G$, $\rho_L$ and $\rho_w$ are respectively the density of air, of the gas phase, of the liquid phase and of water, $\mu_L$ and $\mu_w$ are respectively the dynamic viscosity of the liquid phase and of water, $\sigma_L$ and $\sigma_w$ are respectively the surface tension of the liquid phase and of water. Talmor (1977) presented a flow map in terms of superficial gas to liquid mass flow rate ratio and a force ratio relating inertia plus gravity forces to viscous plus interphase forces.

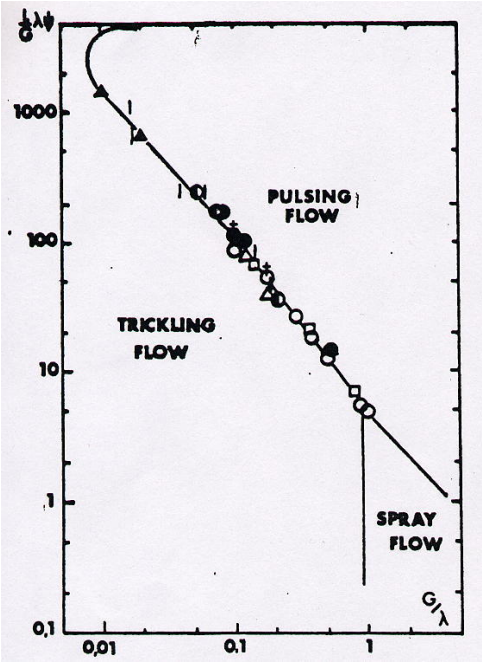


**Figure I-6** Flow pattern diagram (Charpentier and Favier, 1975)

Many flow regime charts and attempts at modeling flow regime transitions have been proposed. Other flow charts did not lead to a better agreement with experimental data at different pressures. A thorough evaluation of available models and empirical correlations for the prediction of trickle-to-pulse flow transition boundaries with pressure was made by Wild et al. (1991), Larachi (1991) and Larachi et al. (1993). Larachi et al. (1993) have suggested the use of a modified Charpentier's diagram. Unfortunately, all recent

experimental studies reach the same conclusion that none of them is yet entirely successful and no single approach can be recommended. Using the flow regime transition database, Larachi et al. (1999) developed an explicit correlation for trickle-to-pulse flow transition based on neural network modeling. Table I-2 summarizes some empirical correlations and theoretical models that have been either based or tested on high-pressure transition data.

Charpentier and Favier (1975) proposed a flow map based on an empirical coordinate system originally developed by Baker (1954) for gas-liquid flow regime transitions in empty horizontal pipes. The reactor pressure has been incorporated in the gas mass flux $G$. The parameters $\lambda$ and $\psi$ are empirical dimensionless numbers which contain the physical properties of the gas-liquid system as related to the air-water system. The boundary line in the flow diagram separating the trickle flow from the pulse flow regime is based on atmospheric experiments and several gas-liquid systems.

The coordinate system of the flow map proposed by Talmor (1977) is based on a semi-theoretical approach. Which flow regime is encountered depends on the ratio of the superficial gas to liquid velocities and on the ratio of the inertia and gravity driving forces to the viscous and surface tension resisting forces. The line separating the trickle flow regime from the pulse flow regime is mainly based on data obtained with air and water-glycerol mixtures.

According to their model, Fukushima and Kusaka (1977) stated that if the dimensionless number $(D_r / d_p)^{0.5}$ plays a role then the contribution of the wall flow to the hydrodynamic behaviour was relatively large. No influence of $D_r / d_p$ on the hydrodynamics was found by Blok et al. (1983) and Sicardi et al. (1979).

Sicardi et al. (1979) and Sicardi and Hofmann (1980) considered the trickle bed as consisting of parallel channels with constrictions. They assumed that the pulse flow regime occurs when large waves on the liquid surface occlude the constrictions. A dimensionless correlation was derived by which the ratio of the wave amplitude to the mean liquid film thickness $(A/\delta)_{tr}$ is described as a function of tangential stress on the liquid surface at the point of transition, the surface tension and the constriction geometry. The two constants in their model were determined by means of transition experiments.

Blok et al. (1983) have found experimentally the mean actual velocity $u_L$ to be constant at each point of transition between trickle and pulse flow. Therefore they postulated that the initiation of pulses is determined by a critical minimum value of the Froude number, based on the mean actual velocity $u_L$. For the air-water system and for several types of packing the critical value was experimentally found to be 0.09.

The model of Ng (1986) is based on theoretical considerations about the hydrodynamics at the scale of a particle in the packed bed. To calculate the value of the parameter $\alpha$, the fraction of flow channels occupied by the liquid films, Ng (1986) used the liquid holdup correlation of Wijffels et al. (1974). In this model the role of the gas density is explicitly taken into account.

Hasseni et al. (1987) examined the effect of pressure on the transitions between different flow regimes by visually observing the two-phase flow patterns in the reactor. Hasseni et al. (1987) compared the flow pattern observations at conditions of high pressure with the predictions of the theoretical model of Ng (1986). It was concluded that the Ng (1986) model does not represent well the influence of the liquid viscosity on the trickling to pulsing flow transition. The following conclusions were drawn by Hasseni et al. (1987) from the theoretical use of the Ng (1986) model to predict flow regime transitions for the purpose of testing its sensitivity to the physical parameters of total pressure, particle parameter and liquid surface tension:

At a given liquid mass flow flux, the corresponding mass flow flux of the gas at the transition between the low and high interaction regimes increases with increasing total pressure.

At a fixed total pressure, the respective mass flow fluxes of gas or liquid at the transition increase with increased particle diameter

At a given liquid mass flow flux and irrespective of total pressure, the mass flow flux of the gas at the transition between the flow regimes increases with increasing liquid surface tension.

The effect of reactor pressure in the range of 0.2 – 2 MPa on the transition between the trickle and pulse flow regime was investigated by Wammes et al. (1990). They observed that most models and flow charts, which are all based on atmospheric pressure, were able to describe the transition experiments performed at 0.2 MPa reasonably well. However, this was not found at elevated pressures except for the water-nitrogen system for which their data for the transition of the trickle flow regime to pulse flow regime was in good agreement with the predicted transition line of the flow map of Talmor (1977). For both gas-liquid systems Wammes et al. (1990b) found that at constant superficial gas velocity and higher reactor pressures the transition of trickle flow to pulse flow occurs at a relatively higher liquid flow rate. The reason for this effect is that due to pressure elevation at constant superficial gas and liquid velocities the liquid holdup will be lowered because of increased pressure gradient at higher gas densities. The mean liquid film thickness, which is proportional to the liquid holdup, becomes smaller and subsequently the liquid films cannot collapse any more to initiate the pulses.

Larachi et al. (1993) investigated the pressure effect on the trickle to pulse flow regime transition. They observed that at low liquid flow rates, the transition takes place at lower gas flow rate values when the pressure increases.

**Table I-2** Model equations or coordinates used in the flow charts for the trickle-to-pulse flow transition

| Reference | Model / Flow chart | |
|---|---|---|
| Charpentier and Favier (1975) | $\log\left[\frac{L}{G}\lambda\psi\right]$ vs. $\log\left[\frac{G}{\lambda}\right]$ | (I-3) |
| Talmor (1977) | $\log\left[\frac{L}{G}\left(\frac{\rho_L}{\rho_G}\right)_{av}\right]$ vs. $\log\left[\frac{1+1/Fr_{LG}}{We_{LG}+1/\mathrm{Re}_{LG}}\right]$ | (I-4) |
| Fukushima and Kusaka (1977) | $\phi^{-0.2}\,\mathrm{Re}_L^{0.27}\,\mathrm{Re}_G^{0.20}\left(\frac{d_p}{D_r}\right)^{-0.5} = 18$ | (I-5) |

$$\phi = \frac{S}{d_p^2} \quad \text{(surface shape factor)} \tag{I-6}$$

Sicardi et al. (1979)

Sicardi and Hofmann (1980)
$$\left(\frac{A}{\delta}\right)_{tr} = 16.2\sqrt{\frac{\tau_p \varepsilon}{\sigma a_v}} \tag{I-7}$$

Blok et al. (1983)
$$Fr = \frac{u_L^2}{g d_p} = 0.09 \qquad u_L = \frac{v_L}{\varepsilon \beta_{tot}} \tag{I-8}$$

Ng (1986)
$$\frac{1}{2}\rho_G u_G^2 \left(1 - \left(\frac{d}{d'}\right)^4\right) = 4\frac{\sigma_L}{d_p} - \frac{1}{2}\rho_L g d_p \tag{I-9}$$
$$G = \varepsilon u_G (1-\alpha)\rho_G \quad \alpha = 4\left[\sqrt{1-\beta} - (1-\beta)\right] \tag{I-10}$$

Grosser et al. (1988)
$$\rho_L \varepsilon_L \left(\frac{\partial U_L}{\partial t} + U_L \frac{\partial U_L}{\partial z}\right) + \varepsilon_L \frac{\partial P_L}{\partial z} - g\rho_L \varepsilon_L - F_L(z) + \frac{\partial\left(\varepsilon_L \mu_L^* \frac{\partial U_L}{\partial z}\right)}{\partial z} = 0 \tag{I-11}$$
$$\rho_G \varepsilon_G \left(\frac{\partial U_G}{\partial t} + U_G \frac{\partial U_G}{\partial z}\right) + \varepsilon_G \frac{\partial P_G}{\partial z} - g\rho_G \varepsilon_G - F_G(z) + \frac{\partial\left(\varepsilon_G \mu_G^* \frac{\partial U_G}{\partial z}\right)}{\partial z} = 0 \tag{I-12}$$
$$F_L(z) = -\left[\frac{A\mu_L (1-\varepsilon)^2 \varepsilon_L^2}{d_p^2 \varepsilon^3} U_L + \frac{B\rho_L (1-\varepsilon)\varepsilon_L^3}{d_p \varepsilon^3} U_L^2\right]\left(\frac{\varepsilon - \varepsilon_{Ls}}{\varepsilon_L - \varepsilon_{Ls}}\right)^{2.43} - F_G(z) \tag{I-13}$$
$$F_G(z) = -\left[\frac{A\mu_G (1-\varepsilon)^2 \varepsilon^{1.8}}{d_p^2 \{\varepsilon_G\}^{2.8}} + \frac{B\rho_G (1-\varepsilon)\varepsilon^{1.8}}{d_p \{\varepsilon_G\}^{1.8}} |U_G - U_L|\right](U_G - U_L) \tag{I-14}$$

Wammes et al. (1990b)
$$\beta_{e,trans} = \frac{c}{U_G^{0.26} \rho_G^{0.04}} \tag{I-15}$$
c = 0.27 for water/$N_2$ and 0.32 for water/40% ETG/$N_2$

Holub et al. (1992, 1993)
$$\frac{2.9\,\mathrm{Re}_L E_1^{5/11}}{\psi_L^{0.17} Ga_L^{0.41} Ka^{1/11}} \le 1 \tag{I-16}$$

Larachi et al. (1993)
$$\frac{L\lambda\psi\phi}{G} = \left(\frac{G}{\lambda}\right)^{-1.25} \tag{I-17}$$

$$\lambda = \sqrt{\frac{\rho_G}{\rho_a}\frac{\rho_L}{\rho_w}} \qquad \psi = \frac{\sigma_w}{\sigma_L}\left(\frac{\mu_L}{\mu_w}\right)^{1/3}\left(\frac{\rho_w}{\rho_L}\right)^{2/3} \qquad \phi = \frac{1}{4.76 + 0.5\frac{\rho_G}{\rho_a}} \qquad \text{(I-18)}$$

It may be noted that all the flow maps are based on experiments conducted at ambient conditions. So the validity of these flow maps at elevated temperature and/or pressure is in doubt because they can change considerably under different operating conditions. In the literature a number of studies have been presented on the transitions between the several regimes and their dependence on the gas and liquid flow rates, the liquid properties and the packing geometry and size. Regretfully – at least to our knowledge – no research has yet been carried out on the effect of temperature. Hence there is still a lag between the published experimental research and industrial practice at elevated temperatures.

## Pressure Drop

The two-phase pressure drop across the trickle bed reactor is a crucial parameter in the design, scale-up and operation of the trickle bed reactor because it is a measure of the energy required to move the fluids through the reactor. The throughput as well as the mass transfer coefficients depend on the energy supplied, which is a function of pressure drop. The pressure drop and liquid holdup influence each other mutually since the greater the liquid holdup, the more resistance to gas flow is observed. Pressure drop is also important in predicting the gas-liquid and the liquid-solid mass transfer.

Gas-liquid flow resistance in porous media is mainly caused by:

friction forces due to fluid viscosity at the gas-liquid, gas-solid (partially wetted conditions) and liquid-solid interfaces; inertial forces caused by successive acceleration and/or deceleration of the fluids across the packing; turbulence because of local velocity field fluctuations in both the gas and the liquid phases; interfacial (capillary) forces, which become significant when the liquids foam; gravity acting positively for downward flows but exerting a resistance to upward flows.

The relative importance of these forces naturally depends upon the flow regime in the reactor. Hence, in the high interaction regime, the main part of the mechanical energy

dissipation is due to inertia of the gas and/or the liquid flows, but in the trickle regime, the resistance to flow is essentially controlled by shear forces and capillary forces.

Extensive literature exists on the two-phase pressure drop and numerous correlations for the prediction of two-phase pressure drop have been proposed by various investigators. The correlations can be classified into two categories:

1. Correlations based on Lockhart-Martinelli Parameter

2. Correlations based on flow variables and packing characteristics

The first group of correlations has followed the pattern of the Lockhart-Martinelli approach for gas-liquid two-phase flow in open horizontal pipe. Lockhart-Martinelli (1949) showed that in the case of two-phase flows in horizontal tubes, it is possible to correlate the two-phase pressure drop as a function of the ratio of the single phase pressure drops of the gas and the liquid at the same flow rates:

$$\chi_G = \sqrt{\frac{\Delta P_G}{\Delta P_L}} \tag{I-19}$$

If both the gas and the liquid phase flows are turbulent, this ratio is equal to:

$$\chi_G = \frac{G}{L}\left(\frac{\rho_L}{\rho_G}\right)^{0.555}\left(\frac{\mu_G}{\mu_L}\right)^{0.111} \tag{I-20}$$

Ellman et al. (1988) showed that omitting the viscosity term did not lead to notable errors. They proposed the following approximation:

$$\chi_G \approx X_G = \frac{G}{L}\sqrt{\frac{\rho_L}{\rho_G}} \tag{I-21}$$

The basic assumptions used in the development of this correlation were:

a) Static pressure drop for the liquid phase must equal the static pressure drop for the gaseous phase regardless of the flow pattern, as long as an appreciable radial static pressure difference does not exist.

b) The volume occupied by the liquid phase plus the volume occupied by the gas phase at any instant must equal the volume of the pipe.

In fact, Weekman and Myers (1964) and Larkins (1961) have shown that the experimental data for two-phase pressure drop in a packed bed with vertical downward flow do not differ significantly from those obtained by Lockhart and Martinelli (1949). The salient feature of this group of correlations is that single-phase pressure drop of both liquid and gas must be found out prior to using these correlations (Midoux et al., 1976; Morsi et al., 1982; Holub et al., 1992, 1993). The single-phase pressure drop can be determined either experimentally or by prediction from an equation for single-phase flow. For predicting the single-phase pressure drop, Ergun's equation is widely used, assuming the same constants to be valid for gas and liquid flow. Ergun (1952) proposed the use of an equivalent spherical particle diameter and suggested universal values, independent of packing type, of the leading constants of the two terms of the equation:

$$\frac{\Delta P}{Z} = \frac{150\mu(1-\varepsilon)u}{\varepsilon^3 d_p^2} + \frac{1.75(1-\varepsilon)\rho u^2}{\varepsilon^3 d_p} \qquad \text{(I-22)}$$

Macdonald et al. (1979) found that very large errors were caused by the use of universal Ergun constants and suggested that constants be determined separately for each packing. They used what they called modified Ergun equation which is simply the Ergun equation with the specific constants 150 and 1.75 replaced by $E_1$ and $E_2$, respectively. The equation is:

$$F_k' \frac{\varepsilon^3}{1-\varepsilon} = E_2 + \frac{E_1(1-\varepsilon)}{\mathrm{Re}'} \qquad \text{(I-23)}$$

where

$$F_k' \equiv -\frac{\Delta P}{\rho u^2} d_{eq} \qquad \text{and} \qquad \mathrm{Re}' \equiv \frac{\rho u d_{eq}}{\mu} \qquad \text{(I-24)}$$

One choice for $d_{eq}$ is the equivalent mean sphere diameter $\bar{d}_{vs}$, defined as

$$d_{eq} \equiv \bar{d}_{vs} \equiv 6\frac{\upsilon_p}{s_p} \qquad \text{(I-25)}$$

where $\upsilon_p/s_p$ is the volume-to-surface ratio for the particulate system. An equivalent choice is

$$d_{eq} = \phi_s \bar{d}_v = 6\frac{\upsilon_p}{s_p} \qquad \text{(I-26)}$$

where $\bar{d}_v$ is the diameter of a different hypothetical sphere having the average volume of the actual particles, and $\varphi_s$, the sphericity, is the ratio of surface area of the hypothetical sphere to the average surface area of the actual particles.

The second group of correlations is based on the measurable operating variables and fluid and packing properties (diameter, porosity, shape etc.) or on combining them in dimensionless groups (*Re*, *We*, *Ga*, etc.). Turpin and Huntington's correlation uses a ratio of gas and liquid Reynolds numbers ($Re_L = d_pL/\mu_L$) as an independent variable.

Specchia and Baldi (1977) used the same ratio but with a correction factor $\psi$ containing the physical properties of the fluid referred to those of water. Clements and Schmidt (1980) used the ratio of the gas and liquid Reynolds numbers ($Re_G = dpG/\mu_G$) as well as the Weber number ($We = u_G^2 d_p \mu_G/\sigma$) for the gas – which contains the gas viscosity and the liquid surface tension.

The pressure drop is very much dependent on the voidage of the packed bed. The voidage near the reactor wall will be different from the rest of the packed bed. The voidage of the trickle bed reactor depends on the shape of the catalyst and the way in which the bed is packed. In most of the correlations falling under this category bed voidage is raised to the power of three which means a slight variation in the bed voidage will have a large effect on two-phase pressure drop (Saroha and Nigam, 1996).

All previous correlations are based on experiments carried out at atmospheric pressure. But the industrial trickle bed reactors are operated in the range of 25 – 40 MPa. At elevated pressures the physical properties of the liquid changes considerably and hydrodynamics of

the reactor changes drastically; therefore, the validity of using these correlations in the design of trickle bed reactors is in doubt.

Only recently some work has been performed at elevated pressures and correlations have been proposed for the determination of two-phase pressure drop which are summarized in Table I-3.

**Table I-3** Two Phase Pressure Drop Correlations at Elevated Pressure

| Reference | Correlation |
|---|---|
| Ellman et al. (1988) | low interaction regime: $f_{LGG} = 200(X_G A)^{-1.2} + 85(X_G A)^{-0.5}$ (I-27) |
| | high interaction regime: $f_{LGG} = 6.96(X_G B)^{-2} + 53.27(X_G B)^{-1.5}$ (I-28) |
| | $A = \frac{\mathrm{Re}_L^2}{(0.001 + \mathrm{Re}_L^{1.5})}$ $B = \frac{\mathrm{Re}_L^{0.25} We_L^{0.2}}{(1 + 3.17\,\mathrm{Re}_L^{1.65} We_L^{1.2})^{0.1}}$ (I-29) |
| Larachi et al. (1991a) | $f_{LGG} = \frac{1}{K^{1.5}}\left(A + \frac{B}{K^{0.5}}\right)$ (I-30) |
| | where $K = X_G(\mathrm{Re}_L We_L)^{0.25}$ $f_{LGG} = \frac{(\Delta P / Z) d_H \rho_G}{2G^2}$ (I-31) |
| | with A = 31.3 ± 3.9 ; B = 17.3 ± 0.6 |
| | $X_G = \frac{u_G}{u_L}\sqrt{\frac{\rho_L}{\rho_G}}$ $\mathrm{Re}_L = \frac{\rho_L u_L d_p}{\mu_L}$ $We = \frac{\rho_L u_L^2 d_p}{\sigma_L}$ (I-32) |
| Wammes et al. (1991a) | $\frac{\Delta P}{0.5\rho_G u_G^2}\left(\frac{d_p}{Z}\right) = 155\left(\frac{\rho_G u_G d_p}{\mu_G(1-\varepsilon)}\right)^{-0.37}\left(\frac{1-\varepsilon}{\varepsilon(1-\beta)}\right)$ (I-33) |
| Holub et al. (1992) | $\psi_L = \frac{\Delta P}{\rho_L g Z} + 1 = \left(\frac{\varepsilon_B}{\varepsilon_L}\right)^3\left[\frac{E_1 \mathrm{Re}_L}{Ga_L} + \frac{E_2 \mathrm{Re}_L^2}{Ga_L}\right]$ (I-34) |
| | $\psi_G = \frac{\Delta P}{\rho_G g Z} + 1 = \left(\frac{\varepsilon_B}{\varepsilon_B - \varepsilon_L}\right)^3\left[\frac{E_1 \mathrm{Re}_G}{Ga_G} + \frac{E_2 \mathrm{Re}_G^2}{Ga_G}\right]$ (I-35) |
| | $\psi_L = 1 + \frac{\rho_G}{\rho_L}(\psi_G - 1)$ (I-36) |

Hasseni et al. (1987) are the first who have presented a study of the effect of the pressure on the two-phase pressure drop in the trickle bed reactor. They measured the pressure drop, primarily in trickle, pulse flow regimes and in the transition regime, by using nitrogen as gas phase and various liquids for the liquid phase (ethylene glycol, cyclohexane and gas-oil). Their experimental data on the trickle-pulse flow transition regime at high pressure were compared with the model of Ng (1986). By this model the pressure effect on the flow regime transitions (in a diagram of L versus G) was represented for the water/nitrogen system. Ellman et al. (1988) proposed two pressure drop correlations for the low interaction (trickle flow) and high interaction (pulse, dispersed bubble and spray flow) regimes.

Larachi et al. (1991a) presented a simplified version of Ellman's correlation. A friction factor, $f_{LGG}$, is represented as a function of dimensionless groups which take inertia, viscosity and surface tension effects into account by using, respectively, $X_G$, $Re_L$ and $We_L$.

Wammes et al. (1991a) also proposed a theoretical correlation to estimate the two-phase pressure drop. The following assumptions were made:

The trickle bed reactor operates under stationary and isothermal conditions, the gas density is constant, the gas-liquid surface tension does not play a role.

However the validity of the correlation of Wammes et al. (1991a) is more limited than that of Larachi et al. (1991a), as it is based on a narrower range of operating conditions. Moreover, it needs prior evaluation of the liquid holdup, $\beta$. Al-Dahhan and Dudukovic (1994) extended Holub et al.'s (1992) model to describe the effect of high pressure on pressure drop and liquid holdup in trickle flow regime. The effect of gas density at constant superficial gas velocity on two-phase pressure drop was studied by Al-Dahhan and Dudukovic (1994) using hexane-nitrogen- helium systems. Helium pressure about seven times higher than that of nitrogen yields helium density equal to nitrogen density. It was observed that for a given value of gas density and liquid mass velocity both systems have approximately the same pressure drop. This shows that the effect of high pressure operation is due to the increase in gas density.

The conclusions drawn from the studies at elevated pressure are as follows:

1) The pressure drop per unit length increases with an increase in gas and liquid mass flow rates. This result is in agreement with the findings observed at atmospheric pressure.

2) At a particular liquid and gas mass flow rate the pressure drop decreases when the gas density increases either via the operating pressure or by using a gas of high molar weight. This is due to the decrease in superficial velocity and inertia of the gas phase with an increase in gas density.

3) The pressure drop increases with the liquid viscosity and decreases with the particle diameter

4) The pressure drop for foaming liquids at elevated pressure is higher than for non-foaming systems in the high interaction regime.

At the present time, the best new correlation for two-phase pressure drop, both for low and high interaction regimes, is that proposed by Iliuta et al. (1999), and derived using a neural network dimensionless-group-approach (Bertucco and Vetter, 2001).

## Liquid Holdup

Liquid holdup is an important parameter for the design, scale-up and operation of trickle bed reactors. The total liquid holdup ($\varepsilon_{Lt}$) (the ratio of the amount of liquid in the bed at any time to the volume of the empty reactor) can be divided into two types: external and internal. Internal liquid holdup ($\varepsilon_{Lint}$) is the ratio of the volume of the liquid held by capillary forces in the pores of porous catalysts to the reactor volume (usually the catalyst pores are filled with liquid due to capillary forces, especially when the bed is flooded before operation), while the external liquid holdup ($\varepsilon_{Lext}$) is the ratio of the volume of the liquid outside the catalyst pores partially occupying the void volume of the bed to the reactor volume. The external liquid holdup can further be divided into dynamic ($\varepsilon_{Ld}$) and static ($\varepsilon_{Ls}$) liquid holdup. The dynamic liquid holdup is the free flowing fraction of the liquid which is usually measured as the ratio, to the reactor volume, of the volume of liquid that would drain from the reactor when the inlets to the reactor are shut off simultaneously and the liquid is allowed to drain until it stops draining freely. In such measurement however, the name so-called dynamic holdup is not accurate since part of the remaining

external liquid which contributes to the dynamic holdup during the normal operation is not accounted for (Al-Dahhan and Highfill, 1999). The dynamic liquid holdup is dependent upon the hydrodynamics of the flow. The static liquid holdup is the ratio of the volume of stagnant liquid and the liquid retained between and around the contact points of the catalyst particles after draining to the reactor volume. It is independent of the reactor pressure, gas flow rate and liquid flow rate. However, it depends on liquid physical properties, particle shape, size and wettability (Al-Dahhan, 1993; Wammes et al., 1991; Charpentier et al., 1968; Shulman et al., 1955). It is called static holdup, although part of it would contribute to the dynamic holdup. Liquid holdup sometimes is called liquid saturation, which is based on the void volume of the reactor. For example, the external liquid saturation ($\beta_{Lext}$) is defined as the ratio of the volume of liquid present outside the catalyst particles to the void volume of the reactor. The relationship between the various types of holdups can be described by the following equations:

$$\varepsilon_{Lt} = \varepsilon_{Lext} + \varepsilon_{Lint} = \varepsilon_{Ls} + \varepsilon_{Ld} + \varepsilon_{Lint} \quad \text{(I-37)}$$

$$\varepsilon_{Lext} = \varepsilon \beta_{Lext} \quad \text{(I-38)}$$

Different techniques have been used to measure liquid holdup in laboratory trickle bed reactors. They can be classified as follows (Al-Dahhan and Highfill, 1999):

a) Draining Method: Liquid holdup is measured by draining the liquid when inlets and outlets to the reactor are shut off simultaneously. Both dynamic and static liquid holdup can be measured (Larkins et al., 1961; etc.).

b) Weighing Method: Liquid holdup is measured by weighing the reactor while liquid flows through it and either subtracting from this the weight of dry bed to obtain total holdup or by subtracting the weight of drained bed to obtain dynamic holdup (Crine and Marchot, 1981; Holub, 1990; etc.).

c) Tracer Method: Liquid holdup is measured by measuring the liquid residence time distribution and its mean to obtain total holdup (Mills and Dudukovic, 1981; Larachi 1991; etc.).

d) Closed Loop Method: Liquid holdup is measured by circulating in a closed loop of a known amount of liquid through the packed bed. The total holdup is the difference between the loop volume and the volume of the liquid outside the bed (Charpentier et al., 1968).

e) Electrical Conductivity Method: Liquid holdup is measured by measuring the apparent electrical conductivity in the presence of a conducting liquid between two electrode positioned at the top and the bottom of the bed or at two positions across the cross section of the bed (Achwal and Stepanek, 1976). This method can be used for various applications depending on how to configure and design the experiment. Prost (1967) and Blok and Drinkenburg (1982b) used such a method to study the pulsing flow regime in trickle bed reactors and to monitor locally the fluctuations of liquid in this regime.

Three of these methods, which are the drainage, tracer and weighing methods, have been used extensively in laboratory trickle bed reactors and they have been performed at either atmospheric pressure (Ellman et al., 1990; Holub et al., 1992; etc.) or at elevated pressures (Wammes et al., 1991a, b; Larachi et al., 1991, a, b, c; Al-Dahhan and Dudukovic, 1994; Tsamatsoulis and Papayannakos, 1994). Kushalkar and Pangarkar (1990) have shown that the static liquid holdup determined by a tracer technique is always smaller than the value determined by drainage technique. For the total liquid holdup it was found that tracer and drainage techniques give comparable values. Although several investigators recommended the weighing method over the others based on their experiments performed at atmospheric conditions, it was found that the weighing method failed to measure liquid holdup properly at high pressure operation (Al-Dahhan and Highfill, 1999).

## *Tracer Technique*

The tracer technique involves measuring the residence time distribution (RTD) in a reactor by analyzing the response curve of a tracer injection (Mills and Dudukovic, 1981; El-Hisnawi, 1982; Dudukovic, 1986; Larachi et al., 1991 a, b, c; Al-Dahhan, 1993; Iliuta et al., 1996; Saroha et al., 1998). Dudukovic (1986) gave a summary of the techniques of tracer methods and provided examples of their use for packed beds. Typically, an impulse injection of tracer or a step increase or decrease in tracer concentration is used. The impulse injection can be used to find total external holdup (in beds of nonporous particles), the

dynamic holdup and the static holdup. However, the step decrease in tracer concentration is considered as a better approach for finding static holdup (Schubert et al., 1986). By plotting the total external holdup versus the volumetric liquid flow rates and extrapolating to zero liquid flow rate, static liquid holdup can be determined (Bennett and Goodridge, 1970). The concentration of tracer at the outlet is measured, as a function of time, by some signal which is proportional to tracer concentration, such as light absorption, current, voltage, reflection, etc. In order to interpret this signal in terms of the residence times of tracer, 1) the tracer must be non-volatile and nonadsorbing, 2) it must enter and leave the system only by bulk flow, 3) the tracer injection must be proportional to flow, 4) the rate at which tracer leaves the system must be the integral of the product of the velocity times concentration integrated in a vectorial sense over the whole exit boundary, 5) the system must be at steady state except with respect to the tracer concentration, 6) the response curve must be proportional to the mass of tracer injected, 7) the tracer must behave almost identically to the carrier fluid, 8) there must be only one inlet and outlet, 9) system must be at steady state and 10) the tracer injection must not perturb the system (Dudukovic, 1986). Also, the liquid volume external to the reactor should be minimized compared to the reactor volume and it is very important to close the tracer mass balance (i.e. account for the entire tracer mass).

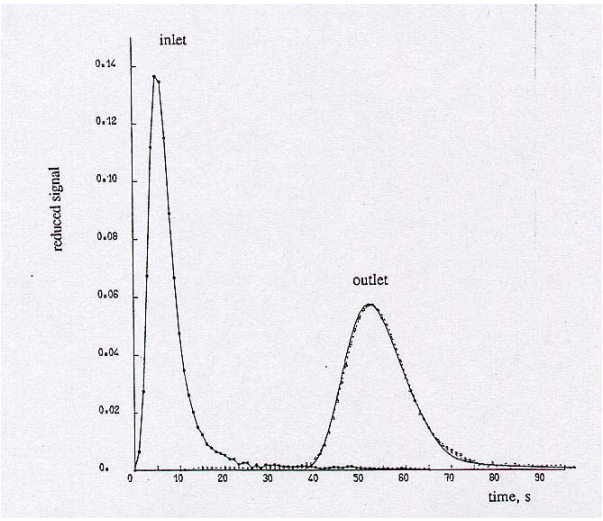


**Figure I-7** Schematic representation of the model fit and the experimental data

For an impulse injection of tracer, the total liquid holdup, $\varepsilon_{Lt}$, can be evaluated as follows (Dudukovic, 1986; Al-Dahhan and Dudukovic, 1995):

$$\tau = \int_0^\infty tE(t)dt \tag{I-39}$$

where

$$E(t) = \frac{QC(t)}{m_T} \tag{I-40}$$

If the tracer concentration is linearly proportional to the output signal of the analytical equipment used, E(t) then can be evaluated directly from the measured signal as:

$$E(t) = \frac{R(t)}{\int_0^\infty R(t)dt} \tag{I-41}$$

By using the equations above, liquid saturation (or holdup) can be calculated as:

$$\beta = \frac{L\tau}{\varepsilon\rho_L Z} \tag{I-42}$$

Here $\tau$ is the mean residence time, $t$ is the time, $E(t)$ is the residence time distribution function, $Q$ is the liquid volumetric flow rate, $C$ is the tracer concentration, $m_T$ is the injected tracer mass, $R$ is the signal response of analytical equipment (i.e. voltage, resistance etc.), $\beta$ is the liquid saturation, $L$ is the liquid superficial mass flow rate, $\varepsilon$ is the bed porosity, $\rho_L$ is the liquid density and $Z$ is the bed height.

For the analysis of the RTD (residence time distribution) curves different models were developed. However, the models that correspond best with reality are models that also divide the liquid phase in a dynamic and a stagnant zone, e.g., “the PDE model” with Piston flow with axial Dispersion and mass Exchange between the dynamic and the stagnant zone, of Van Swaaij et al. (1969) (Stegeman et al., 1996). The equations for this model were given as follows:

$$\frac{\partial C_{dyn}}{\partial x} + \varphi\frac{\partial C_{dyn}}{\partial \theta} + NTU\left(C_{dyn} - C_{st}\right) = \frac{1}{Pe}\frac{\partial^2 C_{dyn}}{\partial x^2} \tag{I-43}$$

$$\frac{\partial C_{st}}{\partial \theta} + \frac{NTU}{1-\varphi}\left(C_{st} - C_{dyn}\right) = 0 \tag{I-44}$$

The axial dispersion Peclet number (*Pe*), the number of transfer units (*NTU*) between the static and the dynamic zone, and the ratio of the dynamic to the total saturation ($\varphi$) can be determined by non-linear least square fitting in the time domain in order to obtain the best fit of the model. Recently, Iliuta et al. (1999a) proposed a model which illustrates the three zones (a dry zone, a wetted zone covered by the flowing dynamic liquid and a wetted zone covered by the stagnant liquid) typically encountered on the catalyst outer surface. The model views the external liquid stream as divided into an axially dispersed dynamic zone and an external stagnant zone contiguous to both the dynamic zone and the partially wetted porous particles. The equations of this model are:

Dynamic liquid zone:

$$\varepsilon_{L,d}\frac{\partial C_d}{\partial t}+\frac{\upsilon_{SL}}{H}\frac{\partial C_d}{\partial x}+N\frac{\upsilon_{SL}}{H}\left(C_d-C_{st}\right)=\frac{1}{Pe}\frac{\upsilon_{SL}}{H}\frac{\partial^2 C_d}{\partial x^2}-D^{eff}\,\frac{a_s f_d}{r_p}\frac{\partial C_p}{\partial \xi}\bigg|_{\xi=1} \qquad \text{(I-45)}$$

Static liquid zone:

$$\varepsilon_{L,st}\frac{\partial C_{st}}{\partial t}+N\frac{\upsilon_{SL}}{H}\left(C_{st}-C_d\right)+D^{eff}\,\frac{a_s f_{st}}{r_p}\frac{\partial C_p}{\partial \xi}\bigg|_{\xi=1}=0 \qquad \text{(I-46)}$$

Solid particle :

$$\varepsilon_{L,\text{int}}\frac{\partial C_p}{\partial t}=\frac{D^{eff}}{r_p^2\xi^2}\frac{\partial}{\partial \xi}\left(\xi^2\frac{\partial C_p}{\partial \xi}\right) \qquad \text{(I-47)}$$

where $\varepsilon_{L,d}$ and $\varepsilon_{L,st}$ are dynamic and static liquid holdups; $C_d$, $C_{st}$ and $C_p$ are the dimensionless tracer concentrations at the dynamic liquid zone, static liquid zone and the particle respectively; $\upsilon_{SL}$ is the superficial liquid velocity; $H$ is the bed height; $x$ is the dimensionless axial co-ordinate; $N$ is the number of transfer units; $D^{eff}$ is the effective diffusivity; $a_s$ is the packing specific area; $f_d$ and $f_{st}$ are the dynamic and static wetted fraction of catalyst; $\xi$ is the dimensionless radial co-ordinate; $r_p$ is the particle radius.

The tracer technique and the drainage technique give comparable values for the total liquid holdup at high pressures, similar to what was found by Tukac and Hanika (1992) at

atmospheric pressure. The tracer technique is a more practical technique on an industrial scale than either the drainage method or the weighing method, due to the tracer technique's capability of being performed without interrupting the flow and the fact that it does not involve weighing any large reactors or liquid volumes. Although Crine and Marchot (1981) found good agreement between weighing and draining methods at atmospheric pressure, the weighing method failed to measure properly liquid holdup at high pressure operation. Hence it is not recommended for use at elevated pressure. It overestimates significantly the liquid holdup due to the force imparted by the flowing fluids on the packing at elevated pressure (high gas density) (Al-Dahhan and Highfill, 1999).

The first measurements of liquid holdup in fixed bed reactors operated at high pressure were made by Abbott et al. (1967) in the range 2.4 – 3.8 MPa. Later, by means of a tracer injection technique, Kohler and Richarz (1985) measured static and total liquid holdups up to 1 MPa. Under zero gas flow and in the trickle flow regime, the data were well described by the low interaction correlation of Specchia and Baldi (1977). For two-phase flow, their data were correlated using the modified high interaction correlation of Specchia and Baldi (1977). Andreussi et al. (1988) applied the impedance method for the measurement of the liquid holdup in two-phase flow. The experimental technique is based on the measurement of the electrical impedance between two or more electrodes mounted on a specially designed section of the pipe. Tsochatzidis et al. (1992) determined cross-sectionally-averaged liquid holdup and the performance of ring electrodes by measuring the conductance of gas-liquid mixtures in pipes and packed beds using the similar design of Andreussi et al. (1988).

Ellman et al. (1990) derived two correlations for liquid holdup, one for the high and the other for the low interaction regimes. Wammes et al. (1991b) investigated static and noncapillary liquid holdups by the stop-flow technique and bed drainage for the same operating conditions as used in the two-phase pressure drop studies. They reported that liquid holdup decreased when the pressure was increased for given gas and liquid superficial velocities. Such a decrease was interpreted as due to a shift in the reactor fluid dynamics from a state predominantly controlled by gravity (trickle flow with zero gas flow rate) to a state controlled by gas-liquid shear stress (or pressure drop). The Specchia and

Baldi correlation (1977) for the low interaction regime described correctly their two-phase flow liquid holdup data. Larachi et al. (1991 a – d) and Wild et al. (1991) used the tracer impulse technique to investigate total liquid holdups within the same operating range as used in two-phase pressure drop measurements. The experimental reported results confirm observations made by Wammes et al. (1991b), but over a wider range of operating conditions: at very low gas velocities, the total holdup is independent of pressure regardless of the type of gas-liquid system. The practical value of the data pertaining to the very low gas velocity range (< 10 $mm.s^{-1}$) is evident since recourse to high pressure measurements is unnecessary. However for larger gas superficial velocities, the influence of pressure has to be taken into account (Bertucco and Vetter, 2001).

Ring and Missen (1991) investigated total, static and dynamic liquid holdups during the catalytic hydrodesulfurization of dibenzothiophene in trickle flow at 10 MPa and 330 – 370 ºC. The results showed the independence of liquid holdup upon temperature and pressure for the very low hydrogen mass fluxes tested ($53 \times 10^{-5} < G < 32 \times 10^{-4}$ $kg/m^2.s$) and found that the available correlations derived for atmospheric conditions can be useful for estimation purposes.

Al-Dahhan and Dudukovic (1994) measured liquid holdups using the stop-flow technique and bed drainage for the same conditions as for the pressure drops, *i.e.* trickle flow regime. Their high pressure data were well described with the parameter-free phenomenological model of Holub et al. (1992). The correlations for the high pressure operation are given below (Table I-4).

**Table I-4** Correlations and Models for Liquid Holdup in High Pressure Trickle Bed Reactors

| Reference | Correlation |
|---|---|
| Abbott et al. (1967) (2.41-3.79 MPa) | $\log_{10}(\beta_{nc}) = -0.44 + 0.40\log_{10}(\chi) - 0.12(\log_{10}(\chi))^2$ (I-47) |

Kohler and Richarz (1985) (0.1-1.0 MPa)

$$\beta_{nc} = 0.71\left(\frac{a_v d_p}{\varepsilon}\right)^{0.65}\left(\frac{\rho_L^2 g d_p^3}{\mu_L^2}\right)^{-0.42}\left(\frac{\rho_L u_L d_p}{\mu_L}\right)^{0.53}\left(\frac{\rho_G u_G d_p}{\mu_G}\right)^{-0.31} \quad \text{(I-48)}$$

Ellman et al. (1990) $\log\beta_{nc} = -RX_G^m \,\mathrm{Re}_L^n We_L^p\left(\frac{a_v d_K}{1-\varepsilon}\right)^q$ (0.1-8.0 MPa) (I-49)

high interaction regime
R = 0.16, m = 0.325, n = 0.163, p = -0.13, q = -0.163
low interaction regime
R = 0.42, m = 0.24, n = 0.14, p = 0, q = -0.14

Ring and Missen (1991) $\varepsilon\beta_a = 15.6u_L^{0.679}$ (10 MPa) (I-50)

Wammes et al. (1991) (0.3-6.0 MPa)
Trickling, no gas flow

$$\beta_{nc} = 16.3\left(\frac{\rho_L u_L d_p}{\mu_L}\right)^c\left(\frac{\rho_L^2 g d_p^3}{\mu_L^2}\right)^d \quad \text{(I-51)}$$

c = 0.36 if Re < 11 0.55 if Re > 15
d = -0.39 if Re < 11 -0.42 if Re > 15

gas-liquid flow (Specchia and Baldi (1977) correlation)

$$\beta_{nc} = 3.8\left(\frac{\rho_L u_L d_p}{\mu_L}\right)^{0.55}\left(\frac{\rho_L^2 g d_p^3}{\mu_L^2}\left(1+\frac{\Delta P}{\rho_L g Z}\right)\right)^{-0.42}\left(\frac{a_v d_p}{\varepsilon}\right)^{0.65} \quad \text{(I-52)}$$

Larachi et al. (1991a) $\log(1-\beta_e) = -\frac{1.22We_L^{0.15}}{\mathrm{Re}_L^{0.20} X_G^{0.15}}$ (0.2-8.1 MPa) (I-53)

Holub et al. (1992) $\psi_L = \frac{\Delta P}{\rho_L g Z} + 1 = \left(\frac{\varepsilon}{\varepsilon_L}\right)^3\left[\frac{E_1 \mathrm{Re}_L}{(1-\varepsilon)Ga_L} + \frac{E_2 \mathrm{Re}_L^2}{(1-\varepsilon)^2 Ga_L}\right]$ (I-54)

$$\psi_G = \frac{\Delta P}{\rho_G g Z} + 1 = \left(\frac{\varepsilon}{\varepsilon - \varepsilon_L}\right)^3\left[\frac{E_1 \mathrm{Re}_G}{(1-\varepsilon)Ga_G} + \frac{E_2 \mathrm{Re} G^2}{(1-\varepsilon)^2 Ga_G}\right] \quad \text{(I-55)}$$

$$\psi_L = 1 + \frac{\rho_G}{\rho_L}(\psi_G - 1) \quad \text{(0.31-5 MPa)} \quad \text{(I-56)}$$

Tsamatsoulis and Papayannakos (1994) $\varepsilon\beta_e = au_L^b$ (5 MPa) (I-57)
where a and b depend on boundary conditions

In the correlations above $\beta_{nc}$ is the non-capillary liquid saturation, $a_v$ is the bed-specific surface area, $d_p$ is the particle diameter, $\rho$ and $\mu$ are the density and viscosity, $u$ is the superficial velocity, $X_G$ is the modified Lockhart-Martinelli ratio, *Re*, *We* and *Ga* are the Reynolds, Weber and Galileo numbers respectively, $d_K$ is the Krischer-Kast hydraulic diameter, $\varepsilon$ and $\varepsilon_L$ are the bed porosity and liquid holdup, $\beta_a$ and $\beta_e$ are the active and external liquid holdup, $\Delta P/Z$ is the pressure drop, $Z$ is the bed length, $E_1$ and $E_2$ are Ergun constants and $\psi$ is a dimensionless parameter.

As mentioned above, the static liquid holdup situated around the contacting points of the particles, results from the balance between the capillary and gravitational forces and is independent of the gas flow, liquid flow and liquid viscosity (Bertucco and Vetter, 2001).

Van Swaaij (1969) and Charpentier et al. (1968) proposed a relationship between the static liquid holdup and the dimensionless Eötvos number, *Eö*. At high Eötvos numbers the static liquid holdup is inversely proportional to *Eö*, whereas at low Eötvos numbers, the static liquid holdup reaches a maximum value.

This correlation gives, for perfectly wettable solids, fairly good estimates of the static holdup for different particle geometries and sizes. Saez and Carbonell (1985) used the hydraulic diameter instead of the nominal particle diameter, as the characteristic length in the Eötvos number, to include the influence of the particle geometry on the static liquid holdup. According to the experimentally determined static holdup data Wammes et al. (1991b) concluded that the static liquid holdup is not affected by the total reactor pressure.

The experimental reported results of Larachi et al. (1991 a, c) confirm observations made by Wammes et al. (1990, 1991), but over a wider range of operating conditions: at very low gas velocities, the total liquid holdup is independent of pressure regardless of the type of gas-liquid system. However for larger gas superficial velocities, the influence of pressure has to be taken into account.

Moreover, Larachi (1991) found that: At given gas and liquid mass flow rates, the total liquid holdup increases with pressure, owing to the lower superficial gas velocity as a consequence of the increase in gas density. The total liquid holdup is reduced when the

liquid viscosity decreases. The total liquid holdup is much smaller for foaming liquids, regardless of the operating pressure, owing to the high stability of fine gas bubbles adhering to the solid particles.

In brief, the external liquid holdup is an increasing function of liquid velocity, viscosity and particle diameter. It is a decreasing function of the gas superficial velocity and of the liquid surface tension. Liquid holdup reduces as the gas density increases, except for very low gas velocities, where it is insensitive to gas density. Non-coalescing liquids exhibit much smaller holdups than coalescing liquids. Gas viscosity appears to have a marginal effect on the liquid holdup.

With the same approach as described for the two-phase pressure drop, Iliuta et al. (1999) also proposed a new correlation for the external liquid holdup in the high interaction regime.

## Models for the hydrodynamics of TBR

In the literature, approaches to modeling the hydrodynamics of TBR can be divided into two categories:

- a microscopic approach which examines the flows at the pore level;

- a macroscopic approach (volume-averaged) which captures the gross flow characteristics

An example of a microscopic approach has been proposed by Ng (1986). This model tries to represent what is happening locally at the place where pulsing is likely to be initiated. The objective was to put the previous flow maps on a theoretical basis by providing analytical predictions of flow regime transitions in order to demonstrate the interplay of various factors such as interfacial tension, bed porosity and others on transitions between flow regimes. It was stated that for the trickle flow regime the minimum superficial mass flow rate of liquid, $L$, to attain complete wetting can be estimated by multiplying the flow rate per unit length with the total length of grain boundary per unit sectional area:

$$L = mS \qquad \text{(I-58)}$$

This equation gives the transition curve from partial wetting to complete wetting where *m* is the minimum flow rate per unit length for complete wetting and *S* is the length of grain boundary per unit sectional area.

As illustrated by figure I-8, the place is just above the constrictions of the porous medium. The gas velocity here is the highest. The gas flow tends to induce the formation of a bridge, while the surface tension tends to keep the films apart. Ng applies Bernoulli's law between the points A and C. When the pulse is about to be initiated and the film breaks down, the liquid flow stops momentarily and the pressure difference between B and A is given by the Young-Laplace equation. By writing that the total gas flow rate is the same at C and A, the following relationship is obtained at the flow transition from trickle to pulse flow:

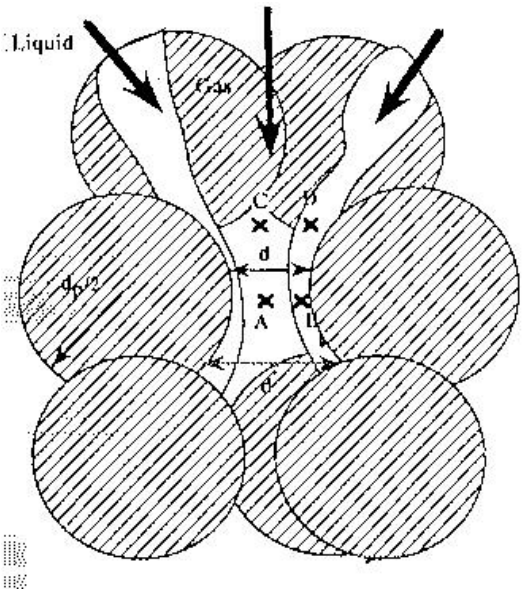


**Figure I-8** Mechanism of formation of a liquid pulse (Bertucco and Vetter, 2001)

$$\frac{1}{2}\rho_G u_G^2\left[1-\left(\frac{d}{d'}\right)^4\right]=\frac{4\sigma_L}{d_p}-\rho_L g\frac{d_p}{2} \qquad \text{(I-59)}$$

where $d$, $d'$ and $d_p$ are respectively the diameter of the pore, the diameter of the constriction and the diameter of the particle; $\sigma_L$ is the liquid phase surface tension and $\rho_L$ and $\rho_G$ are the liquid and gas phase densities respectively.

Here $u_G$, the interstitial velocity of the gas, is related to the superficial mass flow rate, $G$, by the following equation:

$$G = \varepsilon u_g (1-\alpha)\rho_G \tag{I-60}$$

where α is the fraction of the throat area occupied by liquid which is formulated as:

$$\alpha = 4\left[\sqrt{1-\beta} - (1-\beta)\right] \tag{I-61}$$

and $\varepsilon$ is the porosity of the packed bed.

The liquid saturation, $\beta$, is estimated by the correlation proposed by Wijffels et al. (1974):

$$\beta = \left[\left(\frac{200}{\mathrm{Re}_L} + 1.75\right)\frac{u_L^2}{g d_p}\frac{1-\varepsilon}{\varepsilon^3}\right]^{1/4} \tag{I-62}$$

These above equations provide the transition curve from trickle to pulse flow. For the trickle to spray flow transition curve the following equations were given:

$$u_G \propto \sqrt{\frac{\sigma}{\rho_G d_{t,\min}}} \qquad G = \frac{\pi}{4} d_{t,\min}^2 N_c u_G \rho_G \tag{I-63}$$

where $u_G$, $G$ and $\rho_G$ are the interstitial velocity, superficial mass flow rate and the density of gas respectively; $\sigma$ is the surface tension; $d_{t,min}$ is the minimum throat diameter in the column and $N_c$ is the number of circles irrespective of size per unit sectional area. The formulas for the calculation of $N_c$ and $d_{t,min}$ were as follows:

$$N_c = \frac{6(1-\varepsilon)}{\pi d_g^2} \qquad d_{t,\min} = \sqrt{\frac{2}{\pi}\sin\frac{\pi}{3} - \frac{1}{2}}\, d_g \tag{I-64}$$

where $\varepsilon$ is the porosity and $d_g$ is the particle diameter.

Wild et al. (1991) showed the comparison between predictions of Ng's model with measurements with water, nitrogen and 3 mm glass beads at different pressures made by Hasseni et al. (1987) and they stated that the agreement is acceptable. However, when they

considered the results obtained with ethyleneglycol, the liquid flow rate at the trickle/pulse boundary predicted by Ng's model is one order of magnitude smaller than the value measured by Hasseni et al. (1987). It seems, therefore, that this model does not represent well the influence of the liquid viscosity under pressure on the trickle/pulse flow transition (Bertucco and Vetter, 2001).

A large number of models consider the macroscopic approach for the prediction of the hydrodynamic behavior of trickle bed reactor.

Holub et al. (1992) developed a mechanistic pore-scale 1-D two-fluid segregated flow model in the form of two-phase flow Ergun like momentum equation inside an inclined slit. The model sketches the two-phase flow structure as a gas-free liquid flowing film totally covering the slit walls (complete wetting) and a gas flow in the central core of the slit. One of the models intrinsic assumptions is that full wetting predominates, regardless of the operating conditions (Figure I-9). Initially they modeled the complex geometry of the actual void space in the catalyst bed at the pore level by correlating it with the phenomenon of flow inside a rectangular slit. In their model, the width of the slit is a function of bed porosity and the angle of inclination of the slit to the vertical axis is related to a tortuosity factor for the packed bed. They introduced the concept of slip of the velocity and shear at the gas-liquid interface by introducing two slip parameters.

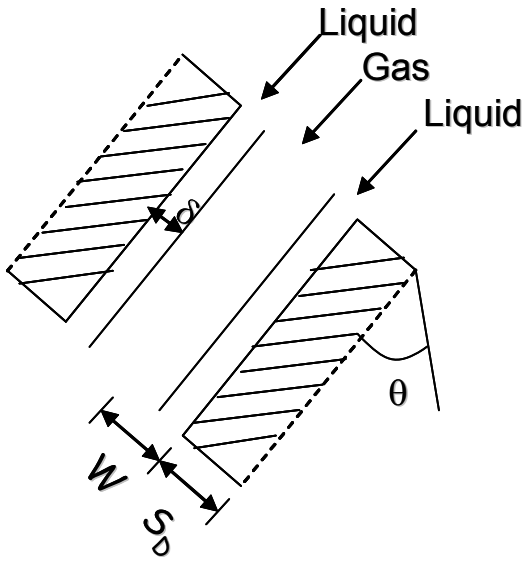


**Figure I-9** Schematic representation of Slit model

In the original model, the gas-liquid interface was assumed hermetic to momentum transfer (shear-free boundary) and the interfacial gas velocity was zero. This assumption implies that the gas flow does not influence the liquid flow. However, the experimental studies have shown that the gas flow has a considerable influence on the hydrodynamics of trickle bed reactor, especially at high operating pressure (Wammes 1990; Wammes et al. 1990a, 1991a; Larachi 1991, Larachi et al. 1991 a – c, Al-Dahhan et al. 1994, 1997).

An extension, by accounting for gas-liquid interfacial interactions via velocity and shear slip factors was then proposed by Al-Dahhan et al. (1998) to lift the model disparities observed for conditions of high gas throughputs and elevated pressures. Later, Iliuta et al. (1998) derived more general slip-corrective correlations. They developed state-of-the-art correlations for shear and velocity slip factors and Ergun single-phase flow bed constants. The shear and velocity slip factors were expressed as a function of the six most expressive dimensionless groups ($Re_L$, $Re_G$, $Fr_L$, $We_L$, $X_L$, $St_L$) whereas Ergun constants were correlated to particle equivalent diameter, sphericity factor, bed porosity and column diameter. These extended correlations are given as:

$$\psi_L = \frac{\Delta P / H}{\rho_L g} + 1 = \left( \frac{\varepsilon}{\varepsilon_{L,t}} \right)^3 \left[ \frac{E_1 \operatorname{Re}_L}{Ga_L} + \frac{E_2 \operatorname{Re}_L^2}{Ga_L} \right] + f_s \frac{\varepsilon_G}{\varepsilon_{L,t}} \left( 1 - \frac{\rho_G}{\rho_L} - \psi_L \right) \tag{I-65}$$

$$\psi_G = \frac{\Delta P / H}{\rho_G g} + 1 = \left( \frac{\varepsilon}{\varepsilon - \varepsilon_{L,t}} \right)^3 \left[ \frac{E_1 \left( \operatorname{Re}_G - f_v \varepsilon_G \operatorname{Re}_i \right)}{Ga_G} + \frac{E_2 \left( \operatorname{Re}_G - f_v \varepsilon_G \operatorname{Re}_i \right)^2}{Ga_G} \right] \tag{I-66}$$

$$\psi_L = 1 + \frac{\rho_G}{\rho_L} \left( \psi_G - 1 \right) \tag{I-67}$$

Iliuta and Larachi (1999b) developed a generalized slit model for the prediction of frictional two-phase pressure drop, liquid holdup and wetting efficiency in trickle bed reactor operated under partially and fully wetted conditions. This proposed model mimicked the actual bed void by two geometrically identical inclined slits, a wet slit and a dry slit.

In the first slit, the liquid wets the wall with a film of uniform thickness; the gas being in the central core (wet slit). The second slit is visited exclusively by the gas (dry slit). The high-pressure and high-temperature wetting efficiency, liquid holdup and pressure drop data reported in the literature for trickle bed reactor in the trickle flow regime were successfully forecasted by the model (Bertucco and Vetter, 2001).

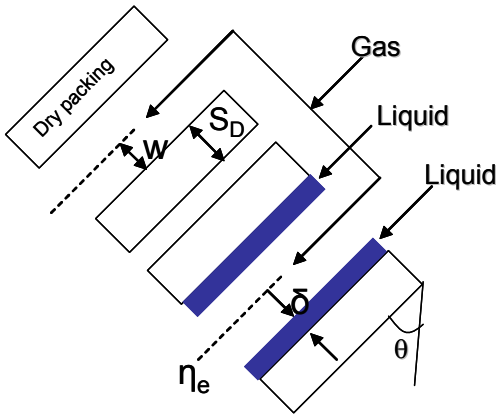


**Figure I-10** Double-slit model representation of two-phase flow in trickle flow reactors (Iliuta and Larachi, 1999b)

The equations for this model are as follows:

$$\psi_L = \left(\frac{\varepsilon}{\varepsilon_{L,t}}\right)^3 \left[\eta_e^2 \frac{E_1 \,\mathrm{Re}_L}{Ga_L} + \eta_e \frac{E_2 \,\mathrm{Re}_L^2}{Ga_L}\right] + f_s \eta_e \frac{\varepsilon - \left(\varepsilon_{L,t}/\eta_e\right)}{\varepsilon_{L,t}} \left(1 - \frac{\rho_G}{\rho_L} - \psi_L\right) \tag{I-68}$$

$$\begin{aligned} \psi_G = {} & \eta_e \frac{\varepsilon^3}{\left(\varepsilon - \left(\varepsilon_{L,t}/\eta_e\right)\right)^2 \left(\varepsilon - \varepsilon_{L,t}\right)} \left\{ E_1 \frac{\mathrm{Re}_G - f_v\left(\varepsilon - \left(\varepsilon_{L,t}/\eta_e\right)\right)\mathrm{Re}_i}{Ga_G} \right. \\ & \left. + E_2 \frac{\left[\mathrm{Re}_G - f_v\left(\varepsilon - \varepsilon_{L,t}/\eta_e\right)\mathrm{Re}_i\right]^2}{Ga_G} \right\} + \left(1 - \eta_e\right) \frac{\varepsilon}{\varepsilon - \varepsilon_{L,t}} \left\{ E_1 \frac{\mathrm{Re}_G}{Ga_G} + E_2 \frac{\mathrm{Re}_G^2}{Ga_G} \right\} \end{aligned} \tag{I-69}$$

$$\eta_e = \frac{1}{2E_1}\left(\frac{\varepsilon_{L,t}}{\varepsilon}\right)^2\left(\psi_L - 1 + \frac{\rho_G}{\rho_L}\right)\frac{Ga_L}{\mathrm{Re}_L} f_s + \left\{\left[\frac{1}{2E_1}\left(\frac{\varepsilon_{L,t}}{\varepsilon}\right)^2\left(\psi_L - 1 + \frac{\rho_G}{\rho_L}\right)\frac{Ga_L}{\mathrm{Re}_L} f_s\right]^2 - \frac{1}{E_1}\left(\frac{\varepsilon_{L,t}}{\varepsilon}\right)^2\left(\psi_L - 1 + \frac{\rho_G}{\rho_L}\right)\frac{Ga_L}{\mathrm{Re}_L} f_s + \frac{2}{3E_1}\left(\frac{\varepsilon_{L,t}}{\varepsilon}\right)^3 \psi_L \frac{Ga_L}{\mathrm{Re}_L}\right\}^{1/2} \quad \text{(I-70)}$$

$$\psi_L = 1 + \frac{\rho_G}{\rho_L}\left(\psi_G - 1\right) \quad \text{(I-71)}$$

Attou et al. (1999) developed a physical one-dimensional model to describe the hydrodynamics of a steady-state cocurrent gas-liquid trickle flow regime through a trickle bed reactor. The trickle flow regime is idealized by a flow in which the gas and liquid phases are completely separated by a smooth and stable interface. As a consequence, each fluid behaves as a continuous medium for which the macroscopic balance laws can be applied in the Eulerian formalism. The formulation of the trickle flow model involves the global mass and momentum balance equations applied to each fluid across the interstitial void volume. The closure equations describing the various interactions between the phases are formulated on the basis of theoretical considerations, by taking into account the assumed idealized flow pattern. The authors indicated that the resulting model has the fundamental characteristic of involving no parameter from fitting single-phase or two-phase flow data. The application of the 1-D CFD model implies knowledge of the two momentum-transfer coefficients between phases and the mean fraction of the interstitial void volume occupied by the gas phase. A good agreement is generally observed between the predictions of pressure-gradient and liquid saturation from the 1-D CFD model and the respective experimental results obtained over a large range of operating pressure (1-100 bar). The proposed model underestimates the pressure gradient in the conditions of high operating pressures and superficial gas velocities owing to the appearance of the phenomena of roll waves pattern of the gas-liquid interface and the entrainment of droplets (Bertucco and Vetter, 2001). The resulting equations for the trickle flow were given as below:

$$\frac{1}{p}\frac{dp}{dz}+\frac{1}{\alpha}\frac{d\alpha}{dz}+\frac{1}{u_G}\frac{du_G}{dz}=0 \qquad \frac{1}{1-\alpha}\frac{d(1-\alpha)}{dz}+\frac{1}{u_L}\frac{du_L}{dz}=0 \tag{I-72}$$

$$\alpha\frac{dp}{dz}=-\frac{\Gamma_G}{RT}\alpha p u_G\frac{du_G}{dz}-\alpha\left(A_{GL}(\alpha)\mu_G(j_r+j_G)+B_{GL}(\alpha)\rho_G\left(j_r^2+j_G^2\right)\right)+\alpha\rho_G g \tag{I-73}$$

$$\begin{aligned}(1-\alpha)\frac{dp}{dz}&=-\Gamma_L(1-\alpha)\rho_L u_L\frac{du_L}{dz}+\alpha\left(A_{GL}(\alpha)\mu_G j_r+B_{GL}(\alpha)\rho_G j_r^2\right)\\&-\left(A_{LS}(\alpha)\mu_L j_L+B_{LS}(\alpha)\rho_L j_L^2\right)+(1-\alpha)\rho_L g\end{aligned} \tag{I-74}$$

The momentum transfer coefficients A and B, functions of gas fraction α and geometrical characteristics of the packed bed ($\varepsilon$, bed porosity and $d_p$, particle diameter) are calculated from the expressions given as follows:

$$A_{LS}=180\frac{(1-\varepsilon)^2}{(1-\alpha)^3\varepsilon^3 d_p^2} \quad \text{and} \quad B_{LS}=1.8\frac{(1-\varepsilon)}{(1-\alpha)^3\varepsilon^3 d_p} \tag{I-75}$$

$$A_{GL}=180\frac{(1-\alpha\varepsilon)^2}{\alpha^3\varepsilon^3 d_p^2}\left(\frac{1-\varepsilon}{1-\varepsilon\alpha}\right)^{2/3} \text{ and } \quad B_{GL}=1.8\frac{(1-\alpha\varepsilon)}{\alpha^3\varepsilon^3 d_p}\left(\frac{1-\varepsilon}{1-\alpha\varepsilon}\right)^{1/3} \tag{I-76}$$

In the above equations $p$ is the pressure, $z$ is the axial coordinate, $\alpha$ is the mean fraction of the interstitial void volume occupied by the gas phase, u is the average interstitial velocity, $\Gamma$ is the shape factor for the momentum flux, $j$ is the superficial velocity, $j_r$ is the reference superficial velocity associated to the gas-liquid slip motion, $\rho$ is the density and $g$ is the gravitational acceleration.

Iliuta et al. (1999) published an overview of hydrodynamics and mass transfer in trickle bed reactor based on extensive historic experimental flow data (22000 experiments) from the literature. The state-of-the art of trickle bed fluid dynamics was presented and a set of unified and updated estimation methods relying on neural work, dimensional analysis and phenomenological hybrid approaches were discussed.

In the same way, Larachi et al. (2000) evaluated with an important trickle flow regime database (4000 experiments) different phenomenological models for liquid holdup and two-phase pressure drop in trickle bed reactor. According to Larachi et al. (2000) and Bertucco and Vetter (2001) the following main remarks are emerged from the analysis of the models:

- the slit model predicted well the liquid holdup but its performance at forecasting pressure drop was as weak as that from the two empirical correlations

- the Attou's 1-D CFD model and the extended slit model constitutive shear and slip correlations did not improve much the pressure drop prediction

- the Attou's 1-D CFD model was tested with different simplifying assumptions, which do not provide significant gains. It is suggested that one should use this model in its simplest form

- the extended slit model of Iliuta et al. (1998) and the double slit model outperformed all the available models in term of the pressure drop prediction

- all models performed almost equally well and can be recommended equally in liquid holdup prediction

- the double slit model was the only model able to predict the wetting efficiency.

Iliuta et al. (2002) introduced a new mechanistic film model for pressure drop and liquid holdup in the low interaction regime. The model mimics the two-phase flow by a double-slit network consisting of a dry and a wet slit. The degree of interaction between the gas and the liquid has been described by incorporating a gas-liquid interaction factor. After testing the model by ca. 5000 experiments they predicted that this new approach has been successful to predict the reactor hydraulics under various operational conditions such as atmospheric or high pressure/temperature conditions.

## Objectives

Trickle bed reactors host a variety of commercially important three-phase catalytic reactions in different processes and industries. Any small improvement in the reactor

productivity can translate into substantial benefits. A basic understanding of the hydrodynamic parameters is essential for their design, scale-up and performance prediction. Cyclic operation could be introduced as one of the methods for the process intensification in TBR. The studies on the hydrodynamics of the cyclic operation were performed at atmospheric pressure and ambient temperature.

This work presents mainly the effect of temperature on the hydrodynamic parameters of a TBR for different systems during constant throughput mode and cyclic operation. Chapter one presents the effect of temperature on the trickle-to-pulse flow transition boundary, pressure drop, liquid holdup, liquid backmixing and the pulse velocity for Newtonian and non-Newtonian power-law liquids. The experimental data was compared with the suggested models and correlations.

Chapter two is focused on the influence of elevated temperature and moderate pressure on the shock wave characteristics (shock wave breakthrough and decay times, shock wave plateau and shock wave breakthrough amplitude) during slow-mode induced pulsing for Newtonian and non-Newtonian liquids.

Chapter three enlightens the influence of temperature on the trickle-to-pulsing transition, pulse characteristics (e.g. pulse velocity and pulse frequency) in cyclic operation as well as in constant-throughput flow for Newtonian and non-Newtonian liquids.

Chapter four concerns the effect of temperature and pressure, superficial gas and (base and pulse) liquid velocities, and bed depth on the structure of the trickle-to-pulsing transition in cyclic operation and spontaneous pulsing flow in terms of liquid holdups and velocities. Additionally the pulse characteristics in the pulsing flow regime are given for both cyclic operation and spontaneous pulsing for Newtonian and non-Newtonian liquids.

Chapter five presents experimental results on the effect of temperature and pressure on the liquid holdup and pressure drop time series in terms of pulse breakthrough and decay times, pulse intensity, and pulse velocity for the air-water system.

Chapter six reports the effects of temperature and pressure on the shift of the transition from trickle to foaming-pulsing flow regimes, on the two-phase pressure drop, the liquid

holdup, and the pulse frequency and velocity for Newtonian (air-cetyltrimethylammoniumbromide (CTAB)) foaming and non-Newtonian (air-0.25% CTAB-carboxymethylcellulose (CMC)) foaming systems.

Chapter seven suggests an alternating gas/liquid fast-mode cyclic operation procedure to enlarge the operational domain of the low interaction regime at elevated temperature and moderate pressure for the air-aqueous cetyltrimethylammoniumbromide (CTAB) foaming system.

TBR hydrodynamic studies could also be performed at particle scale e.g. the extra-granular hydrodynamic effects could be distinguished from intraparticle mass transfer effects of catalytic particles which is noteworthy in scaling up/down of TBR. Chapter eight presents a simple and scaleable method to suppress the internal porosity in various porous particles for the complete filling of the pores by a cross-linked organic polymer. The liquid holdup and Péclet number were compared for a trickle-bed reactor packed with impregnated spherical particles and glass beads at ambient conditions for the air-water system.

## Nomenclature

| | |
|---|---|
| $a$ | specific interfacial area between dynamic and stagnant zone, $m^2/m^3$ |
| $a_v$ | bed-specific surface area, $m^2/m^3$ |
| $C$ | tracer concentration, mol/l |
| $d_p$ | particle diameter, m |
| $D_{ax}$ | axial dispersion coefficient, $m^2/s$ |
| $D^{eff}$ | effective diffusivity, $m^2/s$ |
| $D_r$ | reactor diameter, m |
| $E$ | residence time density function |
| $E_1$, $E_2$ | Ergun constants |

| | |
|---|---|
| $f_d$ | dynamic wetted fraction of catalyst |
| $f_{st}$ | static wetted fraction of catalyst |
| $f_{LGG}$ | two-phase friction factor $\left(\frac{\Delta P / Zd_K}{2\rho_G u_G^2}\right)$ |
| $F_i$ | volume-averaged forces exerted on phase *i* by the other phases, $N/m^3$ |
| Fr | Froude number ($u^2/gd_p$) |
| g | gravitational acceleration, $m/s^2$ |
| G | gas mass flux, $kg/m^2.s$ |
| Ga | Galileo number ($d_p^3\rho^2 g\varepsilon^3/\mu^2(1-\varepsilon)^3$) |
| H | bed height, m |
| $k_L$ | mass transfer coefficient between the zones, m/s |
| Ka | Kapitza number ($\sigma_L^3\rho_L/\mu_L^4 g$) |
| L | liquid mass flux, $kg/m^2.s$ |
| $m_T$ | mass of tracer injected, kg |
| NTU | number of transfer units ($k_L aL/u_L$) |
| P | pressure, MPa |
| Pe | Péclet number ($u_{dyn}Z/D_{ax}$) |
| $\Delta P$ | pressure drop, $N/m^2$ |
| Q | volumetric liquid flow rate, $m^3/s$ |
| r | radial position within solid particle, m |

| | |
|---|---|
| $r_p$ | particle radius, m |
| R | signal response of analytical equipment (i.e. voltage, conductance etc.) |
| Re | Reynolds number ($\rho u d_p/\mu$) |
| We | Weber number ($\rho u^2 d_p/\sigma$) |
| S | selectivity |
| t | time |
| u | superficial velocity, m/s |
| $\upsilon_L$ | liquid superficial velocity, m/s |
| $X_G$ | modified Lockhart-Martinelli ratio |
| Z | bed length, m |

**Greek letters**

| | |
|---|---|
| $\alpha$ | fraction of the area occupied by liquid |
| $\beta$ | liquid saturation |
| $\xi$ | radial co-ordinate ($r/r_p$) |
| $\varepsilon$ | bed porosity |
| $\lambda$ | dimensionless parameter |
| $\mu$ | viscosity, Pa.s |
| $\rho$ | density, $kg/m^3$ |
| $\sigma$ | surface tension, N/m |
| $\tau$ | mean residence time, s |

| | |
|---|---|
| $\psi$ | dimensionless parameter |
| $\delta$ | liquid film height, m |
| $\gamma$ | vapor-to-feed molar ratio, |
| $\chi_G$ | Lockhart-Martinelli parameter |

**Subscripts**

| | |
|---|---|
| a | air |
| d | dynamic |
| e | external |
| ext | external |
| G | gas |
| int | internal |
| L | liquid |
| LG | two-phase |
| P | particle |
| st | static |
| w | water |

## References

Abbott, M.D.; Moore, G.R.; Ralph, J.L. Paper S-4, *Proc. 7th ABG Conf.*, cited by Y.T. Shah (1979) and M. Purwasasmita (1985), 1967.

Achwal, S.K.; Stepanek, J.B. Holdup Profiles in Packed Beds. *Chem. Eng. J.*, 12, 69, 1976.

Al-Dahhan, M.H. Effects of High Pressure and Fines on the Hydrodynamics of Trickle Bed Reactors, PhD Dissertation, Washington University, St.Louis, MO, 1993.

Al-Dahhan, M.H.; Dudukovic, M.P. Pressure drop and liquid holdup in high pressure trickle bed reactors. *Chem. Eng. Sci.*, 49, 5681, 1994.

Al-Dahhan, M.H.; Larachi, F.; Dudukovic, M.P.; Laurent, A. High Pressure Trickle Bed Reactors: A Review, *Ind. Eng. Chem. Res.*, 36, 3292, 1997.

Al-Dahhan, M.H.; Khadilkar, M.R.; Wu, Y.; Dudukovic, M.P. Prediction of pressure drop and liquid holdup in high pressure trickle bed reactors. *Ind. Eng. Chem. Res.*, 37, 793, 1998.

Al-Dahhan, M.H.; Highfill, W. Liquid Holdup Measurement Techniques in Laboratory High Pressure Trickle Bed Reactors. *Can. J. Chem. Eng.*, 77, 759, 1999.

Andreussi, P.; Di Donfrancesco, A.; Messia, M. An impedance method for the measurement of liquid holdup in two-phase flow. *Int. J. Multiphase Flow*, 14, 777, 1988.

Attou, A.; Boyer, C.; Ferschneider, G. Modeling of the hydrodynamics of the cocurrent gas-liquid trickle flow through a trickle bed reactor. Chem. Eng. Sci., 54, 785, 1999.

Attou, A.; Ferschneider, G. A two-fluid model for flow regime transition in gas-liquid trickle bed reactors. Chem. Eng. Sci., 54, 5031, 1999.

Bailey, J.E.; Ollis, D.F. *Biochemical Engineering Fundamentals*, 2nd ed., McGraw-Hill Book Co. New York, 1986.

Baker, O. Simultaneous flow of oil and gas. *Oil Gas J.*, 53, 185, 1954.

Berruti, F.; Hudgins, R.R.; Rhodes, E.; Sicardi, S. Oxidation of sulphur dioxide in a trickle bed reactor: A study of reactor modeling. *Can. J. Chem. Eng.*, 62, 644, 1984.

Bartelmus, G.; Gancarczyk, A.; Stasiak, M. Hydrodynamics of cocurrent fixed bed three-phase reactors: Part I. The effect of physicochemical properties of the liquid on pulse velocity. *Chem. Eng. Proc.*, 37, 331, 1998.

Battin, F. Hydrodynamique d'un réacteur catalytique à lit fixe fonctionnant sous pression à co-courant de gaz et de liquide vers le bas. Diplôme d'Etudes Approfondies, LSGC, ENSIC, INPL, Nancy, France, 1987.

Bennett, A.; Goodridge, F. Hydrodynamic and Mass Transfer Studies in Packed Absorption Columns. *Trans. Instn. Chem. Engrs.*, 48, 232, 1970.

Bertucco, A.; Vetter, G. *High Pressure Process Technology: Fundamentals and Applications*, Elsevier, Amsterdam, 2001.

Blok, J.R.; Drinkenburg, A.A.H. Hydrodynamics and mass transfer in pulsing trickle bed columns. *ACS Symposium series No.196*, Chemical Reaction Engineering, Washington D.C., 393, 1982a.

Blok, J.R.; Drinkenburg, A.A.H. Hydrodynamic properties of pulses in two-phase downflow operated packed columns. *Chem. Eng. J.*, 25, 89, 1982b.

Blok, J.R.; Varkevisser, J.; Drinkenburg, A.A.H. Transition to pulsing flow, holdup and pressure drop in packed columns with cocurrent gas-liquid downflow. *Chem. Eng. Sci.*, 38, 687, 1983.

Boelhouwer, J.G.; Piepers, H.W.; Drinkenburg, A.A.H. Particle-liquid heat transfer in trickle bed reactors. *Chem. Eng. Sci.*, 56, 1181, 2001.

Boelhouwer, J.G.; Piepers, H.W.; Drinkenburg, A.A.H. Nature and characteristics of pulsing flow in trickle bed reactors. *Chem. Eng. Sci.*, 57, 4865, 2002.

Charpentier, J.C. ; Prost, C. ; Van Swaaij, W. ; Le Goff, P. Etude de la retention de liquide dans une colonne à garnissage arrosé à co-courant et à contre-courant de gaz-liquide. *Chimie et Industrie – Génie Chimique*, 99, 803, 1968.

Charpentier, J.C.; Favier, M. Some liquid holdup experimental data in trickle bed reactors for foaming and nonfoaming hydrocarbons. *AIChE J.*, 21, 1213, 1975.

Chou, T.S.; Worley, F.L.; Luss, D. Transition to pulsed flow in mixed phase cocurrent downflow through a fixed bed. *Ind. Eng. Chem. Process Des. Dev.*, 16, 424, 1977.

Chou, T.S.; Worley, F.L.; Luss, D. Local particle-liquid mass transfer fluctuations in mixed phase cocurrent downflow through a fixed bed in the pulsing regime. *Ind. Eng. Chem. Fund.*, *18*, 279, 1979.

Christensen, G.; McGovern, S.J.; Sundaresan, S. Cocurrent downflow of air and water in a two-dimensional packed column. *AIChE J.*, 32, 1677, 1986.

Chuang, K.T.; Cheng, S.; Tong, S. Removal and destruction of benzene, toluene and xylene from wastewater by air stripping and catalytic oxidation. *Ind. Eng. Chem. Res.*, 31, 2466, 1992.

Clements, L.D.; Schmidt, P.C. Two-phase pressure drop in cocurrent downflow in packed beds: Air-Silicone oil systems. *AIChE J.*, 26, 314, 1980.

Crine, M.; Marchot, P. Measuring Dynamic Liquid Holdup in Trickle Bed Reactors Under Actual Operating Conditions. *Chem. Eng. Commun.*, 8, 365, 1981.

Dudukovic, M.P. Tracer Methods in Chemical Reactors. Techniques and Applications in Chemical Reactor Design and Technology, H.I. de Lasa, Editor, *NATO ASI Series E: No. 110*, Nijhoff, 1986.

Dudukovic, M.P.; Larachi, F.; Mills, P.L. Multiphase catalytic reactors: A perspective on current knowledge and future trends. Catal. Rev. – Sci. Eng., 44, 123, 2002.

El-Hisnawi, A.A.; Dudukovic, M.P.; Mills, P.L. Trickle bed reactors: Dynamic tracer tests, reaction studies and modeling of reactor performance. Chemical Reaction Engineering-Boston, J. Wei and C. Georgakis, eds., *Am. Chem. Soc. Symp. Ser.*, No. 196, 421, 1982.

Ellman, M.J.; Midoux, N.; Laurent, A.; Charpentier, J.C. A new, improved pressure drop correlation for trickle bed reactors. *Chem. Eng. Sci.*, 43, 2201, 1988.

Ellman, M.J.; Midoux, N.; Wild, G.; Laurent, A.; Charpentier, J.C. A New, Improved Liquid Holdup Correlation for Trickle Bed Reactors. *Chem. Eng. Sci.*, 45, 1677, 1990.

Ergun, S. Fluid Flow through Packed Columns. *Chem. Eng. Prog.*, 48, 89, 1952.

Fukushima, S.; Kusaka, K. Interfacial area and boundary of hydrodynamic flow region in packed column with cocurrent downward flow. *J. Chem. Eng. Jpn.*, 10, 461, 1977.

Gianetto, A.; Specchia, V. Trickle Bed Reactors: State of Art and Perspectives. *Chem. Eng. Sci.*, 47, 3197, 1992.

Goto, S.; Smith, J.M. Trickle Bed Reactor Performance. *AIChE J.*, 21, 706, 1975.

Goto, S.; Chatani, T.; Matouq, M.H. Hydration of 2-Methyl-2-Butene in gas-liquid cocurrent upflow and downflow reactors. *Can. J. Chem. Eng.*, 71, 821, 1993.

Grosser, K.; Carbonell, R.G.; Sundaresan, S. Onset of Pulsing in Two-phase Cocurrent Downflow Through a Packed Bed. *AIChE J.*, 34, 1850, 1988.

Hartman, M.; Coughlin, R.W. Oxidation of $SO_2$ in a trickle bed reactor packed with Carbon. *Chem. Eng. Sci.*, 27, 867, 1972.

Hasseni, W.; Laurent, A.; Midoux, N.; Charpentier, J.C. Régimes d'écoulement dans un réacteur catalytique à lit fixe arrosé fonctionnant sous pression (0.1 - 10 MPa) à co-courant de gaz et de liquide vers le bas. *Entropie*, 137/138, 127, 1987.

Haure, P.M.; Hudgins, R.R.; Silveston, P.L. Periodic operation of a trickle bed reactor. *AIChE J.*, 35, 1437, 1989.

Haure, P.M.; Hudgins, R.R.; Silveston, P.L. Investigation of $SO_2$ oxidation rates in trickle bed reactors operating at low liquid flow rates. *Can. J. Chem. Eng.*, 70, 600, 1992.

Helwick, J.A.; Dillon, P.O.; McCready, M.J. Time varying behavior of cocurrent gas-liquid flows in packed beds. *Chem. Eng. Sci.*, 47, 3249, 1992.

Herskowitz, M.; Carbonell, R.G.; Smith, J.M. Effectiveness factors and mass transfer in trickle bed reactors. *AIChE J.*, 25, 272, 1979

Herskowitz, M.; Mosseri, S. Global rates of reaction in trickle bed reactors: Effects of gas and liquid flow rates. *Ind. Eng. Chem. Fundam.*, 22, 4, 1983.

Holub, R.A.; Dudukovic, M.P.; Ramachandran, P.A. Phenomenological Model of Pressure Drop, Liquid Holdup and Flow Regime Transition in Gas-Liquid Trickle Flow. *Chem. Eng. Sci.*, 47, 2343, 1992.

Holub, R.A.; Dudukovic, M.P.; Ramachandran, P.A. Pressure drop, liquid holdup and flow regime transition in trickle flow. *AIChE J.*, 39, 302, 1993.

Huang, T-C.; Ben-Chang, K. Kinetic study of naphthalene hydrogenation over $Pt/Al_2O_3$ catalyst. *Ind. Eng. Chem. Res.*, 34, 1140, 1995.

Iliuta, I.; Thyrion, F.C.; Muntean, O. RTD of the Liquid in Two-Phase Cocurrent Downflow in Packed Beds: Air/Newtonian and Non-Newtonian Liquid Systems. *Can. J. Chem. Eng.*, 74, 783, 1996.

Iliuta, I.; Larachi, F.; Grandjean, B.P.A. Pressure drop and liquid holdup in trickle flow reactors: improved Ergun constants and slip correlations for the slit model. *Ind. Eng. Chem. Res.*, 37, 4542, 1998.

Iliuta, I.; Ortiz-Arroyo, A.; Larachi, F.; Grandjean, B.P.A.; Wild, G. Hydrodynamics and mass transfer in trickle bed reactors: an overview. *Chem. Eng. Sci.*, 54, 5329, 1999.

Iliuta, I.; Larachi, F.; Grandjean, B.P.A. Residence time, mass transfer and back-mixing of the liquid in trickle flow reactors containing porous particles. *Chem. Eng. Sci.*, 54, 4099, 1999a.

Iliuta, I.; Larachi, F. The generalized slit model: Pressure gradient, liquid holdup and wetting efficiency in gas-liquid trickle flow. *Chem. Eng. Sci.*, 54, 5039, 1999b.

Iliuta, I.; Grandjean, B.P.A.; Larachi, F. New mechanistic film model for pressure drop and liquid holdup in trickle flow reactors. *Chem. Eng. Sci.*, 57, 3359, 2002.

Koh, C-S.; Butt, J.B. Experimental and modeling study of kinetics and selectivity in the oxidation of a poly (α-olefin) lubricant. *Ind. Eng. Chem. Res.*, 34, 524, 1995.

Kohler, M.; Richarz, W. Investigation of liquid holdup in trickle bed reactors. *Ger. Chem. Eng.*, 8, 295, 1985.

Kolb, W.B.; Melli, T.R.; de Santos, J.M.; Scriven, L.E. Cocurrent downflow in packed beds. Flow regimes and their acoustic signatures. *Ind. Eng. Chem. Res.*, 29, 2380, 1990.

Krishna, R.; Ellenberger, J.; Sie, S.T. Reactor development for conversion of natural gas to liquid fuels: a scaleup strategy relying on hydrodynamic analogies. *Chem. Eng. Sci.*, 51, 2041, 1996.

Kushalkar, K.B.; Pangarkar, V.G. Liquid holdup and dispersion in packed columns. *Chem. Eng. Sci.*, 45, 759, 1990.

Larachi, F. “Etude hydrodynamique d’un réacteur catalytique à lit fixe arrosé fonctionnant sous pression à co-courant de gaz et de liquide vers le bas : Pertes de charge, taux de rétention du liquide et régimes d’écoulement”, Diplôme d’Etudes Approfondies, LSGC, ENSIC, INPL, Nancy, France, 1988.

Larachi, F. Les Réacteurs Triphasiques à Lit Fixe à Écoulement à Co-courant vers le Bas et vers le Haut de Gaz et de Liquide. Étude de l’Influence de la Pression sur l’Hydrodynamique et le Transfert de Matière Gaz-Liquide, PhD Dissertation, Institut National Polytechnique de Lorraine, Nancy, France, 1991.

Larachi, F.; Laurent, A.; Midoux, N.; Wild, G. Experimental Study of a Trickle Bed Reactor Operating at High Pressure: Two-Phase Pressure Drop and Liquid Saturation. *Chem. Eng. Sci.*, 46, 1233, 1991a.

Larachi, F.; Laurent, A.; Wild, G.; Midoux, N. Some Experimental Liquid Saturation Results in Fixed Bed Reactors Operated under Elevated Pressure in Cocurrent Upflow and Downflow of the Gas and the Liquid. *Ind. Eng. Chem. Res.*, 30, 2404, 1991b.

Larachi, F.; Laurent, A.; Midoux, N.; Wild, G. Liquid Saturation Data in Trickle Beds Operating under Elevated Pressure. *AIChE J.*, 37, 1109, 1991c.

Larachi, F.; Laurent, A.; Midoux, N. Pressure Effects on the Liquid Saturation of a Trickle Bed Reactor. *Technol. Today*, 1, 146, 1991d.

Larachi, F.; Laurent, A.; Wild; G.; Midoux, G. Effet de la Pression sur la Transition Ruisselant-Pulsé dans les Réacteurs Catalytiques à Lit Fixe Arrosé. *Can. J. Chem. Eng.*, 71, 319, 1993.

Larachi, F.; Iliuta, I.; Chen, M.; Grandjean, B.P.A. Onset of pulsing in trickle beds: Evaluation of current tools and state-of-the-art correlation. *Can. J. Chem. Eng.*, 77, 751, 1999.

Larachi, F.; Iliuta, I.; Al-Dahhan, M.A.; Dudukovic, M.P. Discrimating trickle flow hydrodynamic models – some recommendations. *Ind. Eng. Chem. Res.*, 39, 554, 2000.

Larkins, R.P.; White, R.R.; Jeffrey, D.W. Two-Phase Cocurrent Flow in Packed Beds. *AIChE J.*, 7, 231, 1961.

Latifi, M.A.; Rode, S.; Midoux, N.; Storck, A. The use of microelectrodes for the determination of flow regimes in a trickle bed reactor. *Chem. Eng. Sci.*, 47, 1955, 1992.

Lemay, Y.; Pineault, G.; Ruether, J.A. Particle-liquid mass transfer in a three-phase fixed bed reactor with cocurrent flow in the pulsing regime. *Ind. Eng. Chem. Process Des. Dev.*, 14, 280, 1975.

Lerou, J.J.; Glasser, D.; Luss, D. Packed bed liquid phase dispersion in pulsed gas-liquid downflow. *Ind. Eng. Fund.*, 19, 66, 1980.

Levec, J.; Smith, J.M. Oxidation of Acetic Acid Solutions in a Trickle Bed Reactor. *AIChE J.*, 22, 159, 1976.

Lockhart, R.W.; Martinelli, R.C. Proposed correlation of data for isothermal two-phase, two-component flow in pipes. *Chem. Eng. Prog.*, 45, 39, 1949.

Macdonald, I.F.; El-Sayed, M.S.; Mow, K.; Dullien, F.A.L. Flow through Porous Media-the Ergun Equation Revisited. *Ind. Eng. Chem. Fundam.*, 18, 199, 1979.

Mata, A.R.; Smith, J.M. Oxidation of sulphur dioxide in a trickle bed reactor. *Chem. Eng. J.*, 22, 229, 1981.

McManus, R.L.; Funk, G.A.; Harold, M.P.; Ng, K.M. Experimental study of reaction in trickle bed reactors with liquid maldistribution. *Ind. Eng. Chem. Res.*, 32, 570, 1993.

Melli, T.R.; de Santos, J.M.; Kolb, W.B.; Scriven, L.E. Cocurrent downflow in networks of passages. *Ind. Eng. Chem. Res.*, 29, 2367, 1990.

Meyers, R.A. *Handbook of Petroleum Refining Processes*, 2nd ed., McGraw-Hill, New York, 1996.

Midoux, N.; Favier, M.; Charpentier, J.C. Flow Pattern, Pressure Loss and Liquid Holdup Data in Gas-Liquid Downflow Packed Beds with Foaming and Nonfoaming Hydrocarbons. *J. Chem. Eng. Japan*, 9, 350, 1976.

Mills, P.L.; Dudukovic, M.P. Evaluation of Liquid-Solid Contacting in Trickle Bed by Tracer Methods. *AIChE J.*, 27, 893, 1981.

Morita, S.; Smith, J.M. Mass transfer and contacting efficiency in a trickle bed reactor. *Ind. Eng. Chem. Fundam.*, 17, 113, 1978

Morsi, B.I.; Midoux, N.; Laurent, A.; Charpentier, J.C. Hydrodynamics and interfacial areas in downward cocurrent gas-liquid flow through fixed beds. Influence of the nature of the liquid. *Int. Chem. Eng.*, 22, 142, 1982.

Narasimhan, C.S.L.; Verma, R.P.; Kundu; A.; Nigam, K.D.P. Modeling Hydrodynamics of Trickle-Bed Reactors at High Pressure. *AIChE J.*, 48, 2459, 2002.

Ng, K.M. A model for flow regime transitions in cocurrent downflow trickle bed reactors. *AIChE J.*, 32, 115, 1986.

Pavko, A.; Levec, J. Wetting efficiency in the trickle bed reactor. *Proc. of 2nd World Congress of Chem. Eng.*, Montreal, Canada, October 4-9, 1981.

Prost, C. Etude des fluctuations de la texture liquide s'écoulant à contre-courant ou à co-courant de gaz dans une garnisage de colonne d'absorption. *Chem. Eng. Sci.*, 22, 1283, 1967.

Ramachandran, P.A.; Chaudhari, R.V. *Three-phase Catalytic Reactors*, Gordon and Breach New York, 1983.

Rao, V.G.; Drinkenburg, A.A.H. Pressure drop and hydrodynamic properties of pulses in two-phase gas-liquid downflow through packed beds. *Can. J. Chem. Eng.*, 61, 158, 1983.

Rao, V.G.; Drinkenburg, A.A.H. Solid-liquid mass transfer in packed beds with cocurrent gas-liquid downflow. *AIChE J.*, 31, 1059, 1985.

Ring, Z.E.; Missen, R.W. Trickle bed reactors: Tracer study of liquid holdup and wetting efficiency at high temperature and pressure. *Can. J. Chem. Eng.*, 69, 1016, 1991.

Saez, A.E.; Carbonell, R.G. Hydrodynamic parameters for gas-liquid cocurrent flow in packed beds. *AIChE J.*, 31, 52, 1985.

Saroha, A.K.; Nigam, K.D.P. Trickle Bed Reactors. *Reviews in Chemical Engineering*, Vol. 12, Chapters 3 - 4, p. 207, 1996.

Saroha, A.K.; Nigam, K.D.P.; Saxena, A.K.; Dixit, L. RTD Studies in Trickle Bed Reactors Packed with Porous Particles. *Can. J. Chem. Eng.*, 76, 738, 1998.

Sato, Y.; Hirose, T.; Takahashi, F.; Toda, M.; Hashiguchi, Y. Flow Pattern and Pulsation Properties of Cocurrent Gas-Liquid Downflow in Packed Beds. *J. Chem. Eng. Jpn.*, 6, 315, 1973.

Satterfield, C.N.; Pelossof, A.A.; Sherwood, T.K. Mass transfer limitations in a trickle bed reactor. *AIChE J.*, 15, 226, 1969.

Schubert, C.N.; Lindner, J.R.; Kelly, R.M. Experimental Methods for Measuring Static Liquid Holdup in Packed Columns. *AIChE J.*, 32, 1920, 1986.

Shulman, H.L.; Ullrich, C.F.; Proulx, A.Z.; Zimmerman, J.O. Performance of Packed Column II: Wetted and Effective Interfacial Area, Gas and Liquid Mass Transfer Rates. *AIChE J.*, 1, 253, 1955.

Sicardi, S.; Gerhard, H.; Hofmann, H. Flow regime transition in trickle bed reactors. *Chem. Eng. J.*, 18, 173, 1979.

Sicardi, S.; Hofmann, H. Influence of gas velocity and packing geometry on pulsing inception in trickle bed reactors. *Chem. Eng. J.*, 20, 251, 1980.

Specchia, V.; Baldi, G. Pressure drop and liquid holdup for two-phase cocurrent flow in packed beds. *Chem. Eng. Sci.*, 32, 515, 1977.

Stegeman, D.; van Rooijen, F.E.; Kamperman, A.A.; Weijer, S.; Westerterp, K.R. Residence Time Distribution in the Liquid Phase in a Cocurrent Gas-Liquid Trickle Bed Reactor. *Ind. Eng. Chem. Res.*, 35, 378, 1996.

Sundaresan, S. Mathematical modeling of pulsing flow in large trickle beds. *AIChE J.*, 33, 455, 1987.

Talmor, E. Two-phase downflow through catalyst beds. *AIChE J.*, 23, 868, 1977.

Tsamatsoulis, D.; Papayannakos, N. Axial Dispersion and Holdup in a Bench Scale Trickle Bed Reactor at Operating Conditions. *Chem. Eng. Sci.*, 49, 523, 1994.

Tsochatzidis, N.A.; Karabelas, A.J. Hydrodynamic properties of pulses in trickle beds. *2nd World Conference on Experimental Heat Transfer, Fluid Mechanics and Thermodynamics*, Dubrovnik, Yugoslovia, 1991.

Tsochatzidis, N.A.; Karapantsios, T.D.; Kostoglou, M.V.; Karabelas, A.J. A Conductance Probe for Measuring Liquid Fraction in Pipes and Packed Beds. *Int. J. Multiphase Flow*, 18, 653, 1992.

Tsochatzidis, N.A.; Karabelas, A.J. Properties of pulsing flow in a trickle bed. *J. Appl. Electrochem.*, 24, 670, 1994.

Tsochatzidis, N.A.; Karabelas, A.J. Properties of pulsing flow in a trickle bed. *AIChE J.*, 41, 2371, 1995.

Tukac, V.; Hanika, J. Influence of Catalyst Particles Orientation on the Pressure Drop and the Liquid Dispersion in the Trickle Bed Reactor. *Chem. Eng. Sci.*, 47, 2227, 1992.

Turpin, J.L.; Huntington, R.L. Prediction of pressure drop for two-phase two-component cocurrent flow in packed beds. *AIChE J.*, 13, 1196, 1967.

Van Swaaij, W.P.M.; Charpentier, J.C.; Villermaux, J. Residence time distribution in the liquid phase of trickle flow in packed columns. *Chem. Eng. Sci.*, 24, 1083, 1969.

Wammes, W.J.A. Hydrodynamics in a cocurrent gas-liquid trickle bed reactor at elevated pressures. PhD Dissertation, Twente University, Enschede, Holland, 1990.

Wammes, W.J.A.; Mechielsen, S.J.; Westerterp, K.R. The influence of the reactor pressure on the hydrodynamics of cocurrent gas-liquid trickle bed reactor. *Chem. Eng. Sci.*, 45, 2247, 1990a.

Wammes, W.J.A.; Mechielsen, S.J.; Westerterp, K.R. The Transition Between Trickle Flow and Pulse Flow in a Cocurrent Gas-Liquid Trickle Bed Reactor at Elevated Pressures. *Chem. Eng. Sci.*, 45, 3149, 1990b.

Wammes, W.J.A.; Middekamp, J.; Huisman, W.J.; Debaas, C.M.; Westerterp, K.R. Hydrodynamics in a cocurrent gas-liquid trickle bed at elevated pressures, Part 2: liquid holdup, pressure drop, flow regimes. *AIChE J.*, 37, 1855, 1991a.

Wammes, W.J.A.; Mechielsen, S.J.; Westerterp, K.R. The Influence of Pressure on the Liquid Holdup in a Cocurrent Gas-Liquid Trickle Bed Reactor Operating at Low Gas Velocities. *Chem. Eng. Sci.*, 46, 409, 1991b.

Weekman, V.W.; Myers, J.E. Fluid flow characteristics of cocurrent gas-liquid flow in packed beds. *AIChE J.*, 10, 951, 1964.

Westerterp, K.R.; Wammes, W.J.A. Three-phase trickle bed reactors. Vol. B4, 309, Principles of Chemical Reaction Engineering and Plant Design, *Ullman's Encyclopedia of Industrial Chemistry*, 5th ed., 1992.

Wijffels, J.B.; Verloop, J.; Zuiderweg, F.J. Wetting of catalyst particles under trickle flow conditions. Chem. Reac. Eng. II, *Adv. Chem. Ser.*, 133, 151, 1974.

Wild, G.; Larachi, F.; Laurent, A. The Hydrodynamic Characteristics of Cocurrent Downflow and Cocurrent Upflow Gas-Liquid-Solid Fixed Bed Reactors: The Effect of Pressure. *Rev. Inst. Fr. Pet.*, 46, 467, 1991.

Wu, R.; McCready, M.J.; Varma, A. Effect of pulsing on reaction outcome in a gas-liquid catalytic packed bed reactor. *Catalysis Today*, 48, 195, 1999.

# Chapter 1

# Trickle bed hydrodynamics at elevated temperature for (non-)Newtonian liquids*

## Résumé

Bien que l'hydrodynamique des réacteurs de type « trickle bed » à haute pression est largement documentée dans la littérature récente, au contraire, le comportement hydrodynamique à haute température demeure en grande partie inconnu. L'objectif de cette étude est d'étudier expérimentalement l'effet de la température sur la transition de régime d'écoulement ruisselant-pulsé, la vitesse de la pulsation, la perte de pression biphasique, la rétention liquide et le coefficient de dispersion axiale. Ces paramètres ont été déterminés pour des systèmes newtonien (air-eau) et non-newtonien (air–0.25% carboxymethylcellulose, CMC), et les résultats expérimentaux obtenus ont été comparés aux modèles et corrélations existants pour confrontation et recommandations. La ligne de la transition ruisselant-pulsé est déplacée vers les grandes vitesses superficielles de gaz et de liquide avec l'élévation de la température en alignement avec le comportement déjà connu sur l'effet de la pression. Le diagramme de Charpentier-Favier modifié (Larachi et al. 1993) a permis de suivre de manière adéquate le déplacement de cette transition avec la température pour les liquides newtoniens. En revanche, toute chose égale par ailleurs, l'élévation de la température occasionne une baisse de perte de pression et de rétention liquide, alors que la vitesse de la pulsation croît avec la température. Le modèle de fentes « slit model » d'Iliuta et Larachi pour les fluides non-newtoniens (Iliuta et Larachi, 2002) prédit avec une très bonne précision à la fois la perte de pression et la rétention liquide, indépendamment des niveaux de pression et de température, et sans nécessiter de réglage de paramètres. La corrélation de Burghardt et al. (2004) pour la vitesse de la pulsation peut être recommandée pour des calculs préliminaires d'ingénierie de la vitesse de la pulsation à

* Aydin, B.; Larachi, F. Chemical Engineering Science, 60, 6687-6701, 2005

température et pression élevées aussi bien pour les liquides newtonien que non-newtonien. Le coefficient de dispersion liquide axiale (Dax) estimé à partir du modèle piston avec dispersion axiale a révélé que la température n'a pas affecté de manière substantielle ce paramètre. Les deux types de fluides (newtonien et non-newtonien en loi de puissance) se sont comportés qualitativement de façon similaire en ce qui concerne l'effet de la température.

# Abstract

Despite the hydrodynamics of trickle beds experiencing high pressures has become largely documented in the recent literature, trickle bed hydrodynamic behavior at elevated temperatures, on the contrary, largely remains *terra incognita*. This study's aim was to demonstrate experimentally the temperature shift of trickle-to-pulse flow regime transition, pulse velocity, two-phase pressure drop, liquid holdup and liquid axial dispersion coefficient. These parameters were determined for Newtonian (air-water) and non-Newtonian (air-0.25% Carboxymethylcellulose (CMC)) liquids, and the various experimental results were compared to available literature models and correlations for confrontation and recommendations. The trickle-to-pulse flow transition boundary shifted towards higher gas and liquid superficial velocities with increasingly temperatures, aligning with the findings on pressure effects which likewise were confirmed to broaden the trickle flow domain. The Larachi-Charpentier-Favier diagram (Larachi et al. 1993) provided good predictions of the transition locus at elevated temperature for Newtonian liquids. Conversely, everything else being kept identical, increasingly temperatures occasioned a decrease in both two-phase pressure drop and liquid holdup; whereas pulse velocity was observed to increase with temperature. The Iliuta and Larachi slit model for non-Newtonian fluids (Iliuta and Larachi, 2002) predicted with very good accuracy both the pressure drops and the liquid holdups regardless of pressure and temperature without requiring any adjustable parameter. The Burghardt et al. (2004) pulse velocity correlation can be recommended for preliminary engineering calculations of pulse velocity at elevated temperature, pressure, Newtonian and non-Newtonian liquids. The liquid axial dispersion coefficient ($D_{ax}$) extracted from the axial dispersion RTD model revealed that temperatures

did not affect in a substantial manner this parameter. Both Newtonian and power-law non-Newtonian fluids behaved qualitatively similarly regarding the effect of temperature.

**Keywords** Trickle bed, elevated temperature, hydrodynamics, transition boundary, pulsing flow, non-Newtonian fluids

## 1.1 Introduction

Trickle-bed reactors (TBR) are perhaps the simplest and the most ubiquitous three-phase reactor configurations wherein gaseous and liquid streams are forced to flow co-currently downwards across a porous medium of randomly packed catalytic grains. Though not being its exclusive user, the petroleum industry nowadays tremendously relies on trickle bed for its hydrotreating and hydrocracking operations. This stems from the gradual reserve depletion of the so-called conventional oil which is forcing the oil sector to exploit *dirtier* non-conventional hydrocarbon deposits such as heavy crude oils, bitumen and residues (Speight, 1999; Speight, 2001; Wauquier, 1994; Lepage et al., 1990).

Ongoing research on trickle bed efficiency demonstrates the significance of spotting the optimal operational modes and of quantifying the incidence of its most influential factors. As several industrial applications require elevated pressure and temperature, understanding of TBR hydrodynamics at these conditions is imperative. A great deal of experimental studies dealing with the effect of elevated pressures on TBR hydrodynamics concerned the trickle flow regime. Though the advantages of pulsing flow are well documented in the literature (Rao and Drinkenburg, 1985; Tsochatzidis and Karabelas, 1995; Boelhouwer et al., 2002) interest on pulse flow regime characteristics at elevated pressures is very recent (Burghardt et al., 2002, 2004). Since this flow regime takes place in several industrial applications often at high temperature, it is necessary to unveil the temperature effects on basic characteristics, e.g., pulse velocity, that occur in this particular flow regime.

To the best of our knowledge, experimental studies on TBR hydrodynamics involving non-Newtonian systems concerned only friendly atmospheric pressure and ambient temperature conditions. As TBR applications also touch the realm of biochemical processes, the effects

of temperature and pressure ought to be unveiled for the hydrodynamic parameters of trickle-bed reactors traversed by the flow of non-Newtonian liquids.

Flow regime transitions at elevated pressure were first investigated by Hasseni et al. (1987) up to 10 MPa. Trickle-to-pulse flow regime transitions were determined both visually and from locating slope inflation using pressure drop-flow rate curves obtained for different pressure values for aqueous and organic liquids, and two particle sizes. Using the gas mass flux scale and the original Charpentier and Favier flow regime diagram (Charpentier and Favier, 1975), Hasseni et al. (1987) noted a collapse with increasing pressures of the $L/G\lambda\psi$ versus $G/\lambda$ lines. Wammes et al. (1990) determined visually the shift with pressure of flow regime transition for air-nitrogen system up to 1.5 MPa. They observed a shift in transition boundary to higher liquid velocities with increasingly pressures for a constant gas superficial velocity. Larachi et al. (1993) derived a graphical correlation based on elevated pressure experimental data by modifying the Charpentier and Favier flow chart through introducing a new gas density sensitive correction function $\Phi$, on top of the two traditional physical-property Baker $\lambda$ and $\psi$ coordinates. The amended flow regime diagram embraced most of the high-pressure flow regime transition data published in the 1990's. Burghardt et al. (2002) observed the gas continuous to pulsing flow regime for air-water system up to 0.9 MPa and ambient temperature by means of electrical conductivity cells. They confirmed their predecessors' observations regarding the shift from trickle to pulse flow transition to higher superficial velocities of the two phases. Experimental investigations on flow regimes in trickle beds involving non-Newtonians liquids (mainly pseudo-plastic inelastic power-law aqueous solutions) were scanty and concerned exclusively ambient temperature and pressure, *e.g.*, Sai and Varma (1998) visual observation of transition for air-0.25%carboxymethylcellulose (CMC) system, and Iliuta et al. (1996) and Iliuta and Thyrion (1997) studies for different power-law aqueous CMC solutions. Their findings were coherent with a trickle flow region that retracts with increased liquid viscosity.

Experimental data on pulse flow characteristics in trickle beds has begun to be reported in the early 1960's. Weekman and Myers (1964) measured pulse frequency and velocity for different particle sizes for the air-water system using photo-resistors. They reported an increase in pulse velocity with gas and/or liquid flow rates. Sato et al. (1973) used motion

pictures, pressure transducer and electrical conductivity probes for the determination of pulse velocity, and pointed out to the negligible dependence of pulse velocity upon phase flow rates. Blok and Drinkenburg (1982), using electrical conductivity probes for the measurement of pulse velocity and frequency for air-water system, found no influence of liquid flow rate on pulse velocity. Similarly, according to experiments with different particle sizes, Rao and Drinkenburg (1983) also observed marginal effect of liquid flow rate and proposed a pulse velocity correlation functionalizing interstitial gas velocity and packing geometry. However, at high liquid flow rate, Tsochatzidis and Karabelas (1995) observed significant influence of this parameter on pulse velocity for the air-water system. They suggested an empirical correlation functionalizing interstitial gas velocity and superficial liquid velocity. Bartelmus et al. (1998) and Burghardt et al. (2002, 2004) implemented optical and electrical conductivity techniques for measuring pulse velocity, pulse frequency and pulse length for different particle sizes, gas-liquid systems and pressures. Increasingly pressures were found to decrease pulse velocity and to increase pulse frequency, whereas pulse length was shortened. They proposed a pulse velocity correlation as a function of packing size, and gas and liquid interstitial velocities. Boelhouwer et al. (2002) measured pulse frequency and pulse velocity for different particle sizes using an electrical conductance technique and observed an increase in pulse velocity with gas flow rate but indicated insignificant effects of liquid flow rate.

The effect of pressure on two-phase pressure drop was investigated by many previous researchers. Experimental two-phase pressure drop data was first reported in the late 1980's by Hasseni et al. (1987) for the nitrogen-water system up to 10.1 MPa based upon which Ellman et al. (1988) proposed correlations for the calculation of pressure drop both in low (trickle flow) and high interaction (mainly pulse flow) regimes. Wammes et al. (1990, 1991) measured and correlated pressure drops up to 7.5 MPa for different aqueous and organic liquid systems under various flow regimes, including trickle and pulse flow regimes. Larachi et al. (1991) and Wild et al. (1991) provided pressure drop experiments up to 8.1 MPa for diverse systems and a pressure drop correlation thereof. In their correlation, pressure drop is expressed by means of two-phase flow friction factor and the modified Lockhart-Martinelli ratio. Al-Dahhan and Dudukovic (1994) conducted experiments up to 5 MPa for different aqueous and non-aqueous systems in trickle flow regime. Recently,

Burghardt et al. (2004) reported pressure drop data up to 0.9 MPa for air-water and air-glycerin systems at elevated pressure; whereas Guo and Al-Dahhan (2004) studied pressure drop up to 0.8 MPa for air-water system. Pressure drop data for non-Newtonian liquids is much scantier and only concerned ambient conditions. Larkins et al. (1961) were the first who studied the behavior of pressure drops in trickle beds for different CMC systems. Iliuta and Thyrion (1997) investigated the pressure drop for different CMC concentrations and Sai and Varma (1987) presented a correlation in terms of Lockhart-Martinelli parameters, flow variables and packing characteristics.

Liquid holdup plays a crucial role in several trickle bed processes such as control of catalyst wetting efficiency, radial heat evacuation, gas-liquid mass transfer of gaseous reactant, solvent evaporation and exposure of bare dry catalytic surfaces thereof, etc. Ongoing research on this parameter has mainly been concerned with the incidence of elevated pressures as described in the pressure drop references above. Besides the reported experimental work at elevated pressure, to our knowledge there is at least only one study published for liquid holdup measurements at elevated temperature. Ring and Missen (1991) measured the liquid holdup between 330-370ºC in trickle flow regime in the conditions of dibenzothiophene catalytic hydrodesulfurization. According to the data obtained from pulse-tracer experiments, no clear cut emerged regarding the effect of temperature which was difficult to interpret.

As seen briefly from the above literature survey, even if an adequate body of knowledge on TBR hydrodynamics has become available for the elevated pressures over the past decade or so, the effect of temperature was largely overlooked by the existing systematic TBR hydrodynamic studies. This situation is paradoxical considering that temperature affects virtually all the gas and liquid physical properties whereas pressure is known to influence almost exclusively density and molecular diffusivity for sub-critical gases that are above atmospheric pressure. It is therefore felt opportune to address this issue and supplement the literature with a study fully devoted to the implications of temperature on the macroscopic hydrodynamic transport properties of trickle beds. As the hydrodynamic parameters are incumbent upon the prevailing flow regime, it is worthwhile to identify the trickle to pulsing flow transition boundary for elevated temperature. Also the hydrodynamic

parameters such as pulse velocity, two-phase pressure drop, liquid holdup and axial dispersion coefficient, which are informative of the degree of liquid backmixing, are also reported for elevated temperature.

## 1.2 Experimental Setup and Procedure

Experiments were carried out in a stainless steel reactor able to withstand temperatures up to 100°C and pressures up to 5 MPa. Hydrodynamic measurements concerned flow regime changeover from trickle to pulse flow, pulse velocity, two-phase pressure drop, liquid holdup and liquid axial dispersion coefficient. A systematic study was devoted to study the effect of temperature for Newtonian and non-Newtonian liquids between 25°C and 75°C and up to a pressure of 0.7 MPa. The main elements of the experimental setup are schematically represented in Fig. 1-1. The reactor (I.D.= 4.8 cm) was packed with 3 mm glass beads to complete a total bed height of 107 cm with an overall porosity 39%. The resulting column-to-particle diameter ratio of 16 was not very far from the criterion $D_c/d_p$>20 recommended for avoiding wall flow maldistribution (Al-Dahhan et al., 1997). Though this ratio was not sufficiently high to completely get rid of such undesirable phenomena, an assessment of the quality of data and the marginal extent of wall flow distribution will be revealed post facto from the matching quality with some literature models and correlations. The packing was maintained by means of a rigid stainless steel screen placed at the column bottom, and had a mesh openness large enough to prevent artifactual bed flooding but narrow enough to impede particles crossings. In all the experiments, air was the process gas, whereas water or aqueous 0.25%w/w carboxymethylcellulose (CMC) solution were the process liquids. The CMC solution, prepared by dissolving powdered CMC in water at ambient temperature, exhibited an inelastic pseudoplastic rheological behavior which was well represented by means of a simple power-law Ostwald-DeWaele model. The consistency index, k, and the power-law index, n, were fitted for each process temperature after measuring the solution shear stress-shear rate responses on an ARES (Advanced Rheometric Expansion System) rheometer in the 0-1000 $s^{-1}$ shear-rate ranges. The rheological parameters for each process temperature are summarized in Table 1-1.

**Table 1-1** Rheological properties of 0.25% CMC at elevated temperatures

| Temperature (ºC) | k (kg/m.s$^{2-n}$) | n | σ (kg/s$^2$) |
|---|---|---|---|
| 25 | 0.072 | 0.666 | 0.056 |
| 50 | 0.041 | 0.707 | 0.054 |
| 75 | 0.033 | 0.659 | 0.051 |

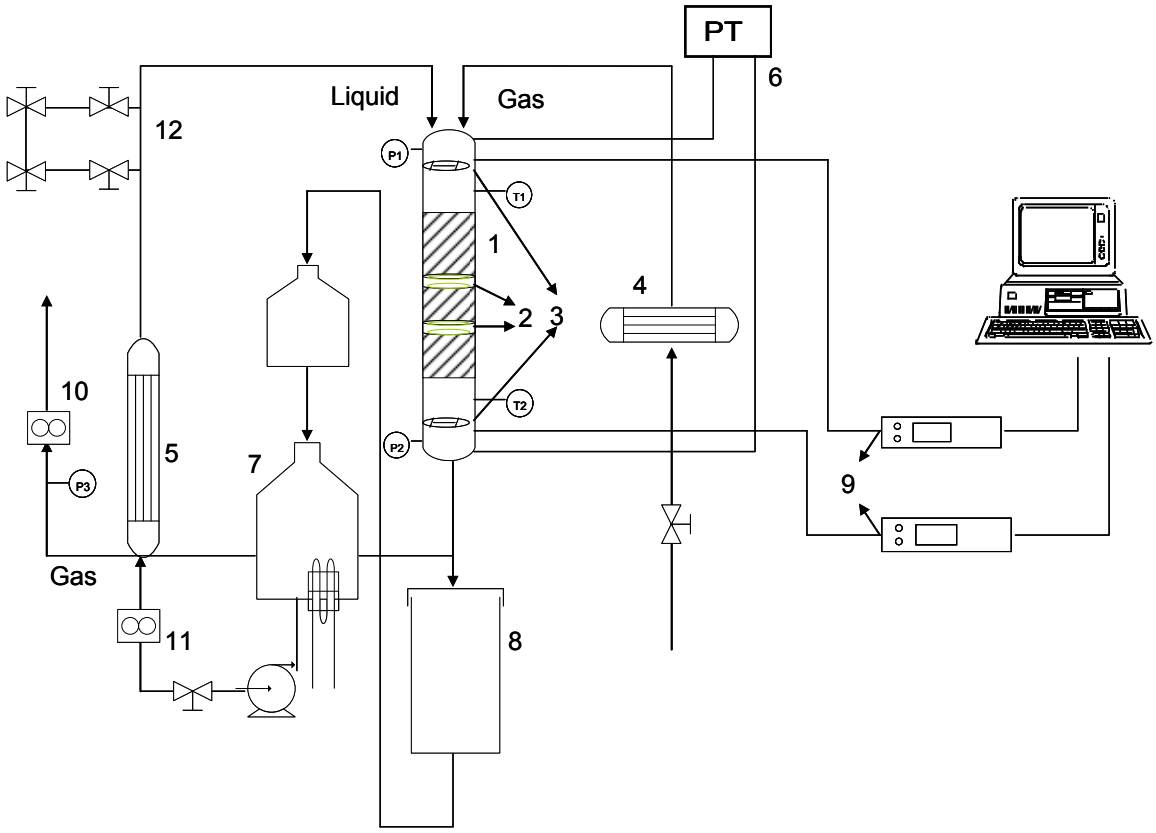


**Figure 1-1** Experimental setup: (1) packed bed, (2) conductance probes, (3) conductimetric sensors, (4) preheater for the gas phase, (5) preheater for the liquid phase, (6) pressure transducer, (7) reservoir, (8) gas-liquid separator, (9) lock-in amplifiers, (10) gas flowmeter, (11) liquid flowmeter, (12) tracer injection loop

After the liquid was heated in the reservoir (up to max. 60ºC), it was pumped by means of a rotary valve pump (Procon model 1309XH) through a liquid preheater via calibrated flowmeters then to the reactor. The gas was fed from a compressed air supply able to deliver a maximum pressure of 0.7 MPa. It passed through a gas preheater before encountering the liquid on the reactor top to be both fed cocurrently downwards through it. Once leaving the reactor, the outgoing stream was intercepted in a gas-liquid separator. The gas was then expanded and its flow rate measured through calibrated flowmeters before being vented to the atmosphere. The liquid was circulated in a closed loop from the reservoir. Before starting the experiments the reactor was operated till the desired operating temperature was reached. Prior to performing any experiment, the reactor was preventively operated in the pulsing flow regime for 1 hour to achieve perfect bed prewetting.

In order to measure the pulse properties, an electrical conductance technique was implemented using recommendations and design details provided by Tsochatzidis and Karabelas (1995) and Boelhouwer et al. (2002). Two conductance probes were mounted in the middle of the reactor, a distance of 0.225 m apart from each another. Each probe consisted of two ring electrodes 0.001 m in thickness and 0.03 m separation distance between the two electrodes (Fig. 1-2). Each probe was connected to a lock-in amplifier to acquire the output signal. After amplification, the signals were transmitted to a computer by means of a data acquisition system.

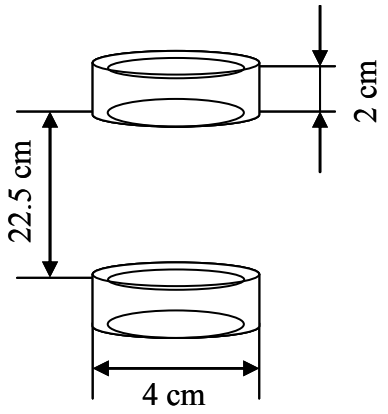


**Figure 1-2** Ring electrical conductivity probes for measuring pulse velocity

Identification of flow regime transition was carried out using a moment method (Rode, 1992). The coefficient of variation T was calculated from the 2nd-order central moment (variance) and the 1st-order moment (arithmetic average) of the probability density function of the fluctuating signals. The coefficient of variation simply compares the amplitude of the fluctuations with respect to the average signal value (Eqs. 1.1, 1.2):

$$\bar{x}^n = \int_{-\infty}^{\infty} \left(X - \overline{X}\right)^n p(X) dX \tag{1.1}$$

$$T = \frac{\sqrt{\bar{x}^2}}{\overline{X}} \tag{1.2}$$

in which $\overline{X}$ is the mean value, and $\bar{x}^2$ is the variance of the conductivity signal. Fig. 1-3 shows an example of location of the coefficient of variation $T$ corresponding to the occurrence of trickle-to-pulse flow regime transition as a function of superficial liquid flow velocity for a constant superficial gas velocity. The maximum in the curve at ($u_L$, $T$) = (0.01 m/s, 0.13) corresponds to the change of flow regime whereof the critical values for superficial liquid and gas velocities can be picked up. The instability of the transitional flow occurs due to low frequency pulsations leading to higher coefficient of variation values whereof a maximum emerges on the curve.

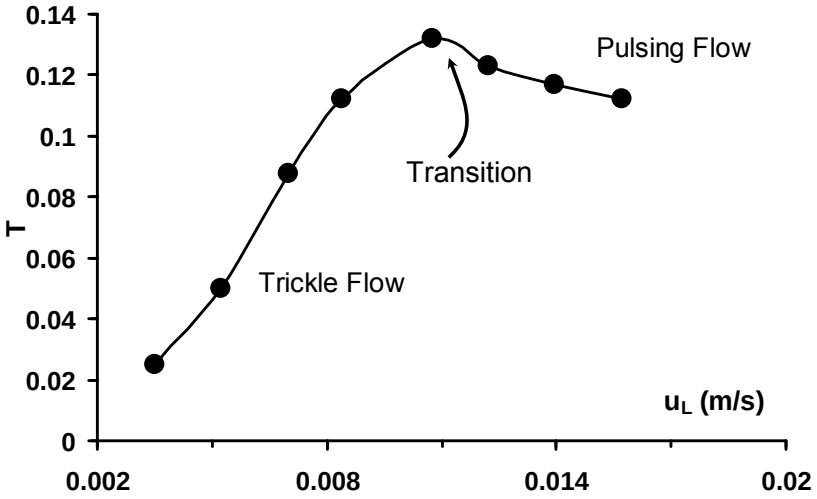


**Figure 1-3** Schematic illustration of the coefficient of variation $T$ as a function of $u_L$, $T_r$ = 50ºC, $P_r$ = 0.7 MPa, $u_G$ = 0.2088 m/s. Vertex corresponds to transition between trickle flow and pulse flow regimes

For the determination of the pulse velocity, the distance between the two ring probes was divided by the time delay of maximum cross-correlation between signals. The cross-correlation function peaks at a time delay equal to the time required for the pulses to travel between probes 1 and 2. An example for pulse time-of-flight determination from the cross-correlation of the fluctuating conductivity signals is shown in Figs. 1-4a, b for a sampling frequency of 50 Hz and a deduced time-of-flight of 2 s.

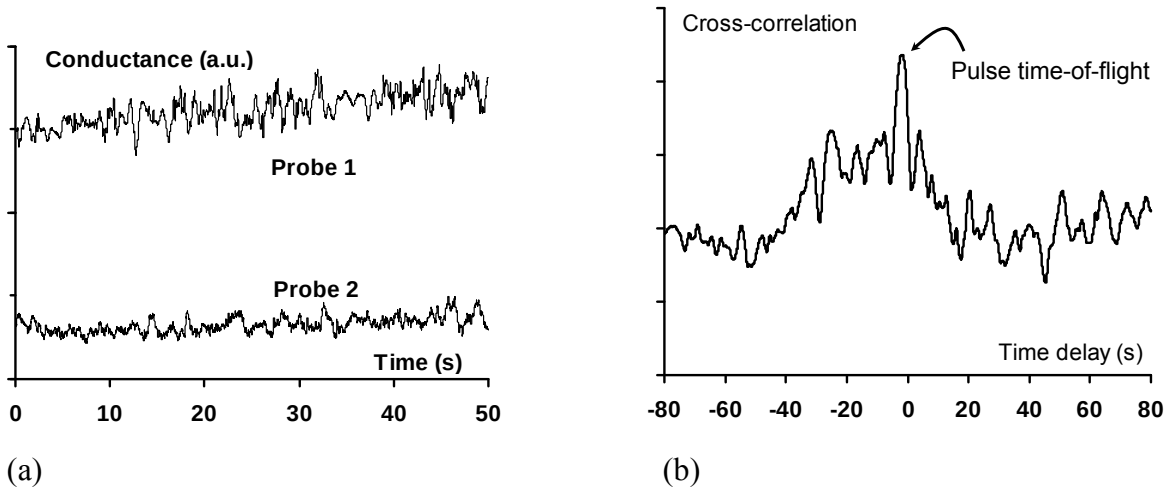


**Figure 1-4** An example for the electrical conductance recordings in pulse flow regime (a) and the corresponding cross-correlation function (b), $T_r$ = 50ºC, $P_r$ = 0.7 MPa, $u_G$ = 0.0522 m/s, $u_L$ = 0.00698 m/s. Arrow indicates time-of-flight of pulse from probe 1 to probe 2

The two-phase pressure drop was measured with a differential pressure transducer (Endress+Hauser Model PMD 235) connected to the packed bed top and bottom sections.

For liquid holdup measurements, the Aris's double-detection tracer response method was implemented. Appropriateness of this technique for elevated pressure trickle-bed reactors due to its capability of being performed without interrupting the flow was already proven by previous investigators (Al-Dahhan and Highfill, 1999). Two electric conductivity probes - one at the top and another at the bottom of the column - were used. The output signals from the probes were received by a conductivity controller (Omega model CDCN-91) and transmitted to a computer by a data acquisition system. Each conductivity probe consisted of three series of three stainless steel wires of which each series is connected by a transverse stainless steel wire. Each probe was separated by a Teflon lining from the (stainless steel) column wall to confine the electrical field only to within the region of influence of the probes (Fig. 1-5).

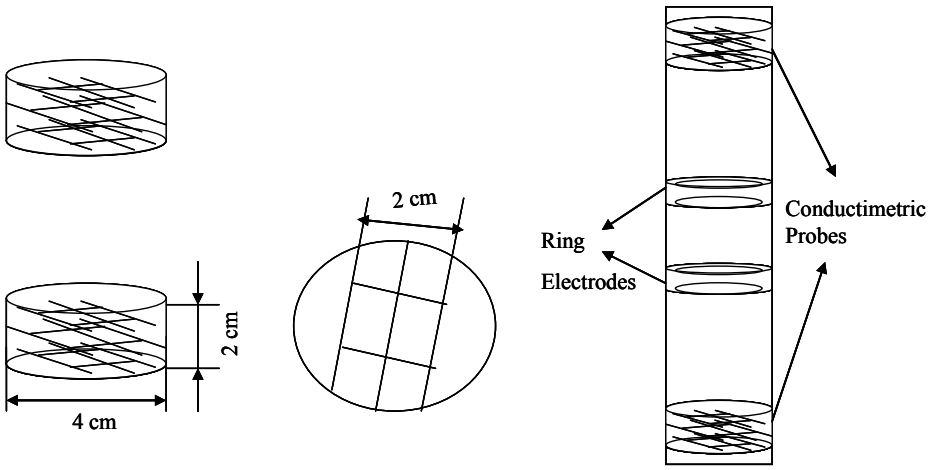


**Figure 1-5** Schematic illustration of the electrical conductivity probes for RTD measurements and probes position in reactor

An aqueous sodium chloride solution was used as a tracer and injected upstream of the column by means of a specially designed injection loop similar to that proposed by Larachi et al. (1991). This system consists of four three-way pneumatic valves: two of them being used for injecting the tracer while the other two valves being used for feeding the injection line from a tracer reservoir by means of a peristaltic pump (Omega model FPU112). Liquid residence time distribution (RTD) curves were calculated using the imperfect pulse Aris method in which the inlet and outlet tracer response conductivity signals are used to fit the two-parameter impulse response RTD model. The plug flow with axial dispersion (PD) model was used to describe the liquid backmixing state. The space time ($\tau$) and the axial dispersion Péclet number (*Pe*) were determined using a non-linear least-squares fitting where the convolution method was used for a time-domain analysis of the non-ideal pulse tracer response data. (Wakao and Kaguei, 1982). Fig. 1-6 gives an example of match between measured and PD-model predicted outlet curves for a run at 75ºC.

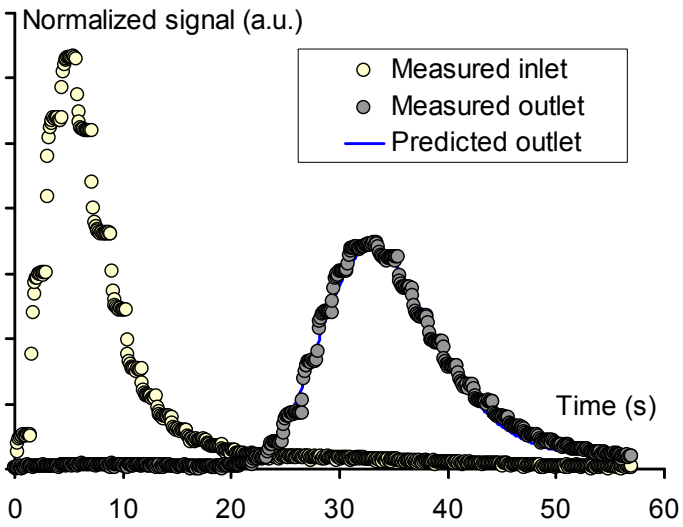


**Figure 1-6** Example of experimental inlet and outlet conductance response curves along with the fit of the outlet response using a two-parameter PD RTD model, $T_r$ = 75ºC, $P_r$ = 0.7 MPa, $u_G$ = 0.1044 m/s, $u_L$ = 0.00349 m/s

## 1.3 Results and Discussion

### 1.3.1 Transition Boundary

The interaction between phases in a trickle bed causes different flow regimes which depend, among other things, on flow rate and physical properties of the fluids as well as particle size. In order to better understand the effect of operating conditions on the system's hydrodynamics, it is always useful to portray the type of flow regime prevailing inside the reactor. As the trickle flow and the pulse flow regimes are most commonly encountered in industrial applications, accurate fingerprinting of their demarcating line as a function of temperature is a key issue in this work. In Figs. 1-7 and 1-8, the transition boundary from trickle flow to pulse flow is plotted as a function of the superficial gas and liquid velocities, reactor pressure and temperature for the air-water and the air-0.25% CMC systems.

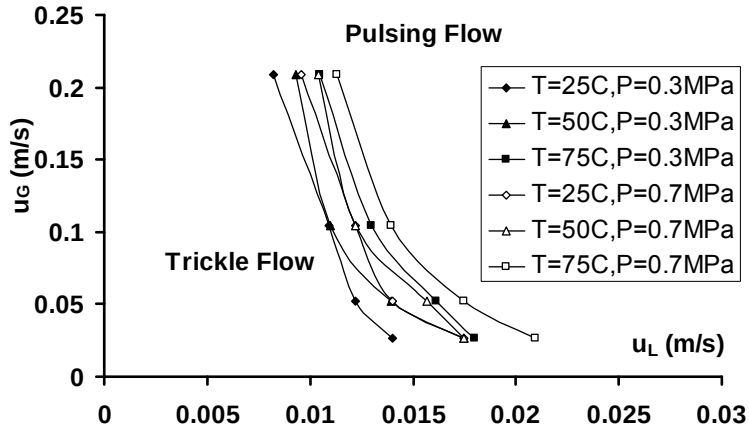


**Figure 1-7** Effect of pressure and temperature on the transition boundary between trickle and pulse flow regimes for the air-water system

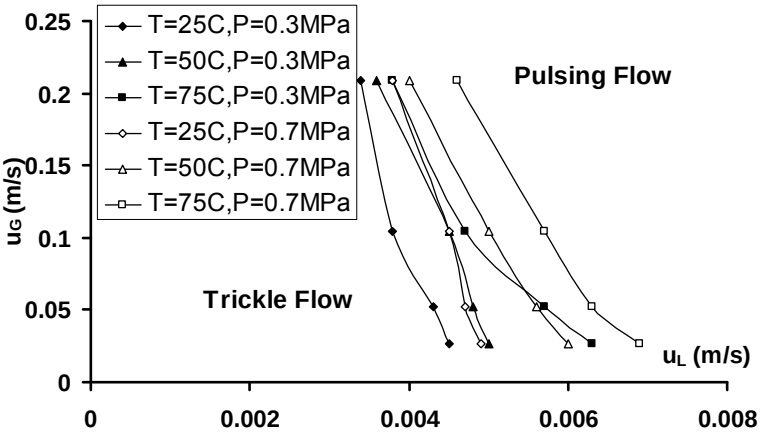


**Figure 1-8** Effect of pressure and temperature on the transition boundary between trickle and pulse flow regimes for the air-0.25% CMC system

Figs. 1-7 and 1-8 clearly show that the transition depends on both reactor pressure and temperature regardless whether the liquid is Newtonian or non-Newtonian power law fluid. At constant superficial gas velocity and ambient temperature, there is a shift towards higher liquid velocities with an increase in reactor pressure. This effect is coherent with literature observations (Wammes et al., 1990; Burghardt et al., 2002). The flow regimes encountered in the reactor are established as a result of a balance between the driving forces (inertia and gravity) and the shear-stress and surface tension resisting forces. It is well known from the literature (and also confirmed in this study, see later) that increasingly gas densities (via

increased reactor pressures) lead to increased pressure drops, everything else being kept constant. Besides gravity, the pressure drop driving force acts on the liquid phase causing its dynamic holdup to decrease. Likewise, the liquid films get thinner preventing pulse phenomena to be initiated in the bed. Pulse flow regime is characterized by alternate traveling pockets in the form of gas rich plugs and liquid rich slugs. Therefore, a higher liquid flow rate is required at elevated pressure to enhance the chances of pulse formation linked to increased liquid holdup. Similar to the effect of pressure, broadening of the trickle flow regime region in the $u_G$ versus $u_L$ diagram (Figs. 1-7, 1-8) was observed with an increase in reactor temperature at constant pressure. The effect of temperature on the transition boundary shift can be explained qualitatively using the same mechanism with regard to a decrease in liquid holdup with temperature as will be explained in detail in the following paragraph.

One of the resisting forces acting on the liquid phase is the shear stress. As temperature increases, the liquid dynamic viscosity decreases whereas gas dynamic viscosity slightly increases. The liquid-side shear stress at the gas-liquid and liquid-solid interfaces weakens, accordingly, with temperature. This causes a decrease in the amount of liquid held within the bed. Therefore, a higher liquid flow rate is required to give a chance to the liquid films to collapse for the emergence of pulses. The decrease of liquid surface tension with increased temperature, albeit less dramatic than for the dynamic liquid viscosity, facilitates gas penetrability in the liquid films causing unlikelihood of liquid films to collapse on the solid surface, in addition to the aggravated liquid film thinning brought about by decreasing viscosities with elevated temperatures. Both reductions in liquid viscosity and surface tension with temperature lead to decreasing liquid holdups. This effect may also be given an explanation for the necessity of higher liquid throughput to achieve sufficient liquid holdup for pulse formation to occur at increasingly temperatures. As can be seen from Fig. 1.7, the transition boundary for 25ºC at 0.7MPa nearly collides with that of 50ºC and 0.3MPa. This may be ascribed to the conflicting effects of pressure and temperature on gas phase density. For the air-0.25%CMC system the same effect of temperature and pressure was observed. The consistency index decrease with temperature leads the liquid-side shear stress to decrease at the gas-liquid and liquid-solid interfaces. Note that the shift in the transition boundary is more distinctive here than that for the air-water system.

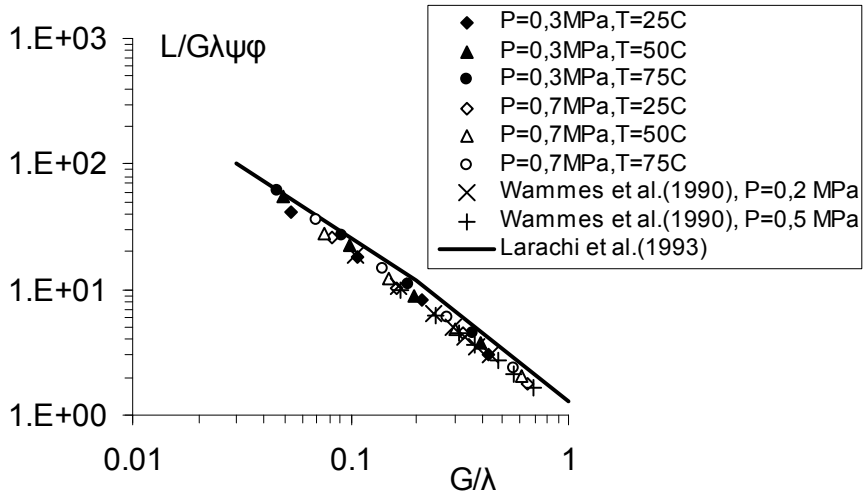


**Figure 1-9** Comparison between the measured transitions, experimental data of Wammes et al. (1990) and the predictions by the Larachi et al. (1993) trickle-to-pulse flow regime transition correlation at elevated pressure and temperature for the air-water system

The experimental data obtained in this study for the air-water system is plotted in Fig. 1-9 along with that of Wammes et al. (1990) for ambient temperature conditions and moderate pressure levels. With a pressure increase, the shift from trickle to pulse flow regime transition to higher flow rates of the phases is in congruity. However, in our experiments the transition boundary is observed at slightly lower liquid and gas velocities. A comparison of the experimentally obtained data for the transition line of the air-water system for all the temperature and pressure levels explored in this study indicates a good agreement with the correlation of Larachi et al. (1993) (Fig. 1.9). Recall that this correlation is an extension of Charpentier and Favier diagram for the trickle-pulse flow regime portion to the high pressure conditions via inclusion of the function $\Phi$. The fact that no additional fitting was required indicates that the natural Baker coordinates $\lambda$ and $\psi$ as well as the gas density correction function $\Phi$ are sufficient to handle the temperature dependence of the gas and liquid physical properties intervening in these property functions. However, no attempt was directed at rationalizing the transition data for the power-law non-Newtonian fluids at elevated temperatures and moderate pressures as these systems require special treatment (see Table 1-2).

**Table 1-2** Properties of water and air at elevated temperatures

| Temperature (ºC) | $\rho_{water}$ ($kg/m^3$) | $\mu_{water}$ x $10^4$ (kg/m.s) | $\sigma_{water}$ ($kg/s^2$) | $\rho_{air}$ ($kg/m^3$) | $\mu_{air}$ x $10^5$ (kg/m.s) |
|---|---|---|---|---|---|
| 25 | 997.1 | 8.86 | 0.0720 | 1.184 | 1.84 |
| 50 | 988.2 | 5.36 | 0.0679 | 1.092 | 1.96 |
| 75 | 974.9 | 3.77 | 0.0635 | 1.012 | 2.07 |

### 1.3.2 Pulse Velocity

One of the important basic characteristics of pulsing flow is the pulse velocity which was determined at elevated pressure and temperature. The pulse velocity decreases with increasing pressures thereby confirming Burghardt et al. (2002) experimental findings (Figs. 1-10 and 1-11). The effect of pressure was more pronounced at higher superficial gas velocities. For the air-0.25%CMC system at a given superficial gas velocity, the augmentation of pulse velocity as a function of superficial liquid velocity was less spectacular comparatively with that for the air-water system. Also for the air-water system, larger values of pulse velocities were reached.

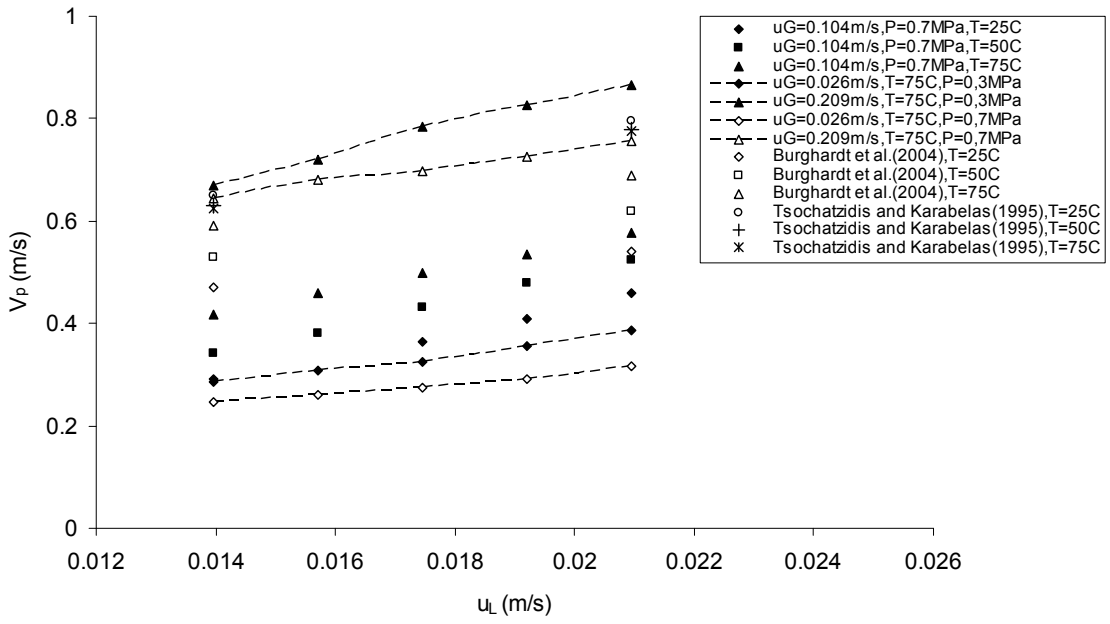


**Figure 1-10** Influence of temperature, pressure, gas and liquid superficial velocities on pulse velocity. Comparison with some literature pulse velocity correlations

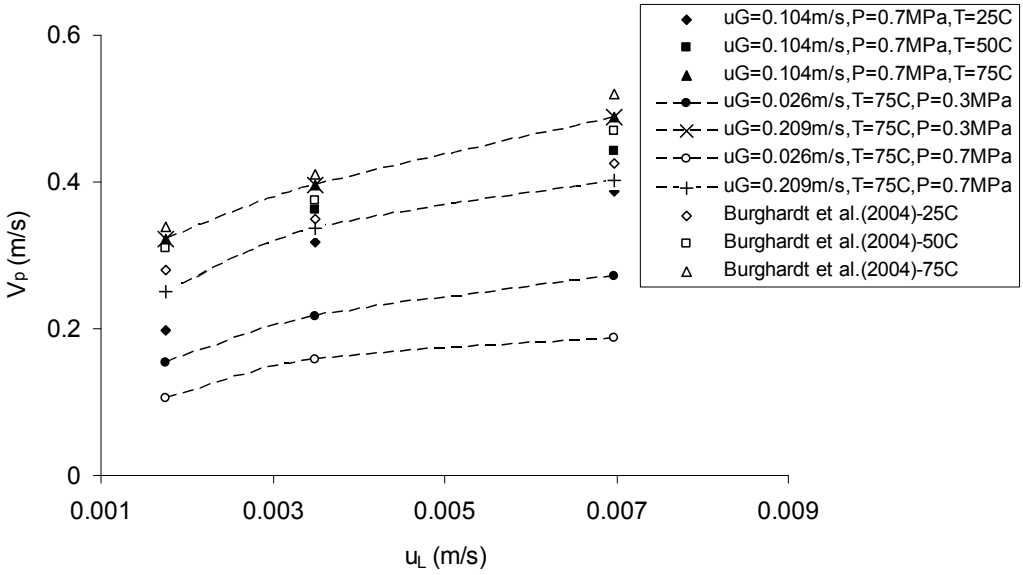


**Figure 1-11** Effect of temperature, pressure, gas and liquid superficial velocities on pulse velocity, experimental and calculated values for air-0.25% CMC system

However, pulse velocities increased with increasingly temperatures. This increase can be rationalized, as will be discussed later, in terms of decreasing liquid holdups when temperature is increased. It is very plausible to anticipate a profound effect of liquid holdup

on the control of pulse propagation velocity. Said otherwise, the pulse velocity increase with increasingly temperatures (Figs. 1-10 and 1-11) is a consequence of a decrease in dynamic liquid viscosity and an increase in interstitial liquid velocity. The monotonic increase of pulse velocity with temperature was qualitatively similar regardless whether Newtonian or non-Newtonian liquids were tested.

The pulse velocity correlations of Tsochatzidis and Karabelas (1995) and Burghardt et al. (2004) were chosen for performing comparisons with our measured pulse velocities for the air-water system (Fig. 1-10). The correlation of Burghardt et al. (2004) gave the same qualitative tendency as the experimental pulse velocity data regarding the effect of temperature. This was not the case for the Tsochatzidis and Karabelas (1995) correlation which exhibited poor temperature sensitivity. This mismatch could be a consequence of an insufficient correlating power of the chosen velocities since the interstitial gas velocity and the superficial liquid velocity intervened in their correlation. Whereas, the Burghardt et al. (2004) correlation involved both liquid and gas interstitial velocities via the corresponding Reynolds numbers. Temperature indeed had a remarkable effect on liquid holdup which was taken into account in the calculation of the Reynolds number and the corresponding interstitial liquid velocity. The Tsochatzidis and Karabelas (1995) correlation predictions were higher in comparison to those by Burghardt et al. (2004) correlation. This latter one provided, however, close estimations of the pulse velocity which can be recommended for approximate estimation of this parameter for aqueous systems at high temperature in addition to its capability to capture high pressure pulse velocity data. The Burghardt et al. (2004) correlation can also be recommended for the case of non-Newtonian liquids at elevated temperature as shown in the plot of Fig. 1-11 for the air-0.25%CMC system.

### 1.3.3 Two-Phase Pressure Drop

Two-phase pressure drop is one of the driving forces acting on the liquid phase which has an effect on energy dissipation in the packed-bed reactor. Pressure drop is a function of the fluids' physical properties as well as of the operating conditions, and bed and particle geometries. Thus, it is important to understand the effect of temperature on the pressure drop via the system characteristics.

Figs. 1-12 shows the effect of temperature on the two-phase pressure drop for different values of superficial liquid and gas velocities for Newtonian and non-Newtonian power law fluid. As expected, two-phase pressure drop increased with superficial liquid and gas velocities regardless of the temperature level and whether the liquid is Newtonian or not. As can be seen from the figures, two-phase pressure drop decreased with increased temperatures. In the present conditions, pressure drop mainly depends on viscosity, density and velocity of the fluids. As the liquid viscosity decreases though the gas viscosity follows an opposite trend with respect to temperature, the net effect of shear stress at the gas-liquid and liquid-solid interfaces is not obvious. Since the effect of temperature on gas viscosity is less pronounced in comparison to that on liquid viscosity, increased temperatures are likely to weaken the frictional forces at the gas-liquid and liquid-solid interfaces. The global outcome would be a reduction in two-phase pressure drop with increasing temperature. It can be seen that at high superficial gas and liquid velocities, the effect of temperature on pressure drop is more significant. Moreover, at constant pressure, both gas and liquid densities decrease as temperature increases resulting in a decrease in pressure drops. These results illustrate how pressure drop evolves as a function of shear stresses and inertial forces. For comparison with literature work carried out at ambient temperature in agreement with observations made by previous researchers (Larachi et al., 1991; Wild et al., 1991; Al-Dahhan and Dudukovic, 1994), the two-phase pressure drop also increases with both flow rates at higher temperature.

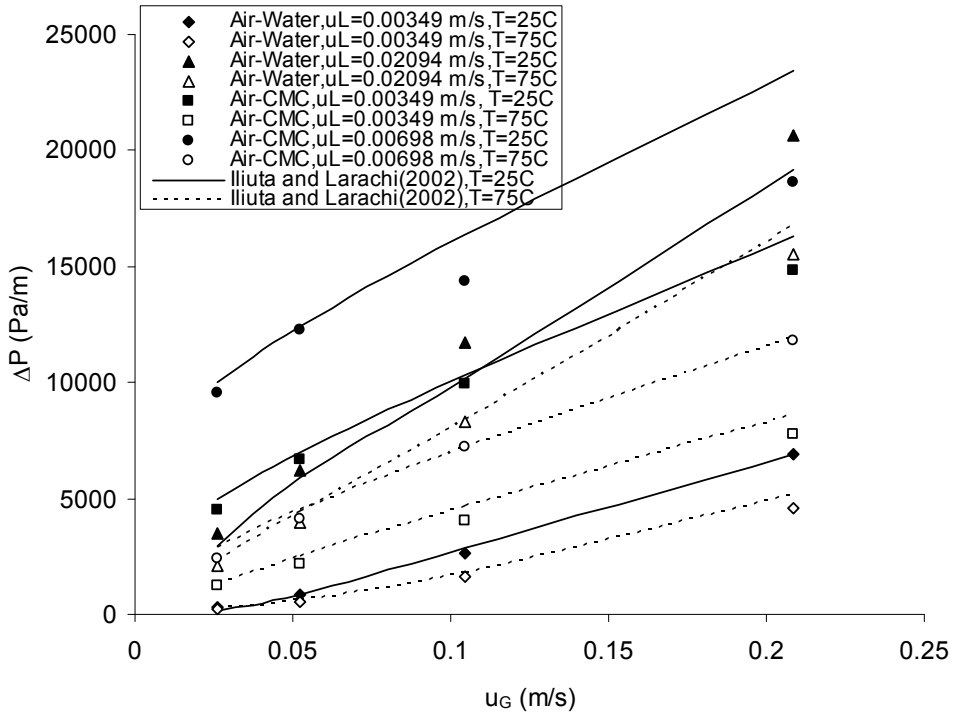


**Figure 1-12** Effect of temperature on two-phase pressure drop at various superficial gas and liquid velocities for air-water and air-0.25% CMC systems. $P_r$ = 0.7 MPa. Lines show predictions using the Iliuta and Larachi (2002) slit model for Newtonian and non-Newtonian fluids

For the air-0.25%CMC system, the two-phase pressure drop increases monotonically with the superficial gas and liquid velocities. The pressure drop values are obviously larger than those measured for the air-water system at the same fluid fluxes, pressure and temperature. This is easily understandable in light of the liquid-side shear stress at the gas-liquid and liquid-solid interfaces which are much larger in this case. In a similar manner than the air-water system, the two-phase pressure drop decreases as temperature is increased (Fig. 1-12) as a result of a decrease in apparent viscosity of the non-Newtonian CMC aqueous solutions. Due to the decrease in gas phase inertia with temperature (via gas density), the two-phase pressure drop decreases at a given particular pressure and fluid superficial velocities. The surface tension of CMC also decreases with temperature resulting in less gas resistance to push the liquid outwards from the reactor. This may also be advanced as an additional contributing factor in favor of an explanation for the pressure drop to decrease with elevated temperatures.

Iliuta and Larachi (2002) generalized the slit model of Holub et al. (1992) for the determination of pressure drop and liquid holdup for non-Newtonian power-law fluids. Their approach extended the double-slit representation (Iliuta et al., 2000) (dry slit + wet slit) of Newtonian fluids to the non-Newtonian case. The generalized bed-scale two-fluid model for pressure drop and liquid holdup was obtained by mapping from slits- to bed-scale the momentum balance equations for the gas phase in the dry and wet slits, and the liquid phase in the wet slit. This model can be further reduced assuming first that non-Newtonian viscous liquids behave similarly to Newtonian viscous liquids so that full bed wetting is virtually achieved at the typical gas and liquid superficial velocities encountered in this work as a result of larger liquid holdups. In addition, for moderate pressures and low to high superficial gas velocities corresponding to cases 2 and 3 according to Al-Dahhan and Dudukovic interaction classification (1994), the correction required for enhanced gas-liquid interactions is not required. Under those circumstances, the hydrodynamic model after dimensionless transformations becomes for power law fluids and spherical particles (refer to the nomenclature for the different variables):

Liquid phase pressure drop:

$$\Psi_\ell = -\frac{\Delta P}{\rho_\ell g H} + 1 = \frac{\varepsilon^3}{\varepsilon_\ell^3}\left[ E_1^{\frac{n+1}{2}} 2^{\frac{n-1}{2}} \frac{\mathrm{Re}_\ell}{\mathrm{Ga}_\ell} \mathrm{Fr}_\ell^{n-1} \frac{(1-\varepsilon)^{n-1}}{\varepsilon_\ell^{2n-2}} + E_2 \frac{\mathrm{Re}_\ell^2}{\mathrm{Ga}_\ell} \mathrm{Fr}_\ell^{n-1} \right] - \Psi_g \frac{\rho_g}{\rho_\ell} \frac{\varepsilon - \varepsilon_\ell}{\varepsilon_\ell} \tag{1.3}$$

Gas phase pressure drop:

$$\Psi_g = -\frac{\Delta P}{\rho_g g H} + 1 = \frac{\varepsilon^3}{(\varepsilon - \varepsilon_\ell)^3}\left\{ E_1 \frac{\mathrm{Re}_g - (\varepsilon - \varepsilon_\ell)\mathrm{Re}_i}{Ga_g} + E_2 \frac{\left[\mathrm{Re}_g - (\varepsilon - \varepsilon_\ell)\mathrm{Re}_i\right]^2}{Ga_g} \right\} \tag{1.4}$$

Interfacial gas and liquid velocity:

$$\mathrm{Re}_i = \frac{\rho_g d_p}{(1-\varepsilon)\mu_g}\left(\frac{72}{E_1}\right)^{\frac{n+1}{2n}} \frac{n}{n+1} \frac{k^{-\frac{1}{n}}}{\Psi_\ell \rho_\ell g} \times \left\{ \left[ \Psi_\ell \rho_\ell g \frac{\varepsilon_\ell}{a_s} + \Psi_g \rho_g g \frac{\varepsilon - \varepsilon_\ell}{a_s} \right]^{\frac{n+1}{n}} - \left[ \Psi_g \rho_g g \frac{\varepsilon - \varepsilon_\ell}{a_s} \right]^{\frac{n+1}{n}} \right\} \tag{1.5}$$

Note that this model is completely predictive provided the Ergun constants $E_1$ and $E_2$, the consistency index ($k$) and the power-law index ($n$) are known. The bed Ergun constants determined from the measured single-phase pressure drops for the 3 mm glass beads bed were, respectively, 215 and 1.4. Putting n=1 in Eqs. 1-3 – 1-5 restores the model in its Newtonian version. Strictu sensu, the founding hypothesis of the slit model is the existence of a liquid film-like structure reminiscent of trickle flow regime necessary for the derivation of the drag forces resulting from the gas-liquid, gas-solid and liquid-solid interactions. Notwithstanding, in what follows no distinction will be made between the trickle flow and the pulse flow regime hydrodynamic data during model confrontation. As shown in Fig. 1-12, the lines represent the slit model predictions by Eqs. 1-3 – 1-5 for the air-water and the air-0.25%CMC systems for the trickle flow and pulse flow pressure drops alike. The effect of temperature was well captured by the model, although at the highest liquid superficial velocities, the predictions tended to be underestimated for the air-water system and over-estimated for the air-0.25%CMC system at the lowest temperature. These discrepancies could likely be ascribed to the choice of negligible gas-liquid interaction function and full wetting hypothesized in the simplified slit model. Nonetheless, the mean relative error was equal to 15% for the air-water system and 9% for the air-0.25%CMC system for all the investigated temperature and pressure values, and flow regimes. These levels of errors remained compatible with the order of magnitude of experimental errors. Note also, that extension of the slit-based drag force closures inherent to trickle flow hypothesis towards the pulse flow regime did not degrade dramatically the model predictions. Therefore, although this choice is open to criticism from a physical standpoint, it does provide good engineering estimates of the pressure drops in the pulse flow regime.

### 1.3.4 Liquid Holdup

Knowledge of the liquid holdup is a key in reactor design model calculations of reaction performances. For exothermic reactions, higher liquid holdup enables better pellet-scale temperature and wetting efficiency control thus contributing to the prevention of hot spots formation. From this point of view, investigation of the liquid holdup at elevated temperature in trickle beds arises as a natural justification.

The effect of temperature, superficial gas and liquid velocities and reactor pressure on the liquid holdup for the two gas–liquid systems is illustrated in Figs. 1-13 and 1-14. At the highest temperature, the liquid holdup increases with superficial liquid velocity for the air–water system. As discussed above, the trickle-to-pulse flow regime transition is repelled towards larger superficial liquid velocities at a given superficial gas velocity. Thus, the increase in holdup with liquid throughput is first through film thickening in trickle flow followed by more frequent liquid-rich slug events in the pulse flow regime. The decrease of liquid holdup with increasingly superficial gas velocities and/or with reactor pressure was also persistent for the elevated temperatures confirming maintenance of this behavior as in the previous literature works regarding ambient temperature and elevated pressure conditions. The drag force at the gas–liquid interface, which is a driving force for the liquid flow, depends on gas velocity and density. Hence since the drag force increases with gas velocity and density, shorter liquid mean residence time arise occasioning a reduction in liquid holdup.

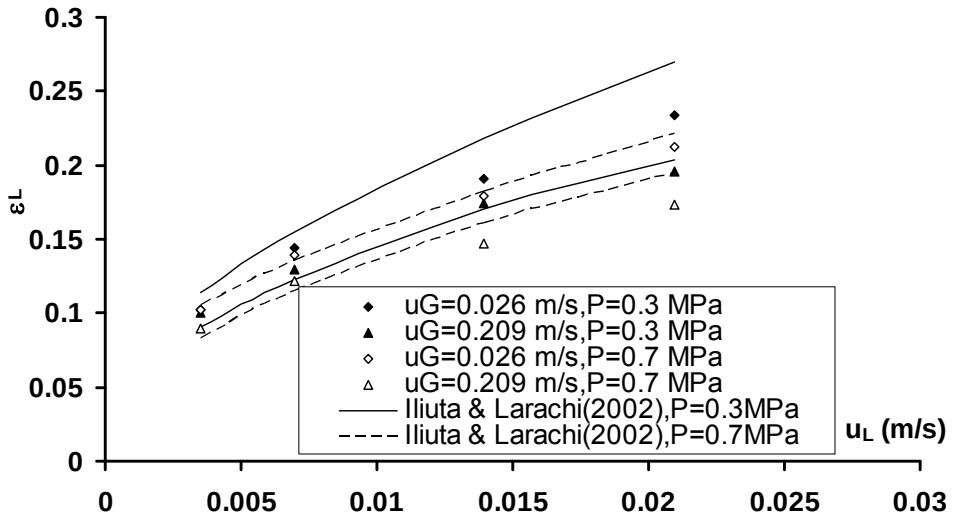


**Figure 1-13** Effect of pressure, gas and liquid velocities on liquid holdup for air-water system. Lines show prediction using the Iliuta and Larachi (2002) slit model for Newtonian and non-Newtonian fluids

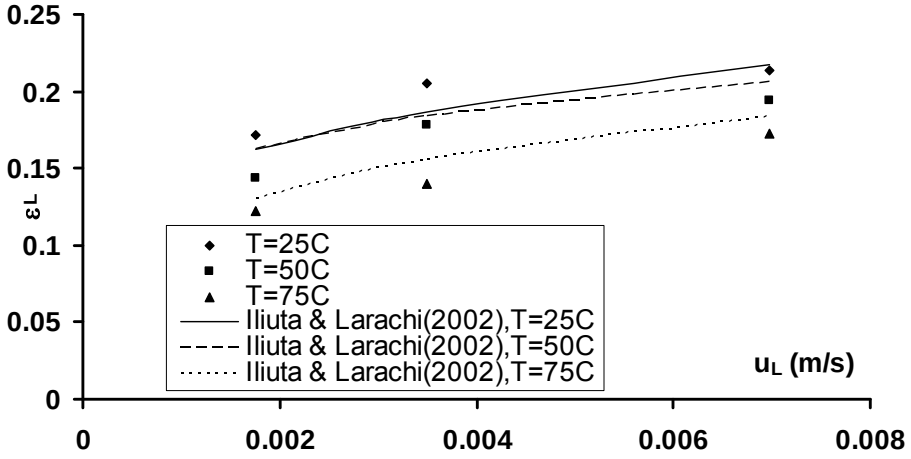


**Figure 1-14** Effect of temperature and liquid velocities on liquid holdup for air-0.25% CMC system. Lines show prediction using the Iliuta and Larachi (2002) slit model for Newtonian and non-Newtonian fluids

The air-0.25%CMC system, at constant gas and liquid superficial velocities and the highest temperature, exhibits liquid holdups decreasing with increasingly pressure similarly to the air-water system. However, the effect of pressure for this system is more visible at high superficial gas velocity. As expected, the liquid holdup values are larger than those for the air-water system due to higher viscosity.

For air–water system, the liquid holdup decreases with increasing temperature at constant superficial liquid and gas velocities. This can be explained by a decrease in liquid viscosity as temperature is increased (Table 1-2). The shear stress at the gas–liquid and liquid–solid interfaces decreases resulting in lower liquid holdup. One of the resisting factors to gas flow, i.e., surface tension, decreases with temperature thereby reducing the number of events corresponding to film collapse around and between particles. The effect of temperature on liquid holdup is more remarkable at high liquid throughputs. Thus, gas-side and liquid-side shear stresses play an important role on the liquid holdup in the high interaction regime.

For the air-0.25%CMC system, the liquid holdup decreases also with temperature as the flow consistency index decreases with temperature (Table 1-1). The increase of liquid holdup with superficial liquid velocity is however less substantial in comparison with the

air-water system due to the propensity of the bed to operate at already large holdup values for viscous liquids.

In a similar manner to pressure drops, the liquid holdup values for both systems were analyzed in the light of the Iliuta and Larachi (2002) slit model described in the previous section. As shown in Figs. 1-13 and 1-14 the lines represent the slit model predictions using Eqs. 1-3 – 1-5 for the air-water and the air-0.25%CMC systems for the trickle flow and pulse flow liquid holdups alike. The model captures properly the temperature and pressure dependencies observed experimentally. Quantitatively, the model is in good agreement with experimental data with a mean relative error of 9.6% and 9.5% for the air-water and the air-0.25%CMC systems, respectively. Despite occasional overestimations especially at the highest temperatures (Figs. 1-13 and 1-14), these errors remained acceptable and compared pretty well with the level of experimental accuracy. Note that although the mechanistic role of surface tension can be understood as an impeding phenomenon against inception of pulse flow, and therefore as being a potential factor affecting liquid holdup, surface tension phenomena were not described in the simple Poiseuille flow type of flows based upon which the slit model was derived. Moreover, extension of the slit-based drag force closures inherent to trickle flow hypothesis towards the pulse flow regime did not appear to degrade dramatically the liquid holdup model predictions. For engineering accuracy computations therefore, the slit model can also be recommended for predictions of holdup even in the pulse flow regime.

### 1.3.5 Axial Dispersion

Besides liquid holdup, applying the PD model to our RTD experimental data enabled extraction of the liquid axial dispersion coefficients ($D_{ax}$) for various temperatures, pressures, and gas and liquid superficial velocities for the air-water and the air-0.25%CMC systems. At constant temperature, $D_{ax}$ was found to slightly decrease with reactor pressure for both systems though for the air-0.25%CMC system the effect of pressure was the most remarkable especially at the lowest superficial gas velocity (Figs. 1-15 and 1-16). For the air-water system, an abrupt increase of $D_{ax}$ was noticed for low superficial liquid flow velocities with a tendency of leveling off as liquid velocities get larger. Such an increase in

liquid backmixing is to be mirrored qualitatively with the trend exhibited by the liquid holdup versus liquid velocity plots. For the air-0.25%CMC system, the increase in $D_{ax}$ with liquid flow rate is less pronounced. This may be ascribed to the early emergence of trickle-to-pulse flow regime transition at lower superficial liquid velocities. Larger liquid throughputs yield larger $D_{ax}$ values due to increased backmixing. The effect of temperature on $D_{ax}$ values is also illustrated in Figs. 1-15 and 1-16, respectively, for the air-water and the air-0.25%CMC systems. The temperature effect was more noticeable for the air-0.25%CMC system. The decrease of $D_{ax}$ especially at 75ºC is the most significant. This may be explained by a lowering in backmixing due to a decrease in liquid holdup with temperature.

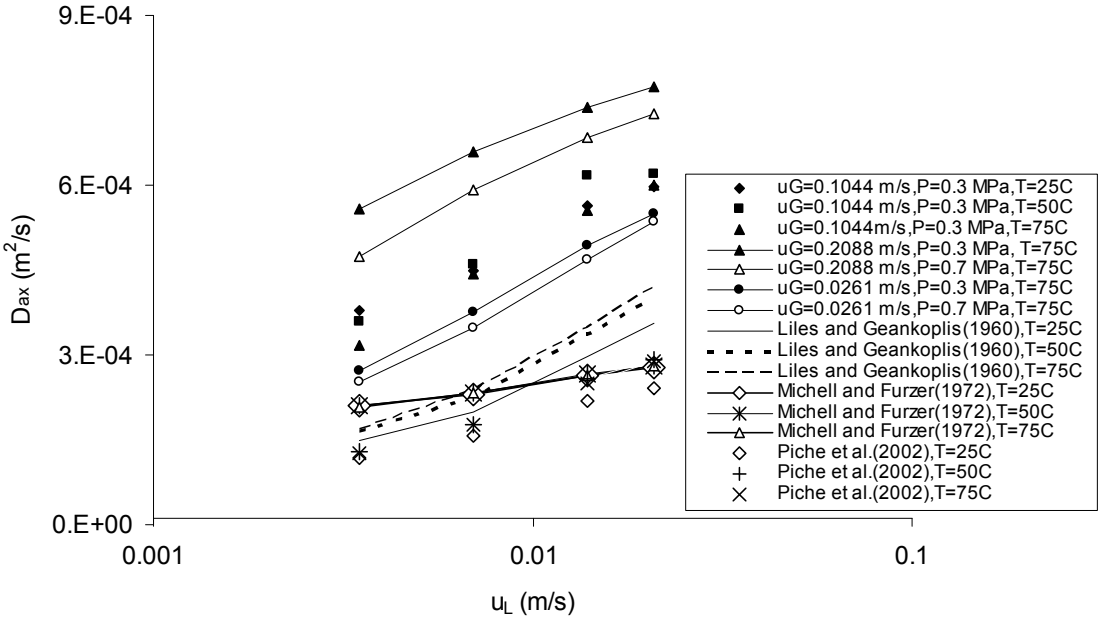


**Figure 1-15** Liquid axial dispersion coefficient as a function of superficial liquid velocity for various superficial gas velocities for air-water system. Effect of reactor temperature and pressure. Comparison with some literature liquid axial dispersion coefficient correlations

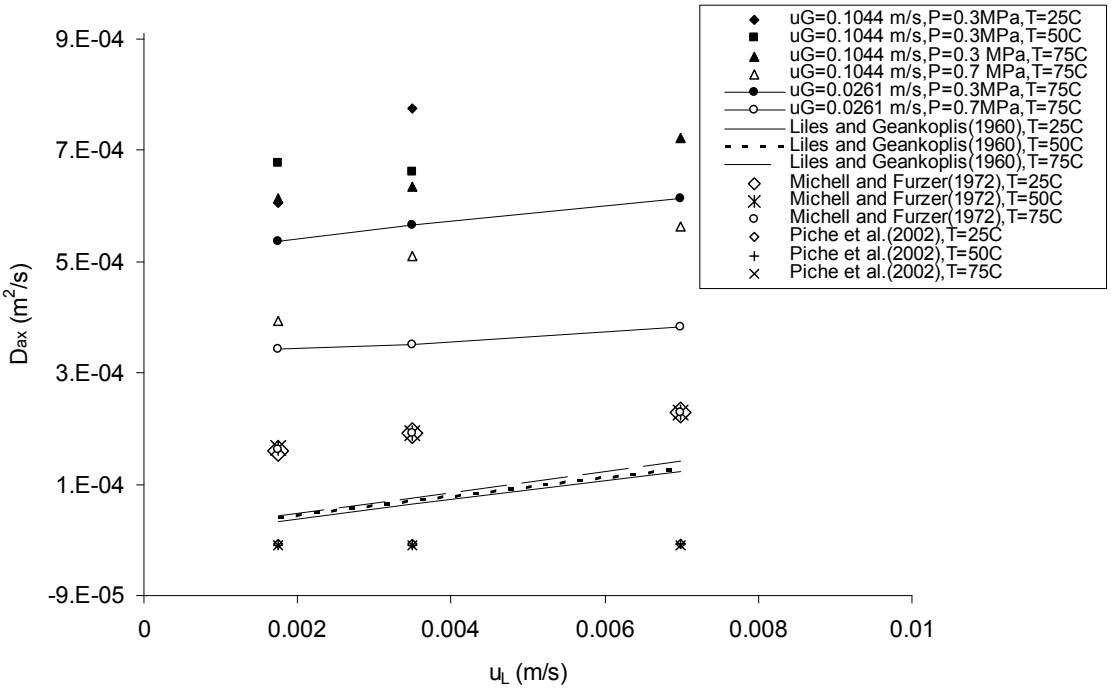


**Figure 1-16** Influence of operating temperature and pressure on liquid axial dispersion coefficient for air-0.25% CMC system, experimental and calculated values. Comparison with some literature liquid axial dispersion coefficient correlations

Experimental $D_{ax}$ data is plotted along with the values calculated from the correlation of Michell and Furzer (1972), Liles and Geankoplis (1960) and Piché et al. (2002) (Table 1-3). The correlation of Liles and Geankoplis (1960) shows that $D_{ax}$ increases with temperature for both systems. The correlation of Michell and Furzer (1972) shows no significant effect of temperature on $D_{ax}$. The correlation of Piché et al. (2002) shows also no systematic effect of temperature on $D_{ax}$, in agreement with experimental data. The values of $D_{ax}$ found with these correlations are systematically lower than our experimental data. Especially for the non-Newtonian liquid where the difference between experimental data and Piché et al. (2002) predictions was dramatically high pointing to a violation of the validity range of the correlation. It seems that even if this correlation has been developed using a broad $D_{ax}$ database, it will necessitate parameters recalibration for moderate-to-high pressures and non-ambient temperatures for Newtonian and non-Newtonian liquids. The average absolute mean errors for the air-water system were equal to 49%, 46% and 59%, respectively for the correlations of Michell and Furzer (1972), Liles and Geankoplis (1960) and Piché et al.

(2002). For the air-water system, the effect of superficial liquid velocity on the axial dispersion coefficient is more pronounced than for the air-0.25%CMC system. This is also in agreement with literature correlations. The effect of temperature on 0.25%CMC viscosity is relatively high. This considerable decrease in viscosity can be advanced as an explanation for the decrease of axial dispersion with temperature.

**Table 1-3** Correlations predicting the liquid axial dispersion coefficient in trickle beds

| Author | Correlation |
|---|---|
| Michell and Furzer (1972) | $\frac{u_L d_p}{\varepsilon_L D_{ax}} = \left(\frac{d_p \rho_L u_L}{\mu_L \varepsilon_L}\right)^{0.70} \left(\frac{d_p^3 g \rho_L^2}{\mu_L^2}\right)^{-0.32}$ (1.6) for $80 < \frac{d_p \rho_L u_L}{\mu_L \varepsilon_L} < 8000$ |
| Liles and Geankoplis (1960) | $D_{ax} = 0.261 d_p^{0.73} \left(\frac{u_L}{\varepsilon_L}\right)^{0.93}$ (1.7) for $2 < \frac{d_p \rho_L u_L}{\mu_L \varepsilon_L} < 500$ |
| Piché et al. (2002)[a] | $S = \frac{\log\left(\frac{Bo_L}{5.91\times10^{-4}}\right)}{2.495}, Bo_L = \frac{u_L}{a_P D_{ax}}, S = \frac{1}{1+\exp\left(-\sum_{j=1}^{10}\omega_j H_j\right)}$ $H_j = \frac{1}{1+\exp\left(-\sum_{i=1}^{8}\omega_{ij} U_i\right)}, U_1 = \frac{\log\left(\frac{\mathrm{Re}_L}{2.17\times10^{-4}}\right)}{6.025}, U_2 = \frac{\log\left(\frac{Eo_L}{9.71\times10^{-6}}\right)}{4.799}$ $U_3 = \frac{\log\left(\frac{Ga_L}{6.02\times10^{-3}}\right)}{7.199}, U_4 = \frac{\log\left(\frac{Ga_G}{2.65\times10^{-5}}\right)}{7.272}, U_5 = \frac{\log\left(\frac{Sa}{1.44\times10^{-5}}\right)}{7.320}$ $U_6 = \frac{K-0.823}{0.173}, U_7 = \frac{RTD-1}{2}$ (1.8) |

[a]See reference for meaning of the different symbols and variables

## 1.4 Conclusion

In this study, the effects of temperature and moderate pressure on the hydrodynamics of trickle-bed reactors were discussed for Newtonian and non-Newtonian liquids. Previous works on trickle bed hydrodynamics dealt mainly with the effects of elevated pressures. This work attempted to fill the gap by adjoining new data on the temperature effect on flow regime transition, pulse velocity, two-phase pressure drop, liquid holdup and liquid axial dispersion coefficient. The following conclusions can be drawn:

- The trickle-to-pulse flow regime transition boundary shifts to higher fluid velocities with increasingly temperatures;

- Pulse velocity was an increasing function of temperature;

- A decline of two-phase pressure drop was observed with climbing temperatures;

- So did the liquid holdup regarding its response with respect to temperature due likely to a decrease in liquid viscosity and gas density.

## 1.5 Nomenclature

$a_s$ bed-specific surface area, $m^2/m^3$

$d_p$ particle diameter, m

$D_{ax}$ axial dispersion coefficient, $m^2/s$

$E_1$, $E_2$ Ergun constants

$Fr_l$ liquid phase Froude number $\left(\frac{u_L^2}{gd_p}\right)$

g gravitational acceleration, $m/s^2$

$Ga_g$ gas phase Galileo number $\left(\frac{d_p^3 g\rho_G^2\varepsilon^3}{(1-\varepsilon)^3\mu_G^2}\right)$

$Ga_l$ liquid phase Galileo number $\left(\frac{d_p^{2+n} g^{2-n} \rho_L^2 \varepsilon^3}{(1-\varepsilon)^3 k^2}\right)$

k flow consistency index, $kg/m.s^{2-n}$

n flow behavior index

P pressure, MPa

ΔP/H two-phase pressure drop, Pa/m

Pe Péclet number $\left(\frac{u_L d_p}{\varepsilon_L D_{ax}}\right)$

$Re_g$ gas phase Reynolds number $\left(\frac{u_G d_p \rho_G}{(1-\varepsilon)\mu_G}\right)$

$Re_l$ liquid phase Reynolds number $\left(\frac{u_L^{2-n} d_p^n \rho_L}{(1-\varepsilon)k}\right)$

$Re_{\alpha,r}$ Reynolds number based on the real velocity of the α phase $\left(\frac{v_r \rho_\alpha d_p}{\mu_\alpha}\right)$

T temperature, ºC

u superficial velocity, m/s

v real velocity, m/s

Vp pulse velocity, m/s

**Greek letters**

ε bed void fraction

$\varepsilon_L$ liquid holdup

| | |
|---|---|
| $\rho$ | density, ($kg/m^3$) |
| $\mu$ | viscosity, (kg/m.s) |
| $\sigma$ | surface tension, ($kg/s^2$) |
| $\psi_\alpha$ | dimensionless body force of the α phase |

**Subscripts**

| | |
|---|---|
| a | air |
| G | gas |
| i | gas-liquid interface |
| L | liquid |
| N | normal conditions |
| r | reactor |

## 1.6 References

Al-Dahhan, M.H.; Dudukovic, M.P., 1994. Pressure Drop and Liquid Holdup in High Pressure Trickle Bed Reactors. Chemical Engineering Science 49, 5681-5698.

Al-Dahhan, M.H.; Larachi, F.; Dudukovic, M.P.; Laurent, A., 1997. High-Pressure Trickle-Bed Reactors: A Review. Industrial and Engineering Chemistry Research 36, 3292-3314.

Al-Dahhan, M.H.; Highfill, W., 1999. Liquid Holdup Measurement Techniques in Laboratory High-Pressure Trickle Bed Reactors. The Canadian Journal of Chemical Engineering 77, 759-765.

Bartelmus, G.; Gancarczyk, A.; Stasiak, M., 1998. Hydrodynamics of Cocurrent Fixed-Bed Three-Phase Reactors. Part I. The Effect of Physicochemical Properties of the Liquid on Pulse Velocity. Chemical Engineering and Processing 37, 331-341.

Blok, J.R.; Drinkenburg, A.A.H., 1982. Hydrodynamic Properties of Pulses in Two-Phase Downflow Operated Packed Columns. The Chemical Engineering Journal 25, 89-99.

Boelhouwer, J.G.; Piepers, H.W.; Drinkenburg, A.A.H., 2002. Nature and Characteristics of Pulsing Flow in Trickle Bed Reactors. Chemical Engineering Science 57, 4865-4876.

Burghardt, A.; Bartelmus, G.; Janecki, D.; Szlemp, A., 2002. Hydrodynamics of a Three-Phase Fixed-Bed Reactor Operating in the Pulsing Flow Regime at an Elevated Pressure. Chemical Engineering Science 57, 4855-4863.

Burghardt, A.; Bartelmus, G.; Szlemp, A., 2004. Hydrodynamics of Pulsing Flow in Three-Phase Fixed-Bed Reactor Operating at an Elevated Pressure. Industrial and Engineering Chemistry Research 43, 4511-4521.

Charpentier, J.C.; Favier, M., 1975. Some Liquid Holdup Experimental Data in Trickle Bed Reactors for Foaming and Nonfoaming Hydrocarbons. A.I.Ch.E. Journal 21, 1213-1218.

Cheng, S.; Chuang, K.T., 1992. Simultaneous Methanol Removal and Destruction from Wastewater in a Trickle Bed Reactor. The Canadian Journal of Chemical Engineering 70, 727-733.

Ellman, M.J.; Midoux, N.; Laurent, A.; Charpentier, J.C., 1988. A New, Improved Pressure Drop Correlation for Trickle-Bed Reactors. Chemical Engineering Science 43, 2201-2206.

Guo, J.; Al-Dahhan, M.H., 2004. Liquid Holdup and Pressure Drop in the Gas-Liquid Cocurrent Downflow Packed-Bed Reactor Under Elevated Pressures. Chemical Engineering Science 59, 5387-5393.

Hasseni, W.; Laurent, A.; Midoux, N.; Charpentier, J.C., 1987. Régimes d'Écoulement dans un Réacteur Catalytique à Lit Fixe Arrosé Fonctionnant sous Pression (0.1-10 MPa) à Co-courant de Gaz et de Liquide vers le Bas. Entropie 137/138, 127-133.

Holub, R.A.; Dudukovic, M.P.; Ramachandran, P.A.A., 1992. Phenomenological Model for Pressure Drop, Liquid Holdup and Flow Regimes Transition in Gas-Liquid Trickle Flow. Chemical Engineering Science 47, 2343-2348.

Iliuta, I.; Thyrion, F.C.; Muntean, O., 1996. Residence Time Distribution of the Liquid in Two-Phase Cocurrent Downflow in Packed Beds: Air/Newtonian and non-Newtonian Liquid Systems. The Canadian Journal of Chemical Engineering 74, 783-796.

Iliuta, I.; Thyrion, F.C., 1997. Flow Regimes, Liquid Holdups and Two-Phase Pressure Drop for Two-Phase Cocurrent Downflow and Upflow Through Packed Beds: Air/Newtonian and non-Newtonian Liquid Systems. Chemical Engineering Science 52, 4045-4053.

Iliuta, I.; Larachi, F.; Al-Dahhan, M.H., 2000. Double-Slit Model for Partially Wetted Trickle Flow Hydrodynamics. A.I.Ch.E. Journal 46, 597-609.

Iliuta, I.; Larachi, F., 2002. Hydrodynamics of Power-Law Fluids in Trickle Flow Reactors: Mechanistic Model, Experimental Verification and Simulations. Chemical Engineering Science 57, 1931-1942.

Larachi, F.; Laurent, A.; Midoux, N.; Wild, G., 1991. Experimental Study of a Trickle Bed Reactor Operating at High Pressure: Two-Phase Pressure Drop and Liquid Saturation. Chemical Engineering Science 46, 1233-1246.

Larachi, F.; Laurent, A.; Wild, G.; Midoux, N., 1993. Effet de la Pression sur la Transition Ruisselant-Pulsé dans les Réacteurs Catalytiques à Lit Fixe Arrosé. The Canadian Journal of Chemical Engineering 71, 319-321.

Larkins, R.P.; White, P.R.; Jeffrey, D.W., 1961. Two-Phase Concurrent Flow in Packed Beds. A.I.Ch.E. Journal 7, 231-239.

Lepage, J.F., Chatila, S.G., Davidson, M., 1990. Raffinage et conversion des produits lourds du pétrole. Éditions Technip., Paris.

Liles, A.W.; Geankoplis, G.J., 1960. Axial Diffusion of Liquids in Packed Beds and End Effects. A.I.Ch.E. Journal 6, 591-595.

Michell, R.W.; Furzer, I.A., 1972. Mixing in Trickle Flow through Packed Beds. The Chemical Engineering Journal 4, 53-63.

Piché, S.; Larachi, F.; Iliuta, I.; Grandjean, B.P.A., 2002. Improving the Prediction of Liquid Back-Mixing in Trickle-Bed Reactors Using a Neural Network Approach. Journal of Chemical Technology and Biotechnology 77, 989-998.

Rao, V.G.; Drinkenburg, A.A.H., 1983. Pressure Drop and Hydrodynamic Properties of Pulses in Two-Phase Gas-Liquid Downflow Through Packed Columns. The Canadian Journal of Chemical Engineering 61, 158-167.

Rao, V.G.; Drinkenburg, A.A.H., 1985. Solid-Liquid Mass Transfer in Packed Beds with Cocurrent Gas-Liquid Downflow. A.I.Ch.E. Journal 31, 1059-1068.

Ring, Z.E.; Missen, R.W., 1991. Trickle-Bed Reactors: Tracer Study of Liquid Holdup and Wetting Efficiency at High Temperature and Pressure. The Canadian Journal of Chemical Engineering 69, 1016-1020.

Rode, S., 1992. Analyse Spatio-Temporelle des Phénomènes Hydrodynamiques et de Transfert de Matière au Sein d'un Réacteur à Lit Fixe Opérant en Écoulement Monophasique de Liquide ou en Co-Courant vers le Bas de Gaz et de Liquide; Mise en Oeuvre de la Technique des Microsondes Électrochimiques. PhD Dissertation, Institut National Polytechnique de Lorraine, Nancy, France.

Sai, P.S.T.; Varma, Y.B.G., 1987. Pressure Drop in Gas-Liquid Downflow Through Packed Beds. A.I.Ch.E. Journal 33, 2027-2035.

Sai, P.S.T.; Varma, Y.B.G., 1988. Flow Pattern of the Phases and Liquid Saturation in Gas-Liquid Concurrent Downflow Through Packed Beds. The Canadian Journal of Chemical Engineering 66, 353-360.

Sato, Y.; Hirose, T.; Takahashi, F.; Toda, M., 1973. Flow Pattern and Pulsation Properties of Cocurrent Gas-Liquid Downflow in Packed Beds. Journal of Chemical Engineering of Japan 6, 315-319.

Speight, J.G., 1999. The chemistry & technology of petroleum. Marcel Dekker Inc., New York.

Speight, J.G., 2001. Handbook of petroleum analysis, John Wiley & Sons Inc., New York.

Suarez-Ojeda, M.E.; Stuber, F.; Fortuna, A.; Fabregat, A.; Carrera, J.; Font, J., 2005. Catalytic Wet Air Oxidation of Substituted Phenols Using Activated Carbon as Catalyst. Applied Catalysis B: Environmental 58, 107-116.

Tsochatzidis, N.A.; Karabelas, A.J., 1995. Properties of Pulsing Flow in a Trickle Bed. A.I.Ch.E. Journal 41, 2371-2382.

Wakao, N.; Kaguei, S., 1982. Heat and Mass Transfer in Packed Beds. Gordon and Breach Science Publishers, New York.

Wammes, W.J.A.; Mechielsen, S.J.; Westerterp, K.R., 1990. The Transition Between Trickle Flow and Pulse Flow in a Cocurrent Gas-Liquid Trickle Bed Reactor at Elevated Pressures. Chemical Engineering Science 45, 3149-3158.

Wammes, W.J.A.; Mechielsen, S.J.; Westerterp, K.R., 1990. The Influence of the Reactor Pressure on the Hydrodynamics in a Cocurrent Gas-Liquid Trickle Bed Reactor. Chemical Engineering Science 45, 2247-2254.

Wammes, W.J.A.; Westerterp, K.R., 1991. Hydrodynamics in a Pressurized Cocurrent Gas-Liquid Trickle-Bed Reactor. Chemical Engineering Technology 14, 406-413.

Wammes, W.J.A.; Middelkamp, J.; Huisman, W.J.; deBaas, C.M.; Westerterp, K.R., 1991. Hydrodynamics in a Cocurrent Gas-Liquid Trickle Bed at Elevated Pressures. A.I.Ch.E. Journal 37, 1849-1862.

Wauquier, J.-P., 1994. Pétrole brut, produits pétroliers, schémas de fabrication, Éditions Technip., Paris.

Weekman, V.W.; Myers, J.E., 1964. Fluid Flow Characteristics of Concurrent Gas-Liquid Flow in Packed Beds. A.I.Ch.E. Journal 10, 951-960.

Wild, G.; Larachi, F.; Laurent, A., 1991. The Hydrodynamic Characteristics of Cocurrent Downflow and Cocurrent Upflow Gas-Liquid-Solid Catalytic Fixed Bed Reactors: The Effect of Pressure. Revue de l'Institut Francais du Petrole 46, 467-490.

Wübker, S.M.; Laurenzis, A.; Werner, U.; Friedrich, C., 1997. Controlled Biomass Formation and Kinetics of Toluene Degradation in a Bioscrubber and in a Reactor with a Periodically Moved Trickle Bed. Biotechnology and Bioengineering 55, 686-692.

# Chapter 2

# Slow-mode induced pulsing in trickle bed reactors at elevated temperature*

## Résumé

Le fonctionnement périodique reconnu comme une des stratégies d'intensification de procédés dans les réacteurs de type «trickle bed» reste encore non intégré dans l'industrie malgré les nombreux avantages soulignés dans la littérature scientifique et technique. Cette observation est en partie imputable à l'absence de données expérimentales à des pressions et températures élevées caractéristiques des conditions réelles de la plupart des réactions catalytiques. Actuellement, l'hydrodynamique des réacteurs de type «trickle bed» à fonctionnement périodique à des températures et pression élevées demeure un champ d'activité inexploité. Plus spécifiquement, cette étude examine, d'un point de vue hydrodynamique, les avantages et les inconvénients d'un régime d'écoulement à pulsations induites en mode cyclique lent de la phase liquide, en surpression et à des températures élevées. Cette étude s'applique aussi bien aux liquides newtoniens que non-newtoniens caractérisés par une loi de puissance. Quatre morphologies caractéristiques de la structure périodique de la rétention en liquide ont été analysées : temps de percée de l'onde de choc, temps de décroissance de cette dernière, plateau de l'onde de choc ainsi que son amplitude. Les temps de percée et de décroissance de l'onde de choc diminuent alors que celui correspondant à l'apparition du plateau augmente avec la pression et la température. Réciproquement, l'amplitude de percée de l'onde de choc diminue de manière significative si la température (et/ou la pression) augmente. L'atténuation de la rupture des pulsations avec l'augmentation des températures et des pressions résulte d'une compensation progressive des niveaux de rétention en liquide entre la base et la pulsation, lors de la propagation de l'onde le long du lit. Qualitativement, des effets similaires de la température et de la pression ont également été observés pour les liquides newtoniens et non-

* Aydin, B.; Fries, D.; Lange, R.; Larachi, F. AIChE Journal, 52, 3891-3901, 2006

newtoniens. Le contraste moins accentué entre ces niveaux remet en cause l'opportunité de la mise en œuvre des stratégies de fonctionnement cyclique des réacteurs industriels de type «trickle bed» en surpression et à des températures élevées.

## Abstract

Periodic operation, as a process intensification measure for trickle beds, is still tepidly greeted by industry despite numerous benefits underlined in the literature. This state of aloofness is partly ascribed to the paucity of experimental data acquired under elevated temperature and pressure, which, in practice, most catalytic reactions are subjected to. Currently, the hydrodynamics of trickle bed periodic operation at elevated temperature and pressure remains by and large an uncharted territory. This study specifically approaches from a hydrodynamic perspective the pros and cons of slow-mode induced pulsing for Newtonian and non-Newtonian power-law liquids at elevated temperature and moderate pressure. Four morphological features of the liquid holdup periodic pattern were analyzed: shock wave breakthrough, shock wave decay times, shock wave plateau, and shock wave breakthrough amplitude. The shock wave decay and breakthrough times were found to shorten, while correspondingly the shock wave plateau to lengthen, with increasing pressure and temperature. Conversely, the breakthrough amplitude of the shock wave underwent palpable collapse the higher the temperature (and/or pressure). The collapse of the bursting pulses with increasing temperatures and pressures was the result of the reduction of base and pulse liquid holdup levels, delivery of liquid cargo from pulse to baseline flow, and occurrence of dispersive hydrodynamic effects with a tendency to flatten the pulses. Qualitatively, similar effects of temperature and pressure were equally observed whether Newtonian or non-Newtonian liquids were used. The less sensational contrasts prevailing between base and pulse holdups might question the opportunity for implementing induced pulsing strategies in high-temperature, high-pressure tall trickle beds.

**Keywords** Trickle bed, elevated temperature, hydrodynamics, liquid holdup, induced pulsing, non-Newtonian fluids

## 2.1 Introduction

Trickle-bed reactors (TBR) are among the most pervasive configurations industry makes use of, where gas and liquid streams downwardly traverse a porous randomly-packed catalyst layer. Despite the continuous-flow TBR operation still typifies an overwhelming orthopraxy; a growing literature is advocating the merits of liquid-induced pulsing as process intensification means for promoting a multitude of facets of TBR performances (Boelhouwer et al., 2002 a, b, c; Dudukovic et al., 2002, Nigam and Larachi, 2005).

In liquid-induced pulsing flow, a continuous flow of gas encounters a binary-coded liquid stream that is made to switch periodically at the bed entrance between a low-level (also referred to as base) and a high-level (or pulse) velocity. Such a procedure is known to mitigate mass transfer resistances and to enhance reactor conversion especially for gas-limited reactions (Boelhouwer et al., 2002 b). Controlling, in addition, wetting efficiency as a function of time enables averting catalyst life time loss and certain undesirable secondary reactions, on top of, quenching incipient hot spots and curbing flow maldistribution (Boelhouwer et al., 2002 c).

Induction of pulses can be accomplished by switching liquid velocity, back and forth, either between zero and a specified value, i.e., so-called “on-off mode”, or between non-zero base and high-level pulse values, *i.e.*, so-called “base-pulse cycling”. In terms of characteristic times, such an unsteady operation can be effected in slow mode for liquid feed periodic changes over few-minute time spans, or in fast mode using brief liquid pulse incursions lasting for few seconds.

The *spontaneous* pulse flow regime takes place at high enough fluid throughputs in TBRs achieving therein the high transfer rates (Wilhite et al., 2001; Wu et al., 1999) which can be tentatively taken advantage of by liquid-induced pulsing emulation. For a given bed length, on the other hand, trickle flow regime offers longer residence times pulse flow regime lacks to. Therefore, superimposing high enough pulse velocity, causing pulse flow regime, onto low enough base velocity, retrieving trickle flow, enables liquid-induced pulsing to embody the two antagonistic, but yet both desirable, features into one single flow pattern.

The vast majority of experimental work performed to demonstrate the advantages of periodic operation was directed towards probing the changes undergone by the catalytic reaction response. The experimental studies in reaction systems have begun to spring in the early 1990s. Haure et al. (1989) studied the influence of periodic water flow on $SO_2$ catalytic oxidation whereby 30 – 45% increase in reaction rate was reported. Lange et al. (1994) studied the hydrogenation of $\alpha$-methylstyrene under periodic liquid operation up to 1MPa and 40ºC and observed up to 10% increase in the time-average $\alpha$-methylstyrene conversion. Tukac et al. (2003), studying periodic-operation in the temperature range of 125-170ºC and pressure range of 1-7MPa, improved phenol oxidation conversion by *ca*. 10% with respect to that measured at steady state. Wilhite et al. (2003) reported 45% improvement in product selectivity for the catalytic hydrogenation of phenylacetylene into styrene during induced pulsing flow at 90ºC and up to 1.5MPa. More recently, Urseanu et al. (2004) examined the effect of periodic operation for the hydrogenation of $\alpha$-methylstyrene at 40ºC and 0.2MPa, and pinpointed an improvement of 50% in reaction rate.

Apart from investigations on chemical response enhancement, "fluid mechanics" experimentation on induced pulsing flow has been scantier. Xiao et al. (2001), by binarizing air flow *feed* rate, achieved better approach to uniformity of axial and radial liquid distributions in forced pulse flow than for spontaneous pulse flow. Forced air feed superficial velocity and pulse frequency were responsible for further fall off of the liquid holdup. Investigations on liquid flow modulation were instigated by Drinkenburg and coworkers for different particle sizes using an electrical conductivity technique to measure shock wave velocity and liquid holdup under liquid-induced pulsing flow. Hence, Boelhouwer et al. (2002a) distinguished between slow mode and fast mode feed strategies, and measured shock wave characteristics such as shock wave velocity, shock wave tail and plateau, and pulse frequency. The literature reported that shock waves decay while moving down the column by leaving liquid behind their tail (Boelhouwer et al., 2002a). This effect is conducive to eroding the shock wave plateaus which are progressively torn off, according to a linear pattern, as a function of bed depth (Boelhouwer et al., 2002a), while, in return, an increase in the duration of the shock wave tail is diagnosed. The shock wave decay rate, expressed as the decrease in shock wave plateau duration per unit distance, was

found to correlate well with the shock wave velocity (Boelhouwer et al., 2002a). In case of too short durations of base liquid feed, the individual shock waves may start to merge with each other at some depth in the bed erasing thus any positive effect of induced pulsing. Similarly, a decrease in shock wave tail with increased base liquid superficial velocity was observed. Giakoumakis et al. (2005) carried out fast mode liquid-induced pulsing flow experiments on the air-water system. Pulse attenuation was reported from cross-sectionally averaged liquid holdup measurements using ring electrical conductivity probes placed along a glass-bead bed. Experimental data on liquid holdup, pressure drop, and pulse velocity was discussed in terms of gas and liquid flow rates and liquid feed frequency. It is noteworthy that as far as experimental studies on induced pulsing flow characteristics are concerned, none of them afforded to interrogate the effects of elevated temperature and pressure.

As the vast majority of industrial trickle bed applications obtrude stiff stream operation, increasing temperature and pressure becomes virtually inescapable. Any prospect of induced pulsing for industrial implementation therefore dictates further fundamental investigations spotting expressly the incidence of temperature and pressure. Because detailed information about shock wave behavior is important for an operation at optimal conditions, it is the intent of our present study to unveil some of the effects of temperature and pressure on the slow-mode induced pulsing characteristics.

## 2.2 Experimental Setup

The experiments were performed using a stainless steel 48mm I.D. and 1070mm long single-module column capable of withstanding temperatures up to 100°C and pressures up to 5MPa (see Fig. 2-1). Details of the experimental setup were given elsewhere (Aydin and Larachi, 2005). Nonporous glass beads with a diameter of 3mm were used as the packing yielding bed porosity equal to 0.39.

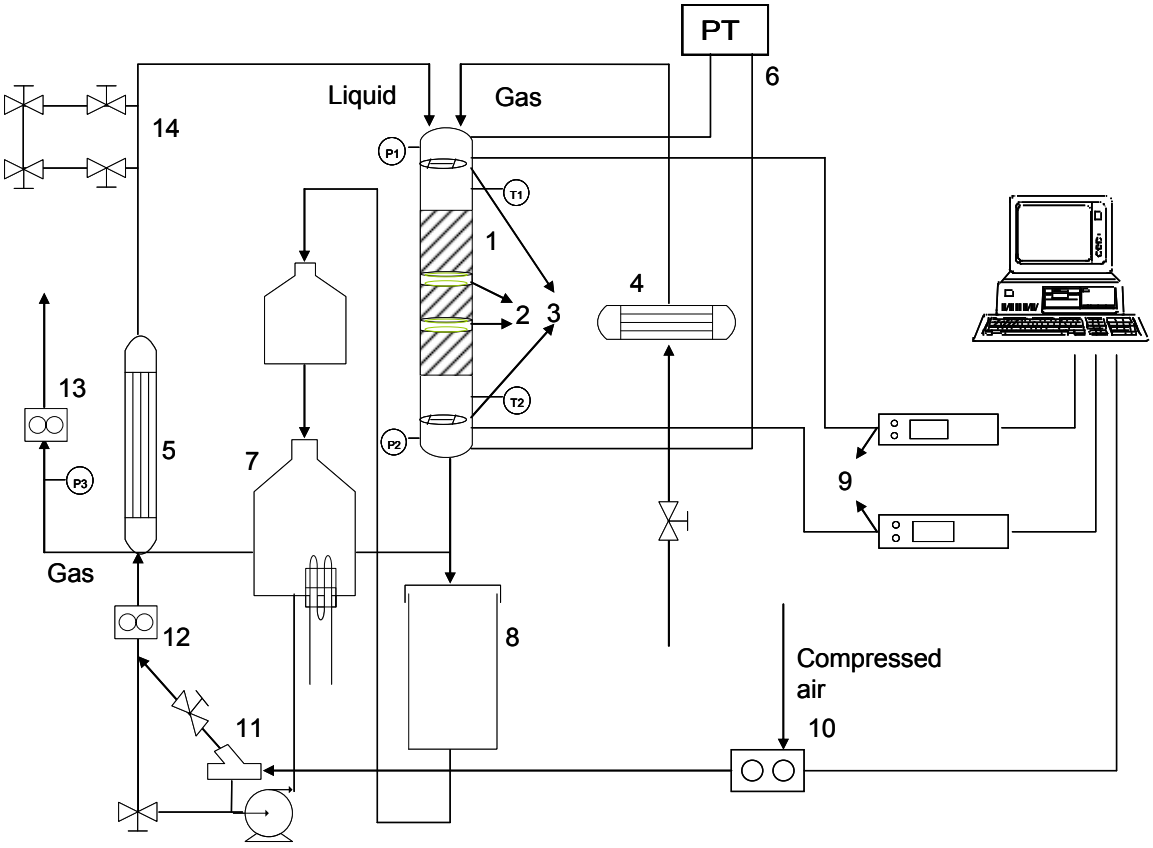


**Figure 2-1** Experimental setup: (1) packed bed, (2) ring electrical conductivity probes, (3) RTD electrical conductivity probes, (4) gas preheater, (5) liquid preheater, (6) pressure transducer, (7) reservoir, (8) gas-liquid separator, (9) lock-in amplifiers, (10) three-way solenoid valve, (11) on-off valve for the additional liquid feed, (12) liquid flowmeter, (13) gas flowmeter, (14) tracer injection loop.

The slow-mode induced pulsing characteristics, in addition to the shock wave velocity and pulse frequency, concerned four morphological features of the dynamic evolution of the liquid holdup: i) the shock-wave breakthrough time, $B_\tau$, which measures the transient time for the liquid holdup to rise from base level to pulse value when liquid feed rate is tipped up; ii) the decay time, $D_\tau$, corresponds to the time elapsed for the liquid holdup to retrieve back its base level when liquid pulse feed is tipped out; iii) the shock-wave plateau time, $P_\tau$, measures the duration, intertwined between the breakthrough and decay times, over which *pulse* liquid holdup remains at, or fluctuates around, a constant value; iv) the shock-wave breakthrough amplitude, $B_\alpha$, measures the increment liquid holdup between base and pulse values. Fig. 2-2a pictorially sketches each of these four features.

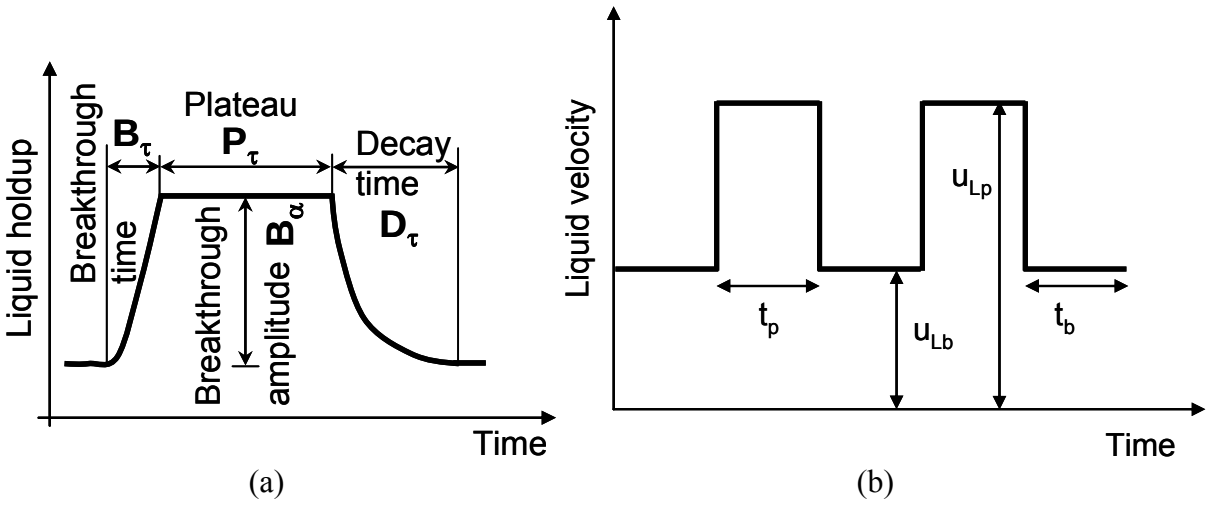


**Figure 2-2** Schematic illustration of the parameters characterizing (a) morphological features of liquid holdup under cycled liquid feed. (b) square-wave cycled liquid feed. $t_b$ = base liquid feed period, $t_p$ = pulse liquid feed period, $u_{Lb}$ = base superficial liquid velocity, $u_{Lp}$ = pulse superficial liquid velocity.

Among the previous quartet, the breakthrough amplitude is the only non-temporal property extracted from the liquid holdup time series. This property is computed as an ensemble- and time-average liquid holdup increment advected by the pulse on top of the base liquid holdup. It is computed after determining the pulse duration, $\tau_{pulse}$, and the number of pulses, $N_{pulse}$, acquired in each experiment for a given bed depth:

$$B_\alpha = \left\langle \varepsilon_{Lp} - \varepsilon_{Lb} \right\rangle = \frac{1}{N_{pulse}} \sum_{1}^{N_{pulse}} \frac{1}{\tau_{pulse}} \int_{0}^{\tau_{pulse}} \left( \varepsilon_{Lp} - \varepsilon_{Lb} \right) \mathrm{d}t \qquad (2.1)$$

The experiments were performed to study the effects of temperature and pressure for Newtonian and non-Newtonian liquids between 25°C and 75°C and up to a pressure of 0.7 MPa. For all the experiments, air was used as the gas phase, whereas water or aqueous 0.25% w/w carboxymethylcellulose (CMC) solution were the process liquids. Note that ease and commodity were the basic criteria that drove our choice of CMC to obtain a model fluid mimicking pseudo-plastic powerlaw behaviors—besides the obvious industrial relevance of viscous pseudo-plastic fluids in areas such as biotechnology and bio-treating in fixed beds (Tsochatzidis and Karabelas, 1995).

The CMC solution, prepared by dissolving powdered CMC in water at ambient temperature, exhibited an inelastic pseudoplastic rheological behavior which was well represented by means of a simple power-law Ostwald-DeWaele model. The consistency index, *k*, and the power-law index, *n*, were fitted for each process temperature after measuring the solution shear stress-shear rate response on an ARES (Advanced Rheometric Expansion System) rheometer in the 0-1000 $s^{-1}$ shear-rate ranges. The physical properties of this solution are given in Table 2-1.

**Table 2-1** Physical Properties of Water-0.25% CMC at Elevated Temperatures

| Temperature (ºC) | k (kg/m.$s^{2-n}$) | n | σ (N/m) | Standard Deviation |
|---|---|---|---|---|
| 25 | 0.072 | 0.666 | 0.056 | 0.99 |
| 50 | 0.041 | 0.707 | 0.054 | 0.99 |
| 75 | 0.033 | 0.659 | 0.051 | 0.99 |

After the liquid was preheated in the reservoir (up to max. 60ºC), it was pumped by means of a rotary valve pump through a liquid preheater via calibrated flowmeters then to the reactor. The line used for feeding the liquid from the pump to the preheater was divided into two streams. The first line was used for handling the continuous liquid flow

corresponding to the base (or low-level) feed by means of a controlled valve. The second line was used to supply the additional liquid feed required during the high-level (or pulse) feed. An on-off valve which was actuated by a digital timer was placed on the second line to trigger and shut off the shock wave bursts. With this strategy it was feasible to obtain base ($u_{Lb}$) and pulse ($u_{Lp}$) liquid superficial velocities over a wide range of operating conditions. The period for the base and pulse liquid feed was kept to 60 seconds for the air-water system and to 120 seconds for the air-0.25%CMC system. The four common parameters used to characterize the feed square-wave cycled liquid feed are schematically shown in Fig. 2-2b.

The preheaters for the gas and the liquid phases, which were installed before the reactor entrance, were utilized in order to maintain the target reactor temperatures constant during the slow-mode induced pulsing experiments. The gas and liquid feeds were distributed from the top of the column across a distributor designed in a way to achieve homogeneous distribution. After leaving the reactor, the gas-liquid stream was demixed into a separator before cooling down and pressure release. The gas was then released from the separator to the atmosphere via a calibrated flowmeter, while the liquid was recirculated back into the feed tank.

For the measurements of induced pulsing flow characteristics, two electrical conductivity probes of the design adopted by Tsochatzidis and Karabelas (1995) and Boelhouwer et al. (2002b) and described in detail elsewhere (Aydin and Larachi, 2005), were placed in the middle of the reactor with a separation distance of 245mm. Each probe, consisting of two ring electrodes 1mm thick and 30mm apart, was connected to a lock-in amplifier to acquire the output signal. After amplification, the signals were transmitted to a computer by means of a data acquisition system. In order to convert the conductance signals issued from two different axial positions in the bed into liquid holdup ones, the conductivity probes were calibrated by means of two additional residence time distribution (RTD) probes using salt injection and Aris's imperfect impulse method with downstream double detection. At constant temperature, pressure and superficial gas velocity, the output signals of the two RTD electrical conductivity probes – buried in thin porous medium layers, one at the top and another at the bottom of the column – were received by an electrical conductimeter and

transmitted to a computer by a data acquisition system. Liquid residence time distribution curves were obtained by fitting the measured outlet tracer normalized response conductance signal to a two-parameter axial-dispersion impulse response RTD model convoluted to the measured inlet tracer normalized response conductance signal. The space time ($\tau$) was determined by using non-linear least-squares fitting and a time-domain analysis of the non-ideal pulse tracer response data. The thus determined liquid holdup values *versus* the conductance values received from the two ring probes at the same operating conditions were so plotted to obtain individual calibration curves for each ring probe. This procedure was repeated for different superficial liquid velocities at different constant temperature, pressure and superficial gas velocity values. Typical calibration curves and relationships between the electrical conductance measured with the ring electrodes and the RTD-determined liquid holdup are shown in Fig. 2-3.

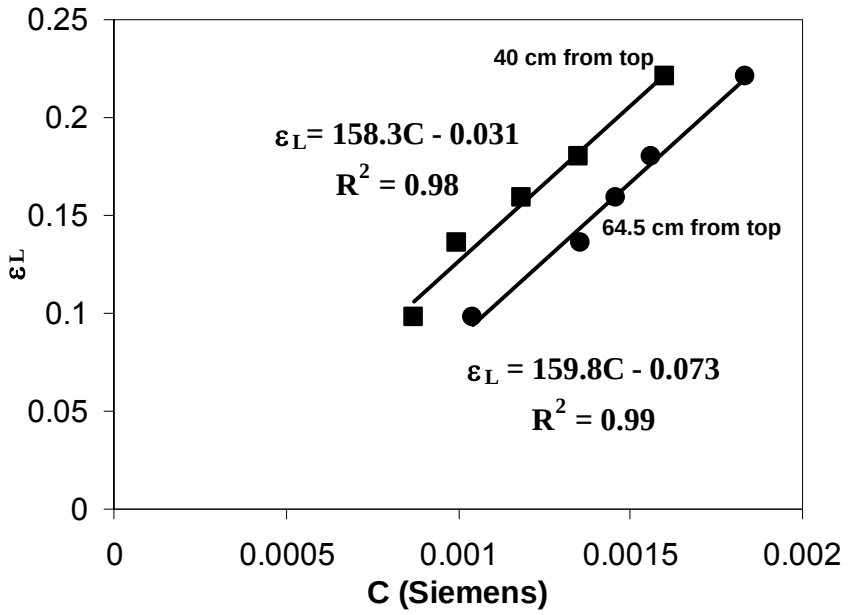


**Figure 2-3** Example of experimental liquid holdup versus conductance plot for the calibration of the conductance probes for the air-water system. $T_r$ = 75ºC, $P_r$ = 0.3 MPa, $u_G$ = 0.21 m/s.

In addition, the pulse frequency was determined with an algorithm implemented in MATLAB for counting the number of peaks (holdup maxima or minima) occurring in the conductance signal and dividing by the observational time window locked on the pulse

portion or the base (if pulse flow regime is observed there) portion of the liquid holdup time series. On the other hand, the velocity of the shock waves was determined by dividing the distance between the two ring-electrode probes (*i.e.*, 245 mm) by the time delay between two signals obtained at pulse superficial liquid velocity.

## 2.3 Results and Discussion

### 2.3.1 Shock wave patterns versus bed depth

The influence of liquid induced pulsing was studied with respect to the behavior of liquid holdup, $\varepsilon_L$, at three temperature and two pressure levels. Regardless of the combination of base and pulse liquid velocities, a constant split ratio of 50% was used for both liquids. Figs. 2-4a,b exemplify typical liquid holdup traces from the two conductivity probes for the air-water and air-0.25%CMC systems, respectively. The runs were conducted at 75ºC and 0.7MPa and at a gas superficial velocity of 0.2m/s in the slow-mode of operation. The conductivity probes were embedded deep in the bed at 40cm and 64.5cm. In terms of systems dynamics, the trickle bed can be viewed as a filter whose impulse response is convoluted with the inlet liquid feed policy to generate signals such as those shown in Fig.4.

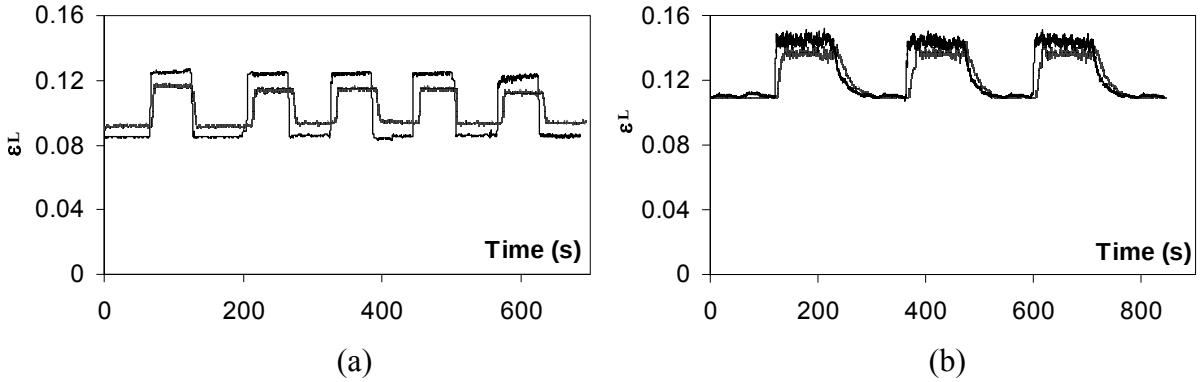


**Figure 2-4** An example of liquid holdup traces during induced pulsing flow, $T_r$ = 75ºC, $P_r$ = 0.7 MPa, $u_G$ = 0.2 m/s, (a) air-water system, $u_{Lb}$ = 0.0035 m/s, $u_{Lp}$ = 0.007 m/s, $t_b$ = 60 s, $t_p$ = 60 s, (b) air-0.25%CMC system, $u_{Lb}$ = 0.00087 m/s, $u_{Lp}$ = 0.0035 m/s, $t_b$ = 120 s, $t_p$ = 120 s.

During their flight down the bed, the induced pulses undergo alterations with bed depth which, at first sight, reflect in attenuation in the amplitude of the pulse liquid holdup response. This behavior prevails irrespective of temperature and pressure levels, while similar observations were arrived at by previous investigators for ambient temperature and atmospheric pressure conditions (Boelhouwer et al., 2002a; Tsochatzidis and Karabelas, 1995). As water pulses progress downstream (Fig. 2-4a), depletion of the pulse amplitude appears to be quickly taken up by the baseline holdup which re-equilibrates, within times much shorter than the cycle period, at a higher compensatory liquid holdup value. This would indicate that pulses and bases are not hermetically sealed to each other, and that mixing takes place in-between by driving some of the liquid cargo from the pulse down into the baseline flow. Conversely, the 0.25%CMC aqueous solution (Fig. 2-4b), being much more viscous, exhibits less leakage of liquid from the plateau with virtually undisturbed baseline liquid holdup during pulse migration. Presumably because more viscous liquids drain more slowly, liquid leakage from the plateau reverberates mainly in the long-lasting transient decay branch. Note the larger fluctuations of liquid holdup in the plateau region for the air-0.25% CMC system which indicate that pulse flow regime had occurred because of the larger liquid holdups attained therein.

From the above observations, it is not difficult to foresee that shock waves may vanish at some bed depth should the TBR be sufficiently tall, a phenomenon already documented for the ambient conditions by Boelhouwer et al. (2002a). Ultimately, induced pulsing may be supplanted by a smoothed out continuous-flow TBR operation that would take over at a constant liquid velocity equal to the weighted average base/pulse velocities. It is instructive therefore to assess to which extent such loss in shock wave capacity evolves as temperature and pressure grow beyond ambient conditions.

### 2.3.2 Shock wave patterns versus temperature

Figs. 2-5a,b show the effect of temperature on the shock waves, respectively, for the air-water and air-0.25%CMC systems at a constant pressure of 0.3MPa with the ring electrodes buried at a depth of 40cm. Identical liquid feed policy parameters were used for the different temperatures concerning each liquid. As can be seen from the figures and in line

with the trend depicted for the continuous-flow TBR operation (Aydin and Larachi, 2005), hotter, and thus less viscous, liquids occasion increasingly less liquid holdups. Also, coherent with the corresponding less viscous behavior, increased temperatures appeared to aggravate depletion of the shock wave. Such collapse in pulse amplitude is clearly highlighted by the variations in $B_\alpha$ shown in Figs. 2-6a,b and measured at 40cm bed depth, independently of the viscous character of the liquid phase, for various pressures and, base and pulse velocity combinations. It is very likely that the shock waves would prematurely vanish after crossing shorter depths in trickle beds operated at higher temperatures. The fact that less sensational contrasts prevail between base and pulse holdups, *i.e.*, diminishing $B_\alpha$ values, at increasingly temperatures could in all appearance seriously question the opportunity for implementing induced pulsing strategies in high-temperature and especially tall beds. We will see later on that pulse depletion via mass exchange with baseline flow explains only part of the amplitude reduction, whereas another part is ascribed to the reduction of the levels of the base and pulse holdups themselves as temperature rises, which occurs regardless of whether induced pulsing or non-forced continuous TBR flow are in play.

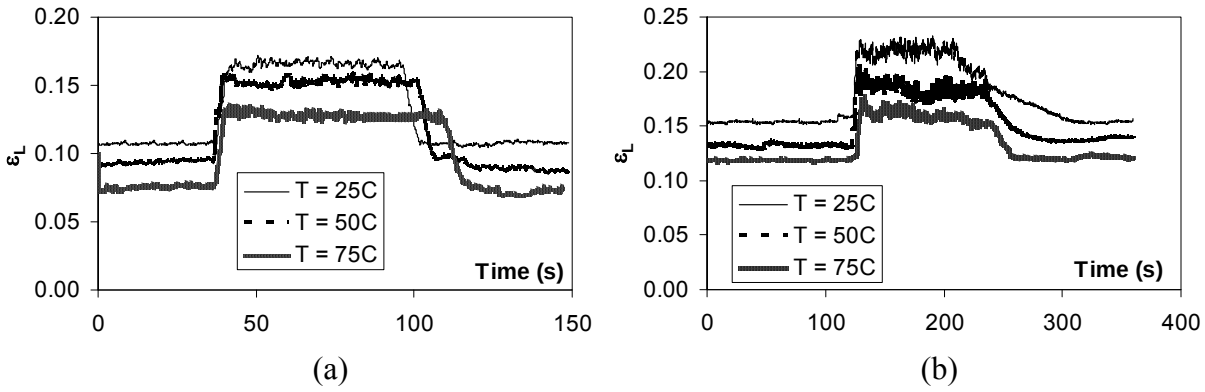


**Figure 2-5** Effect of temperature on shock wave patterns measured 40 cm from bed top, $P_r$ = 0.3 MPa, $u_G$ = 0.2 m/s, (a) air-water system, $u_{Lb}$ = 0.0035 m/s, $u_{Lp}$ = 0.0105 m/s, (b) air-0.25%CMC system, $u_{Lb}$ = 0.00087 m/s, $u_{Lp}$ = 0.0035 m/s.

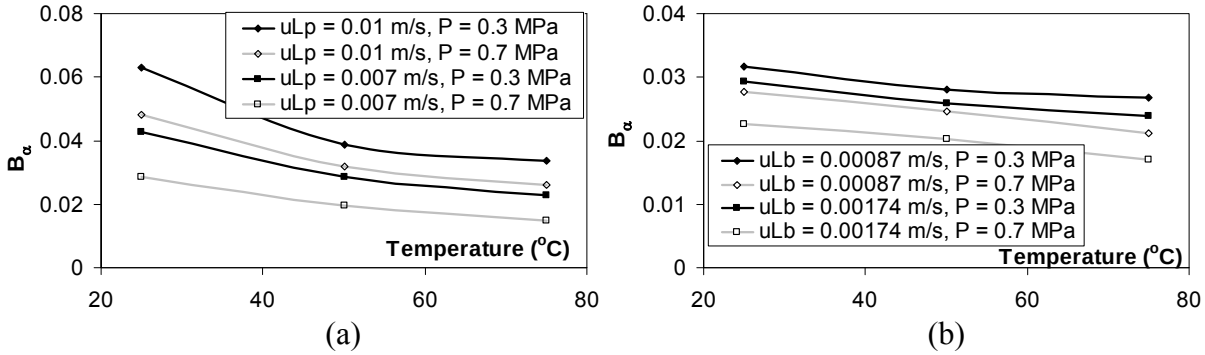


**Figure 2-6** Effect of temperature and pressure on breakthrough amplitude $B_\alpha$ at various base and pulse superficial liquid velocities, $u_G$ = 0.2 m/s, measured 40 cm from bed top (a) air-water system, $u_{Lb}$ = 0.0035 m/s, (b) air-0.25% CMC system, $u_{Lp}$ = 0.0035 m/s.

Figs. 2-5a,b show that all four shock wave characteristics, previously depicted in Fig. 2-2a, are altered by an increase in temperature. These morphological features will be discussed in more details in the forthcoming section. Note that an overshoot in liquid holdup occurs for the air-0.25%CMC system at the burst of the shock wave. It is unclear though to which phenomenon this is to be ascribed since elastic effects were not observed during the rheological characterization of the liquid at such a minute CMC concentration.

The decrease of liquid holdup with temperature appears to be more prominent in the pulse flow regime when higher superficial liquid velocities are used, as exemplified in the case of air-0.25%CMC at $u_{Lp}$ = 3.5mm/s where $\varepsilon_L$ as large as *ca*. 0.22 can occur (see Fig. 2-5b). Furthermore, the decrease with temperature of pulse holdup is more palpable than for base holdup. This causes the shock wave to decay more quickly the higher the temperature as clearly suggested from the viscous liquid (Fig. 2-5b) or as depicted by the temperature-dependent variations in breakthrough amplitude, $B_\alpha$, of Figs. 2-6a,b.

### 2.3.3 Shock wave patterns versus pressure

Figs. 2-7a,b illustrate the effect of pressure on the shock waves, respectively, for the air-water and air-0.25%CMC systems at a constant temperature of 75ºC. In terms of sensitivity of liquid holdup to pressure, our study confirms the decreasing holdup trend with increasing pressures, on a gas superficial basis, as observed already for the continuous-flow TBR operation in the case of ambient (Wammes and Westerterp, 1990; Larachi et al., 1991; Al-Dahhan and Dudukovic, 1994) or of elevated temperatures (Aydin and Larachi, 2005).

Liquid holdup underwent reduction for both the pulse and base portions. However, the reduction was more significant for the pulse portion considering that more gas-liquid interactions occur at higher liquid holdup values. It is interesting to note that the effect of pressure on the shock wave decay time is less substantial than in the case of temperature. However, provided the rest of all the operating parameters is unchanged, it appears that higher pressures tend, at a given bed depth, to smooth out the shock wave and to reduce the breakthrough amplitude (see also Figs. 2-6a,b). Clearly, pulse liquid holdups retract as either temperature or pressure is increased. Hence, as for the negative impact of temperature, shock waves would similarly be afflicted by higher pressures.

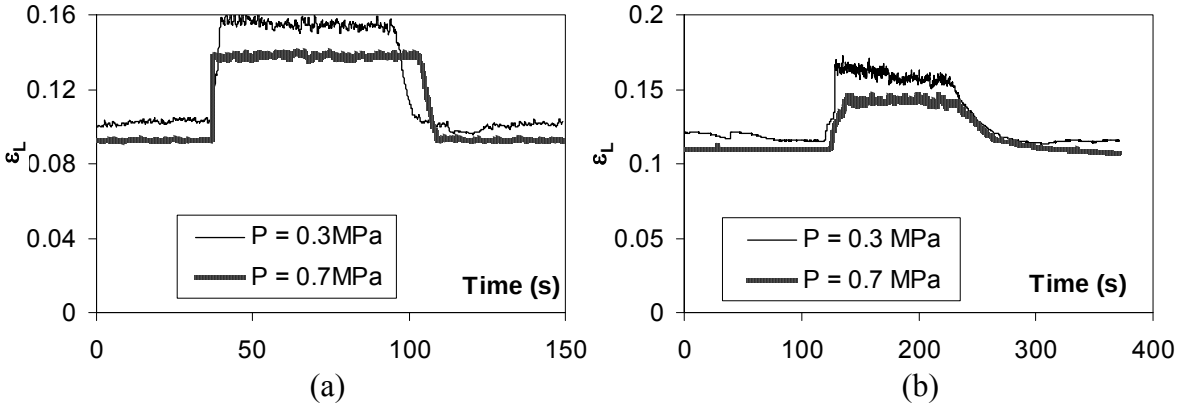


**Figure 2-7** Effect of pressure on shock wave patterns measured 40 cm from bed top, $T_r$ = 75ºC, $u_G$ = 0.2 m/s, (a) air-water system, $u_{Lb}$ = 0.0035 m/s, $u_{Lp}$ = 0.0105 m/s, (b) air-0.25%CMC system, $u_{Lb}$ = 0.00087 m/s, $u_{Lp}$ = 0.0035 m/s.

### 2.3.4 Extent of pulse-base holdup exchange with temperature and pressure

The previous observations tend to support the contention of a non-isolated nature of pulses in the slow-mode induced pulsing (see Fig. 2-8), as well as the inclination of pulses to get squeezed with increasingly temperature and/or pressure. However, such behaviors have been inferred based on comparisons between base, $\varepsilon_{Lb}$, and pulse, $\varepsilon_{Lp}$, holdup homologous series recorded at different temperature and pressure levels under otherwise similar conditions. As alluded to earlier, this comparison may be biased since the liquid holdups, $\varepsilon^o_{Lb}$ (at $u_{Lb}$) and $\varepsilon^o_{Lp}$,(at $u_{Lp}$), for the continuous-flow TBR operation at liquid superficial velocities corresponding to the same base, $u_{Lb}$, and pulse, $u_{Lp}$, velocities are

themselves also prone to changes with temperature and pressure. Therefore, additional liquid holdup experiments have been carried out under continuous-flow TBR operation to quantify the following *deviation indices* between induced pulsing and non-forced continuous flow:

$$\frac{\Delta\varepsilon_{Lp}}{\varepsilon^{o}_{Lp}} = \frac{\varepsilon^{o}_{Lp} - \varepsilon_{Lp}}{\varepsilon^{o}_{Lp}} \tag{2.2}$$

$$\frac{\Delta\varepsilon_{Lb}}{\varepsilon^{o}_{Lb}} = \frac{\varepsilon_{Lb} - \varepsilon^{o}_{Lb}}{\varepsilon^{o}_{Lb}} \tag{2.3}$$

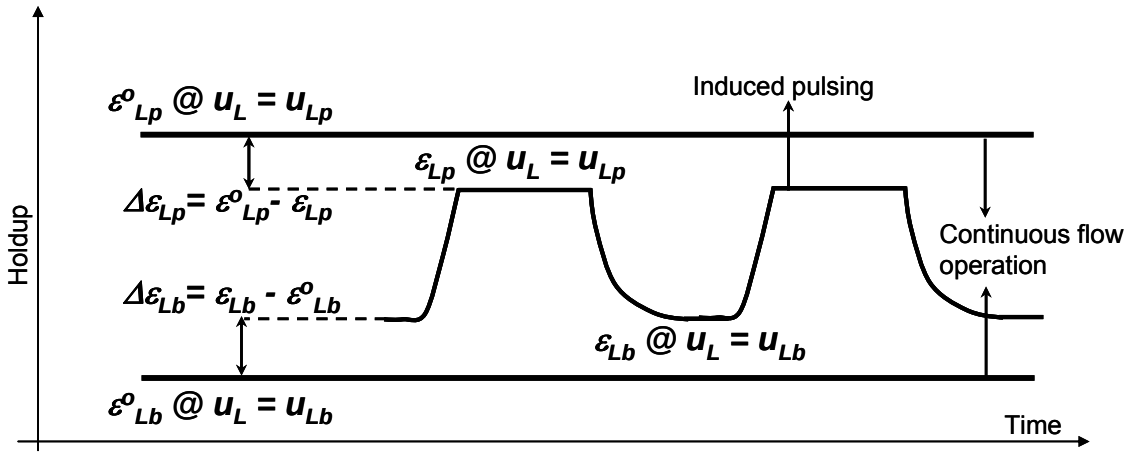


**Figure 2-8** Definition of the deviation indices and distinction between the holdup patterns of induced pulsing and non-forced continuous operation for a given ($u_{Lb}$, $u_{Lp}$) set.

Deviation indices equal to zero would suggest, on the one hand, that pulses are isolated and do not transfer their material content to the baseline flow (*i.e.*, subject to $u_{Lb}$ irrigation); and on the other hand, that induced pulsing under such circumstances would reduce to mere juxtaposition of two non-interacting sequences of continuous-flow hydrodynamic states, one at $u_{Lb}$ and the other at $u_{Lp}$, that would be completely described off induced-pulsing runs. Positive deviation indices would signify that i) the pulse liquid holdup in liquid induced pulsing suffers a loss with respect to continuous flow at same $u_{Lp}$ (Fig. 2-8), ii) the base liquid holdup in liquid induced pulsing undergoes a gain with respect to continuous flow at the same $u_{Lb}$ (Fig. 2-8).

Figs. 2-9a,b show that no other possibility on the signs of the deviation indices exist for our tested conditions. Also, the figures reveal beyond doubt that regardless of the pressure and temperature levels explored here, the pulses in the induced pulsing are indeed non-isolated entities. Since both of $\varepsilon^{o}_{Lb}$ and $\varepsilon^{o}_{Lp}$ slip down to lower values with increased temperature and pressure, Figs. 2-9a,b suggest that, in relative proportions, pulses at 0.3 MPa give up *ca*. 15% of $\varepsilon^{o}_{Lp}$ at 20°C reducing to *ca*. 3.5% of $\varepsilon^{o}_{Lp}$ at 75°C. Similarly, this exchange would go diminishing the higher the pressure because of the correspondingly lesser liquid holdup. The base holdup exhibits a similar behavior as suggested by the evolution of the deviation index given by Eq. 2-3. However, less viscous liquids witness higher exchange levels between pulse and base than more viscous ones.

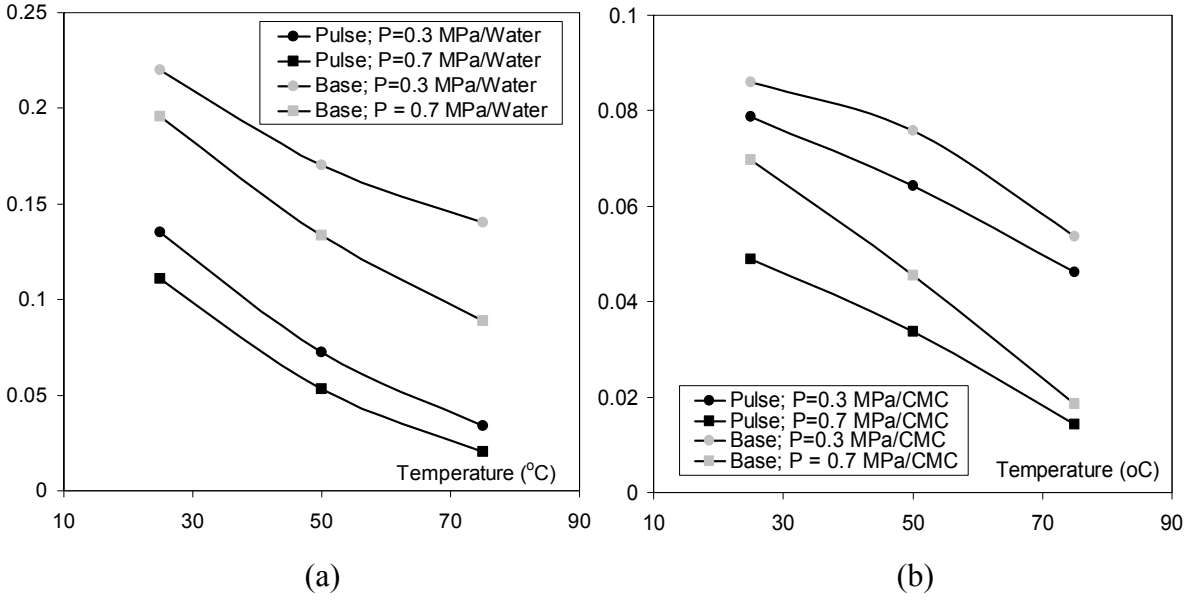


**Figure 2-9** Deviation indices (Eqs.2,3) as a function of temperature and pressure obtained at 40cm depth. $u_G$ = 0.2 m/s, (a) air-water system, $u_{Lp}$ = 0.014 m/s, (b) air-0.25% CMC system, $u_{Lp}$ = 0.0035 m/s.

## 2.3.5 Shock wave breakthrough time

The influence of temperature and/or pressure on the shock wave breakthrough time, $B_\tau$, was also studied for both systems as shown in Figs. 2-10a,b. The shock wave breakthrough time decreases with increasing temperature for the air-water system. A feature presumably ascribable to the water viscosity reduction with temperature enabling, within *ca*. 3-4 s, a

liquid holdup taking up once liquid feed rate is tipped up. At a given temperature, pressure rise brings about higher gas density and therefore more inertia in the gas phase enabling stronger gas-liquid interactions, which, during the transient of the breakthrough, jostle more vigorously the liquid flow and contribute to shorten down to *ca*. 2 s the $B_\tau$ values (Fig. 2-10a). The shock wave breakthrough time also decreases with increasingly base superficial liquid velocity when the same pulse velocity is maintained since, obviously, the gap between pulse and base holdup levels becomes slimmer. For the air-0.25%CMC system, similar effects of temperature, pressure and base velocities were observed (Fig. 2-10b); with nonetheless more pronounced temperature effect plausibly attributable to the drastic viscosity drop.

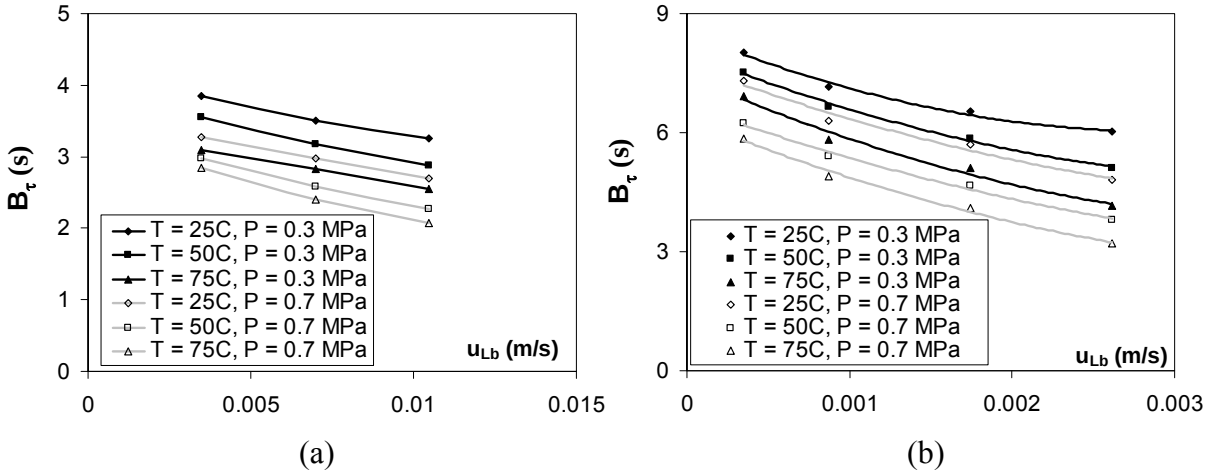


**Figure 2-10** Shock wave breakthrough time as a function of base superficial liquid velocity. Effect of reactor temperature and pressure. $u_G$ = 0.2 m/s, (a) air-water system, $u_{Lp}$ = 0.0175 m/s, (b) air-0.25% CMC system, $u_{Lp}$ = 0.0035 m/s.

## 2.3.6 Shock wave plateau time

One additional parameter characterizing pulse morphology is the shock wave plateau time, $P_\tau$. At constant base superficial liquid velocity, the effects of pulse superficial liquid velocity, reactor temperature and pressure on $P_\tau$ for the air-water and air-0.25%CMC systems are illustrated in Figs. 2-11a,b. Recall that the feed policy delivers perfectly rectangular inlet pulses with plateau times lasting 60 s for water and 120 s for aqueous 0.25%CMC solution. At constant temperature and pressure, the shock wave plateau time increases with pulse superficial liquid velocity. In the same manner, the shock wave plateau

time increases with increasingly temperature and/or pressure for the air-water system; though the effect of temperature is more pronounced. At first sight, plateaus lasting less than 60 s would simply be interpreted as being amputated of their breakthrough time and decay time (to be discussed in next section), especially at the lower pulse superficial velocity values (Fig. 2-11a). However, $P_\tau$ > 60 s were measured particularly when larger pulse velocities coincide with elevated temperatures and pressures (right region of Fig. 2-11a). Hence, an additional feature of the pulse morphology stems here which indicates that pulses collapse not only because they transfer some of their cargo to the baseline flow as noted previously but also because pulses flatten, presumably owing to dispersive effects which result in stretching the plateau times. The air-0.25%CMC system, at constant pulse superficial liquid velocity, exhibits shock wave plateau increasing with increasingly pressure similarly to the air-water system, but this effect is less substantial at high pulse superficial velocity. Note that for this system, $P_\tau$ is always less than 120 s because of the dominant effect of the breakthrough time and especially the decay time as shown in Figs. 2-4b, 2-5b and 2-7b.

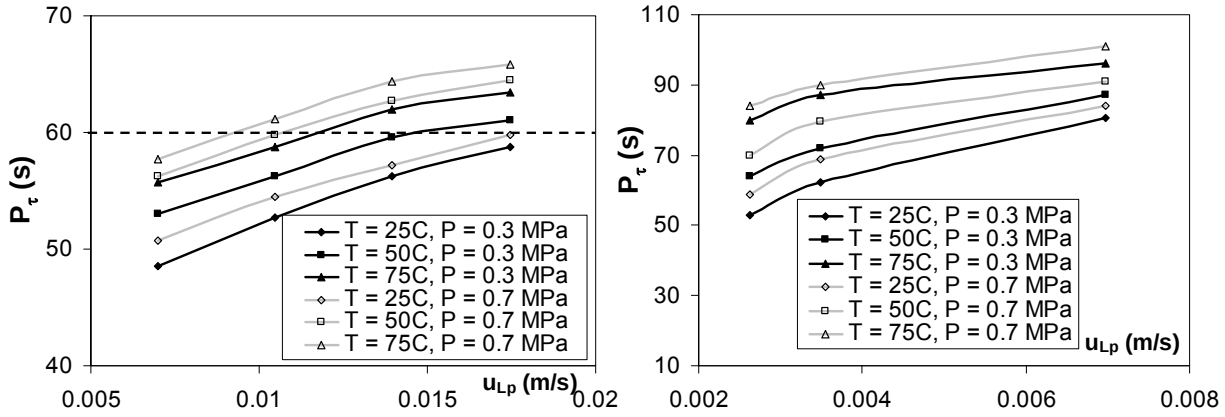


(a) (b)

**Figure 2-11** Influence of pulse superficial liquid velocity, temperature and pressure on plateau time, $u_G$ = 0.2 m/s, (a) air-water system, $u_{Lb}$ = 0.0035 m/s, (b) air-0.25% CMC system, $u_{Lb}$ = 0.00087 m/s.

### 2.3.7 Shock wave decay time

Figs. 2-12a,b depict the evolution of the decay time, $D_\tau$, of the shock wave *versus* the base superficial liquid velocity for the air-water and the air-0.25% CMC systems plotted at different temperatures and pressures. In a fashion similar to the previous observation regarding the breakthrough time, the decay time tendency to thinning is favored by increased base superficial liquid velocity at constant temperature, pressure and pulse velocity. This observation is in agreement with observations made by previous researchers for ambient temperature and atmospheric pressure tests[1]. At constant base superficial liquid velocity, the shock wave decay time decreases with the temperature and pressure and can be easily explained taking again the same interpretative arguments as for the breakthrough time behavior (Fig. 2-10).

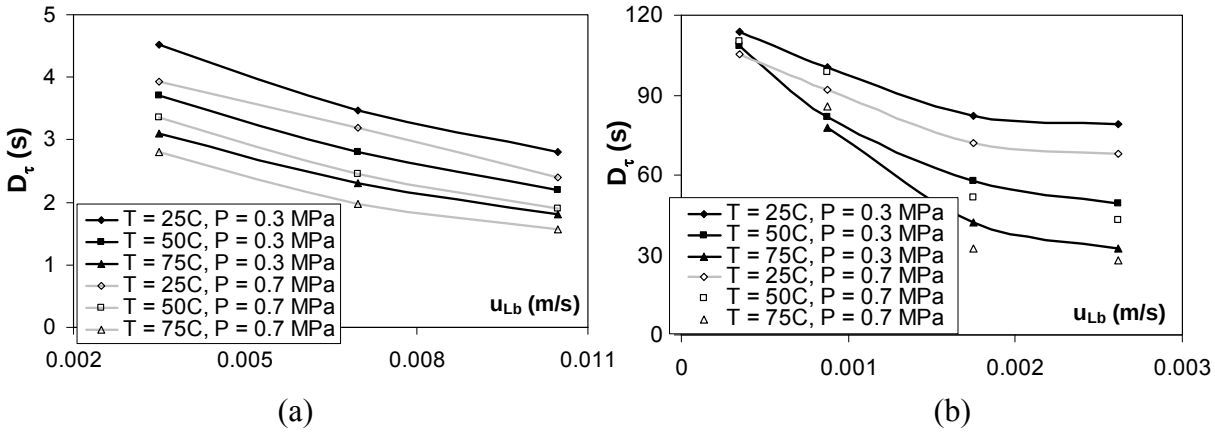


**Figure 2-12** Influence of base superficial liquid velocity, temperature and pressure on decay time, $u_G$ = 0.2 m/s, (a) air-water system, $u_{Lp}$ = 0.0175 m/s, (b) air-0.25% CMC system, $u_{Lp}$ = 0.0035 m/s.

For the air-water system, temperature and pressure appeared to be more influential the lower the base superficial liquid velocity. Furthermore, as the pulse holdup decreases more notably than the base holdup with increased temperature and/or pressure (Fig. 2-5a), the corresponding decrease in breakthrough amplitude, $B_\alpha$, results into less substantial effects from temperature and pressure especially at higher base superficial liquid velocities explaining thus the retracting decay times (Fig. 2-12a) . For the air-0.25%CMC system, the shock wave decay time also decreases with increasingly base superficial liquid velocity, temperature and pressure. Contrarily to the air-water system, the effect of temperature and

pressure on the shock wave decay time is more pronounced the higher the base superficial liquid velocities. Additionally, the effect of pressure on the shock wave decay time for the non-Newtonian liquid is less significant than for the Newtonian liquid. Though $D_\tau$ is characterized by the formation of a long tail (Boelhouwer et al., 2002a), this latter will be less prominent the higher the temperature or the pressure.

### 2.3.8 Shock wave breakthrough amplitude

Going back to Figs. 2-6a,b, these latter illustrate the effect of pressure and temperature on the breakthrough amplitude, $B_\alpha$. For the air-water system, $B_\alpha$ decreases with increased temperature with a marked effect of the latter, the higher the pulse superficial velocities (Fig. 2-6a). The breakthrough amplitude also decreases with increased pressure, especially at low temperature. Similarly, $B_\alpha$ decreases with temperature and pressure for the air-0.25%CMC system though to a much lesser extent in comparison with the air-water system. At elevated temperature and pressure the decrease in $B_\alpha$ also means diminishing pulse liquid holdup. Recall that the most beneficial purpose put forward for liquid induced pulsing is to remove excessive incipient heat of reaction and problematical products from catalyst surface while supplying fresh liquid phase reactants. At industrial conditions where elevated temperature and pressure are often required, it would be difficult to fully benefit from the potential of induced pulsing should the scale up be based on the amplitudes measured in cold flow conditions.

### 2.3.9 Shock wave velocity

The shock wave velocity, Vs, was determined at elevated pressure and temperature at different superficial gas and pulse liquid velocities for air-water and air-0.25%CMC systems (Figs. 2-13a,b) where the experimental data was compared with the Wallis (1969) shock wave velocity relationship. As seen from Fig. 2-13a, the shock wave velocity increases with temperature and pressure at constant superficial gas, base and pulse liquid velocities for the air-water system. The decrease of pulse holdup being more severe compared to the decrease in base holdup with increased temperatures, causes the shock wave velocity to increase. However, our measurements were found to be systematically over-predicted by the Wallis (1969) shock wave velocity equation. This provides a further

confirmation of the deviation of TBR induced pulses from the ideal square-wave cycling assumed by Wallis (1969) relationship. For the air-0.25%CMC system, the shock wave velocity increases with temperature and pressure, everything else being kept constant (Fig. 2-13b). The shock wave velocity values are lower than for the air-water system due to larger viscosity and thus larger liquid holdup exhibited by the 0.25%CMC solution. At constant temperature and pressure the shock wave velocity was found to increase with superficial gas velocity coherent with the corresponding decrease in liquid holdup.

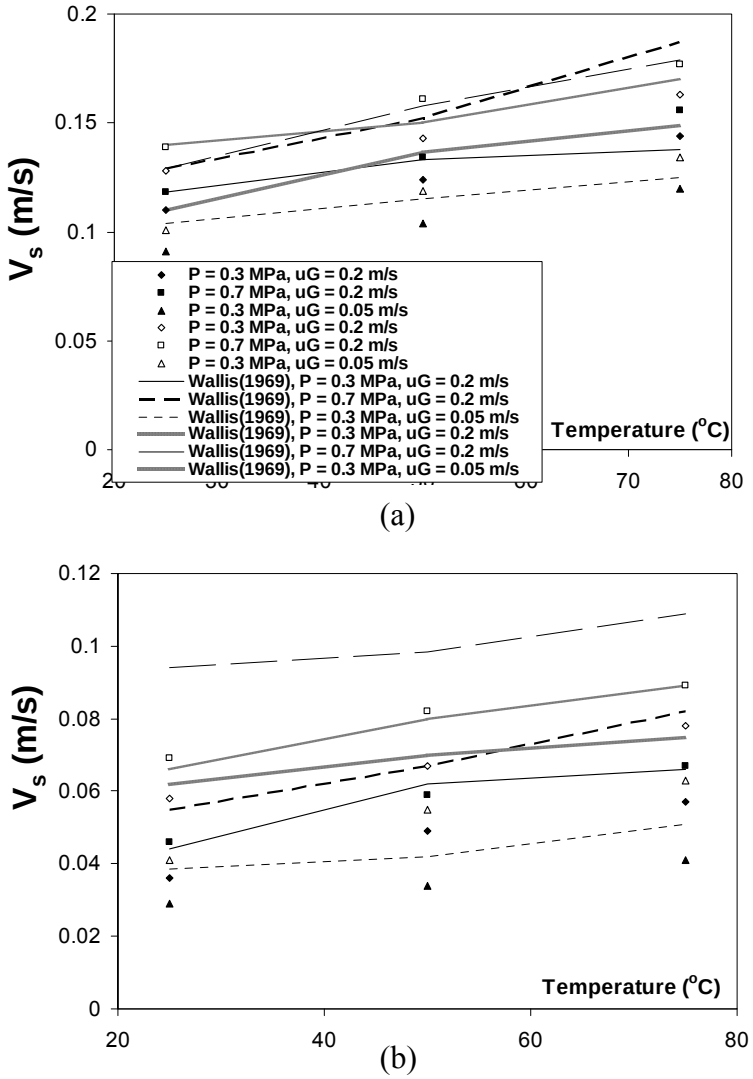


**Figure 2-13** Effect of temperature and pressure on the shock wave velocity. Experimental *vs.* calculated values. (a) air-water system, filled symbols represent data for $u_{Lb}$ = 0.0035 m/s, $u_{Lp}$ = 0.014 m/s; empty symbols represent data for $u_{Lb}$ = 0.0035 m/s, $u_{Lp}$ = 0.0175 m/s, (b) air-0.25% CMC system, filled symbols represent data for $u_{Lb}$ = 0.00087 m/s, $u_{Lp}$ = 0.0035 m/s and empty symbols data for $u_{Lb}$ = 0.00087 m/s, $u_{Lp}$ = 0.007 m/s.

### 2.3.10 Pulse frequency

The base-level portion of the induced pulsing experiments took always place in the trickle flow regime whereas pulse flow regime was allowed to occur in the pulse portion for sufficiently high values of $u_{Lp}$. Maintaining constant base (low-level) superficial liquid velocity constant, the pulse frequency, $f$, was measured in various conditions of high-level (pulse) liquid feed rate experiments when the pulse flow regime was attained for both air-water and air-0.25%CMC systems. The experimental values obtained at elevated temperature and pressure are plotted together with the frequency values calculated by the correlation suggested by Burghardt et al. (2004) for the air-water and air-0.25%CMC systems in Figs. 2-14a,b. Fig. 2-14a shows that the pulse frequency increases with pulse superficial liquid velocity at constant temperature. In the same manner, at constant pulse superficial liquid velocity, pulse frequency increases with increased temperature and pressure for the air-water system. The frequency values predicted with the correlation of Burghardt et al. (2004) are higher than the experimental values. For the air-0.25%CMC system and at lower pressure, the experimental and calculated pulse frequency values are closer. However the correlation predicts lower frequency values at elevated pressure.

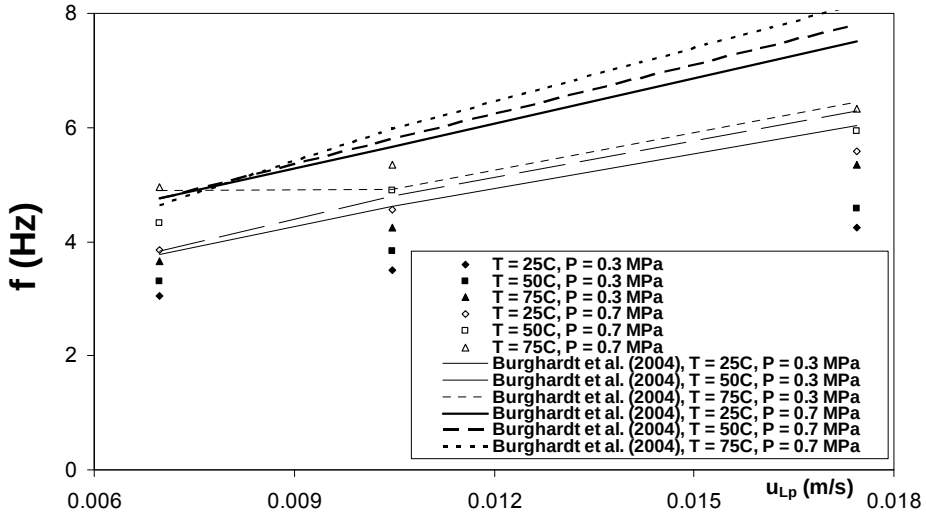


(a)

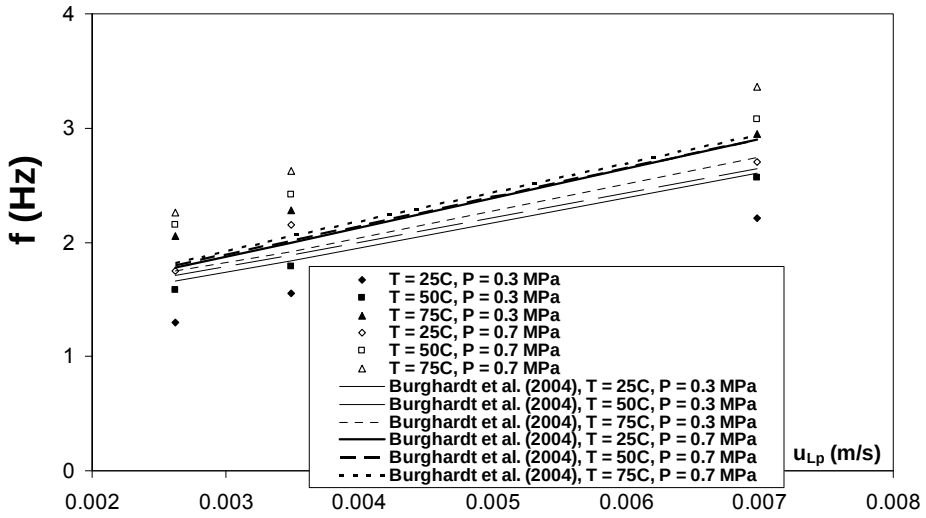


(b)

**Figure 2-14** Effect of temperature and pressure on pulse frequency. Experimental *vs.* calculated values. $u_G$ = 0.2 m/s, (a) air-water system, $u_{Lb}$ = 0.0035 m/s, (b) air-0.25% CMC system, $u_{Lb}$ = 0.00087 m/s.

## 2.4 Conclusion

Operating the column in liquid induced pulsing flow is proposed as one of the strategies for process intensification in TBRs. As industrial TBR operate at elevated temperature and pressure; the necessity of investigating the effect of temperature and/or pressure on the TBR performance exploiting this strategy is a central topic. Previous investigations focusing on liquid induced pulsing flows were performed at atmospheric pressure and ambient temperature. In this study, the aim was to illustrate the effects of temperature and pressure on the shock wave characteristics for both Newtonian and non-Newtonian liquids. The decay process for the shock waves was found to reduce with increased temperature and pressure. The shock wave breakthrough time and shock wave decay time decreased with increasing temperature and pressure. On the contrary, the shock wave plateau time increased with temperature and pressure. This would favor the removal of heat and products from the catalyst during the high liquid feed. However, the liquid holdup decreased with temperature especially at the high liquid feed rates. This phenomenon could be viewed as an obstacle for enhancement of reactor performance with liquid induced pulsing flow at high temperature and pressure operations. The shock wave velocity and the pulse frequency were found to increase with temperature and pressure.

## 2.5 Nomenclature

$B_\alpha$ breakthrough amplitude

$B_\tau$ breakthrough time, s

$D_\tau$ decay time, s

$f$ pulse frequency, Hz

$u$ superficial velocity, m/s

$P_r$ reactor pressure, MPa

$P_\tau$ plateau time, s

$t$ time, s

$T_r$ reactor temperature, °C

$V_s$ shock wave velocity, m/s

**Greek letters**

$\varepsilon_L$ liquid holdup

**Subscripts**

b base

G gas phase

L liquid phase

o continuous-flow TBR operation

p pulse

r reactor

## 2.6 References

Boelhouwer JG, Piepers HW, Drinkenburg AAH. Liquid-induced pulsing flow in trickle-bed reactors. *Chem Eng Sci.* 2002a;57: 3387-3399.

Boelhouwer JG, Piepers HW, Drinkenburg AAH. Nature and characteristics of pulsing flow in trickle-bed reactors. *Chem Eng Sci.* 2002b;57: 4865-4876.

Boelhouwer JG, Piepers HW, Drinkenburg AAH. Advantages of forced non-steady operated trickle-bed reactors. *Chem Eng Technol.* 2002c;25:647-650.

Dudukovic MP, Larachi F, Mills PL. Multiphase catalytic reactors: A perspective on current knowledge and future trends. *Catal Rev-Sci Eng.* 2002;44:123-246.

Nigam KDP, Larachi F. Process intensification in trickle-bed reactors. *Chem Eng Sci.* 2005;60: 5880-5894.

Wilhite BA, Wu R, Huang X, McCready MJ, Varma A. Enhancing performance of three-phase catalytic packed-bed reactors. *AIChE J.* 2001; 47:2548-2556.

Wu R, McCready MJ, Varma A. Effect of pulsing on reaction outcome in a gas-liquid catalytic packed-bed reactor. *Catal Today.* 1999; 48:195-198.

Haure PM, Hudgins RR, Silveston PL. Periodic operation of a trickle-bed reactor. *AIChE J.* 1989; 35:1437-1444.

Lange R, Hanika J, Stradiotto D, Hudgins RR, Silveston PL. Investigations of periodically operated trickle-bed reactors. *Chem Eng Sci.* 1994;49:5615-5621.

Tukac V, Hanika J, Chyba V. Periodic state of wet oxidation in trickle-bed reactor. *Catal Today.* 2003;79-80:427-431.

Wilhite BA, Huang X, McCready MJ, Varma A. Effects of induced pulsing flow in trickle-bed reactor performance. *Ind Eng Chem Res.* 2003;42:2139-2145.

Urseanu MI, Boelhouwer JG, Bosman HJM, Schroijen JC. Induced pulse operation of high-pressure trickle bed reactors with organic liquids: hydrodynamics and reaction study. *Chem Eng Process.* 2004;43:1411–1416.

Xiao Q, Cheng ZM, Jiang ZX, Anter AM, Yuan WK. Hydrodynamic behavior of a trickle bed reactor under "forced" pulsing flow. *Chem Eng Sci.* 2001;56:1189-1195.

Giakoumakis D, Kostoglou M, Karabelas AJ. Induced pulsing in trickle beds—characteristics and attenuation of pulses. *Chem Eng Sci.* 2005;60:5183-5197.

Aydin B, Larachi F. Trickle bed hydrodynamics and flow regime transition at elevated temperature for a Newtonian and a non-Newtonian liquid. *Chem Eng Sci.* 2005;60:6687-6701.

Tsochatzidis NA, Karabelas AJ. Properties of pulsing flow in a trickle bed. *AIChE J.* 1995;41:2371-2382.

Wammes WJA, Westerterp KR. The influence of the reactor pressure on the hydrodynamics in a cocurrent gas-liquid trickle bed reactor. *Chem Eng Sci.* 1990;45:2247-2254.

Larachi F, Laurent A, Midoux N, Wild G. Experimental study of a trickle bed reactor operating at high pressure: Two-phase pressure drop and liquid saturation. *Chem Eng Sci.* 1991;46:1233-1246.

Al-Dahhan MH, Dudukovic MP. Pressure drop and liquid holdup in high pressure trickle bed reactors. *Chem Eng Sci.* 1994;49:5681-5698.

Wallis GB. One-dimensional two-phase flow. New York: McGraw-Hill, Inc., 1969:122-35.

Burghardt, A., Bartelmus, G., Szlemp, A., (2004). Hydrodynamics of pulsing flow in three-phase fixed-bed reactor operating at an elevated pressure. Industrial and Engineering Chemistry Research, 43, 4511-4521.

# Chapter 3

# Slow-mode induced pulsing in trickle beds at elevated temperature for (non)Newtonian liquids*

## Résumé

L'effet de la température sur l'hydrodynamique d'un réacteur de type « trickle bed » a été étudié pendant l'opération cyclique du liquide. La transition ruisselant-pulsé en fonctionnement cyclique ($tpT^{co}$) a été comparée à la transition spontanée ($tpT^{s}$) à débit constant de flux, ainsi qu'aux régimes correspondants d'écoulement pulsé. L'effet de la température sur $tpT^{co}$ et $tpT^{s}$, ainsi que sur la rétention liquide et la durée du pulse de l'onde, a été évalué pour les liquides (non-) newtoniens. Les effets de la température et de la vitesse superficielle de gaz sur la vitesse et la fréquence de pulsation ont été estimés après l'atteinte du régime pulsé sous opération à flux cyclique et à débit liquide constant. Avec l'augmentation de la température, la transition $tpT^{co}$ se déplace vers des vitesses élevées de gaz et liquide, néanmoins le diagramme de Charpentier - Favier modifié continue à prédire de manière satisfaisante les évolutions des transitions $tpT^{co}$ et $tpT^{s}$ avec la température.

## Abstract

The effect of temperature on the hydrodynamics of trickle bed liquid cyclic operation was studied. The ***t***rickling-to-***p***ulsing Transition in ***c***yclic ***o***peration ($tpT^{co}$) was compared to ***s***pontaneous Transition ($tpT^{s}$) in constant-throughput flow, as well as the corresponding pulsing flow regimes. The effect of temperature on $tpT^{co}$ and $tpT^{s}$, and on liquid holdup and shock wave plateau time, was assessed for (non-)Newtonian liquids. The effect of temperature and superficial gas velocity on pulse velocity and pulse frequency was evaluated for pulsing flow in cyclic and constant-throughput flows. With increased temperature, $tpT^{co}$ shifted to higher gas and liquid velocities, however, the modified

* Aydin, B.; Fries, D.; Lange, R.; Larachi, F. Chemical Engineering Science, 62, 5554-5557, 2007

Charpentier-Favier diagram still adequately captured both $tpT^{co}$ and $tpT^{s}$ evolution with temperature.

**Keywords** Trickle bed, elevated temperature, induced pulsing, transition boundary

## 3.1 Introduction

Trickle-bed reactor, TBR, is one of the widely functional designs of gas-liquid packed beds with cocurrent gas and liquid flow. Its versatile functionality in the petroleum industry and applications extending to biochemical process industry favor ongoing research for better utilization of TBRs. Liquid-induced pulsing is one of the methods suggested for TBR periodic operation in terms of productivity increase (Boelhouwer et al., 2002a).

In terms of characteristic times, such an unsteady operation can be effected in slow mode for liquid feed periodic changes over few-minute time spans, or in fast mode using brief liquid pulse incursions lasting for few seconds.

Liquid-induced pulsing can be performed either in fast (brief liquid pulse incursions lasting for few seconds) mode or in slow mode (liquid feed periods over few-minute intervals). During both operation modes the liquid velocity is switched either between zero and a given value (on-off mode) or between low and high value (base-pulse mode). TBR periodic operation was first suggested by Gupta (1985) and subsequently, Haure et al. (1989) reported one of the early studies for periodic operation for a wide range of cycle periods wherein palpable increase in $SO_2$ oxidation rate was observed. The potential benefits of cyclic operation on catalytic reactions cannot be fully understood without taking care of the special hydrodynamics arising as a result of liquid flow modulation. By now, the reported work on the hydrodynamics of periodically operated TBR is still scanty. Xiao et al. (2001) studied the effect of gas flow modulation on liquid distribution and liquid holdup at ambient conditions and observed more uniform liquid distribution and lower liquid holdup during forced gas input. Boelhouwer et al. (2002b) introduced two feed strategies – slow mode and fast mode – and measured ambient liquid holdup and shock wave characteristics (shock wave velocity, shock wave tail, shock wave plateau, pulse frequency) under liquid-induced pulsing flow for different particle sizes using an electrical conductance technique.

Giakoumakis et al. (2005) carried out fast mode liquid-induced pulsing flow experiments for the air water at ambient conditions. Pulse attenuation was reported from axial profiles of cross-sectionally averaged liquid holdups using ring probes placed along a packed bed of 6 mm glass beads. Experimental data on liquid holdup, pressure drop, and pulse celerity and pulse intensity was presented as a function of fluid flow rates and liquid feed frequency.

As the industrial trickle bed applications often impose elevated temperature and pressure; it is required to unveil induced pulsing flow hydrodynamics near these conditions. In this work, the nature of the ***t***rickling-to-***p***ulsing Transition in ***c***yclic ***o***peration ($tpT^{co}$) in the slow mode was compared to that of ***s***pontaneous Transition ($tpT^{s}$) in constant-throughput flow, as well as the corresponding pulsing flow regimes (pulse velocity and frequency) for (non-) Newtonian liquids.

## 3.2 Experimental Procedure

The experiments were performed in a 4.8-cm-ID, 107-cm-long stainless steel reactor bed packed with 3-mm glass beads (bed porosity, 0.39). The experimental setup was described elsewhere (Aydin and Larachi, 2005). During the experiments, air and water or aqueous 0.25 % w/w carboxymethylcellulose (CMC) solution were used. The effect of temperature was studied between 25°C and 75°C. The power-law parameters of the CMC solution were given in Aydin and Larachi (2005). Two feed lines were used for the periodic operation. The base ($u_{Lb}$) and pulse ($u_{Lp}$) superficial liquid velocities were adjusted by needle valves connected to each line. After the liquid was heated in the reservoir, it was sent to the reactor through a liquid preheater via calibrated flowmeter. The gas passed through a gas preheater before encountering the liquid at the reactor top. Prior to the experiments the reactor was preheated at least 1 hour in the pulsing flow regime to achieve a totally pre-wetted bed.

For the investigation of pulse characteristics, an electrical conductance technique was employed. Two probes, each comprised of two ring electrodes, were placed in the reactor (0.245 m apart) to measure averaged liquid holdups along the bed. The probes were calibrated by the tracer method. $u_{Lb}$'s were set to always achieve trickling regime at base flow, whereas $u_{Lp}$'s were varied to comprise both trickling and pulsing regimes. At constant $u_{Lb}$, identification of regime transition was carried out by analyzing the signals specific to

the applied $u_{Lp}$ and by using the moment method (Aydin and Larachi, 2005). Pulse frequency, $f_p$, was determined by counting the number of holdup maxima or minima and dividing by the liquid holdup pulse period. Pulse velocity, $V_p$, was determined by dividing inter-electrode distance by the time delay of maximum cross-correlation between signals. For confirmation of observed trends and differences between cyclic mode and steady operation, the experiments were repeated up to three times and taking afterwards average values.

## 3.3 Results and Discussion

For all the experiments, a split ratio of 50% was applied. The periods for the base and pulse velocities were 60 s for air-water and 120 s for air-0.25% CMC. Different flow regimes emerge due to the interaction between phases which mostly depend on flow rate and fluids properties. On Figs. 3-1a, b, the $tpT^{s}$ as well as $tpT^{co}$ points are plotted on the modified Charpentier-Favier diagram (Larachi et al., 1993) for different temperatures and pressures for air-water and air-0.25% CMC, respectively. Additionally, the transitional data simulated with the Larachi et al. (1999) correlation are shown in a parity plot (inset, Fig. 3-1a) together with the present experimental data for the air-water system. The average error was *ca*. 13% and the ±25% envelopes encompassed most of the data. For the cyclic mode, both Charpentier and Favier diagram and Larachi et al. correlation used the *pulse* superficial liquid velocity. The $tpT^{s}$ points fall along the same line as the $tpT^{co}$ points. The plots suggest that the Charpentier-Favier diagram could be relied upon for localizing transition irrespective of constant-throughput or cyclic operation. They also indicate that increased temperature and pressure are well accounted for by the correction factors, $\lambda$, $\psi$ and $\Phi$, used by the diagram coordinates.

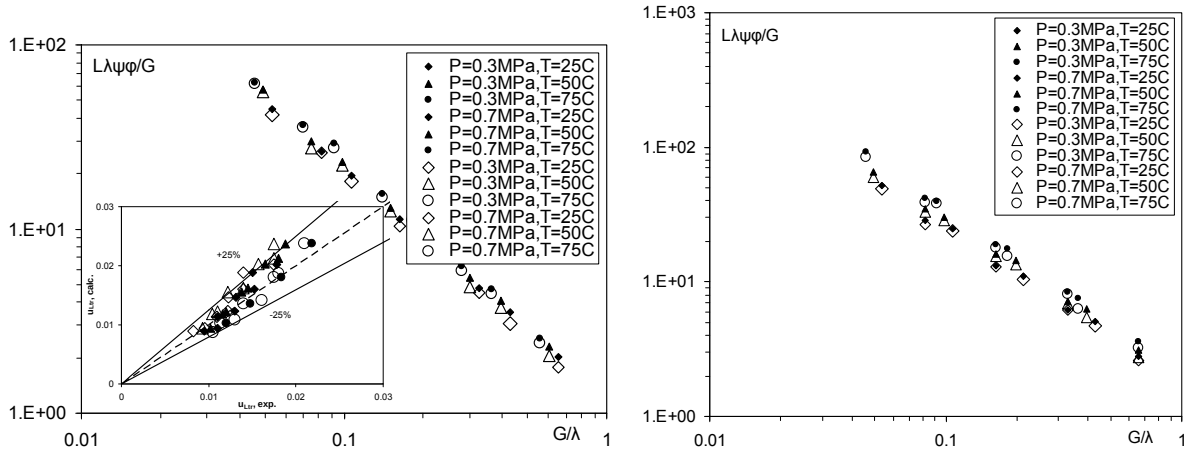


(a) (b)

**Figure 3-1** $tpT^{s}$ (empty symbols) and $tpT^{co}$ (filled symbols) boundary at elevated pressure and temperature for (a) air-water with those calculated from Larachi et al. (1999) correlation (b) air-0.25% CMC system.

Fig. 3-2a illustrates the liquid holdup values at $tpT^{s}$ and $tpT^{co}$ for air-water at 0.3 MPa. At a given $u_G$, liquid holdups ($\varepsilon_L$ and $\varepsilon_{Lp}$) decrease with increasing temperature at the transition points, $tpT^{co}$ and $tpT^{s}$. However, $\varepsilon_{Lp}$ values for $tpT^{co}$ were larger than their $tpT^{s}$ counterparts despite the same temperature and $u_G$ were imposed both in cyclic operation and constant-throughput mode. This suggests that under these conditions, the liquid superficial *pulse* velocity, $u_{Lp}$, at the transition must be higher than the liquid superficial velocity, $u_L$, required for attainment of trickling-to-pulsing transition in the constant-throughput mode. A likely explanation of this behavior could be ascribed to the non-isolated nature of the pulses in the induced pulsing mode whereby some of the liquid at $u_{Lp}$ is being discharged onto the liquid base flow thus diminishing the level of liquid holdup at $u_{Lp}$ with respect to the constant-throughput mode at $u_L = u_{Lp}$. Therefore, higher liquid velocity, and thus increased $\varepsilon_{Lp}$, is required to provoke inception of pulsing flow in cyclic operation. Fig. 3-2b is a deciphered version of the $tpT^{s}$ and $tpT^{co}$ shifts shown in Fig. 3-2a. It confirms the higher liquid superficial velocities in cyclic operation than in constant-throughput mode required to reach the trickling-to-pulsing transition. In addition, the flow regimes in the reactor result from a balance between driving (inertia, gravity) forces and resisting (shear-stress, surface tension) forces. As the amount of liquid held decreases with the reduction in

liquid viscosity and surface tension with temperature, higher liquid throughput is required for pulse formation to occur at elevated temperatures.

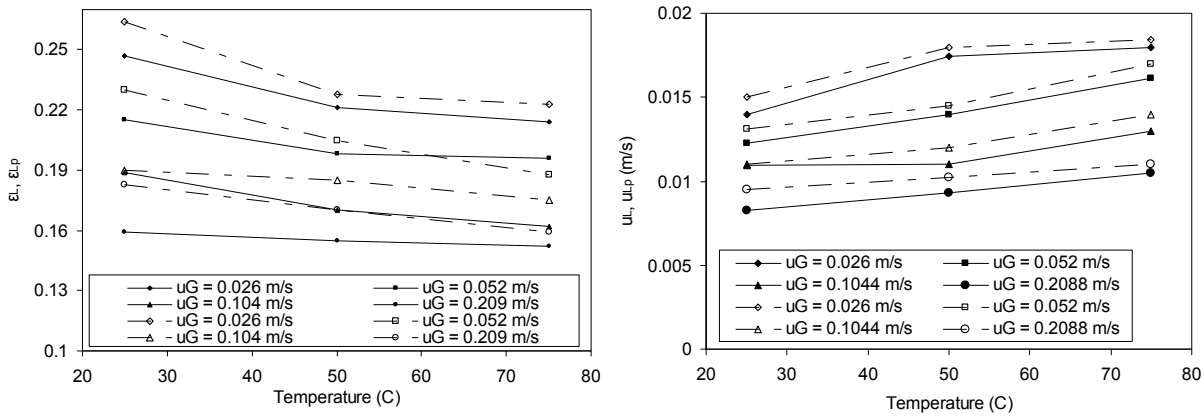


(a) (b)

**Figure 3-2** Effect of temperature and gas superficial velocity on liquid holdup (a) and liquid superficial velocity (b) at $tpT^{s}$ (filled symbols) and $tpT^{co}$ (empty symbols) boundary for air-water, $P$ = 0.3 MPa.

The ratio of the shock wave plateau time at $tpT^{co}$ normalized to that at the reactor entrance, i.e., 60 s for water, is plotted in Fig. 3-3 to show the effect of temperature at various $u_G$. The decrease of liquid holdup at the pulse with increased temperature and $u_G$ signifies the smoothing of the pulses due to the transfer of some of the liquid carried to the base flow. This causes the shock wave plateau time to increase at $tpT^{co}$ with increasingly temperature and/or $u_G$.

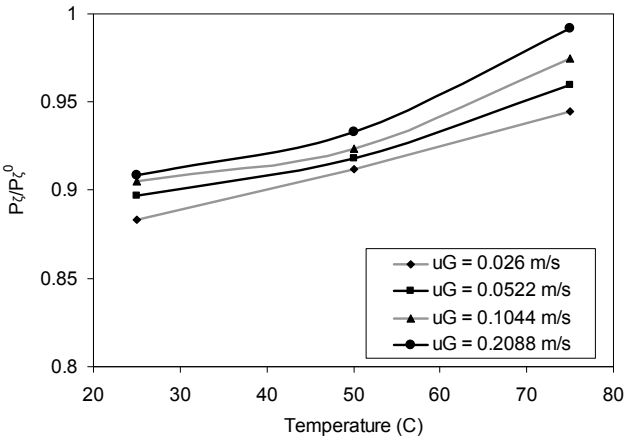


**Figure 3-3** Effect of temperature and $u_G$ on shock wave plateau time at $tpT^{co}$ for air-water, $P$ = 0.3 MPa. $P_\tau$ and $P_\tau^0$ represent experimentally obtained plateau time and applied pulse velocity period (60 s) respectively.

The effect of temperature and $u_G$ on the pulse velocity, $V_p$, and the pulse frequency, $f_p$, is shown in Figs. 3-4a, b for equal values of $u_L$ (constant-throughput mode) and $u_{Lp}$ (pulse velocity in cyclic operation) of 0.0192 m/s. Recall that in cyclic operation, pulsing flow regime is allowed to occur solely for high enough $u_{Lp}$ values while trickling always prevailed at $u_{Lb}$. Also pulse velocity $u_{Lp}$ (cyclic operation) must be distinguished from $V_p$ of pulsing flow regime. While the former was clearly defined, the latter concerns the speed of the fast-propagating pulses that arise in the pulsing flow when $u_{Lp}$ in cyclic operation (or $u_L$ in constant-throughput mode) is sufficiently high to shift reactor from trickling to pulsing flow regime.

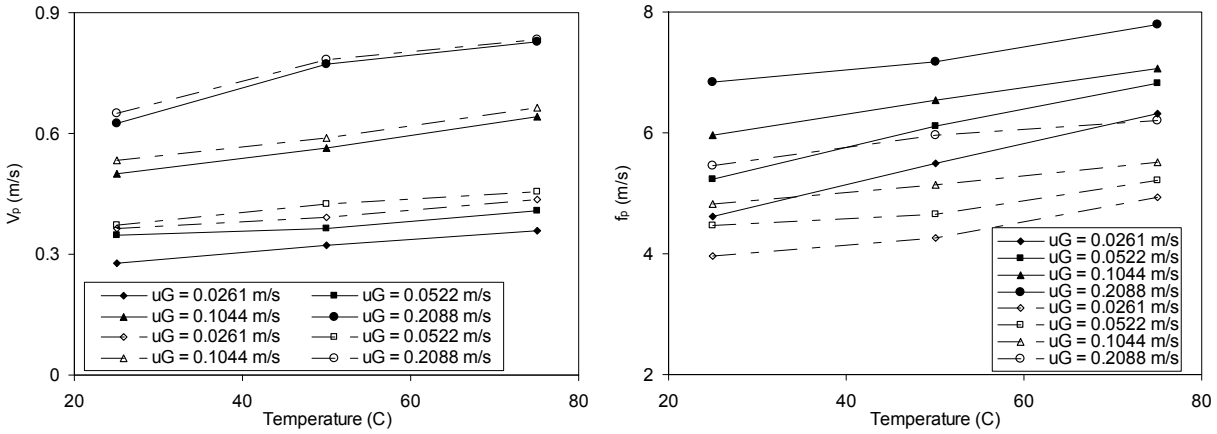


(a) (b)

**Figure 3-4** Effect of temperature and $u_G$ on (a) pulse velocity and (b) pulse frequency for constant-throughput mode (filled symbols) and cyclic operation (empty symbols) for air-water, $u_L$ and $u_{Lp}$ = 0.0192 m/s, $P$ = 0.3 MPa.

At given temperature, and $u_G$ and $u_L$ (or $u_{Lp}$), pulse velocity, $V_p$, in cyclic operation is larger than that in the constant-throughput mode (Fig. 3-4a). The differences between $V_p$ are especially pronounced the lower the $u_G$. Pulses in the liquid would propagate faster across the bed at the expense of reduced liquid holdups equivalent to higher interstitial liquid velocities. This intuitive explanation appears to be coherent with the lesser $\varepsilon_{Lp}$ in the pulse at $u_{Lp}$ than in the constant-throughput mode at $u_L = u_{Lp}$. Also, increased temperature and/or $u_G$ occasioned an increase in $V_p$ because of increased interstitial liquid velocities. As the pulses move faster, higher liquid flow rates are required for the pulses to form during cyclic operation providing *post-facto* confirmation of Figs. 3-2a,b observations.

Coherently, $f_p$ increased with temperature and $u_G$ (Fig. 3-4b). At a given temperature and $u_G$, and $u_L$ (or $u_{Lp}$), cyclic operation $f_p$ is lower than the constant-throughput mode $f_p$.

## 3.3 Conclusion

The following conclusions can be made: 1) at constant temperature and $u_G$, $tpT^{co}$ required a higher $u_{Lp}$ value with respect to $tpT^{s}$ in constant-throughput operation. 2) $\varepsilon_{Lp}$ at $tpT^{co}$ was higher than $\varepsilon_L$ at $tpT^{s}$ at constant temperature and given $u_G$. 3) shock wave plateau time at $tpT^{co}$ was an increasing function of temperature and $u_G$. 4) $V_p$ and $f_p$ increased with temperature and $u_G$ for both cyclic operation and constant-throughput modes. 5) $V_p$ in

cyclic operation was larger than in constant-throughput mode while the opposite was observed for $f_p$.

## 3.4 References

Aydin, B., Larachi, F., (2005). Trickle bed hydrodynamics and flow regime transition at elevated temperature for a Newtonian and a non-Newtonian liquid. Chemical Engineering Science, 60, 6687-6701.

Boelhouwer, J. G., Piepers, H. W., Drinkenburg, A. A. H., (2002a). Advantages of forced non-steady operated trickle-bed reactors. Chemical Engineering and Technology, 25, 647-650.

Boelhouwer, J. G., Piepers, H. W., Drinkenburg, A. A. H., (2002b). Liquid-induced pulsing flow in trickle-bed reactors. Chemical Engineering Science, 57, 3387-3399.

Giakoumakis, D., Kostoglou, M., Karabelas, A. J., (2005). Induced pulsing in trickle beds—characteristics and attenuation of pulses. Chemical Engineering Science, 60, 5183-5197.

Gupta, R., (1985). Pulsed flow vapour-liquid reactor. US Pat. 4, 526, 757.

Haure, P. M., Hudgins, R. R., Silveston, P. L., (1989). Periodic operation of a trickle-bed reactor. AIChE Journal, 35, 1437-1444.

Larachi, F., Laurent, A., Wild, G., Midoux, N., (1993). Effet de la Pression sur la Transition Ruisselant-Pulsé dans les Réacteurs Catalytiques à Lit Fixe Arrosé. The Canadian Journal of Chemical Engineering, 71, 319-321.

Larachi, F., Iliuta, I., Chen, M., Grandjean, B. P. A., (1999). Onset of pulsing in trickle beds: evaluation of current tools and state-of-the-art correlation. The Canadian Journal of Chemical Engineering, 77, 751-758.

Xiao, Q., Cheng, Z. M., Jiang, Z. X., Anter, A. M., Yuan, W. K., (2001). Hydrodynamic behavior of a trickle bed reactor under forced pulsing flow. Chemical Engineering Science, 56, 1189-1195.

# Chapter 4

# Flow regime transition and hydrodynamics of slow-mode liquid-induced pulsing at elevated temperature for (non-) Newtonian liquids*

## Résumé

Les effets de la température et de la pression sur la structure de la transition de régime d'écoulement ruisselant-pulsé en mode cyclique dans les réacteurs type « trickle bed » ont été analysés. La relation entre rétention et débit de liquide à la transition de régime en mode cyclique, le comportement de l'onde en fonction de la hauteur de lit, ainsi que les propriétés du régime d'écoulement pulsé ont été étudiés pour les systèmes newtonien (air-eau) et non-newtonien (air - 0,25% carboxymethylcellulose (CMC)). À une température donnée, les temps de percée, de plateau et de décroissance de l'onde diminuent avec la hauteur du lit. La vitesse et la fréquence de la pulsation en régime pulsé tant en mode cyclique qu'en mode de pulsation naturelle (à débits constants) augmentent avec la température. Toutefois, l'augmentation de la pression dans le réacteur entraîne une augmentation de la fréquence de pulsation accompagnée d'une diminution de sa vitesse. L'analyse de la rétention liquide à la transition pour l'écoulement pulsé naturel (ou spontané) et en mode cyclique a révélé que la rétention liquide diminue avec la température et la pression. La rétention liquide et la vitesse superficielle du liquide à la transition en mode cyclique symétrique excèdent celles en opération à débit constant pour une température, pression et vitesse de gaz données. Ce qui donne accès à une plus large zone de fonctionnement en régime d'écoulement ruisselant en mode cyclique. Le comportement des deux systèmes étudiés (newtonien et non-newtonien) est similaire en ce qui concerne l'effet de la température, de la pression et de la vitesse de gaz.

* Aydin, B.; Larachi, F. Chemical Engineering Science, accepted

## Abstract

The effects of temperature and pressure on the structure of the trickle-to-pulse flow regime transition in slow-mode cyclic operation in trickle-bed reactors were reported. The relationship between liquid holdup and liquid velocities at the trickle-to-pulse flow transition in cyclic operation, the shock wave behavior as a function of bed depth, as well as the pulsing flow regime properties were investigated for Newtonian (air-water) and non-Newtonian (air-0.25% Carboxymethylcellulose (CMC)) liquids. At a given temperature, the breakthrough, plateau and decay times of the shock wave were found to decrease with bed depth. The pulse velocity and pulse frequency for pulsing flow regime both in cyclic operation and in natural pulsing (constant-throughput operation) were observed to increase with temperature. However, increasing the reactor pressure led to increased pulse frequency and decreased pulse velocity. Analysis of the transition liquid holdups for natural pulse flow and cyclic operation revealed that liquid holdup decreased with temperature and pressure. The transition liquid holdups and superficial liquid pulse velocities in symmetric peak-base cyclic operation surpassed those in constant-throughput operation for given temperature, pressure and gas velocity, giving rise to wider trickle flow regime area in cyclic operation. The behavior of both Newtonian and power-law non-Newtonian fluids was similar regarding the effect of temperature, pressure and gas velocity.


**Keywords** Trickle bed, elevated temperature, induced pulsing, transition boundary

## 4.1 Introduction

The concept of unsteady state operation to promote process performances can be traced back to the 1960s under the designation of parametric pumping. Initially concerned with heat exchanger and stirred tank studies, it expanded to comprise thermal cycling and flow reversal to overcome equilibrium constraints or to improve energy efficiency in various systems such as fractionators, adsorbers, regenerators, and ion exchangers (Dudukovic et al., 2002). The advent of unsteady state operation in trickle-bed reactors (TBRs) is more recent and probably associated to Gupta's (1985) patented application to pulse liquid feeds

for replenishing the wetting environment of catalyst particles in large-diameter and shallow-height trickle flow reactors for overcoming catalyst under-utilization and partial wetting. Though cyclic operation can be accomplished in various ways, such as modulation of flow, composition and activity (Dudukovic et al., 2002), the former policy, especially liquid flow modulation, has been witnessing a remarkable effervescence in the academic literature over the past few years. Liquid flow modulation was recommended as it allows more degrees of freedom in tuning the gas-to-liquid reactant concentration ratio on the catalyst surface and in controlling, *via* wetting efficiency, the reactor thermal behavior (Gupta, 1985).

Early systematic investigations informing about potential benefits of cyclic operation in TBRs for catalytic reactions can be traced back to Lange et al. (1987) and Haure et al. (1989). The model reactions studied were $\alpha$-methylstyrene hydrogenation and sulfur dioxide oxidation. Lange et al. (1987, 1994) noted a 10% increase in the time-average conversion by periodic operation for $\alpha$-methylstyrene catalytic hydrogenation whereas Haure et al. (1989) observed a palpable increase in $SO_2$ oxidation rate during periodic operation for a wide range of cycle periods. Lee et al. (1995) studied the effect of period, split and liquid flow rate and obtained up to 98 % $SO_2$ removal. Castellari and Haure (1995) reported a fourfold increase in reaction rate when optimum split and period values were selected. Improvements in conversion were also reported for the same reaction by Urseanu et al. (2004) in periodic operation and Banchero et al. (2004) in on-off fast liquid flow modulation. Khadilkar et al. (1999) studied liquid flow modulation in gas and liquid reactant-limited conditions. Performance enhancement was reported for gas-limited reactions with on-off flow modulation, while for liquid-limited reactions enhancement was observed with base-peak flow modulation at low mean liquid rates. Gas and liquid flow modulation was also tested by Turco et al. (2001). If improvement in reactor performance went unnoticed during gas flow modulation; liquid flow modulation on the contrary contributed to an increase in performance. This improvement was ascribed to the formation of foams in the foaming-pulsing flow during high-liquid flow rate period which were transferred to trickling regime during low liquid flow rate. Stradiotto et al. (1999) investigated the conversion and consumption rate for crotonaldehyde hydrogenation under on-off liquid flow modulation and in steady-state experiments. They observed that high

liquid flow rates brought no improvement during periodic operation contrarily to low liquid flow rates where up to 50% increase in crotonaldehyde consumption was observed. Tukac et al. (2003) studying phenol wet oxidation reported a 10% conversion increase under on-off liquid flow modulation. For the same reaction, Massa et al. (2005) reported insignificant effect of periodic operation on conversion despite an improvement in products' distribution. Recently, Muzen et al. (2005) studied the influence of cyclic period and split ratio on the conversion for the oxidation of ethyl and benzyl alcohols during on-off liquid flow modulation. The wet oxidation of ethyl alcohol was ameliorated at high split values whereas an enhancement of benzyl alcohol oxidation was observed at lower split values.

Parallel to the catalytic reaction studies, the effect of periodic operation on TBR hydrodynamics started to be investigated only relatively recently. Xiao et al. (2001) studied the effect of gas-induced pulsing flow on the hydrodynamics of a 0.1 m in diameter TBR, packed with 5 mm glass beads up to a height of 1 m. They observed that more uniform radial and axial liquid distributions are achievable during gas-induced pulsing flow while a significant decrease in liquid holdup during gas-forced input was observed. Boelhouwer et al. (2001) suggested that enlargement of pulsing flow regime and control of pulse frequency in liquid cyclic operation of TBRs could be advantageous for enhancing mass and heat transfer rates and for improving selectivity in catalytic reactions. In another study by the same authors (Boelhouwer et al., 2002), two feed strategies - slow mode and fast mode - were characterized by measuring the shock wave characteristics such as the shock wave velocity, the tail and plateau times, and the pulse frequency and velocity. The rate of decay and duration of tail were found to decrease with increasing superficial liquid base velocity, and to increase with distance from bed top. Borremans et al. (2004) investigated the effect of periodic operation on the liquid flow distribution by using a multi-compartment liquid collector located beneath a 0.3 m diameter column packed with 3 mm glass beads up to a height of 1.3 m. They observed only marginal effects of periodic operation on bed cross-wise liquid flow distribution. Giakoumakis et al. (2005) quantified the extent of pulse attenuation in fast mode cyclic operation and reported the effects of liquid and gas flow rates and liquid feed frequency on the pressure drop, the liquid holdup, and the pulse intensity and velocity. Recently, Bartelmus et al. (2006) studied the trickle-to-induced pulsing flow regime boundary under slow and fast mode cycling for different

systems. The transition boundary was found to shift towards lower mean liquid superficial velocities by choosing appropriate base and pulse superficial velocities and time durations. Trivizadakis et al. (2006) and Trivizadakis and Karabelas (2006) studied the effect of particle shape and size on pulse characteristics and liquid-solid mass transfer during fast mode induced pulsing. They observed lower pulse attenuation rate and spread of local mass transfer coefficients with spherical particles as compared to cylindrical extrudates. Aydin et al. (2006) reported the effects of temperature and pressure on the shock wave characteristics for both Newtonian and non-Newtonian liquids for slow-mode induced pulsing. One of their work's findings concerned the collapse of the bursting pulses with increasing temperatures and pressures which resulted from the reduction of the base and pulse liquid holdup levels, and from the delivery of liquid cargo from pulse to baseline flow with a tendency to flatten the pulses. Borremans et al. (2007) found that the cyclic variation of the liquid mean residence time was a function of split ratio, cycle period, and bed height in liquid-induced pulsing. A new approach of dynamic similarity was proposed based on residence times in constant-throughput and periodically-operated TBRs thought to be more adequate for the interpretation of the chemical conversion data in cyclic operation.

Despite a fast growing body of knowledge on cyclic operation as briefly alluded to above, it appears that some important facets of liquid-induced pulsing as a prospective process intensification strategy for trickle-bed reactors have not been unveiled yet. For example, the hydrodynamics of periodically operated TBR ought to be investigated at elevated temperature and/or pressure conditions to mimic as closely as possible the conditions of numerous industrial applications. There is still a number of unanswered questions about the behavior near these conditions of TBR flow hydrodynamics subject to cyclic operation. In this work, we propose a detailed comparative study of the structure of the transition between trickle and pulse flow regime as well as of the pulse characteristics in cyclic operation and in constant-throughput conditions. More precisely, we propose to assess some of the effects of temperature and pressure, namely, i) the commonality or difference of the ***t***rickle-to-***p***ulsing ***T***ransition between ***c***yclic ***o***peration ($tpT^{co}$) and ***s***pontaneous pulsing ($tpT^{s}$) conditions (*i.e.*, constant-throughput flow), ii) the pulse characteristics (pulse velocity and frequency) of the pulsing flow regime in cyclic operation and in spontaneous conditions, iii) and the shock wave characteristics, *i.e.*, breakthrough time, plateau time,

decay time as a function of bed depth. Three temperature levels (25ºC, 50ºC, 75ºC) and two pressure levels (0.3MPa, 0.7MPa) were explored for air-water and air-0.25%CMC systems.

## 4.2 Experimental Setup

The experimental setup is shown elsewhere (Aydin and Larachi, 2005). Briefly, 3-mm glass beads were used as packing to fill a stainless steel column of 4.8 cm-ID and 107 cm height to yield a bed with 39% porosity. The resulting column-to-particle diameter ratio of 16 was not very far from the criterion $D_c/d_p>20$ recommended for avoiding wall flow maldistribution (Al-Dahhan et al., 1997). Though this ratio was not sufficiently high to completely get rid of such undesirable phenomena, an assessment of the quality of data and the marginal extent of wall flow distribution was checked by Aydin and Larachi (2005) from the matching quality with some literature models and correlations in the constant-throughput operation. During the experiments, air was used as gas phase whereas water or aqueous 0.25 % w/w carboxymethylcellulose (CMC) solution were used as liquid phases. The CMC solution, prepared by dissolving powdered CMC in water at ambient temperature, exhibited an inelastic pseudoplastic rheological behavior which was well represented by means of a simple power-law Ostwald-DeWaele model. The consistency index, $k$, and the power-law index, $n$, were fitted for each temperature after measuring the solution shear stress-shear rate response on an ARES (Advanced Rheometric Expansion System) rheometer in the 0-1000 $s^{-1}$ shear-rate ranges. The power-law parameters are given in Table 4-1.

After the liquid was preheated in the reservoir, it was pumped to the reactor by means of a rotary valve pump through a liquid preheater via a calibrated flowmeter. The line used for liquid feeding from the pump to the preheater consisted of two streams. The first line was used for feeding a continuous liquid flow rate whereas the second line was used to supply a jerked (*i.e.*, on/off) flow rate of prescribed periodicity which was superimposed on the continuous flux to generate the cyclic operation of the liquid feed. Needle valves connected to each line were used to adjust the desired flow rates. For the cyclic operation, an on-off programmable solenoid valve was used. This type of configuration enabled to operate over a wide range of base ($u_{Lb}$) and pulse ($u_{Lp}$) superficial liquid velocities and feed times ($t_p$ and

$t_b$), see Fig. 4-1a. The gas phase was supplied from a compressed air line and sent to the reactor *via* a gas preheater before encountering the liquid at the reactor top.

An electrical conductance technique was employed for the identification of regime transition and investigation of the pulse characteristics in the pulsing flow regime. In order to measure the cross-sectionally averaged liquid holdups along the bed, two probes, each comprised of two ring electrodes, were inserted in the reactor at two bed depths 0.245 m apart. The probes were calibrated using a tracer method which allowed establishment of the needed relationships between the measured liquid holdups and the electrical conductances measured with each probe. Repeatability tests revealed an error of *ca.* 10% on the liquid holdups estimations. The procedure was repeated for different superficial liquid velocities at different constant temperature, pressure and superficial gas velocity values for water and the 0.25 % w/w carboxymethylcellulose (CMC) aqueous solution, see Aydin et al. (2006) for more details. For flow regime identification, the superficial liquid base velocity ($u_{Lb}$) values were selected in the range to *always* correspond to the trickle flow whereas the range for superficial liquid pulse velocity ($u_{Lp}$) was allowed to encompass both the trickle and pulsing flow regimes.

For each given gas superficial velocity ($u_G$), identification of the transition points, $tpT^{co}$ and $tpT^{s}$, consisted in searching the required liquid throughputs, respectively, $u_{Lp}$ in cyclic operation and $u_L$ in constant-throughput mode that demarcated a regime changeover -recall that trickle flow regime is always imposed at the base liquid velocity, $u_{Lb}$-. The trickle-to-pulse flow regime transition points were determined by smoothly increasing the superficial liquid velocities, $u_{Lp}$ or $u_L$, beginning in trickle flow regime. The vertex in the plots as a function $u_{Lp}$ or $u_L$, of the coefficient of variation computed as the standard-deviation-to-mean ratio of the ring-probe conductivity time-series signals (Rode, 1992) was located and assigned to the transition point. The liquid holdup values, $\varepsilon_{Lp}$ and $\varepsilon_L$, corresponding, respectively, to cyclic operation and constant-throughput mode were also measured at the transition points, $tpT^{co}$ and $tpT^{s}$. Once the pulsing flow regime was established, the standard-deviation of the liquid holdup time-series fluctuations, $\sigma_{\varepsilon L}$, around the mean liquid holdup was quantified to allow comparisons between the pulsing flow regimes in cyclic operation and in constant-throughput conditions. The pulse frequency, $f_p$, was determined by counting the number of holdup maxima or minima and dividing by the holdup pulse

period for some selected portions of the liquid holdup time series. In addition, the pulse propagation velocity, $V_p$, was determined by dividing the inter-electrode distance by the time delay of maximum cross-correlation between signals. The cross-correlation function will peak at the time delay equal to the time required for the pulses to move from first to second probe.

For the sake of clarity, a distinction must be made between the pulse velocity $u_{Lp}$ (cyclic operation) and the pulse propagation velocity $V_p$ which characterizes the pulsing flow regime. While the former is clearly identified in Fig. 1a, the latter concerns the speed of the fast-propagating pulses that arise in the pulsing flow regime when $u_{Lp}$ in cyclic operation, or $u_L$ in constant-throughput mode, is high enough.

The induced pulsing characteristics concerned also three morphological features of the dynamic evolution of the pulse liquid holdup: i) the shock-wave breakthrough time, $B_\tau$, which measures the transient time for the liquid holdup to rise from base level to pulse value when the liquid feed rate is tipped up; ii) the decay time, $D_\tau$, corresponds to the time elapsed for the liquid holdup to retrieve back its base level when liquid pulse feed is tipped out; iii) and the shock-wave plateau time, $P_\tau$, which measures the duration, intertwined between the breakthrough and decay times, over which the pulse liquid holdup remains at, or fluctuates around, a constant value. Fig. 1b pictorially sketches each of these parameters.

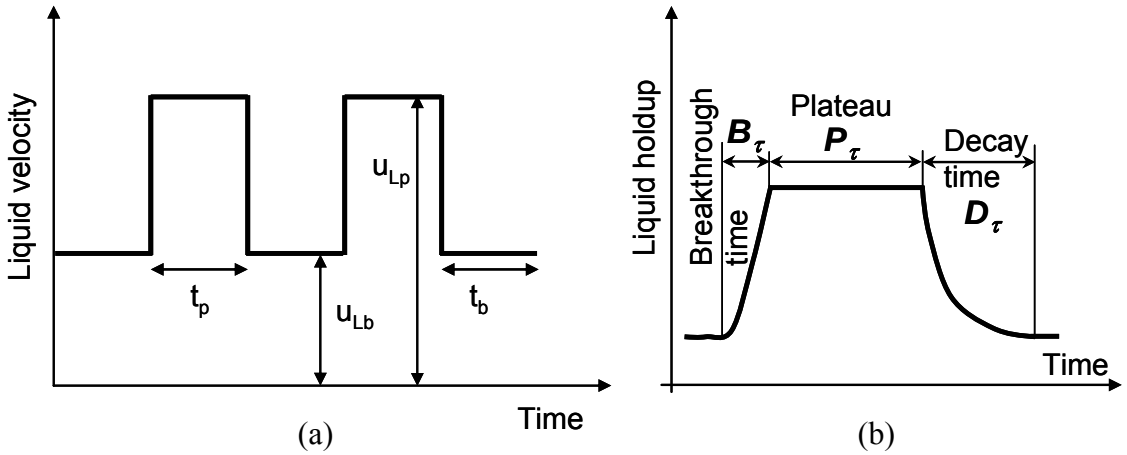


**Figure 4-1** Schematic illustration of the parameters characterizing (a) the square-wave cycled liquid feed. $t_b$ = base liquid feed period, $t_p$ = pulse liquid feed period, $u_{Lb}$ = base superficial liquid velocity, $u_{Lp}$ = pulse superficial liquid velocity, split ratio $S = t_p/(t_p + t_b)$ (b) morphological features of pulse liquid holdup under cycled liquid feed.

## 4.3 Results and Discussion

Table 4-1 displays the physicochemical properties of water, aqueous 0.25%w/w carboxymethyl-cellulose (CMC) solution and air as affected by an increase in temperature from 25ºC to 75ºC and in pressure from 0.3 to 0.7 MPa. The viscosity of both liquids is the most sensitive to temperature where the effective viscosity drop of CMC is expressed with consistency index, *k*, and the power-law index, *n*. The liquid dynamic viscosity reduced by more than a factor two for both liquids, followed by liquid surface tension and liquid density, respectively, dropping by *ca*. 10% and *ca*. 2% between 25ºC and 75ºC. The reactor pressure is most influential on gas density (233% rise from 0.3 to 0.7 MPa) while temperature reduces gas density by 15% and inflates gas dynamic viscosity by 13% over the explored range. Pressure variations as imposed in this study are virtually effectless on the dynamic viscosity of the gas phase. Hence, the hydrodynamic behavior of the trickle bed under slow-mode cyclic operation will be analyzed with respect to changes of liquid viscosity with temperature and of gas density due to reactor pressure.

**Table 4-1** Properties of Water, Aqueous 0.25% wt. CMC solution and Air at Elevated Temperatures and Pressures

| Temperature (ºC) | $\rho_{water}$ # (kg/m3) | $\mu_{water}$ * x $10^4$ (kg/m.s) | $\sigma_{water}$ * ($kg/s^2$) | $k_{CMC}$ $ ($kg/m.s^{2-n}$) | $n_{CMC}$ $ | $\sigma_{CMC}$ ($kg/s^2$) | $\rho_{air}$ * (0.3 MPa) ($kg/m^3$) | $\rho_{air}$ * (0.7 MPa) ($kg/m^3$) | $\mu_{air}$ * x $10^5$ (kg/m.s) |
|---|---|---|---|---|---|---|---|---|---|
| 25 | 997.21 | 8.86 | 0.0720 | 0.072 | 0.666 | 0.056 | 3.49 | 8.15 | 1.84 |
| 50 | 988.22 | 5.36 | 0.0679 | 0.041 | 0.662 | 0.054 | 3.23 | 7.53 | 1.96 |
| 75 | 974.9 | 3.77 | 0.0635 | 0.033 | 0.659 | 0.051 | 2.99 | 6.98 | 2.07 |

*CRC Handbook of tables for Applied Engineering Science (1970)

#CRC Handbook of Chemistry and Physics (1977)

$ consistency index, & power-law index

### 4.3.1 Influence of Temperature and Pressure on Structure of Trickle-to-Pulse Flow Transition

***Transition Liquid Holdup in Cyclic Versus Constant-Throughput Operations*** During all the cyclic operation tests, a split ratio of 50% was imposed for the inlet liquid stream, *i.e.*, symmetric peak-base feed policy. The split ratio is defined as the fractional time $t_p/(t_p + t_b)$ and refers to the lapse of time liquid is fed at pulse velocity $u_{Lp}$. The period values, $t_p + t_b$, were 120 s for the air-water system and 240 s for the air-0.25% CMC system. These corresponded to the slow-mode liquid-rich continuity shock waves when trickle flow prevails both at $u_{Lb}$ and $u_{Lp}$, or slow-mode induced pulsing when trickle flow is imposed at $u_{Lb}$ but pulsing flow regime arises at $u_{Lp}$ (Boelhouwer, 2001). Figs. 4-2a,b exemplify typical liquid holdup time series traces from a conductivity probe embedded deep in the bed at 40 cm for the air-water and air-0.25% CMC systems, respectively. The runs were conducted at 75°C and 0.7 MPa and fixed superficial gas velocity of 0.2 m/s, and the superficial liquid base velocities were, respectively, $u_{Lb}$ = 0.0035 m/s and $u_{Lb}$ = 0.00087 m/s for air-water and air-0.25% CMC. The superficial liquid pulse velocities were progressively increased between $u_{Lp}$ = 0.007 m/s and 0.014 m/s for air-water and $u_{Lp}$ = 0.0035 m/s and 0.007 m/s for air-0.25% CMC to cross over the trickle-to-pulse flow regime transition point. These conditions permitted to evolve the trickle bed from liquid-rich continuity shock waves with trickle flow regime in both base and pulse sequences at low $u_{Lp}$ values. The trickle flow regime was supplanted for high enough $u_{Lp}$ by a pulsing flow regime in the pulse sequence as is visible from the holdup time series of Figs. 4-2a,b.

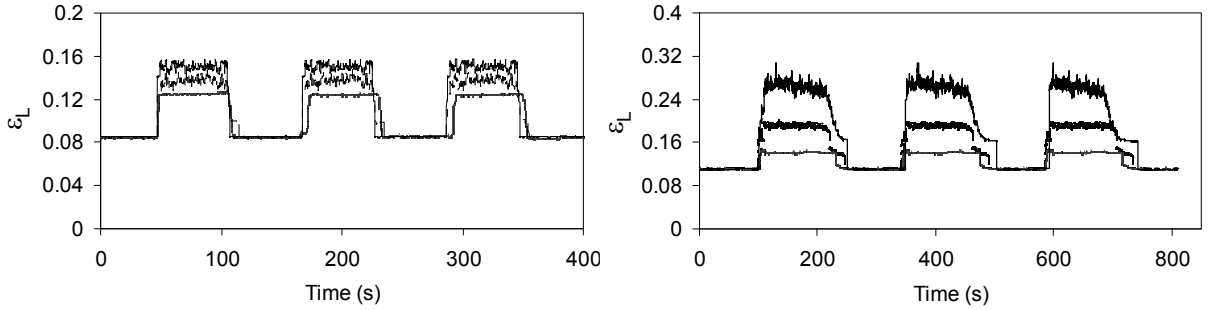


(a) (b)

**Figure 4-2** Examples of liquid holdup time series traces during induced pulsing flow, $T_r$ = 75°C, $P_r$ = 0.7 MPa, $u_G$ = 0.2 m/s. (a) Air-water system, $u_{Lb}$ = 0.0035 m/s, $u_{Lp}$ = 0.007 - 0.014 m/s, $t_b$ = 60 s, $t_p$ = 60 s; (b) air-0.25%CMC system, $u_{Lb}$ = 0.00087 m/s, $u_{Lp}$ = 0.0035 - 0.007 m/s, $t_b$ = 120 s, $t_p$ = 120 s.

Figs. 4-3a,b show the effect of reactor temperature ($T_r$), pressure ($P_r$) and superficial gas velocity ($u_G$) on the liquid holdup at the transition points, $tpT^s$ and $tpT^{co}$, for the air-water (Fig. 4-3a) and the air-0.25% CMC (Fig. 4-3b) systems. Recall that the superscripts "s" and "co" refer, respectively, to spontaneous and to cyclic operation. Unless otherwise stated, the liquid holdup time series that were analyzed corresponded to measurements made with the ring electrodes embedded 40 cm from the bed top.

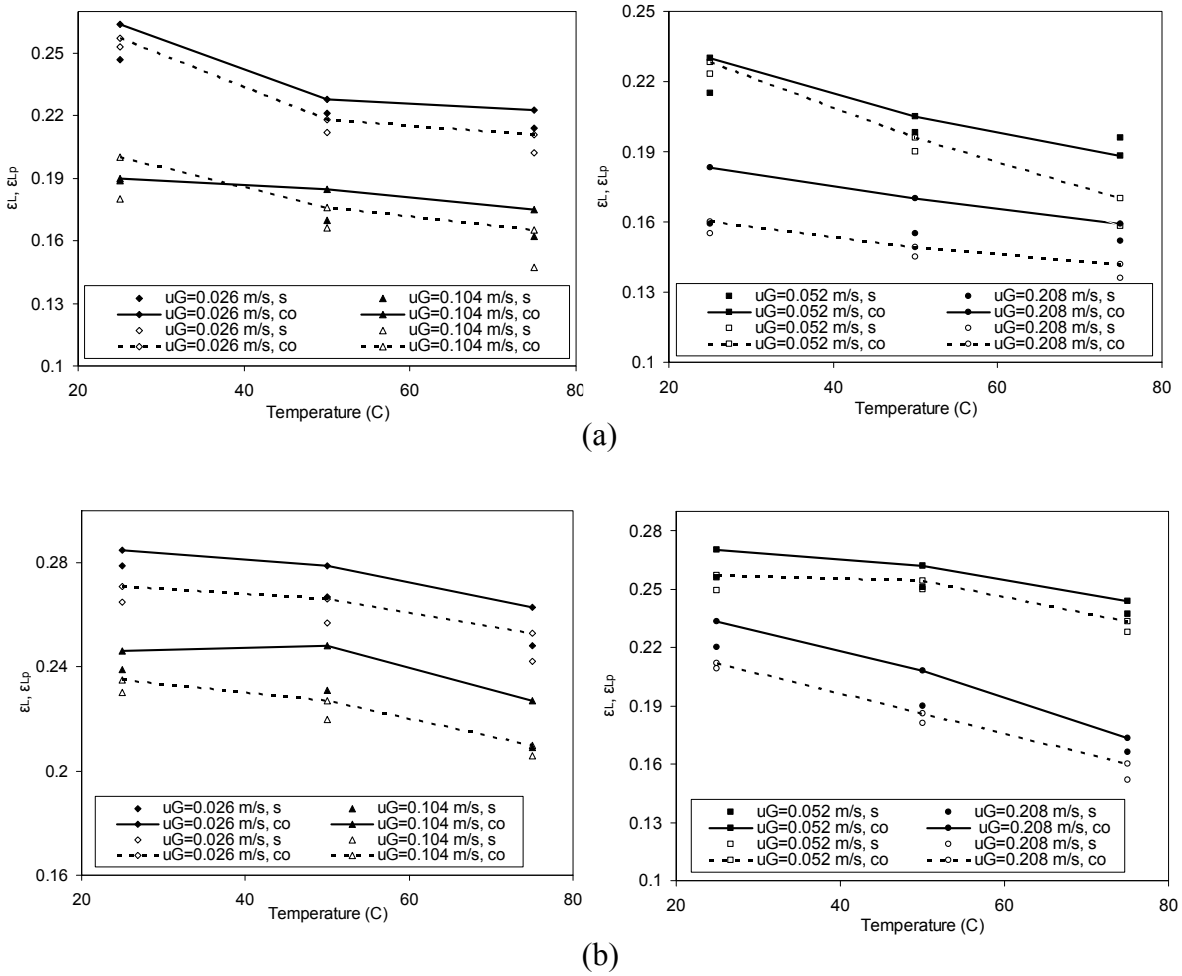


**Figure 4-3** Effect of temperature, pressure and superficial gas velocity on liquid holdup at $tpT^{s}$ and $tpT^{co}$ transition points. (a) air-water system, $u_{Lb}$ = 0.007 m/s, (b) air-0.25% CMC system, $u_{Lb}$ = 0.00175 m/s. Filled symbols represent data for $P_r$ = 0.3 MPa, empty symbols represent data for $P_r$ = 0.7 MPa, and (solid and dotted) lines differentiate co = cyclic operation from s = spontaneous pulsing data. The $tpT^{co}$ corresponds to trickle-to-pulse transition at $u_{Lp}$.

For the air-0.25%CMC system, the liquid holdup values $\varepsilon_L$ at $tpT^{s}$ and $\varepsilon_{Lp}$ at $tpT^{co}$ are larger than those corresponding to the air-water system. As a general rule, the differences between the transition liquid holdup values, $\varepsilon_L$ and $\varepsilon_{Lp}$, appear to be more remarkable for the air-0.25%CMC system.

The liquid holdups, $\varepsilon_L$ at $tpT^{s}$ and $\varepsilon_{Lp}$ at $tpT^{co}$, diminish, irrespective of the liquids, with an increase in temperature at given $u_G$ and $P_r$ values. This can be attributed to the liquid viscosity greater sensitivity to temperature, which amongst the physical gas and liquid properties, is the one that experiences the largest reduction when temperature rises from

ambient to 75 °C as evidenced also by Aydin and Larachi (2005) during the constant-throughput tests in trickle and pulsing flow regimes. This finding is also in agreement with literature studies on the evolution of flow regime transition with liquid viscosity in constant-throughput TBR experimentations and ambient temperature (Hasseni et al., 1987; Sai and Varma, 1988; Wammes et al., 1990; Iliuta and Thyrion, 1997; Larachi et al., 1998). At a constant temperature, on the other hand, the liquid holdups, whether at $tpT^{s}$ or at $tpT^{co}$, generally decrease with increasing $P_r$ and $u_G$ for both tested systems, see for instance arrangement of the solid lines relative to the dotted lines in cyclic operation in Figs. 4-3a,b. Such reduction in liquid holdup can be rationalized considering that the drag force at the gas-liquid interface acting as a driving force on the liquid phase increases with gas inertia *via* gas density and/or gas velocity thus occasioning shorter liquid residence time or lower liquid holdup (Wammes and Westerterp, 1990). In general, the influence of pressure in the 0.3 - 0.7 MPa range is less remarkable for $\varepsilon_L$ at $tpT^{s}$ than for $\varepsilon_{Lp}$ at $tpT^{co}$. There is however some scatter on the pressure dependency of the transition liquid holdup, particularly at the lowest gas superficial velocities, *e.g.*, air-water in cyclic operation for $u_G$ = 2.6 cm/s and in constant-throughput for $u_G$ = 2.6 cm/s and 5.2 cm/s, where in effect the gas inertia is the lowest and thus of lesser influence on the interfacial gas-liquid shear stress and in return on liquid holdup. These data in particular fall close to "case II" classification for pressure and gas velocity ranges of Al-Dahhan et al. (1997) depicting a domain corresponding to marginal effect of pressure on TBR hydrodynamics.

For a given ($T_r$, $P_r$, $u_G$) set the pulse liquid holdup value, $\varepsilon_{Lp}$, at which the trickle-to-pulse flow regime transition occurs exceeds, almost systematically, the liquid holdup counterpart, $\varepsilon_L$, at the verge of the pulsing flow regime in the constant-throughput case (Figs. 4-3a,b). This means that for a given gas/liquid/solid system, the transition from trickle to pulse flow in slow-mode cyclic operation cannot be unequivocally determined only from a knowledge of $T_r$, $P_r$ and $u_G$. This transition also depends on the cyclic operation parameters such as the superficial liquid base velocity, $u_{Lb}$, and the cycle period and split ratio though the influence of this latter tends to vanish at the approach of the symmetric split as proven by Boelhouwer et al. (2001). The observation arising from Figs. 4-3a,b leans towards sustainability of a more *stable* trickle flow regime at the superficial liquid pulse velocity, $u_{Lp}$, considering the noticeably greater transition liquid holdup prevailing there. This

difference in holdups can be ascribed, as will be next seen, to regime changeover taking place at relatively larger values of $u_{Lp}$ as opposed to $u_L$ despite identical $T_r$, $P_r$ and $u_G$; and because instabilities in the pulsing flow regime during the $u_{Lp}$ segments are in all likelihood influenced by the intermittence between base flow segments at $u_{Lb}$ with those at $u_{Lp}$. Such spatially patterned juxtaposition along the bed is believed to provide as many "containment" zones corresponding to $u_{Lb}$, intertwined between as many pulse sequences corresponding to $u_{Lp}$, to help retarding the inception and growth of the instabilities characterizing the pulsing flow regime.

***Transition Liquid Velocities in Cyclic Versus Constant-Throughput Operations***

Boelhouwer et al. (1999) along with others (Bartelmus et al., 2006; Trivizadakis and Karabelas, 2006) found that the $u_G$ *versus* $u_L$ domain relevant to the trickle flow regime retracts in cyclic operation with respect to that in constant-throughput. They reported that for an equal superficial gas velocity, the trickle-to-pulse flow regime transition happens at a lower superficial liquid *average* velocity in cyclic operation than that to be required to trigger spontaneous pulsing. This was portrayed as a significant achievement at inducing pulses, and thus at intensifying the process, in regions normally forbidden to pulse spontaneously had the TBR been operated in constant-throughput mode at the same liquid average velocity. Though Boelhouwer et al. (1999) did not clearly mention how their average velocity was computed, cross-checking their transition map Fig. 12 with Fig. 13 (Boelhouwer et al., 2001) suggests that their average velocities were *barycentric*, *i.e.*, $u_L = (t_p \times u_{Lp} + t_b \times u_{Lb})/(t_p + t_b)$. Trivizadakis and Karabelas (2006) studying the TBR hydrodynamics in ON-OFF cyclic operation adopted the same definition to locate their so-called pseudo-transition boundary which signals inception of pulsing during the ON feed half-period. By recasting the transition line (a') in cyclic operation in Fig. 2 of Trivizadakis and Karabelas (2006) from liquid average mass fluxes to their corresponding $u_{Lp}$ values, we found that this line collapsed nearly at the identical with the transition line (a) corresponding to spontaneous pulsing. Therefore, this might question whether or not it is possible that the spectacular character of inducing pulses in cyclic operation would in a large part be ascribed to an inadequate representational variable. Though the choice of the barycentric velocity for interpreting the transition data in cyclic operation seems in appearance appropriate as it embeds both $u_{Lp}$ and the split ratio, $t_p/(t_p + t_b)$; it nonetheless

disguises the effect of the superficial liquid base velocity, $u_{Lb}$, which always has been stated to correspond to the trickle flow regime. Another conflicting experimental fact acknowledged in several experimental studies that questions premature inception of induced pulses in cyclic operation is that shock waves, while possessing their full potency in the top sections of the reactor, progressively decay while moving down the column by leaving liquid behind their tail. This effect is conducive to eroding the shock wave plateaus which become progressively torn off and eventually fade away at the approach of the bed exit should TBRs be enough tall (Boelhouwer et al., 2002; Aydin et al. 2006). Ultimately, induced pulsing could be supplanted by a *smoothed out* continuous-flow TBR operation that would take over at a constant liquid velocity equal to the barycentric velocity. In this instance, bearing in mind that pulsations usually are initiated close to bed exit and then fill up backwards the entirety of the column by increasing fluid throughputs, it is unlikely for the barycentric velocity to trigger *spontaneous* pulse flow had it been less than the $u_L$ required to attain the transition locus in a $u_G$ *versus* $u_L$ transition plot.

This analysis points to the necessity to reconsider data interpretation for the presumed induced pulsing in cyclic operation. A more pertinent comparison of the transition points would have been to invoke directly the liquid velocity during the $u_{Lp}$ segment with regard to the liquid velocity $u_L$ in constant-throughput operation before to analyze any differences between cyclic and constant-throughput operations.

This is indeed what is adopted in Figs. 4-4a,b which are complementary plots to Figs. 4-3a,b, respectively. They illustrate the effects of temperature, pressure and gas superficial velocity on the liquid superficial velocities, $u_L$ and $u_{Lp}$, at the transition points, $tpT^s$ and $tpT^{co}$, respectively, for both the air-water (Fig. 4-4a) and the air-0.25% CMC (Fig. 4-4b) systems. As can be seen, at given $u_G$ and $P_r$, the liquid velocities at the trickle-to-pulsing transition, $u_{Lp}$ and $u_L$, increase with increasing reactor temperature. This result is coherent with the liquid viscosity drop-off that would require increasing the liquid superficial velocity to bring the pulsing flow regime with increasingly temperatures. Liquid viscosity, as seen in Fig. 4-4b, also occasions the transition points, $tpT^s$ and $tpT^{co}$, to occur at liquid velocities lower for the air-0.25%CMC system than for the air-water system. Increasing reactor pressure likewise entrains the liquid holdups $\varepsilon_{Lp}$ and $\varepsilon_L$ to decrease (Figs. 4-3a,b)

necessitating, as for the temperature effect, larger liquid superficial velocities, respectively, $u_{Lp}$ and $u_L$, to approach the pulsing flow regime at higher pressure.

Figs. 4-4a,b reveal the necessity for a superficial liquid pulse velocity $u_{Lp}$ in cyclic operation larger than the $u_L$ required in the constant-throughput mode to allow a shift of flow regime from trickle to pulsing for a given set $u_G$, $T_r$ and $P_r$ for both tested systems. This finding takes the opposite course to the convention of plotting the transition points as a function of the liquid barycentric velocity (Boelhouwer et al., 1999; Bartelmus et al., 2006; Trivizadakis and Karabelas, 2006) instead of the pulse velocity which is chiefly responsible for any regime changeover.

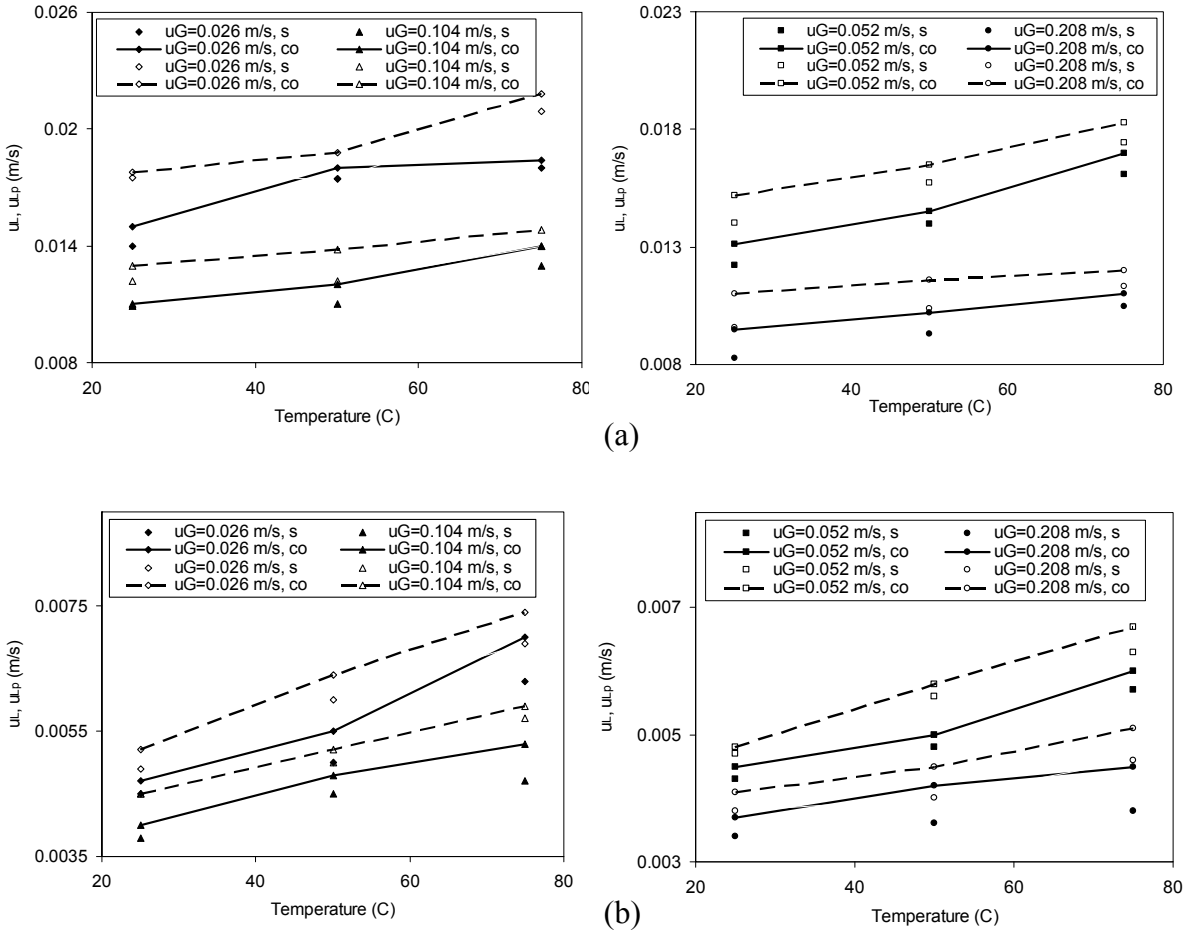


**Figure 4-4** Effect of temperature, pressure and superficial gas velocity on superficial liquid velocity at $tpT^{s}$ and $tpT^{co}$ transition points. (a) air-water system, $u_{Lb}$ = 0.007 m/s, (b) air-0.25% CMC system, $u_{Lb}$ = 0.00175 m/s. Filled symbols represent data for $P_r$ = 0.3 MPa, empty symbols represent data for $P_r$ = 0.7 MPa, and (solid and dotted) lines differentiate co = cyclic operation from s = spontaneous pulsing data. The $tpT^{co}$ corresponds to trickle-to-pulse transition at $u_{Lp}$.

The frequency of slow-mode cyclic operation (*ca*. 4 to 8 mHz) is typically 2 to 3 orders of magnitude lower than the frequency of the pulses, usually a few Hz (to be discussed later with Fig. 4-7) that would enliven the pulsing flow regime at $u_{Lp}$. It is however impossible to state that the pulses that emerge during the pulsing flow regime in cyclic operation are incognizant of the cyclic operation frequency since the cycle period was not changed in our study. In addition, had the pulse sequences subject to $u_{Lp}$ feed been completely isolated vis-à-vis the alternating base sequences being subject to $u_{Lb}$ irrigation, cyclic operation would have been reduced to mere juxtaposition of non-interacting sequences of two continuous-flow hydrodynamic states. Under such instances, there would be no reason that $u_{Lp}$ and $\varepsilon_{Lp}$ at $tpT^{co}$ be different from $u_L$ and $\varepsilon_L$ at $tpT^{s}$. This is exactly what Figs. 4-3a,b and 4-4a,b, do not show suggesting that the structure of the transition differs between the cyclic and the constant-throughput operations.

The effect of temperature and superficial gas velocity on the normalized shock wave plateau time (see its definition in Fig. 4-1b) at $tpT^{co}$ for the two gas-liquid systems is plotted in Figs. 4-5a,b. The normalized plateau time is expressed as the ratio of the shock wave plateau time at $tpT^{co}$ to that imposed at the reactor entrance, *i.e.*, 60 s and 120 s for air-water and air-0.25%CMC systems, respectively. The plateau time increases with increasing temperature and pressure for both systems (Figs. 4-5a,b). It is interesting to observe that the normalized plateau times, corresponding to signals acquired at 40 cm bed depth, remain systematically lower than unity; in line with the erosion of the square-shaped pulses imposed at the reactor entrance (Fig. 4-1a). As discussed in Aydin et al. (2006), with increased temperature and/or pressure, the pulse holdup was found to decrease due to two factors: in the one hand, due to the intrinsic reduction of liquid holdup with pressure and temperature as already noted in constant-throughput experimentations (Aydin and Larachi, 2005), and in the other hand, due to the transfer of some liquid from the pulse to the base flow by virtue of the non-isolated nature of pulses. The latter factor has the tendency to flatten the pulses, despite $P_\tau/P_\tau^0$ is always <1, so that the shock wave plateau time at $tpT^{co}$ increases with temperature, pressure and superficial gas velocity, where the influence of the latter is more pronounced the higher the pressure.

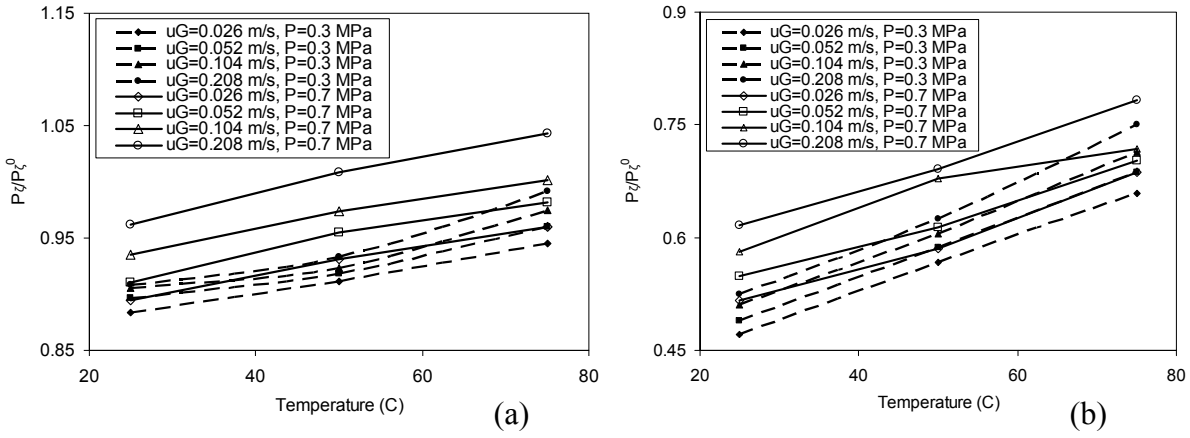


**Figure 4-5** Influence of temperature, pressure and superficial gas velocity on shock wave plateau time at $tpT^{co}$ (a) air-water system, $u_{Lb}$ = 0.007 m/s, (b) air-0.25% CMC system, $u_{Lb}$ = 0.00175 m/s. Filled symbols represent data for $P_r$ = 0.3 MPa, empty symbols represent data for $P_r$ = 0.7 MPa.

### 4.3.2 Influence of Temperature and Pressure on Pulse Characteristics

***Pulse Velocity*** A basic characteristics of pulsing flow regime is the pulse velocity which was determined at elevated pressure and temperature as explained in the Experimental section above. Figs. 6a,b illustrate the effect of temperature, pressure and superficial gas velocity on the pulse velocity, $V_p$, in cyclic operation and in constant-throughput mode, respectively, for the air-water and the air-0.25% CMC systems. Note that the runs were conducted at an equal value for the superficial liquid velocity in constant-throughput operation and for the superficial liquid pulse velocity in cyclic operation, *i.e.*, $u_L = u_{Lp}$ = 0.0192 m/s for air-water and $u_L = u_{Lp}$ = 0.007 m/s for air-0.25% CMC.

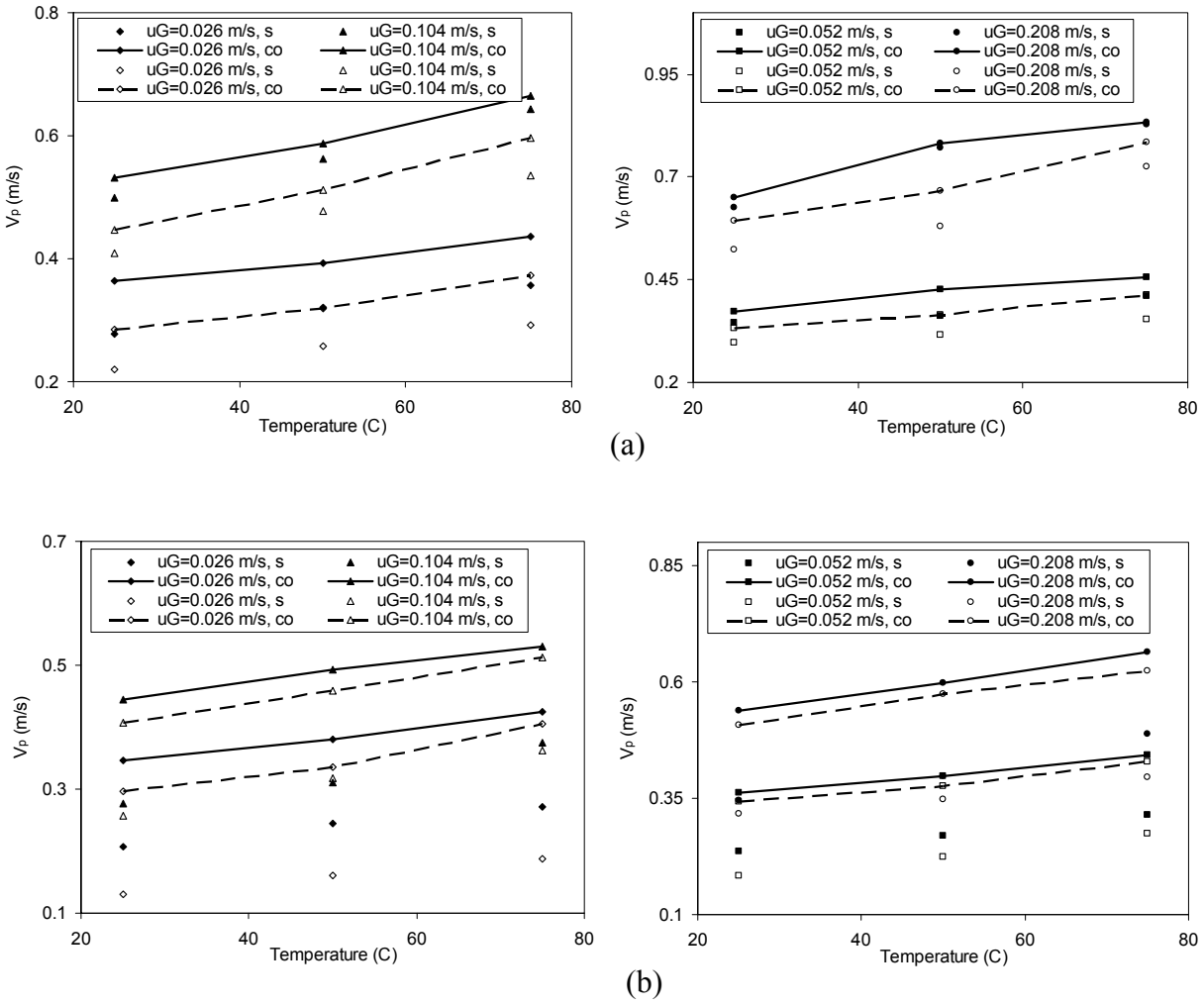


**Figure 4-6** Effect of temperature, pressure and superficial gas velocity on pulse velocity for constant throughput (s) and cyclic operation (co) -solid and dotted line interpolations- for (a) air-water system, $u_{Lb}$ = 0.007 m/s, $u_L$ and $u_{Lp}$ = 0.0192 m/s, (b) air-0.25% CMC system, $u_{Lb}$ = 0.00175 m/s, $u_L$ and $u_{Lp}$ = 0.007 m/s. Filled symbols represent data for $P_r$ = 0.3 MPa, empty symbols are for $P_r$ = 0.7 MPa.

The pulse velocity decreases with increasing pressure in accordance with Burghardt et al. (2004) and Aydin and Larachi (2005) experimental findings for constant-throughput TBRs. The same pressure dependence for $V_p$ holds in cyclic operation as shown in Figs. 4-6a,b. The liquid holdup also decreases with increasing reactor pressure, everything else being identical, pointing to an increase in interstitial liquid velocity which cannot explain in intuitive terms the reduction of pulse velocity. However, a physical picture in which the amplitude of liquid holdup fluctuations around their mean value in pulsing flow regime is

allowed to increase with pressure would turn to be coherent with this trend as high-amplitude pulses can carry more material without recourse to faster pulses. Another coherent scenario would be that even pulses are slowed down with pressure, their number density per unit time can be increased to have higher pulse frequencies, $f_p$. As will be seen, both events took place. In the other hand, the increase with temperature and superficial gas velocity of pulse velocity may be ascribed to increasing indeed the interstitial liquid velocity due to decreasing liquid holdup.

Figs. 4-6a,b reveal that pulse velocity in cyclic operation was higher than in constant-throughput operation, irrespective of temperature and pressure provided $u_L$ and $u_{Lp}$ are the same. This can easily be understood by bearing in mind that constant-throughput liquid holdup $\varepsilon_L$ at $u_L$ is always larger than the $\varepsilon_{Lp}$ corresponding to $u_{Lp}$ (= $u_L$) in cyclic operation because of the non-isolated nature of pulses discharging a fraction of their cargo onto the baseline flow at $u_{Lb}$ (Aydin et al., 2006). This state of affairs gives rise, for identical pressure and temperature, to larger liquid interstitial velocities in cyclic operation and presumably larger pulse velocities.

The pulse velocity for air-0.25%CMC system also increases monotonically with temperature whereas the effect of pressure is less pronounced compared to the air-water system. Despite the contrasts between pulse velocities in cyclic and constant-throughput operations are more dramatic in highly viscous systems, the higher liquid holdups in these latter systems yield much lower interstitial velocities compared to air-water system, and correspondingly much lower pulse velocities.

***Pulse Frequency*** Figs. 4-7a,b indicate that the pulse frequency, $f_p$, slightly increases with temperature whereas its increase with pressure is more noticeable for both the air-water and the air-0.25%CMC systems, irrespective of the operation type, *i.e.*, whether cyclic or constant-throughput. The pulse frequency for the air-water system is larger than that for the air-0.25%CMC system. At constant temperature and pressure, the pulse frequency also increases with the superficial gas velocity where during cyclic operation its effect is more pronounced for the air-water system than for the air-0.25%CMC system. The effect of gas velocity on the pulse frequency is coherent with literature findings where an outgrowth in the number of pulses with increasing gas velocity in pulsing flow regime was reported in ambient conditions experiments (Anadon et al., 2006). For a given assortment ($T_r$, $P_r$, $u_G$,

$u_L$=$u_{Lp}$), the pulse frequency during cyclic operation was found to be systematically less than during constant-throughput. The finding is coherent with the faster pulses detected in cyclic operation as discussed above (Figs. 4-6a,b).

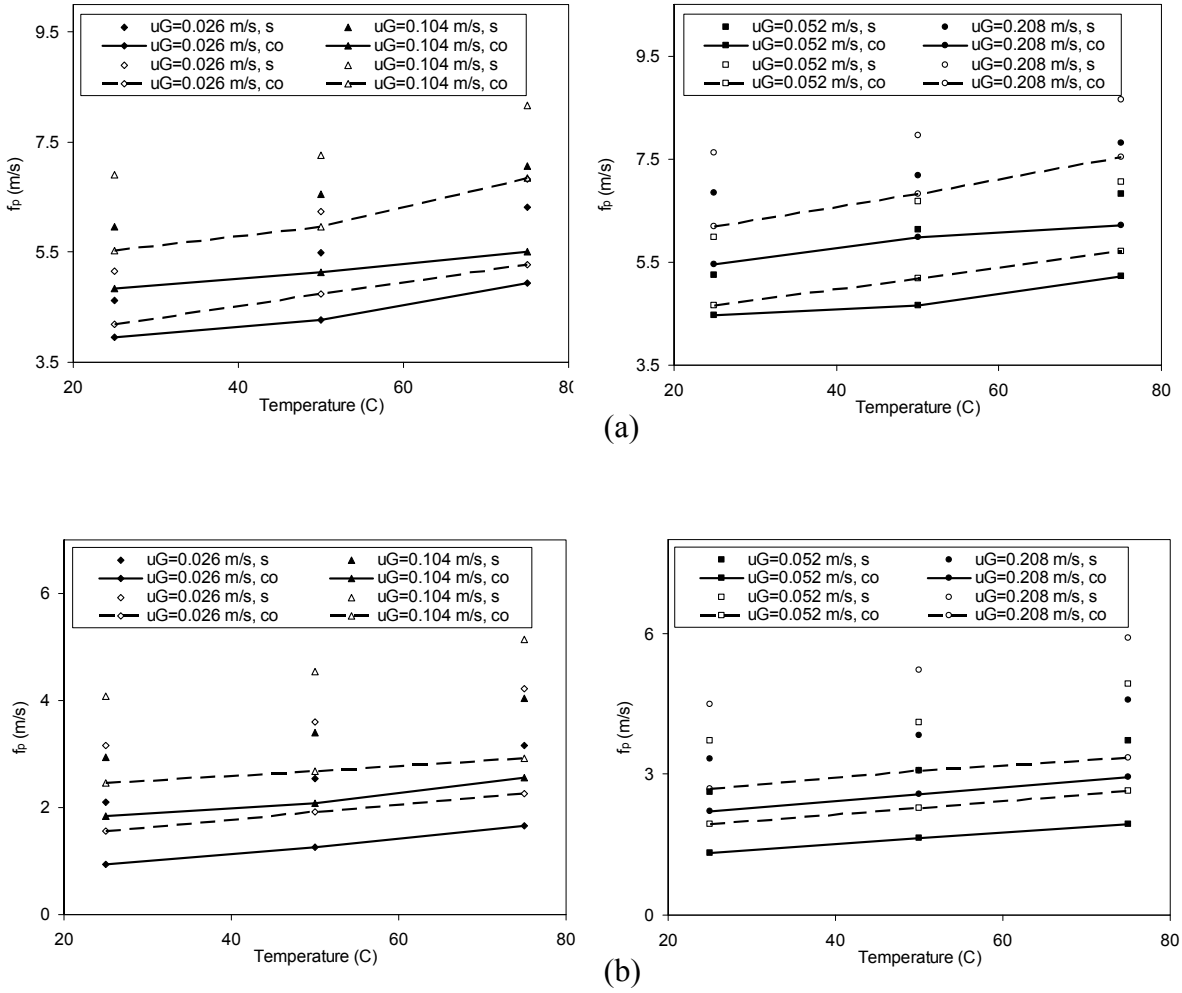


**Figure 4-7** Effect of temperature, pressure and superficial gas velocity on pulse frequency for constant-throughput (s) and cyclic operation (co) -solid and dotted line interpolations- for (a) air-water system, $u_{Lb}$ = 0.007 m/s, $u_L$ and $u_{Lp}$ = 0.0192 m/s, (b) air-0.25% CMC system, $u_{Lb}$ = 0.00175 m/s, $u_L$ and $u_{Lp}$ = 0.007 m/s. Filled symbols represent data for $P_r$ = 0.3 MPa, empty symbols are for $P_r$ = 0.7 MPa.

***Liquid Holdup Standard-Deviation in Pulsing Flow*** In terms of fluctuating behavior of the liquid holdup time series obtained for both types of operations, it was observed that the standard deviation of the fluctuating liquid holdups for the spontaneous pulse flow was more pronounced than that for the cyclic operation at given temperature, pressure and

superficial gas and liquid ($u_L = u_{Lp}$) velocities for both systems (Figs. 4-8a,b). This behavior is compatible with the lower liquid holdup prevailing in cyclic operation as explained earlier. As a general trend, the liquid holdup standard-deviation was found to decrease with increasingly temperatures whereas it increased with pressure. The increase of liquid holdup standard-deviation as pressure increased provides *post-facto* confirmation to our previous speculation regarding the decrease of pulse velocity, $V_p$, with increasing pressure. For both systems, the standard-deviation of the fluctuating liquid holdups increased with increasing superficial gas velocity, with more drastic effects for air-0.25%CMC system.

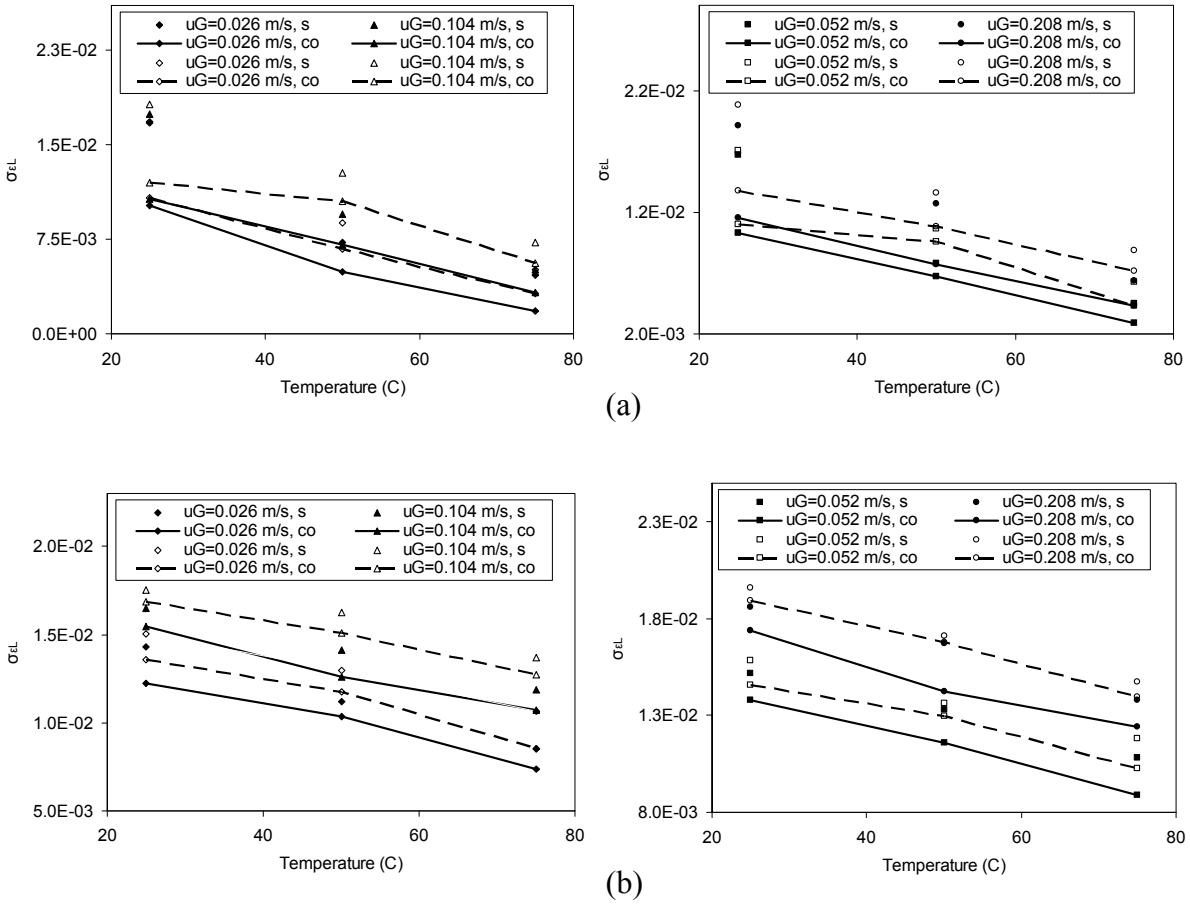


**Figure 4-8** Influence of temperature, pressure and superficial gas velocity on liquid holdup standard deviation for the spontaneous pulse flow (s) and cyclic operation (co) -solid and dotted line interpolations- for (a) air-water system, $u_{Lb}$ = 0.007 m/s, $u_L$ and $u_{Lp}$ = 0.0192 m/s, (b) air-0.25% CMC system, $u_{Lb}$ = 0.00175 m/s, $u_L$ and $u_{Lp}$ = 0.007 m/s. Filled symbols represent data for $P_r$ = 0.3 MPa, empty symbols represent data for $P_r$ = 0.7 MPa.

### 4.3.3 Fate of Shock Wave Characteristics with Bed Depth

In Figs. 4-9a,b, the shock wave breakthrough time, $B_\tau$, at two bed depths (40 and 64.5 cm) is shown for constant gas, and base and pulse superficial liquid velocities at different reactor temperatures and pressures for both air-water and the air-0.25% CMC systems. At constant reactor temperature and pressure, the shock wave breakthrough time decreases with bed height, especially in the case of the less viscous air-water system. This could be explained with the transfer of some amount of liquid from pulse to base which flattens the waves as they move down the bed. At a given axial position in the reactor, the shock wave breakthrough time decreases with increasingly temperature and pressure with a more prominent effect for highly viscous systems (Aydin et al., 2006). Figs. 4-10a,b illustrate the diminution of the plateau time, $P_\tau$, as the shock waves move along the bed at various temperatures and pressures and constant superficial gas, and base and pulse liquid velocities for both systems. The same tendency was also observed for the shock wave decay time, $D_\tau$, though this attenuation with bed depth was pretty slim for the air-0.25% CMC system (Figs. 4-11a,b). The shock wave plateau time was found to increase with temperature and pressure, whereas, on the contrary, the shock wave decay time decreased with increased temperature and pressure.

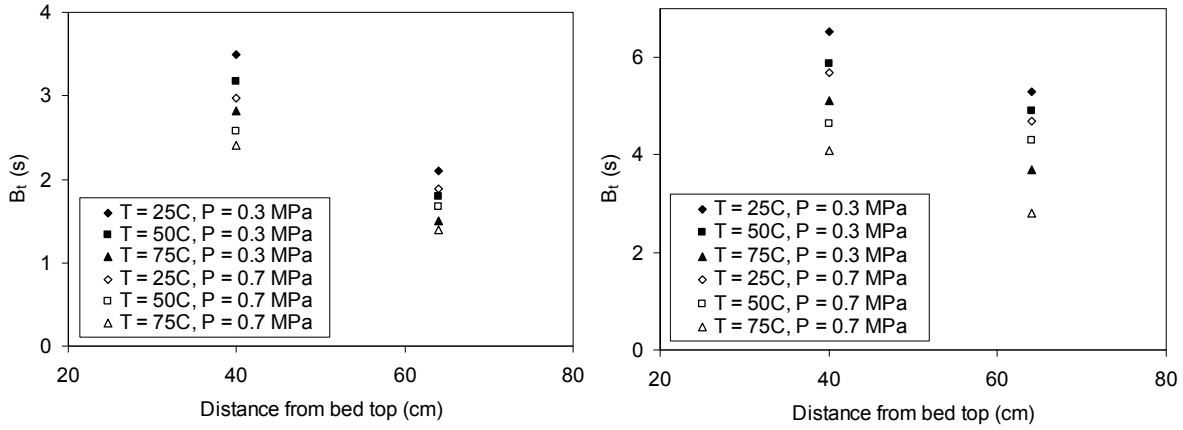


**Figure 4-9** Shock wave breakthrough time as a function of bed length for various reactor temperatures and pressures. $u_G$ = 0.208 m/s, (a) air-water system, $u_{Lb}$ = 0.007 m/s, $u_{Lp}$ = 0.0175 m/s, (b) air-0.25% CMC system, $u_{Lb}$ = 0.00175 m/s, $u_{Lp}$ = 0.007 m/s.

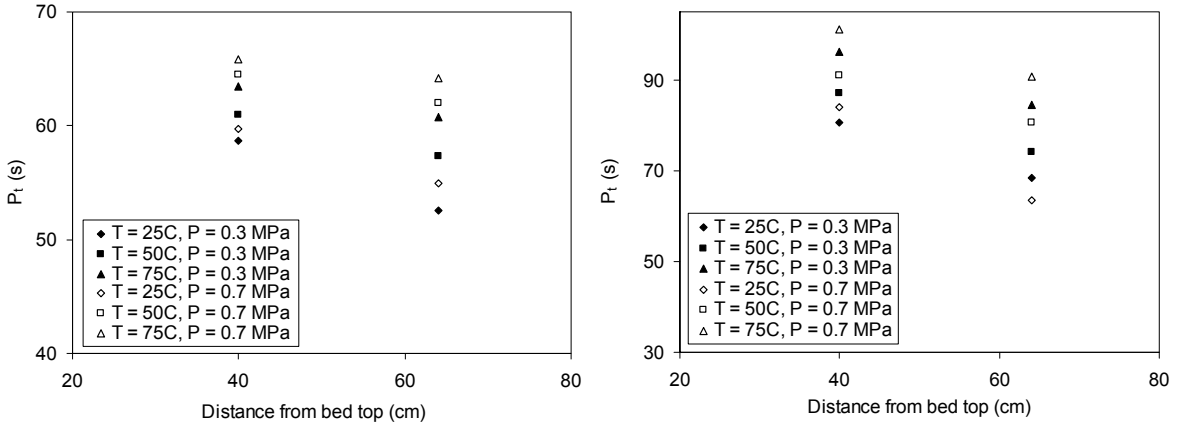


(a) (b)

**Figure 4-10** Shock wave plateau time *versus* bed length for various reactor temperatures and pressures. $u_G$ = 0.208 m/s, (a) air-water system, $u_{Lb}$ = 0.007 m/s, $u_{Lp}$ = 0.0175 m/s, (b) air-0.25% CMC system, $u_{Lb}$ = 0.00175 m/s, $u_{Lp}$ = 0.007 m/s.

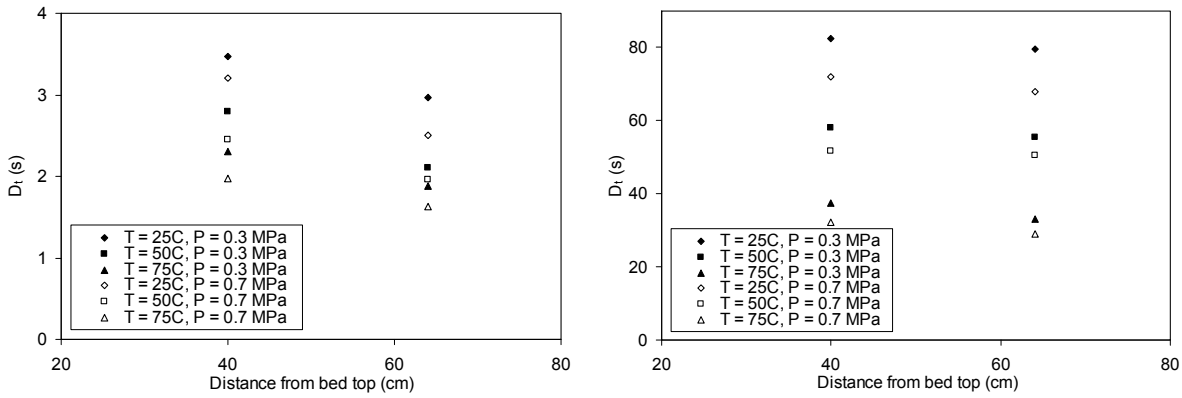


(a) (b)

**Figure 4-11** Shock wave decay time *versus* bed length for various reactor temperature and pressure. $u_G$ = 0.208 m/s, (a) air-water system, $u_{Lb}$ = 0.007 m/s, $u_{Lp}$ = 0.0175 m/s, (b) air-0.25% CMC system, $u_{Lb}$ = 0.00175 m/s, $u_{Lp}$ = 0.007 m/s.

## 4.4 Conclusion

This study's aim was to investigate the effects of temperature and moderate pressure, superficial gas and (base and pulse) liquid velocities, and bed depth on i) the structure of the ***t***rickle-to-***p***ulsing ***T***ransition between ***c***yclic ***o***peration ($tpT^{co}$) and ***s***pontaneous pulsing ($tpT^{s}$) conditions in terms of liquid holdups and velocities, ii) in addition to the pulse characteristics in the pulsing flow regime both in cyclic operation and spontaneous pulsing, iii) and finally some hints on the evolution of the shock wave topological features as a

function of bed depth in a trickle-bed reactor. The following main conclusions can be drawn from the study of Newtonian and non-Newtonian power law liquids:

- In slow-mode cycling, the liquid holdups at $tpT^{s}$ and $tpT^{co}$ were decreasing functions of temperature and pressure due, respectively, to a decrease in liquid viscosity and an increase in gas density.
- The transition liquid holdups and superficial liquid pulse velocities in cyclic operation outperformed those in constant-throughput operation giving rise to more *stable* trickle regime in cyclic operation.
- Irrespective of cyclic or constant-throughput operations, pulse velocities decreased with increasing pressure due to either larger-amplitude liquid holdup fluctuations or larger pulse frequencies.
- Irrespective of cyclic or constant-throughput operations, pulse velocities increased with temperature and superficial gas velocity which was ascribed to increasing the interstitial liquid velocity due to decreasing liquid holdup.
- Pulse velocity in cyclic operation was higher than in constant-throughput operation, irrespective of temperature and pressure for equal $u_L$ and $u_{Lp}$. Conversely, pulse frequency and liquid-holdup standard deviation in cyclic operation were lower than in constant-throughput operation, irrespective of temperature and pressure.
- The shock wave breakthrough, decay and plateau times were decreasing with bed depth regardless of pressure and temperature, and in coherence with the depletion of pulses from their liquid content as they move down the bed.
- As similar gas density effects on hydrodynamics could be effected either by changing pressure or gas molar weight (Al-Dahhan et al., 1997), the present results suggest there is no reason such an equivalence cannot be set between liquid viscosity and temperature hence liquids having equal viscosities (and densities) would impose similar hydrodynamics regardless of whether temperature is changed or different liquids are used.

## 4.5 Nomenclature

$B_\tau$ breakthrough time, s

$D_\tau$ decay time, s

$f$ frequency, Hz

$P_r$ reactor pressure, MPa

$P_\tau$ plateau time, s

$P_\tau^0$ plateau time at reactor entrance, s

$T_r$ reactor temperature, °C

$u$ superficial velocity, m/s

$V_p$ pulse propagation velocity, m/s

**Greek letters**

$\varepsilon_L$ liquid holdup

$\sigma$ standard deviation

**Subscripts**

$b$ base

$G$ gas phase

$L$ liquid phase

$p$ pulse

## 4.6 References

Al-Dahhan, M.H., Larachi, F., Dudukovic, M.P., Laurent, A., 1997. High-Pressure Trickle-Bed Reactors: A Review, Industrial and Engineering Chemistry Research 36, 3292-3314.

Anadon, L.D., Sederman, A.J., Gladden, L.F., 2006. Mechanism of the trickle-to-pulse flow transition in fixed-bed reactors. AIChE Journal 52, 1522-1532.

Aydin, B., Larachi, F., 2005. Trickle bed hydrodynamics and flow regime transition at elevated temperature for a Newtonian and a non-Newtonian liquid. Chemical Engineering Science 60, 6687-6701.

Aydin, B., Fries, D., Lange, R., Larachi, F., 2006. Slow-mode induced pulsing in trickle-bed reactors at elevated temperature. AIChE Journal 52, 3891-3901.

Banchero, M., Manna, L., Sicardi, S., Ferri, A., 2004. Experimental investigation of fast-mode liquid modulation in a trickle-bed reactor. Chemical Engineering Science 59, 4149–4154.

Bartelmus, G., Burghardt, A., Gancarczyk, A., Jaroslawska, E., 2006. Hydrodynamics of a trickle-bed reactor operating at a liquid-induced pulsing flow. Inzynieria Chemiczna i Procesowa, 27, 107-123.

Boelhouwer, J.G., Piepers, H.W., Drinkenburg, A.A.H., 1999. Enlargement of the pulsing flow regime by periodic operation of a trickle-bed reactor. Chemical Engineering Science 54, 4661-4667.

Boelhouwer, J.G., 2001. Nonsteady operation of trickle-bed reactors. PhD thesis, chapter 8, p. 180.

Boelhouwer, J.G., Piepers, H.W., Drinkenburg, A.A.H., 2001. The induction of pulses in trickle-bed reactors by cycling the liquid feed. Chemical Engineering Science 56, 2605-2614.

Boelhouwer, J.G., Piepers, H.W., Drinkenburg, A.A.H., 2002. Liquid-induced pulsing flow in trickle-bed reactors. Chemical Engineering Science 57, 3387-3399.

Borremans, D., Rode, S., Wild, G., 2004. Liquid flow distribution and particle–fluid heat transfer in trickle-bed reactors: the influence of periodic operation. Chemical Engineering and Processing 43, 1403-1410.

Borremans, D., Rode, S., Wild, G., 2007. Cyclic variation of the liquid flow residence time in periodically operated trickle-bed reactors. Chemical Engineering Science 62, 1230-1238.

Burghardt, A., Bartelmus, G., Szlemp, A., 2004. Hydrodynamics of pulsing flow in three-phase fixed-bed reactor operating at an elevated pressure. Industrial and Engineering Chemistry Research 43, 4511-4521.

Castellari, A.T., Haure, P.M., 1995. Experimental study of the periodic operation of a trickle-bed reactor. AIChE Journal 41, 1593-1597.

CRC Handbook of tables for Applied Engineering Science, 1970. CRC Press, Ohio, USA.

CRC Handbook of Chemistry and Physics, 1977. CRC Press, Boca Raton, USA.

Dudukovic, M.P., Larachi, F., Mills, P.L., 2002. Multiphase catalytic reactors: A perspective on current knowledge and future trends. Catalysis Reviews - Science and Engineering 44, 123-246.

Giakoumakis, D., Kostoglou, M., Karabelas, A.J., 2005. Induced pulsing in trickle beds—characteristics and attenuation of pulses. Chemical Engineering Science 60, 5183-5197.

Gupta, R., 1985. Pulsed flow vapor-liquid reactor. US Pat. 4,526,757.

Hasseni, W., Laurent, A., Midoux, N., Charpentier, J.C., 1987. Régimes d'écoulement dans un réacteur catalytique à lit fixe arrosé fonctionnant sous pression (0-10 MPa) à cocourant de gaz et de liquide vers le bas. Entropie 137/138, 127-133.

Haure, P.M., Hudgins, R.R., Silveston, P.L., 1989. Periodic operation of a trickle-bed reactor. AIChE Journal 35, 1437-1444.

Iliuta, I., Thyrion, F.C., 1997. Flow regimes, liquid holdups and two-phase pressure drop for two-phase cocurrent downflow and upflow through packed beds: Air/Newtonian and non-Newtonian liquid systems. Chemical Engineering Science 52, 4045–4053.

Khadilkar, M., Al-Dahhan, M.H., Dudukovic, M.P., 1999. Parametric study of unsteady-state flow modulation in trickle-bed reactors. Chemical Engineering Science 54, 2585-2595.

Lee, J., Hudgins, R., Silveston, P., 1995. A cycled trickle-bed reactor for SO2 oxidation. Chemical Engineering Science 50, 2523-2530.

Lange, R., Hanika, J., 1987. Problems encountered in the periodic operation of catalytic three-phase reactors. Presented at the Ninth Congress, CHISA, Prague.

Lange, R., Hanika, J., Stradiotto, D., Hudgins, R.R., Silveston, P.L., 1994. Investigations of periodically operated trickle-bed reactors. Chemical Engineering Science 49, 5615-5621.

Larachi, F., Iliuta, I., Chen, M., Grandjean, B.P.A., 1999. Onset of pulsing in trickle beds : Evaluation of current tools and stateof-the-art correlation. Canadian Journal of Chemical Engineering 77, 751-758.

Massa, P., Ayude, M.A., Ivorra, F., Fenoglio, R., Haure, P., 2005. Phenol oxidation in a periodically operated trickle bed reactor. Catalysis Today 107-108, 630-636.

Muzen, A., Fraguio, M.S., Cassanello, M.C., Ayude, M.A., Haure, P.M., Martinez, O.M., 2005. Clean oxidation of alcohols in a trickle-bed reactor with liquid flow modulation. Industrial and Engineering Chemistry Research 44, 5275-5284.

Rode, S., 1992. Analyse spatiotemporelle des phénomènes hydrodynamiques et de transfert de matière au sein d'un réacteur à lit fixe opérant en écoulement monophasique de liquide ou en co-courant vers le bas de gaz et de liquide; mise en œuvre de la technique des microsondes électrochimiques. PhD Dissertation, Institut National Polytechnique de Lorraine, Nancy, France.

Sai, P.S.T., Varma, Y.B.G., 1988. Flow pattern of the phases and liquid saturation in gas-liquid cocurrent downflow through packed beds. Canadian Journal of Chemical Engineering 66, 353-360.

Stradiotto, D.A., Hudgins, R.R., Silveston, P.L., 1999. Hydrogenation of crotonaldehyde under periodic flow interruption in a trickle bed. Chemical Engineering Science 54, 2561-2568.

Trivizadakis, M.E., Giakoumakis, D., Karabelas, A.J., 2006. Induced pulsing in trickle beds - particle shape and size effects on pulse characteristics. Chemical Engineering Science 61, 7448-7462.

Trivizadakis, M.E., Karabelas, A.J., 2006. A study of local liquid/solid mass transfer in packed beds under trickling and induced pulsing flow. Chemical Engineering Science 61, 7684-7696.

Tukac, V., Hanika, J., Chyba, V., 2003. Periodic state of wet oxidation in trickle-bed reactor. Catalysis Today 79-80, 427-431.

Turco, F., Hudgins, R.R., Silveston, P.L., Sicardi, S., Manna, L., Banchero, M., 2001. Investigation of periodic operation of a trickle-bed reactor. Chemical Engineering Science 56, 1429-1434.

Urseanu, M., Boelhouwer, J., Bosman, H., Schroijen, J., Kwant, G., 2004. Induced pulse operation of high-pressure trickle bed reactors with organic liquids: hydrodynamics and reaction study. Chemical Engineering and Processing 43, 1411-1416.

Wammes, W.J.A., Mechielsen, S.J., Westerterp, K.R., 1990. The transition between trickle flow and pulse flow in a cocurrent gas-liquid trickle-bed reactor at elevated pressures. Chemical Engineering Science 45, 3149-3158.

Wammes, W.J.A., Westerterp, K.R., 1990. The influence of the reactor pressure on the hydrodynamics in a cocurrent gas-liquid trickle bed reactor. Chemical Engineering Science 45, 2247-2254.

Xiao, Q., Cheng, Z.M., Jiang, Z.X., Anter, A.M., Yuan, W.K., 2001. Hydrodynamic behavior of a trickle bed reactor under “forced” pulsing flow. Chemical Engineering Science 56, 1189-1195.

# Chapter 5

# Influence of temperature on fast-mode cyclic operation hydrodynamics in trickle-bed reactors*

## Résumé

Malgré le bien-fondé du fonctionnement périodique reconnu dans la littérature scientifique comme une des stratégies d'intensification des procédés pour des réacteurs de type « trickle bed », une réticence persiste toujours quant à une mise en œuvre industrielle. Ceci peut en partie être attribué à l'absence de données techniques pertinentes aux températures et pressions élevées caractérisant le fonctionnement des procédés industriels. Actuellement, l'hydrodynamique des réacteurs trickle bed en mode de fonctionnement cyclique, et plus particulièrement en mode de fonctionnement rapide à température élevée et en surpression, reste inconnue. Cette étude se propose d'explorer le comportement hydrodynamique d'un réacteur trickle bed à modulation rapide de l'écoulement du liquide, fonctionnant à température élevée et en surpression. L'effet de la température et de la pression sur les séries chronologiques de la rétention liquide et de la perte de charge, en termes de temps caractéristiques, d'intensité et de vitesse des pulsations, a été examiné pour une gamme étendue de vitesses superficielles de gaz et de liquide. L'évolution de la perte de charge s'atténue avec l'élévation de la température pour des vitesses superficielles données de gaz et de liquide. Les valeurs expérimentales de la vitesse de pulsation ont été comparées à celles obtenues avec la corrélation de Giakoumakis et al. (2005) et les résultats montrent que cette corrélation pourrait être utilisée à température élevée et proche de la pression atmosphérique.

* Aydin, B.; Cassanello, M.C.; Larachi, F. Chemical Engineering Science, 63, 141-152, 2008

# Abstract

Despite the merits of periodic operation praised in the academic literature as one of the process intensification strategies advocated for trickle bed reactors (TBRs), there is still reluctance to implement it in industrial practice. This can partly be ascribed to the lack of engineering data relevant to the elevated temperature and pressure characterizing industrial processes. Currently, the hydrodynamics of trickle beds under cyclic operation, especially in fast mode at *elevated* temperature and pressure remains by and large *terra incognita*. This study proposes exploration of the hydrodynamic behavior of TBRs experiencing fast liquid flow modulation at elevated temperature and moderate pressure. The effect of temperature and pressure on the liquid holdup and pressure drop time series in terms of pulse breakthrough and decay times, pulse intensity, and pulse velocity was examined for a wide range of superficial gas and liquid (base and pulse) velocities for the air-water system. The pulse breakthrough and decay times decreased, whereas the pulse velocity increased with temperature and/or pressure. The pressure drop trace was attenuated with increasing temperature for given superficial gas, and base and pulse superficial liquid velocities. Experimental pulse velocity values were compared to the Giakoumakis et al. (2005) correlation which revealed that it could be relied upon at elevated temperature and close to atmospheric pressure.


**Keywords** Trickle bed, cyclic operation, elevated temperature, liquid holdup, pressure drop

## 5.1 Introduction

Trickle bed reactors (TBR) in which gas and liquid are forced to flow cocurrently downwards through an immobile porous medium are among the most ubiquitous types of catalytic packed bed reactors (Dudukovic et al., 2002). The flexibility in throughput demands TBRs achieve by means of their ample capacity for operating at various flow regimes (*i.e.*, or *L/G* ratios) elect them as the best reactor candidates in a number of industrial processes where they are indeed in use for decades, *e.g.*, hydrotreating,

hydrocracking, Fischer-Tropsch synthesis, to name just a few (Meyers, 1996; Jess et al., 1999; Wang et al., 2003).

There are many industrial examples where, because of process constraints, TBRs have to be operated in trickle flow regime which establishes at low irrigation liquid flow rates inasmuch as gas throughput is not excessively high. An obvious example is syngas conversion through the Fischer-Tropsch synthesis carried out in multi-tubular fixed bed reactors, such as the Shell Middle Distillate Synthesis process (Jess et al., 1999) where an "all-gas" $CO/H_2$/inert feed is progressively converted into liquid wax giving eventually rise to two-phase *trickle flow regime* at some depth in the bed. Another known context where trickle flow regime is imposed in small units is during iso-LHSV trickle-bed scale-up/-down which requires the lowering of liquid superficial velocity in the small unit so that the liquid residence time-holdup ratio prevailing in both the small and large units can be matched. In some instances, trickle flow regime is recognized to be inauspicious in terms of TBR efficiency or operability. As an example, partial wetting may cause a bulky zone of the reactor to be dry giving a chance to hot spots to go off during exothermic reactions as a result of insufficient heat removal. Liquid-limited catalytic reactions are also incompatible with partial wetting as this may result in a loss in reactor productivity and catalyst under-utilization. On the contrary, pulsing flow regime which prevails in TBR at relatively high gas and liquid flow rates is an alternate flow regime which is known to be beneficial for liquid-limited reactions because of the complete catalyst wetting, and of the larger particle-liquid and gas-liquid mass transfer coefficients (Chou et al., 1979).

Periodic operation in trickle beds is being in vogue for some time with expected improvements on TBR performance (Boelhouwer et al., 2002a). Such artifice has been reckoned under the flag of *process intensification* suggesting an economy deriving profit from plant size reduction as a result of improved efficiency (Hüther et al., 2005).

One method for process intensification in TBRs advocated over the past few years in the academic literature is artificial induction of pulses (Boelhouwer et al., 2002a,c; Dudukovic et al., 2002). For instance with this method it would be possible to benefit from the quenching ability of pulsing flow vis-à-vis no hot spot formation and high mass transfer rates while the barycentric flow rates for the liquid phase can be kept low enough to exploit the longer residence times as in trickle flow regime. Depending on the applied period,

liquid-cyclic operation flow can be categorized as slow mode (~ few minutes) or fast mode (~ few seconds) with liquid flow modulation optionally consisting in switching liquid flow rate periodically either between zero and some assigned value, *i.e.*, so-called on-off mode, or between a low (but non-zero) and a high value, *i.e.*, so-called base-peak mode.

Systematic research on periodic operation in trickle-bed reactors has begun to spring in the open literature in the early 1990s'. Haure et al. (1991) noted drastic increases (up to 25 times) in product concentration during the $SO_2$ oxidation in slow mode periodic operation. Some literature work reporting an increase in conversion and selectivity for similar reactions during periodic operation was also summarized by Dudukovic et al. (2002). In another study (Lange et al., 1999), a performance increase in periodically operated TBRs was reported for the hydrogenation of $\alpha$-methylstyrene to cumene, where the time-average conversion was found to exceed its steady-state counterpart. Stradiotto et al. (1999) while studying crotonaldehyde hydrogenation at 25ºC and 1.1 MPa could achieve a 50% increase in reaction rate provided the operating conditions were chosen adequately, *e.g.*, temperature, pressure, time-average (barycentric) liquid flow rate, period and split. Recently, Massa et al. (2005) reported favorable effects of on-off liquid flow modulation on products' distribution during phenol oxidation. Liu and Mi (2005) studied the influence of temperature and pressure on the hydrogenation of 2-ethylanthraquinones for periodically operated TBRs. They interestingly observed that the positive effect of liquid flow modulation becomes increasingly attenuated with an increase in temperature and pressure. Ucan et al. (2005) investigating the influence of periodic operation on $SO_2$ removal at atmospheric pressure and ambient temperature in a trickle bed loaded with activated carbon reached similar qualitative conclusions as Haure et al. (1991) regarding improvements in sulfur dioxide removal. Muzen et al. (2005) reported the favorable effect of on-off liquid flow modulation on the catalytic oxidation of benzyl alcohol and ethyl alcohol. Banchero et al. (2004) studied the effect of fast-mode operation on the conversion of $\alpha$-methyl styrene hydrogenation and identified optimal values for period and split ratio which procured enhancement in reaction conversion. They showed also that improper selection of the fast-mode parameters (*i.e.*, period and split ratio) could have neutral or negative effects on the conversion.

As opposed to numerous studies available on reaction performances, an increasing number of experimental studies concerning the effect of periodic operation on the TBR hydrodynamics is recently appearing in the literature. Xiao et al. (2001) studied the effect of gas-induced pulsing flow on the hydrodynamics of a 0.1 m in diameter TBR, packed with 5 mm glass beads up to a height of 1 m. They observed that more uniform radial and axial liquid distributions are achievable during gas-induced pulsing flow while a significant decrease in liquid holdup during gas-forced input was observed. Boelhouwer et al. (2002b) measured the liquid holdup, and the pulse velocity and pulse duration during the fast-mode cyclic operation flow for 6 mm glass beads which they compared with the measured hydrodynamic counterparts occurring during spontaneous pulsing flow regime. They observed that i) the pulse velocities at two axial locations in the column vary over the same range of the pulse velocities measured in the spontaneous pulsing flow regime, ii) the pulse duration in spontaneous pulsing flow was longer than in induced pulsing flow. Borremans et al. (2004) investigated the effect of periodic operation on the liquid flow distribution by using a multi-compartment liquid collector located beneath a 0.3 m diameter column packed with 3 mm glass beads up to a height of 1.3 m. They observed only marginal effects of periodic operation on bed cross-wise liquid flow distribution. Giakoumakis et al. (2005) studied the effect of cyclic frequency (*i.e.*, reciprocal of cycle period), and gas and liquid flow rates on the dynamic liquid holdup, the pressure drop, and the pulse intensity and pulse velocity during fast-mode cyclic operation flow. No significant effect of cyclic frequency was observed on liquid holdup, pressure drop, and pulse velocity, while pulse intensity decreased with increasing cyclic frequency. Bartelmus et al. (2006) performed fast and slow mode flow experimentations for different liquids and reported the shift of trickle-to-induced pulsing transition boundary to lower superficial liquid velocities with increasing liquid viscosities. Trivizadakis et al. (2006a,b) studied the effect of particle shape and size on pulse characteristics and liquid-solid mass transfer during fast mode cyclic operation. They observed lower pulse attenuation rate and spread of local mass transfer coefficients with spherical particles as compared to cylindrical extrudates. Aydin et al. (2006) reported the effects of temperature and pressure on slow-mode cyclic operation characteristics for both Newtonian and non-Newtonian liquids. One of the key findings of their work was the aggravation in the collapse of the liquid holdup pulses with increasingly temperatures and

pressures due to liquid exchange from pulse to baseline flow which had a tendency to flatten prematurely the pulses. Borremans et al. (2007) found that the cyclic variation of the liquid mean residence time was a function of split ratio, cycle period, and bed height in liquid cyclic operation. A new approach of dynamic similarity was proposed based on residence times in constant-throughput and periodically-operated TBRs thought to be more adequate for the interpretation of chemical conversion data.

Fast modulation has been suggested mostly for improving liquid distribution, thus reducing possible appearance of channeling and hot spots, and allowing for better reactor temperature control. In addition, high-frequency liquid feed cycling has been shown to decrease the product residence time inside the catalyst pellets which can represent a major advantage in circumstances where the prevention of undesirable secondary reactions is crucial or when products are reaction inhibitors or catalyst poisons. Additionally, the increase in the reactant time-average concentration of the liquid phase inside the catalyst favors the target reaction by ensuring high reaction rates (Boelhouwer et al., 2002a).

Except our recent work on slow-mode cyclic operation (Aydin et al., 2006, 2007), it is worthy of notice that none of the available hydrodynamic experimentations has addressed the effect of elevated temperature and pressure on TBR hydrodynamics in *fast-mode* cyclic operation despite the fact that most industrial trickle beds are operated in severe conditions away from those commonly tested in academic conditions. Therefore, there is a gap to fill and an opportunity to seize in investigating the influence of elevated temperature and moderate pressure levels on the hydrodynamics of trickle beds subjected to fast-mode cyclic operation. In this work, we propose to analyze the effect of temperature and moderate pressure, superficial gas and (base and pulse) liquid velocities, and bed depth on the liquid holdup dynamic features, *e.g.*, pulse breakthrough and decay times, pulse intensity, pulse velocity, as well as on the pressure drop time series in fast-mode cyclic operation. Finally, the effect of temperature and pressure will be compared in both fast-mode and slow-mode cyclic operation experiments to assess the extent of liquid mass transfer exchange from peaks to bases during the passage of liquid waves down the bed.

## 5.2 Experimental Setup and Procedure

The experiments were performed in a stainless steel column of 0.048 m inner diameter. The packed bed consisted of 3.0 mm glass spheres filling the tube up to a total height of 1.07 m and yielding a bed porosity of 0.39. The schematic of the experimental facility was given elsewhere (Aydin et al., 2006). The effect of temperature and pressure on the cyclic operation characteristics was studied up to temperatures and pressures of 90ºC and 0.7 MPa, respectively, for the air-water system. All the experiments were performed under a cyclic frequency of 0.25 Hz for base-peak (2 s base - 2 s pulse) fast liquid flow modulation.

For the elevated temperature measurements, the liquid, prior to be routed to the reactor *via* a calibrated flowmeter, was heated in a reservoir through a liquid preheater. The gas was supplied from a compressed air line up to a maximum pressure of 0.7 MPa. After passing through a preheater, the gas phase encountered the heated liquid phase at the top of the reactor. Both phases were introduced cocurrently downwards through a distributor which was designed to spread crosswise the gas and liquid as uniformly as possible. At the reactor outlet both phases were intercepted in a separator where the gas phase was vented to the atmosphere *via* a calibrated flowmeter and the liquid phase was recirculated back to the heated reservoir. As the heat source is external to the reactor, this latter was run in an isothermal mode by insulating the setup. Measurements were taken only when the desired steady-state operating temperature was reached along the packed bed, and the reactor was preventively operated under pulsing flow regime to ensure complete bed wetting.

On top of the base-line liquid flow rate, the additional liquid feed for generating the pulse sequence in the base-peak flow modulation required installation of a computer-controlled three-way pneumatic valve. This valve was connected to the continuous liquid feed line via a needle valve where the high liquid feed rate can be adjusted to the desired value prior to the measurements.

An electrical conductance technique was implemented for the measurement of cyclic operation flow characteristics; the electrode specifications and drawings were given in detail elsewhere (Aydin and Larachi, 2005). For the local liquid holdup measurements, two conductance probes were mounted in the middle of the reactor, a distance of 0.245 m apart from each other. Each probe was connected to a lock-in amplifier to acquire the associated output signal. After amplification, the signals were transmitted to a computer by means of a

data acquisition system. Calibration of these embedded probes was done using a conventional tracer method which consisted in measuring the bed-average liquid holdup by injecting imperfect electrolyte tracer pulses (aqueous sodium chloride solution) and recording on-line, by means of a conductivity controller, the time-dependent liquid electrical conductivity measured by means of two RTD probes located at each extremity of the reactor (Larachi et al., 1994). The liquid space time ($\tau$) was determined by fitting the inlet and outlet tracer response conductivity signals to a two-parameter impulse response RTD axial dispersion model. For the same operating conditions the signal received from the two ring electrodes was also recorded. This process was repeated for different temperatures, pressures and gas and liquid superficial velocities to enable mapping of the response domain of the ring electrodes for reconstructing the local liquid holdup viewed in their vicinity from their recorded conductance signals. A plot example for the calibration of the ring electrodes was presented in a previous study (Aydin et al., 2006).

The two-phase pressure drop was measured with a differential pressure transducer connected to the top and bottom of the packed bed and pressure drop traces were recorded for each operating condition. For the determination of the pulse velocity, the distance between the two ring probes was divided by the time delay of maximum cross-correlation between signals. The pulse intensity was calculated based on the definition given by Giakoumakis et al. (2005) and experimental pulse velocity values were compared with their suggested correlation.

## 5.3 Results and Discussion

Table 5-1 displays the physicochemical properties of water and air as affected by an increase in temperature from 25ºC to 90ºC and in pressure from 0.3 to 0.7 MPa. The liquid dynamic viscosity is the most sensitive to temperature with 284% reduction, followed by liquid surface tension and liquid density, respectively, dropping by 23% and 3% between 25ºC and 90ºC. The reactor pressure is most influential on gas density (233% rise from 0.3 to 0.7 MPa) while temperature reduces gas density by 22% and inflates gas dynamic viscosity by 16% over the explored range. Pressure variations as imposed in this study are virtually effectless on the dynamic viscosity of the gas phase. Hence, the hydrodynamic

behavior of the trickle bed under fast-mode cyclic operation will be analyzed with respect to changes of liquid viscosity with temperature and of gas density due to reactor pressure.

**Table 5-1** Properties of Water and Air at Elevated Temperatures

| Temperature (ºC) | $\rho_{water}^{\#}$ (kg/m3) | $\mu_{water}^{*}$ x $10^4$ (kg/m.s) | $\sigma_{water}^{*}$ ($kg/s^2$) | $\rho_{air}^{*}$ (0.3 MPa) ($kg/m^3$) | $\rho_{air}^{*}$ (0.7 MPa) ($kg/m^3$) | $\mu_{air}^{*}$ x $10^5$ (kg/m.s) |
|---|---|---|---|---|---|---|
| 25 | 997.21 | 8.86 | 0.0720 | 3.49 | 8.15 | 1.84 |
| 50 | 988.22 | 5.36 | 0.0679 | 3.23 | 7.53 | 1.96 |
| 75 | 974.9 | 3.77 | 0.0635 | 2.99 | 6.98 | 2.07 |
| 90 | 964.7 | 3.12 | 0.0608 | 2.87 | 6.7 | 2.13 |

*CRC Handbook of tables for Applied Engineering Science (1970)

#CRC Handbook of Chemistry and Physics (1977)

### 5.3.1 Liquid Holdup and Pressure Drop Times Series

The cyclic operation characteristics were examined according to the relevant liquid holdup time series. Ideally, the well-defined squared sequence of base-peak liquid velocities reaching the bed top would translate into a correspondingly, non-attenuated irrespective of depth location, squared liquid holdup sequence should the trickle bed be totally indifferent to the imposed dynamics. On the contrary, as revealed by Fig. 5-1 at T = 90 ºC and P = 0.3 MPa, the quasi-periodic liquid holdup traces viewed by the ring electrodes, respectively at depths of $z$ = 40 cm and $z$ = 64.5 cm, undergo progressive attenuation during the course of the forced liquid waves down the porous medium. The decay of the pulses along the bed is as persistent at elevated temperatures and moderate pressures, as shown in Fig. 5-1, as it is known to be at ambient temperature and atmospheric pressure, as reported for instance by Boelhouwer et al. (2002b) and Giakoumakis et al. (2005). If the liquid holdup is further time-averaged over a sufficiently long base-peak sequence such as the one displayed in Fig. 5-1, it is possible to assess the effects of temperature (and also pressure) such as those plotted in Fig. 5-2 as a function of bed depth. As seen in Fig. 5-2 the liquid holdup obtained along the bed is constant at a given temperature and pressure. Fig. 5-2 shows a hardly perceptible reduction of the time average liquid holdup as bed depth increases. In our opinion, this almost imperceptible "peaking" can be due to combined error contributions in

the liquid holdup measuring technique and the numerical averaging process because otherwise it does look like violating the "continuity" principle as no sink nor source for the liquid holdup exist in the bed. The liquid holdup at given $u_G$ and barycentric liquid ($S \times u_{Lp}$ + (1-$S$)$\times u_{Lb}$) superficial velocities for cyclic operation is equal to that obtained for constant throughput mode at identical superficial liquid and gas velocities. At constant temperature and pressure, and although measured over an inter-probe distance of 24.5 cm, axial invariance of the time-averaged liquid holdup for any given ($u_G$, $u_{Lb}$, $u_{Lp}$) set, which is in agreement with Giakoumakis et al. (2005) observations at ambient temperature and atmospheric pressure, is therefore just reassuring. It means that, though contiguous peaks and bases might not be hermetic to each other and allow for an exchange of liquid content from peak to base as the waves travel downwards, the amount of liquid in play is nonetheless conserved. Our results are a generalization of such axial invariance of the amount of liquid in transit down the bed from peak to base when elevated temperatures and pressures are involved. Fig. 5-1 evidences that at a given elevated temperature, the drift in liquid holdup base along the column due to the base superficial liquid velocity ($u_{Lb}$ = 0.00175 m/s) is less pronounced in comparison to the drift in liquid holdup peaks corresponding the peak superficial liquid velocity ($u_{Lp}$ = 0.014 m/s). As will be discussed later, the change in the dynamics of these holdup traces can be evaluated from the variation with temperature, pressure, and axial position in the bed of the breakthrough time, $B^{\tau}_{\varepsilon}$, and the decay time, $D^{\tau}_{\varepsilon}$, (as schematically illustrated in Fig. 5-1) it takes for the holdup pulse to, respectively, buildup and then collapse for chosen values of gas, liquid base and pulse superficial velocities.

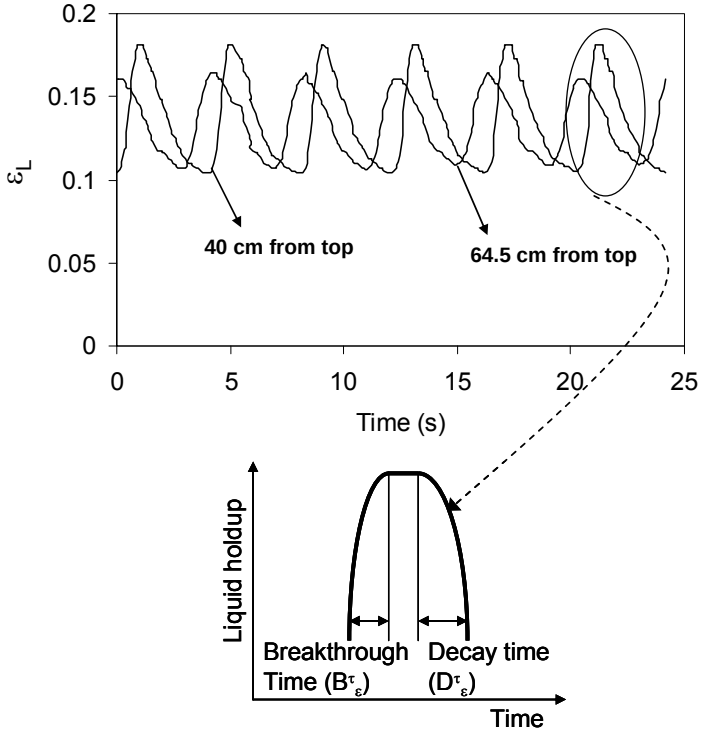


**Figure 5-1** An example of liquid holdup traces obtained along the bed during cyclic operation flow. $T$ = 90ºC, $P$ = 0.3 MPa, $u_{Lb}$ = 0.00175 m/s, $u_{Lp}$ = 0.014 m/s, $u_G$ = 0.1 m/s.

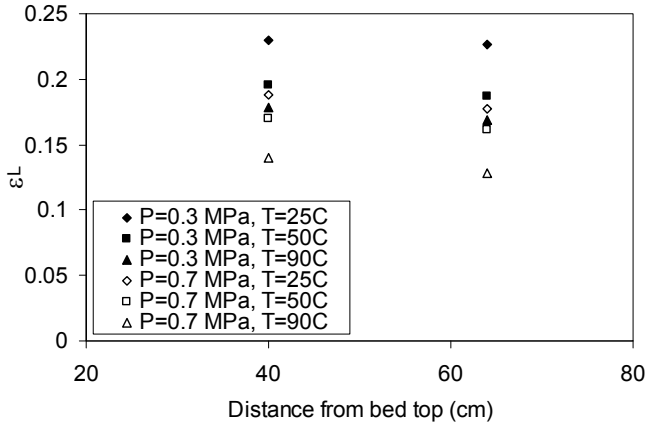


**Figure 5-2** Liquid holdup along the packed bed at various temperatures and pressures for cyclic operation $u_{Lb}$ = 0.0035m/s, $u_{Lp}$ = 0.014m/s, $u_G$ = 0.2m/s.

Figs. 5-3a-c show the effect of temperature on the attenuation of the liquid holdup pulses as felt by the probe located at a depth of 40 cm, for different superficial gas velocities. For given pressure and superficial gas and liquid velocities, the liquid holdup decreases with temperature due most plausibly to a reduction in liquid viscosity. The liquid holdup

decrease in TBRs due to temperature is in agreement with observations relevant to constant-throughput (Aydin and Larachi, 2005) or to slow-mode cyclic operation (Aydin et al., 2006) experimentations. The phenomenon of holdup reduction with temperature is believed to rub off more or less rapidly the liquid holdup pulses as they travel down the bed so that any process intensification expected from the fast-mode would be suppressed at some depth should lengthy beds be used.

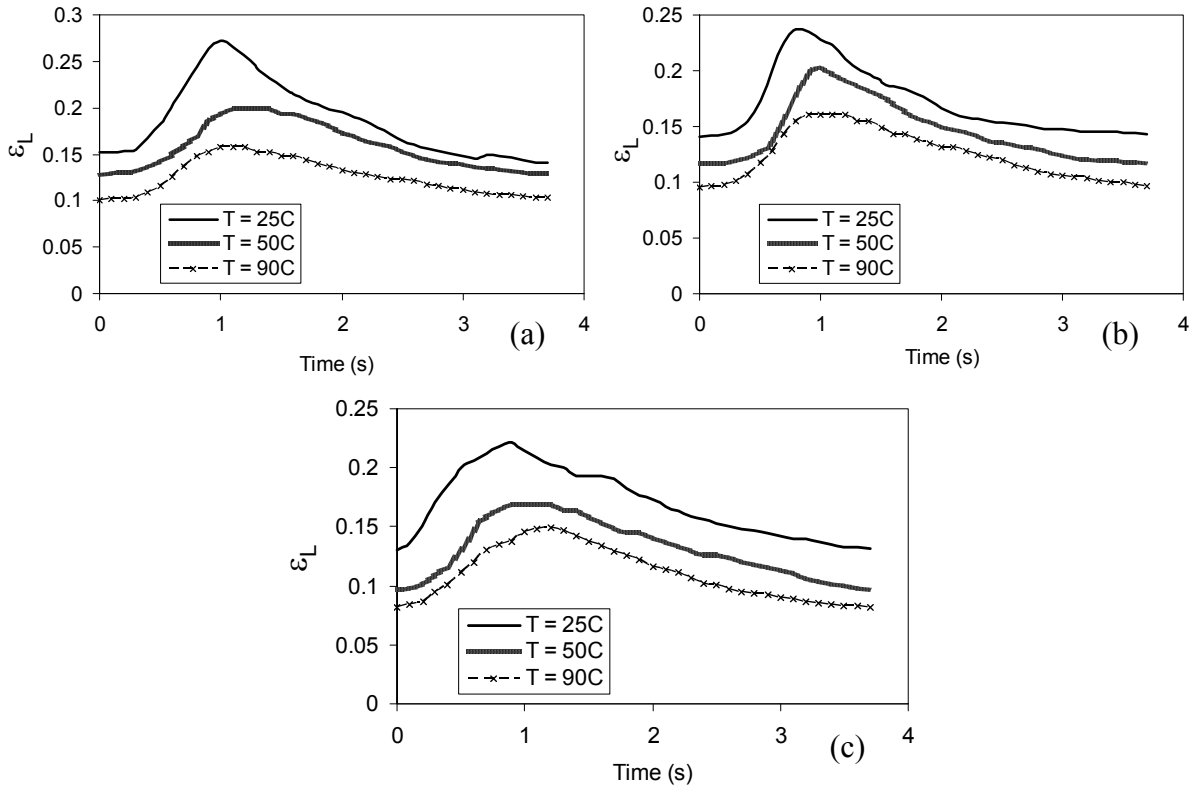


**Figure 5-3** Effect of temperature on pulse pattern measured 40 cm from bed top. $P$ = 0.3 MPa, $u_{Lb}$ = 0.0035 m/s, $u_{Lp}$ = 0.014 m/s, (a) $u_G$ = 0.05 m/s, (b) $u_G$ = 0.1 m/s, (c) $u_G$ = 0.2 m/s.

Figs. 5-4a-c show that, for constant elevated temperature and various superficial gas velocities, liquid holdup pulse attenuation becomes more pronounced with increasing reactor pressure. The origin of this attenuation is much likely tied to the higher gas-liquid interfacial shear stress that elevated pressures are known to be the cause of (Wammes et al., 1991). Also, in addition to pulse attenuation, the effect of increased pressures is to reduce the transient of the pulse tail at a fixed bed location rendering the distinction between base and pulse more noticeable with increased pressures.

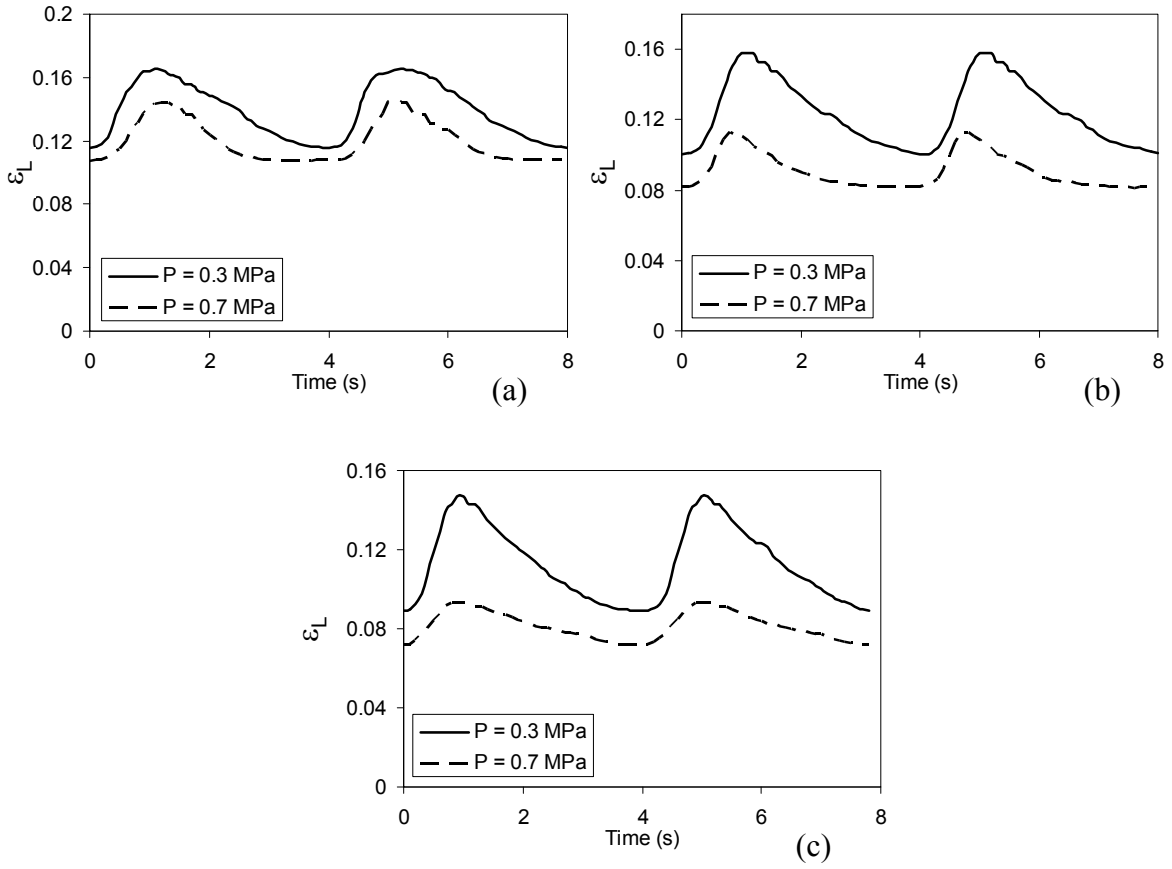


**Figure 5-4** Influence of pressure on pulse pattern at 40 cm from bed top. $T$ = 90ºC, $u_{Lb}$ = 0.0035 m/s, $u_{Lp}$ = 0.014 m/s, (a) $u_G$ = 0.05 m/s, (b) $u_G$ = 0.1 m/s, (c) $u_G$ = 0.2 m/s.

There is a remarkable influence by temperature and pressure on the fast-mode cyclic operation flow. At constant base and pulse superficial liquid velocities and a given axial position in the reactor, the attenuation of the liquid holdup pulses is aggravated by the increased pressure and temperature in the reactor. Therefore, one has to exert some caution

from extrapolating the *cold-flow* liquid holdup pulse amplitudes obtained from literature correlations to the conditions of elevated temperature and pressure.

As indicated above, the pressure drop traces were also recorded during periodic operation for each reactor temperature, pressure and superficial gas and liquid (base and pulse) velocities. An example of such a pressure drop trace obtained at 0.3 MPa for three reactor temperatures is illustrated in Fig. 5-5. Increased temperatures are likely to weaken the frictional forces at the gas-liquid and liquid-solid interfaces, the global outcome of which would also be a reduction in two-phase pressure drop as noted in constant-throughput experimentations (Aydin and Larachi, 2005). It is worthy of notice that the lower pressure drops should be the resultant of a reduction in liquid viscosity, and liquid and gas densities as temperature is raised, while the increased gas viscosity in almost the same ratio as the decrease in gas density is believed to mitigate the temperature effect associated with the gas phase. Hence, the pressure drop traces tend to be attenuated with increasing temperature for the same reason as for the evolution of the liquid holdup traces regarding liquid viscosity attenuation discussed above.

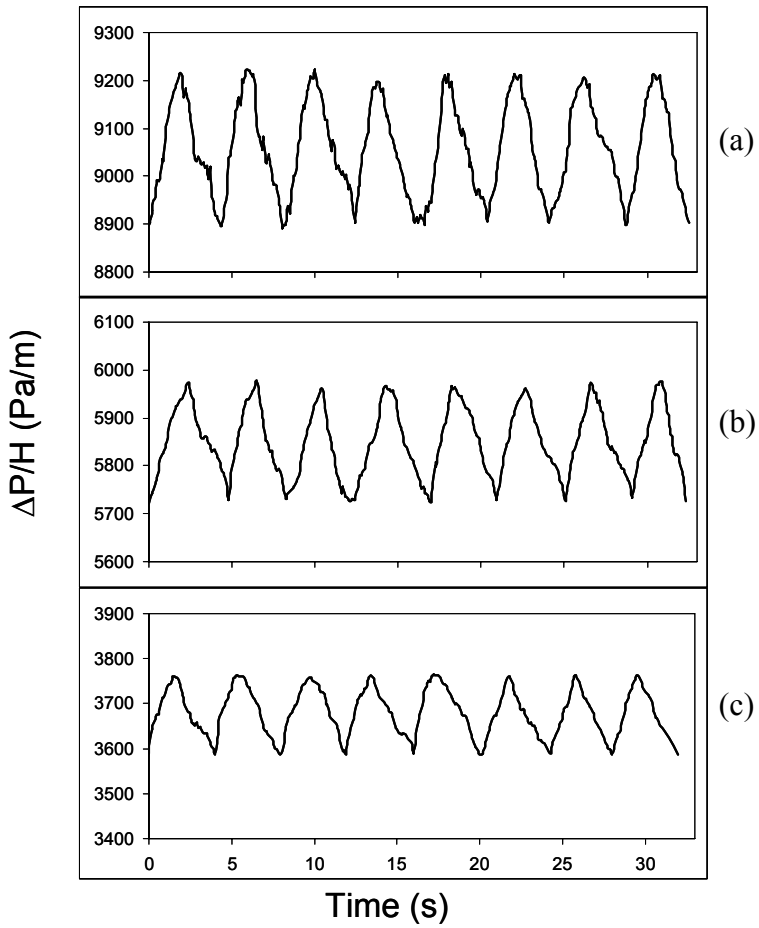


**Figure 5-5** An example of pressure traces obtained during cyclic operation flow. $P$ = 0.3 MPa, $u_{Lb}$ = 0.0035 m/s, $u_{Lp}$ = 0.014 m/s, $u_G$ = 0.1 m/s, (a) $T$ = 25ºC, (b) $T$ = 50ºC, (c) $T$ = 90ºC.

### 5.3.2 Pulse Topological Features

The pressure drop pulse characteristics, *i.e.*, pulse breakthrough time ($B^{\tau}_{\Delta P}$) and decay time ($D^{\tau}_{\Delta P}$), were also determined for various operating conditions. Though in principle the couples ($B^{\tau}_{\Delta P}$, $D^{\tau}_{\Delta P}$) and ($B^{\tau}_{\varepsilon}$, $D^{\tau}_{\varepsilon}$) are time-dependent parameters of the same dynamic system, they will not necessarily take the same values. This is because the former couple is an integral descriptor resulting from the whole-bed pressure drop as sensed by the pressure transducer whereas the latter is more local as it senses only the liquid holdup in the region of the ring electrode. This section therefore discusses the qualitative effect of temperature and pressure on either the liquid holdup or the pressure drop traces in terms of pulse shape features during fast-mode periodic operation.

The effect of temperature and pressure on the pulse breakthrough time for both times series is plotted in Figs. 5-6a,b. At given base and pulse superficial liquid velocities, the pulse breakthrough time of liquid holdup (at $z$ = 40 cm) and pressure drop time series decreases with increasing temperature and pressure, with a more pronounced effect of the latter. The breakthrough time occupies between 0.4 to 2 s from a total of 4 s of the fast-mode period irrespective of the pressure drop or the liquid holdup trace. A reduction of $B^{\tau}{}_{\varepsilon}$ is expected to occur after increasing $u_{Lb}$ to approach $u_{Lp}$. Furthermore, the effect of gas phase inertia becomes more prominent at elevated pressure especially at the higher liquid flow rates, *i.e.*, $u_{Lp}$. This entails reductions in both pulse liquid holdup and pulse breakthrough time since the gap between the base and pulse holdup erodes as pressure is increased, see Fig. 5-4. The same holds true regarding the effect of increased reactor temperature in lowering the liquid viscosity thus leading to briefer pulse breakthrough times as liquid holdup falls. Hence an increase in pressure, temperature and/or base liquid velocity results in a loss in contrast between base and pulse liquid holdups which are in agreement with the observed reductions in the pressure drop increments between base and pulse superficial liquid velocities. Thus, $B^{\tau}{}_{\Delta P}$ also diminishes.

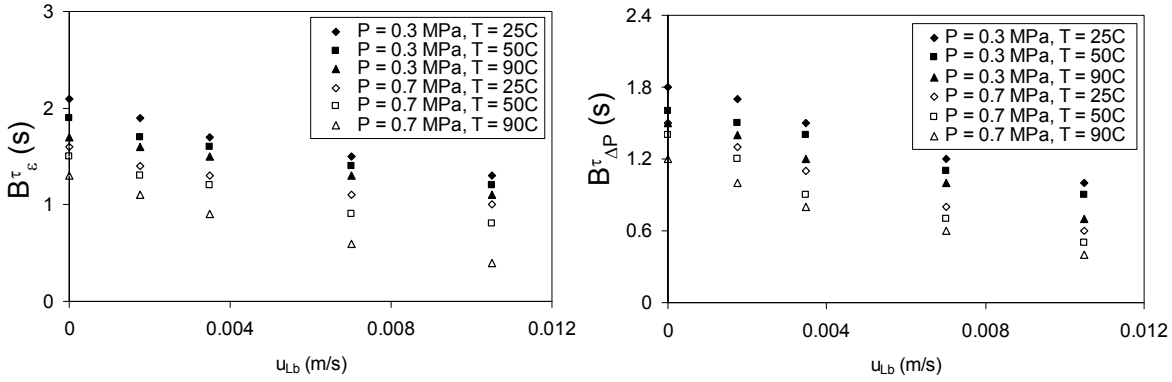


(a) (b)

**Figure 5-6** Pulse breakthrough time as a function of base superficial liquid velocity. Effect of temperature and pressure on (a) liquid holdup trace and (b) pressure drop trace. $u_{Lp}$ = 0.014 m/s, $u_G$ = 0.1 m/s, $z$ = 40 cm.

Figs. 5-7a,b show the effect of superficial gas velocity and base superficial liquid velocity on the pulse breakthrough time of both holdup and pressure drop time series at given elevated temperature and pressure. The pulse breakthrough time for holdup (Fig. 5-7a) and pressure drop (Fig. 5-7b) decreases with increasing gas and base liquid superficial

velocities. The prevailing flow regime in the reactor shifts from trickle flow to pulsing flow regime with increasing gas and liquid superficial velocities. The increased drag force in the high interaction regime *via* gas velocity yields shorter liquid mean residence times and thus less contrast in liquid holdups (and pressure drops) so that the time required for the liquid holdup (pressure drop) to rise from base to pulse level is lessened. For the same reasons mentioned in the previous paragraph, the pulse breakthrough time also decreases with increasing the base superficial liquid velocity due to a lower gap between base and pulse holdup and pressure drop.

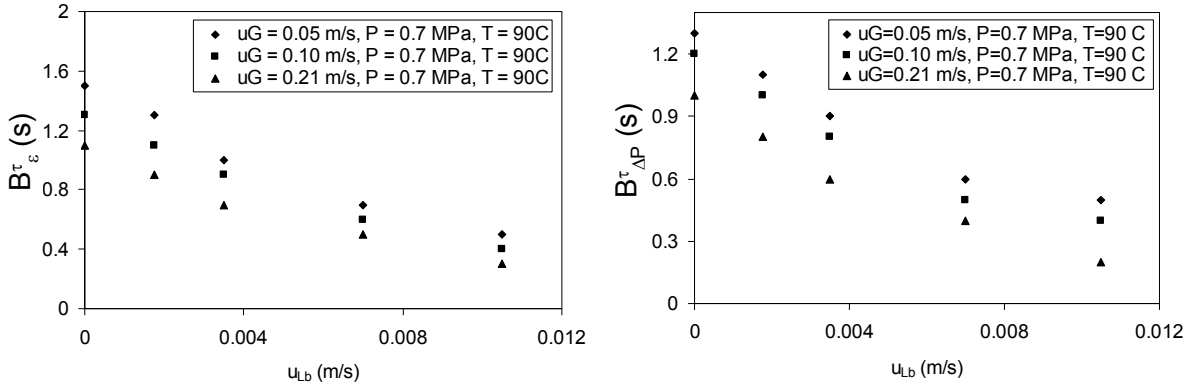


(a) (b)

**Figure 5-7** Effect of gas and base superficial liquid velocities on the pulse breakthrough time at elevated temperature for liquid holdup trace (a) and pressure drop trace (b). $u_{Lp}$ = 0.014 m/s. $z$ = 40 cm.

Figs. 5-8a,b show the effect of temperature, pressure and base superficial liquid velocity on the pulse decay time for both liquid holdup and pressure drop traces, respectively. At constant pressure and base liquid velocity, the pulse decay time diminishes with increased temperature. Similarly, for a given temperature the decay time also decreases with increased pressure and liquid base velocity. However, the effect of temperature is more pronounced than that of pressure. The decay times vary between 1 to 2.6 s irrespective of the pressure drop or the liquid holdup time series and are longer than the breakthrough times reported earlier. The peaks hence in the fast mode exhibit a forward asymmetric distortion. The breakthrough + decay time spans between 40% (high pressure and/or high temperature and/or high $u_{Lb}$) and ca. 100% (low pressure and/or low temperature and/or low $u_{Lb}$) over a 4 s (breakthrough + decay + plateau) period of the fast-mode cycling. The

plateau time (which is short in this case) increases with increased temperature and/or pressure. As the decay time exhibits qualitatively similar dependences regarding pressure, temperature and liquid base velocity as those shown above in the case of the breakthrough time, the same explanations are valid again.

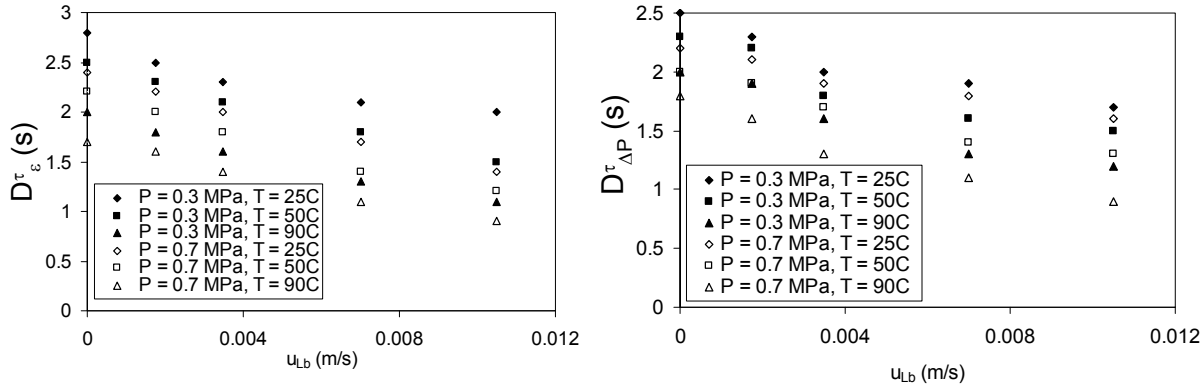


(a) (b)

**Figure 5-8** Pulse decay time as a function of base superficial liquid velocity. Effect of temperature and pressure on liquid holdup (a) and pressure drop (b) traces. $u_{Lp}$ = 0.014 m/s, $u_G$ = 0.05 m/s. $z$ = 40 cm.

At constant elevated temperature, pressure, base and pulse superficial liquid velocity, the pulse decay time for the liquid holdup and pressure drop traces decreases with increasing superficial gas velocity (Figs. 5-9a,b). One of the driving forces acting on the liquid flow is the drag force at the gas-liquid interface which is a function of gas velocity which reduces the amount of liquid held in the bed. Hence, the lesser liquid retained in the void space is expelled more vigorously the higher the gas superficial velocity resulting in the shortened pulse decay durations. The $D^{\tau}_{\Delta P}$ values shown in Fig. 5-9b reflect also this same trend.

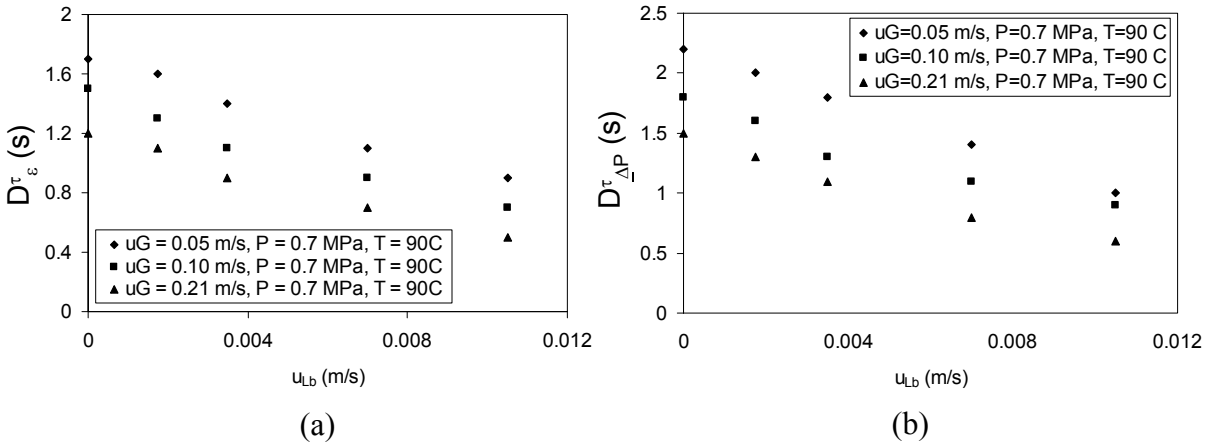


(a) (b)

**Figure 5-9** Influence of gas and base superficial liquid velocities on the pulse tail time at elevated temperature for liquid holdup trace (a) and pressure drop trace (b). $u_{Lp}$ = 0.014 m/s. $z$ = 40 cm.

Another very useful index to assess how the liquid holdup dynamics is affected by temperature, pressure, superficial gas and base liquid velocity is reflected in the pulse intensity introduced by Giakoumakis et al. (2005) during their studies of fast-mode cyclic operation in cold-flow trickle bed experimentations. The pulse intensity is an alternate designation of the statistics commonly known as the coefficient of variation and is merely a measure of a dimensionless standard-deviation of the (time series) variable under scrutiny divided by its corresponding time average. Fig. 5-10a displays the variations of the pulse intensity at 40 cm from the bed top as a function of the superficial liquid base velocity and parameterized by pressure and temperature for given superficial gas and pulse liquid velocities. The pulse intensity increases with increasing temperature while it decreases with pressure for constant superficial liquid base and pulse velocity and gas velocity. For any given temperature and pressure, pulse intensity decreases as $u_{Lb}$ or $u_G$ increases. First, the domain of variation of pulse intensity, typically between 0.3 and 0.05 for $P$ = 0.3 MPa is comparable with that reported by Giakoumakis et al. (2005) for similar gas velocities for ambient conditions. Second, it is expected that pulse intensity becomes vanishingly small - or at least measures only holdup fluctuations reminiscent of *natural* pulsing flow regime- as the base velocity is raised to approach the pulse velocity (Figs. 5-10a,b). Third, the superficial gas velocity affects the pulse intensity variations in a different way than liquid velocity. As a matter of fact, because the average liquid holdup is a decreasing function of gas throughput, increasing $u_G$ would have translated into increased pulse intensity.

However, it seems that the contrasts between the base and peak holdups are dampened more dramatically by the increased $u_G$ resulting in an overall diminishing pulse intensity. The effect of pressure seems to obey the same rationale as gas superficial velocity (Fig. 5-10a). Regarding the effect of temperature, the average liquid holdup decreases drastically in comparison to the corresponding holdup contrast between peak and base holdups yielding an overall increase in pulse intensity (Fig. 5-10a).

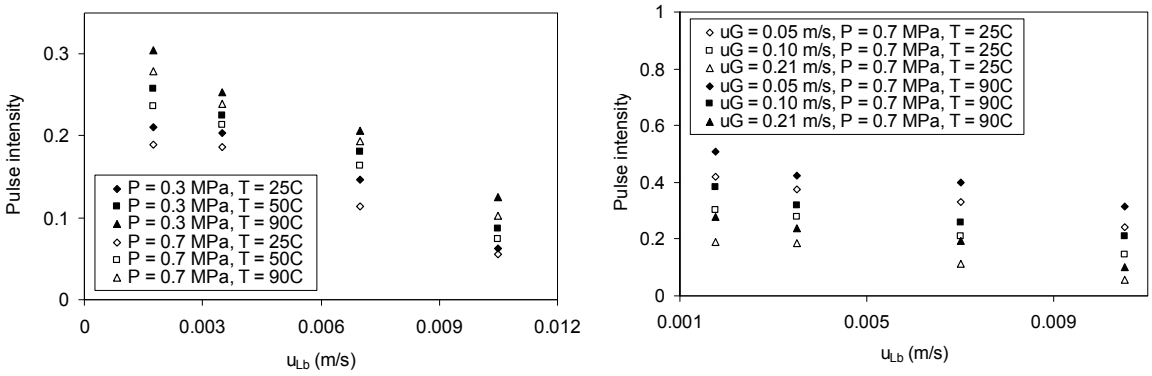


**Figure 5-10** Effect of (a) temperature and pressure ($u_G$ = 0.2 m/s), and (b) gas and base superficial liquid velocities on liquid holdup pulse intensity. $u_{Lp}$ = 0.014 m/s. $z$ = 40 cm.

### 5.3.3 Pulse Velocity

In Figs. 5-11a,b, the experimental pulse velocity data is plotted along with the values estimated from the expressions suggested by Wallis (1969) and by Giakoumakis et al. (2005), respectively. As seen from Fig. 5-11a, the pulse velocity increases with temperature and pressure at constant superficial gas, base and pulse liquid velocities. This can be explained by the decrease of the time needed for the liquid to traverse a given distance in the column due to being less viscous (effect of temperature) and/or being subjected to an increasing gas-liquid interfacial shear stress (effect of pressure). However, the pulse velocity values calculated by Wallis (1969) approach were found to significantly underestimate the experimental results. On the contrary, the correlation proposed by Giakoumakis et al. (2005) was found to slightly over-predict the measurements especially at the highest temperature and pressure levels. Interestingly, the correlation's predictions for the nearly-atmospheric pressure but high temperature are quite satisfactory.

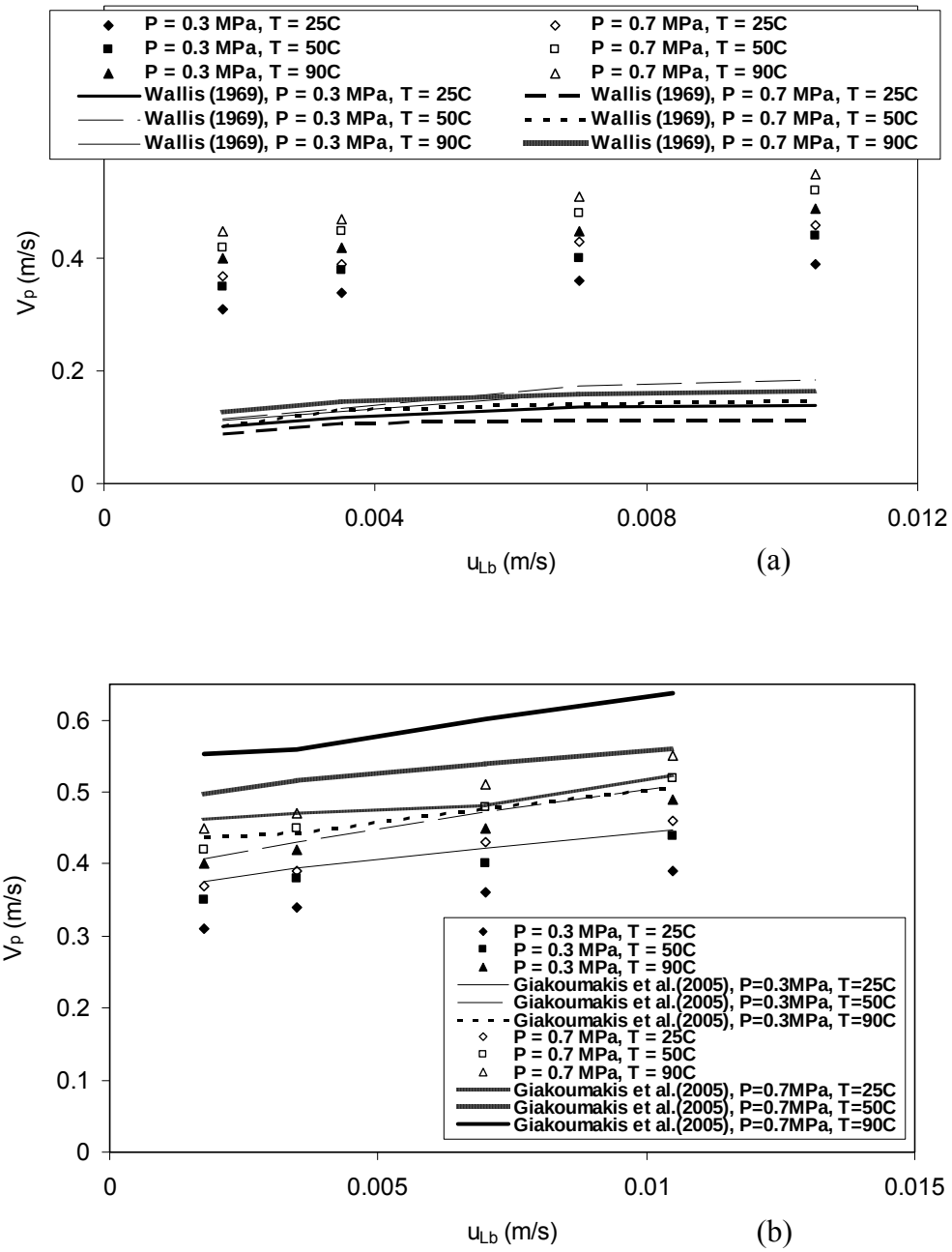


**Figure 5-11** Influence of temperature and pressure on pulse velocity. Experimental vs. calculated values. $u_{Lp}$ = 0.014 m/s, $u_G$ = 0.2 m/s. Comparisons with pulse velocities computed from (a) Wallis (1969) and (b) Giakoumakis et al. (2005).

### 5.3.4 Fast-Mode vs. Slow-Mode Operation

As discussed in detail in a previous study (Aydin et al., 2006), the extent up to which the pulses can preserve their isolated nature while traveling down the bed could be expressed by means of base, $\varepsilon_{Lb}$, and pulse, $\varepsilon_{Lp}$ holdup differences between cyclic and constant-

throughput TBR tests under similar operating conditions as sketched in Fig. 5-12. To be comparable, the holdup values in constant-throughput operation correspond to barycentric superficial liquid velocities calculated as seen above as $u_{L,o} = S \times u_{Lp} + (1\text{-}S) \times u_{Lb}$ either for fast-mode or slow-mode flows. In terms of pulse isolation, the deviation indices between cyclic operation and non-forced continuous flow were plotted for identical pressures, temperatures, superficial gas and liquid velocities in Figs. 5-13a,b for fast ($t_b$ = 2 s, $t_p$ = 2 s) and slow-mode ($t_b$ = 60 s, $t_p$ = 60 s) flows where the deviation indices are formulated as:

$$\frac{\Delta\varepsilon_{Lp}}{\varepsilon^{o}_{Lp}} = \frac{\varepsilon^{o}_{Lp} - \varepsilon_{Lp}}{\varepsilon^{o}_{Lp}} \tag{5-1}$$

$$\frac{\Delta\varepsilon_{Lb}}{\varepsilon^{o}_{Lb}} = \frac{\varepsilon_{Lb} - \varepsilon^{o}_{Lb}}{\varepsilon^{o}_{Lb}} \tag{5-2}$$

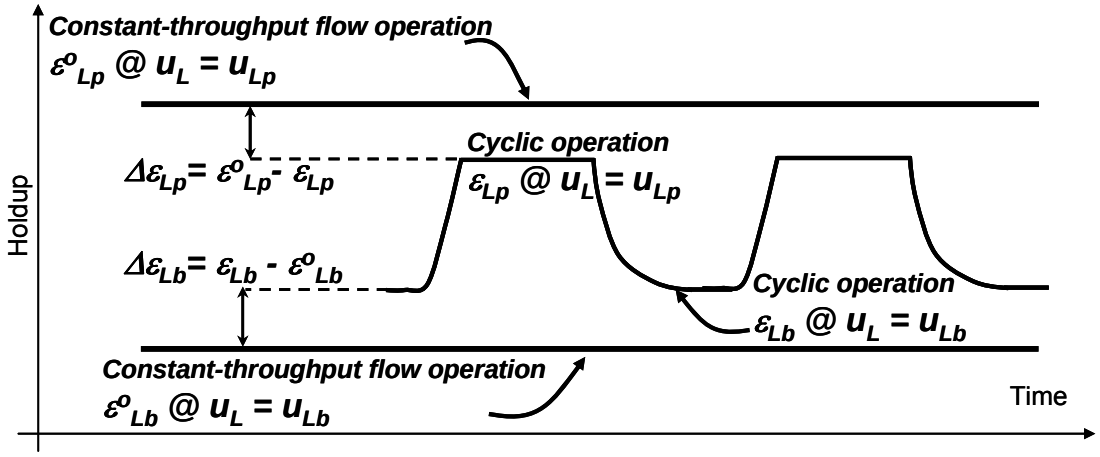


**Figure 5-12** Definition of the deviation indices and distinction between the holdup patterns of cyclic operation and non-forced constant-throughput operation for a given ($u_{Lb}$, $u_{Lp}$) set.

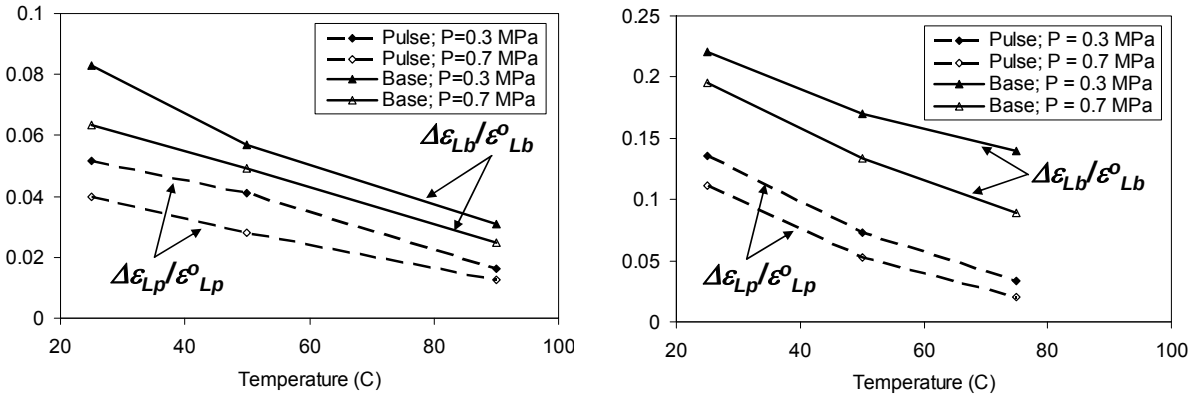


**Figure 5-13** Liquid holdup deviation indices as a function of temperature and pressure obtained at 40cm depth. $u_{Lb}$ = 0.0035 m/s, $u_{Lp}$ = 0.014 m/s, $u_G$ = 0.2 m/s, (a) fast-mode operation ($t_b$ = 2 s, $t_p$ = 2 s), (b) slow-mode operation ($t_b$ = 60 s, $t_p$ = 60 s).

At similar operating conditions, the deviation indices for the base and pulse liquid holdup decrease with increased reactor temperature and/or pressure, irrespective of the applied mode. However, the decrease for the fast mode is typically a factor two less pronounced than for the slow-mode. Under the operating conditions studied here, it can be concluded therefore that the pulses exchange less liquid content with their surroundings in the fast-mode than in the slow-mode operation. This means that, in the one hand, fast mode could be preferable to the slow mode in order to prolong the life time and the strength of waves as they advance downstream through the bed, and in the other hand, this would result in better performance with the former mode for the removal of heat and products from the catalyst during the peak liquid feed.

## 5.4 Conclusion

It is crucial to investigate the behavior of TBR operating at elevated temperature and pressure during liquid cyclic operation to explore the pros and cons of this strategy at conditions representative of industrial contexts. This study's aim was to investigate the effects of temperature and moderate pressure, superficial gas and (base and pulse) liquid velocities, and bed depth on the liquid holdup shape and dynamic features, *s*, pulse breakthrough and decay times, and pulse intensity, pulse velocity, as well as on the pressure drop time series in the fast-mode cyclic operation. The following main conclusions can be drawn from this study:

- fast-mode cyclic operation outperforms slow mode for the same split ratio, pressure, temperature and fluid throughputs as it preserves the holdup content of pulse typically two times better as assessed from the holdup deviation indices.
- For holdup and pressure drop time series, the pulse breakthrough and decay times are decreasing functions of temperature and pressure.
- Pulse intensity is an increasing function of temperature and a decreasing function of reactor pressure.
- In agreement with the behavior observed for the spontaneous pulsing flow regime in constant-throughput TBRs, pulse velocity increases both with temperature and pressure.

## 5.5 Nomenclature

$B^{\tau}$ breakthrough time, s

$D^{\tau}$ decay time, s

u superficial velocity, m/s

P reactor pressure, MPa

$\Delta P/H$ two-phase pressure drop, Pa/m

T reactor temperature, °C

$V_p$ pulse velocity, m/s

z bed height, cm

**Greek letters**

$\varepsilon_L$ liquid holdup

$\rho$ density, $kg/m^3$

$\mu$ viscosity, kg/m.s

$\sigma$ surface tension, $kg/s^2$

**Subscripts**

b base

G gas phase

L liquid phase

o continuous-flow

p pulse

r reactor

## 5.6 References

Aydin, B., Larachi, F., 2005. Trickle bed hydrodynamics and flow regime transition at elevated temperature for a Newtonian and a non-Newtonian liquid. Chemical Engineering Science 60, 6687-6701.

Aydin, B., Fries, D., Lange, R., Larachi, F., 2006. Slow-mode induced pulsing in trickle-bed reactors at elevated temperature. AIChE Journal 52, 3891-3901.

Aydin, B., Fries, D., Lange, R., Larachi, F., 2007. Slow-mode induced pulsing in trickle beds at elevated temperature for (non-)Newtonian liquids. Chemical Engineering Science 62, 5554-5557.

Banchero, M., Manna, L., Sicardi, S., Ferri, A., 2004. Experimental investigation of fast-mode liquid modulation in a trickle-bed reactor. Chemical Engineering Science 59, 4149-4154.

Bartelmus, G., Burghardt, A., Gancarczyk, A., Jaroslawska, E., 2006. Hydrodynamics of a trickle-bed reactor operating at a liquid-induced pulsing flow. Inzynieria Chemiczna i Procesowa, 27, 107-123.

Boelhouwer, J.G., Piepers, H.W., Drinkenburg, A.A.H., 2002a. Advantages of forced non-steady operated trickle-bed reactors. Chemical Engineering and Technology 25, 647-650.

Boelhouwer, J.G., Piepers, H.W., Drinkenburg, A.A.H., 2002b. Liquid-induced pulsing flow in trickle-bed reactors. Chemical Engineering Science 57, 3387-3399.

Boelhouwer, J.G., Piepers, H.W., Drinkenburg, A.A.H., 2002c. Nature and characteristics of pulsing flow in trickle-bed reactors. Chemical Engineering Science 57, 4865-4876.

Borremans, D., Rode, S., Wild, G., 2004. Liquid flow distribution and particle–fluid heat transfer in trickle-bed reactors: the influence of periodic operation. Chemical Engineering and Processing 43, 1403-1410.

Borremans, D., Rode, S., Wild, G., 2007. Cyclic variation of the liquid flow residence time in periodically operated trickle-bed reactors. Chemical Engineering Science 62, 1230-1238.

Chou, T.S., Worley, F.J., Luss, D., 1979. Local particle-liquid mass transfer fluctuations in mixed-phase cocurrent downflow through a fixed bed in the pulsing regime. Industrial and Engineering Chemistry Fundamentals 18, 279-283.

CRC Handbook of tables for Applied Engineering Science, 1970. CRC Press, Ohio, USA.

CRC Handbook of Chemistry and Physics, 1977. CRC Press, Boca Raton, USA.

Dudukovic, M.P., Larachi, F., Mills, P.L., 2002. Multiphase catalytic reactors: A perspective on current knowledge and future trends. Catalysis Reviews 44, 123-246.

Giakoumakis, D., Kostoglou, M., Karabelas, A.J., 2005. Induced pulsing in trickle beds—characteristics and attenuation of pulses. Chemical Engineering Science 60, 5183-5197.

Haure, P., Silveston, P.L., Hudgins, R.R., Bellut, M., 1991. Conversion efficiency in trickle bed reactors. US Patent 5, 011, 675.

Huther, A., Geisselmann, A., Hahn, H., 2005. Prozessintensivierung-Eine strategische option fur die chemische industrie. Chemie Ingenieur Technik 77, 1829-1837.

Jess, A., Popp, R., Hedden, K., 1999. Fischer–Tropsch-synthesis with nitrogen-rich syngas Fundamentals and reactor design aspects Applied Catalysis A: General 186, 321–342.

Lange, R., Gutsche, R., Hanika, J., 1999. Forced periodic operation of a trickle-bed reactor. Chemical Engineering Science 54, 2569-2573.

Larachi, F., Wild, G., Laurent, A., Midoux, N., 1994. Influence of gas density on the hydrodynamics of cocurrent gas-liquid upflow fixed bed reactors. Industrial and Engineering Chemistry Research 33, 519-525.

Liu, G., Mi, Z., 2005. Hydrogenation of 2-ethylanthraquinones in a periodically operated trickle-bed reactor. Chemical Engineering and Technology 28, 857-862.

Massa, P., Ayude, M.A., Ivorra, F., Fenoglio, R., Haure, P., 2005. Phenol oxidation in a periodically operated trickle bed reactor. Catalysis Today 107-108, 630-636.

Meyers, R.A. 1996. Handbook of petroleum refining processes. McGraw-Hill, 2ed ed., New York, USA.

Muzen, A., Fraguio, M.S., Cassanello, M.C., Ayude, M.A., Haure, P.M., Martinez, O.M., 2005. Clean oxidation of alcohols in a trickle-bed reactor with liquid flow modulation. Industrial and Engineering Chemistry Research 44, 5275-5284.

Stradiotto, D.A., Hudgins, R.R., Silveston, P.L., 1999. Hydrogenation of crotonaldehyde under periodic flow interruption in a trickle bed. Chemical Engineering Science 54, 2561-2568.

Trivizadakis, M.E., Giakoumakis, D., Karabelas, A.J., 2006a. Induced pulsing in trickle beds - particle shape and size effects on pulse characteristics. Chemical Engineering Science 61, 7448-7462.

Trivizadakis, M.E., Karabelas, A.J., 2006b. A study of local liquid/solid mass transfer in packed beds under trickling and induced pulsing flow. Chemical Engineering Science 61, 7684-7696.

Ucan, L.H., Ozkan, G., Bicer, A., Pamuk, V., 2005. Removal of sulphur dioxide in a periodically operating trickle-bed reactor with activated carbon bed. Process Safety and Environmental Protection 83, 47-49.

Wammes, W.J.A., Middelkamp, J., Huisman, W.J., deBaas, C.M., Westerterp, K.R., 1991. Hydrodynamics in a cocurrent gas-liquid trickle bed at elevated pressures. AIChE Journal 37, 1849-1862.

Wang, Y.-N., Xu, Y.-Y., Li, Y.-W., Zhao, Y.-L., Zhang, B.-J., 2003. Heterogeneous modeling for fixed-bed Fischer–Tropsch synthesis: Reactor model and its applications. Chemical Engineering Science 58, 867 – 875.

Wallis, G.B. 1969. One-dimensional two-phase flow. McGraw-Hill Inc., New York, pp 122-135.

Xiao, Q., Cheng, Z.M., Jiang, Z.X., Anter, A.M., Yuan, W.K., 2001. Hydrodynamic behavior of a trickle bed reactor under forced pulsing flow. Chemical Engineering Science 56, 1189-1195.

# Chapter 6

# Trickle bed hydrodynamics at elevated temperature for (non-)Newtonian foaming liquids*

## Résumé

Les études hydrodynamiques des réacteurs trickle-bed opérés à des conditions non-ambiantes portent essentiellement sur les systèmes coalescents bien que de nombreuses applications industrielles concernent le traitement de liquides moussants pour lesquelles des données techniques sont rares. Afin de combler ce vide, cette étude rend compte des effets de la température et de la pression sur la transition du régime d'écoulement ruisselant au régime d'écoulement pulsé moussant, sur la perte de charge bi-phasique, sur la rétention en liquide ainsi que sur la fréquence et la vitesse des pulsations pour les systèmes Newtoniens moussants air-bromure de cétyltriméthylammonium (CTAB) et les systèmes non-Newtoniens moussants air-0,25% CTAB-carboxyméthylcellulose (CMC). À une vitesse superficielle du gaz constante, la transition de l'écoulement ruisselant vers l'écoulement pulsé moussant a été observée à de plus faibles vitesses superficielles du liquide comparativement aux systèmes non-moussants. La frontière de la transition est déplacée vers les vitesses superficielles du liquide et du gaz plus élevées lorsque les températures et les pressions augmentent. La fréquence de pulsation augmente aussi bien avec la température que la pression alors que la vitesse de la pulsation augmente avec la température, mais diminue avec l'augmentation de la pression. La comparaison respective avec les systèmes coalescents, en l'occurrence eau-air et air-CMC/eau a montré que les systèmes Newtoniens et non-Newtoniens moussants présentent des comportements qualitatifs similaires relativement aux effets de la température et de la pression.

* Aydin, B.; Larachi, F. Chemical Engineering Journal, submitted

## Abstract

Hydrodynamic studies on trickle-bed reactors at non-ambient conditions overwhelmingly addressed coalescing systems despite numerous industrial applications concern the processing of foaming liquids for which engineering data are scantier. To fill this gap, the effects of temperature and moderate pressure are reported in this study on the shift of the transition from trickle to foaming-pulsing flow regimes, on the two-phase pressure drop, the liquid holdup, and the pulse frequency and velocity for Newtonian (air-cetyltrimethylammoniumbromide (CTAB)) foaming and non-Newtonian (air-0.25% CTAB-carboxymethylcellulose (CMC)) foaming systems. At constant superficial gas velocity, the trickle-to-foaming pulsing flow transition boundary was observed at lower superficial liquid velocity in comparison to non-foaming systems. The transition boundary shifted towards higher gas and liquid superficial velocities with increasingly temperatures and pressures. The pulse frequency increased with temperature and/or pressure whereas the pulse velocity increased with temperature but it decreased with increasing pressure. Respective comparisons with the coalescing alter ego, namely, air-water and air-CMC/water systems, showed that Newtonian and non-Newtonian foaming systems behaved qualitatively similarly regarding the effects of temperature and pressure as the coalescing systems.


## 6.1 Introduction

Trickle bed reactors (TBR), which consist of fixed beds fed co-currently downwards with gas and liquid streams, host a diversity of gas-liquid-solid reactive systems. For instance, TBR has been ushering for decades the oil industry where it is the battle horse in its refining operations. Among the various processes relying on trickle beds, their hydrodynamics when foaming systems are involved remains a poorly explored subject even though foams emanate very often in the petroleum, pharmaceutical and food industries (Prud'homme and Khan, 1996). Especially in the petroleum industry, foams play an important role in productivity and petroleum recovery and processing (Schramm, 1994). Previous experimental work on foaming liquids highlighted the differences of TBR

hydrodynamics in comparison to non-foaming systems (Charpentier and Favier, 1975; Bartelmus and Janecki, 2003, 2004).

Experimental studies on foaming in trickle beds were initiated by Larkins et al. (1961) and Weekman and Myers (1964). Till the late 1990s, the experimental work on flow regimes, pressure drop and liquid holdup were performed for a variety of foaming gas-liquid systems (Charpentier and Favier, 1975; Midoux et al., 1976; Talmor, 1977; Morsi et al. 1978, 1982; Sai and Varma, 1987; Sai, 1997) but were restricted mainly to ambient conditions. However, Wild et al. (1991) showed that the hydrodynamics of foaming systems can be dramatically influenced by increased pressures such as skyrocketing amplitudes of pressure fluctuations after a flow pattern shift beyond the transition line between trickle and foaming-pulsing flow regimes. Some systematic studies were triggered on the effect of pressure on TBR hydrodynamics with weakly and strongly foaming liquids (Bartelmus and Janecki, 2003, 2004; Burghardt et al., 2003a,b; Janecki et al. (2005), such as the trickle-to-pulsing flow regime transition, the pressure drop and liquid holdup up to 2 MPa. To the best of the authors' knowledge, pulse velocity and frequency at non-ambient conditions are missing in the open literature. At much elevated pressures up to 8.1 MPa, Larachi et al. (1991) reported pressure drop and liquid holdup data using as a foaming system nitrogen-1%w/w ethanol/water. It is worthy of notice that none of the published literature addressed the incidence of elevating temperature on the evolution of TBR hydrodynamics with foaming liquids.

This work therefore presents a systematic study on the effect of temperature on the hydrodynamics of TBR for Newtonian and non-Newtonian foaming systems. The influence of temperature on the trickle to foaming-pulsing flow transition boundary, the two-phase pressure drop, the liquid holdup, and the pulse velocity and frequency are reported for the first time. The two-phase pressure drop and liquid holdup at the trickle-to-foaming-pulsing transition are also analyzed at elevated temperature and moderate pressure.

## 6.2 Experimental Setup

The experimental setup was discussed in detail elsewhere (Aydin and Larachi, 2005). The experiments were performed in a bed of 107 cm high and 4.8 cm-ID packed with 3 mm glass beads. As foaming systems, the air-aqueous cetyltrimethylammoniumbromide

(CTAB, 6.25 ppmw or $0.17 \times 10^{-4}$ mol/L) and air-6.25 ppmw CTAB-0.25% w/w aqueous carboxymethylcellulose (CMC) solutions were prepared and their behavior was compared to the air-water and the air-0.25%CMC base case solutions, respectively. To prevent fading of foaminess during the high temperature tests, CTAB was chosen because it is a non-volatile surfactant in the studied temperature range. For the CTAB-containing Newtonian solutions, the CTAB critical micelle concentration increased from $0.95 \times 10^{-3}$ to $2.35 \times 10^{-3}$ mol/L when temperature increased from 25 and 90 ºC. Correspondingly, the surfactant concentrations expressed as a percentage of critical micelle concentration varied from 1.8% to 0.7% (Evans et al., 1984). Fractional surfactant concentrations between 0.6 and 1.8% cmc were already high enough to turn the systems into foaming (air-CTAB/water) and strongly foaming (air-CTAB-CMC/water) ones and to dramatically alter the reactor hydrodynamics with respect to the air-water and air-CMC/water base cases.

Similar to the preparation procedure in Aydin and Larachi (2005), the CTAB-CMC solutions were prepared by dissolving first CTAB and then powdered CMC in water at ambient temperature. The pseudoplastic rheological behavior was well represented by an empirical power law relation. The consistency index, k, and the power-law index, n, were fitted for each temperature after measuring the solution shear stress-shear rate response on an ARES (Advanced Rheometric Expansion System) rheometer in the 0-1000 s-1 shear-rate ranges. Table 6-1 displays the physicochemical properties of 0.25% w/w aqueous CTAB-CMC solution from 25ºC to 90ºC. The viscosity and the surface tension are sensitive to temperature where the effective viscosity drop of CTAB-CMC is expressed with consistency index, k, and the power-law index, n. The properties of the 6.25 ppmw CTAB solution are also given in Table 6-1 along with the density and dynamic viscosity of the gas phase (dry basis).

**Table 6-1** Properties of aqueous CTAB, 0.25% CTAB-CMC and Air at Elevated Temperatures

| Temperature (ºC) | $\rho_{CTAB}$ # (kg/m3) | $\mu_{CTAB}$ # x $10^4$ (kg/m.s) | $\sigma_{CTAB}$ ($kg/s^2$) | $k_{CTAB-CMC}$ ($kg/m.s^{2-n}$) | $n_{CTAB-CMC}$ | $\sigma_{CTAB-CMC}$ ($kg/s^2$) | $\rho_{air}$ * (0.3 MPa) ($kg/m^3$) | $\rho_{air}$ * (0.7 MPa) ($kg/m^3$) | $\mu_{air}$ * x $10^5$ (kg/m.s) |
|---|---|---|---|---|---|---|---|---|---|
| 25 | 997.21 | 8.86 | 0.050 | 0.212 | 0.625 | 0.052 | 3.49 | 8.15 | 1.84 |
| 50 | 988.22 | 5.36 | 0.037 | 0.137 | 0.617 | 0.048 | 3.23 | 7.53 | 1.96 |
| 90 | 964.7 | 3.12 | 0.032 | 0.121 | 0.614 | 0.045 | 2.92 | 6.82 | 2.13 |

*CRC Handbook of tables for Applied Engineering Science (1970)

#estimated to be close to the values for water

For the elevated temperature measurements, the liquid, prior to be routed to the reactor via a calibrated flowmeter was heated in a reservoir through a liquid preheater. The gas was supplied from a compressed air line up to a maximum pressure of 0.7 MPa. After passing through a preheater, the gas phase encountered the heated liquid phase at the top of the reactor. Both phases were introduced co-currently downwards through a distributor which was designed to obtain a uniform distribution. At the reactor outlet both phases were intercepted in a separator where the gas phase was vented to the atmosphere via a calibrated flowmeter and the liquid phase was drained. Measurements were taken only when the desired steady-state operating temperature was reached along the bed after the reactor was systematically and preventively operated under pulsing flow regime to ensure full bed wetting.

An electrical conductance technique using ring electrodes was employed for the identification of regime transition and for the investigation of the pulse characteristics as detailed elsewhere (Aydin and Larachi, 2005). The two electrical conductance probes were mounted in the middle of the reactor, a distance of 0.245 m apart from each other. Each probe was connected to a lock-in amplifier to acquire the output signal. After amplification, the signals were transmitted to a computer by means of a data acquisition system. Identification of flow regime transition was carried out using a moment method (Rode, 1992). Pulse frequency, $f_p$, was determined by counting the number of maxima or minima

of the conductance trace and dividing by the pulse period for a selected portion of the conductance trace. Pulse velocity, $V_p$, was determined by dividing the inter-electrode distance by the time delay of maximum cross-correlation between signals.

The two-phase pressure drop was measured with a differential pressure transducer connected to the top and bottom of the packed bed. For liquid holdup measurements, the Aris's double-detection tracer response method was implemented. Two electric conductivity probes - one at the top and another at the bottom of the column - were used. The plug flow with axial dispersion (PD) model was used to determine the liquid holdup ($\varepsilon_L$) by applying a non-linear least squares fitting where the convolution method was used for a time-domain analysis of the non-ideal pulse tracer response data.

## 6.3 Results and Discussion

### 6.3.1 Temperature and Pressure Evolution of the Transition between Trickling and Foaming-Pulsing

Flow regimes in a trickle bed reactor emerge due to the interaction between phases which depend on fluid flow rates and physical properties as well as on reactor and particle geometrical features. As for coalescing systems, a low interaction regime, referred to as trickle flow regime at low fluid throughputs, and high interaction regimes at either or both high gas and liquid throughputs exist also for foaming systems. In Figs. 6-1a,b, the transition boundary from trickle flow to foaming-pulsing flow is plotted as a function of the superficial gas and liquid velocities, the reactor pressure and temperature for the air-CTAB/water and the air-CTAB-CMC/water systems. The observed results are compared with the air-water (Fig. 6-1c) and air-CMC/water (Fig. 6-1d) systems, respectively. Note that the transition was referred to the displacement from trickling to foaming-pulsing flow, and not from trickling to pulsing flow, as it was difficult to distinguish the pulsing flow regime from the foaming pulsing flow regime. This was due to a systematic presence of foams which was recognizable by the larger fluctuations in comparison with the non-foaming system.

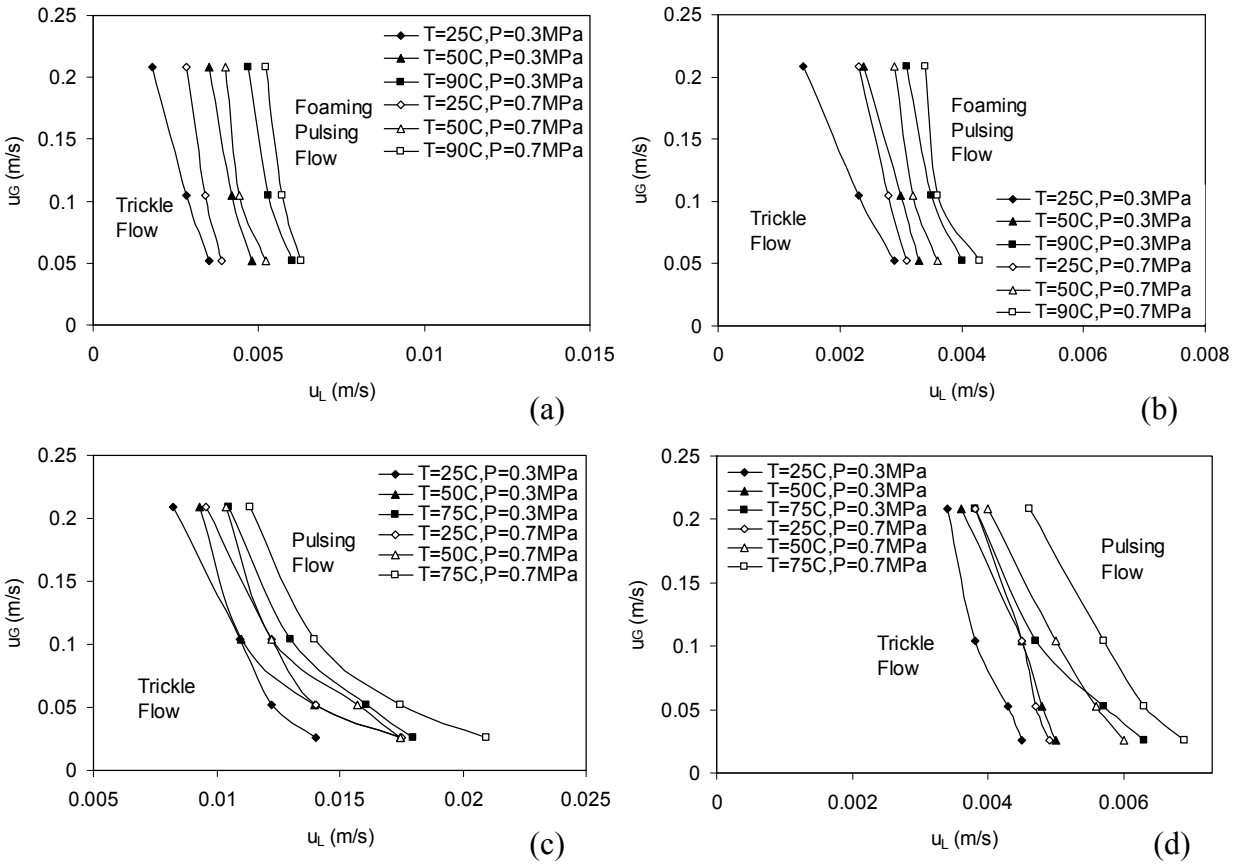


**Figure 6-1** Influence of pressure and temperature on the transition boundary between trickle and foaming-pulsing flow regimes for the (a) air-CTAB/water (b) air-CTAB-CMC/water (c) air-water (d) air-CMC/water systems.

The pronounced influence of both reactor pressure and temperature on the transition is illustrated in Figs. 6-1a,b for both systems. At ambient temperature and constant superficial gas velocity, there is a shift of the transition line towards higher liquid velocities with an increase in reactor pressure. This tendency is classical and is reminiscent of the enlargement of the trickle flow domain as observed for non-foaming Newtonian and non-Newtonian liquids (Aydin and Larachi, 2005) and where the interpretation that a higher liquid volumetric flux is required at elevated pressure to initiate pulse formation is widely accepted. It should be noted that at a given superficial gas velocity, the transition takes place at a much lower superficial liquid velocity for foaming systems than for non-foaming systems (Fig. 6-1a-d) despite minute changes in the physicochemical properties of the liquids by the introduction of CTAB (Table 6-1). This is explained as due to early foam formation at lower liquid fluxes as a result of increased pressures; the foams being characterized by lower liquid holdups (Bartelmus and Janecki, 2003).

Similar to the effect of pressure, the shift towards higher liquid velocities was observed at constant superficial gas velocity with an increase in reactor temperature at constant pressure (Figs. 6-1a,b). Foam stability is very likely lessened with increased temperatures due to the viscosity decrease of the liquid. This promotes the liquid on the bubble surface to drain faster and to yield unstable bubbles the higher the temperature at given gas and liquid volumetric fluxes. In addition, the resisting forces acting on the liquid phase such as the surface tension force and the liquid shear stress (via viscosity) are weakened with temperature. This causes a decrease in the amount of liquid held within the bed as noted in the behavior of coalescing systems (Figs. 6-1c,d). Therefore, a higher liquid flow rate is required for the emergence of pulses in the case of foaming systems the higher the temperature. Furthermore, at constant pressure, the effect of temperature on the transition boundary is more pronounced for the foaming systems (Figs. 6-1a,b) in comparison to non-foaming systems (Figs. 6-1c,d).

Figs. 6-2 and 6-3 show the effect of reactor temperature, pressure and superficial gas velocity on the liquid holdup and the two-phase pressure drop at the trickle-to-foaming-pulsing transition points: air-CTAB/water (Fig. 6-2a,3a) and air-CTAB-CMC/water (Fig. 6-2b,3b) systems. For the air-CTAB-CMC/water, the liquid holdup values ($\varepsilon_L$) are larger by ca. a factor two with respect to those corresponding to the air-CTAB/water system. However, the ranges for the transition pressure drops are almost coincident for both systems, typically between 15 kPa/m and 30 kPa/m. There is a tendency for the transition liquid holdup to decrease especially in the higher temperatures region for both systems and regardless of superficial gas velocity and pressure. This liquid holdup tendency is similar to the one reported for the corresponding coalescing systems by Aydin et al. (2007). The transition pressure drops monotonically decrease with temperature over the whole range of temperatures. Both trends can be related to the liquid viscosity greater sensitivity to temperature, which amongst the physical gas and liquid properties, is the one that experiences the largest reduction when temperature rises from ambient to 90°C. The pressure drop decreases with temperature in comparable proportions for both systems. Here again, increased temperatures are likely to weaken the frictional forces at the gas-liquid and liquid-solid interfaces as well as liquid surface tension forces resulting in less resistance to flow.

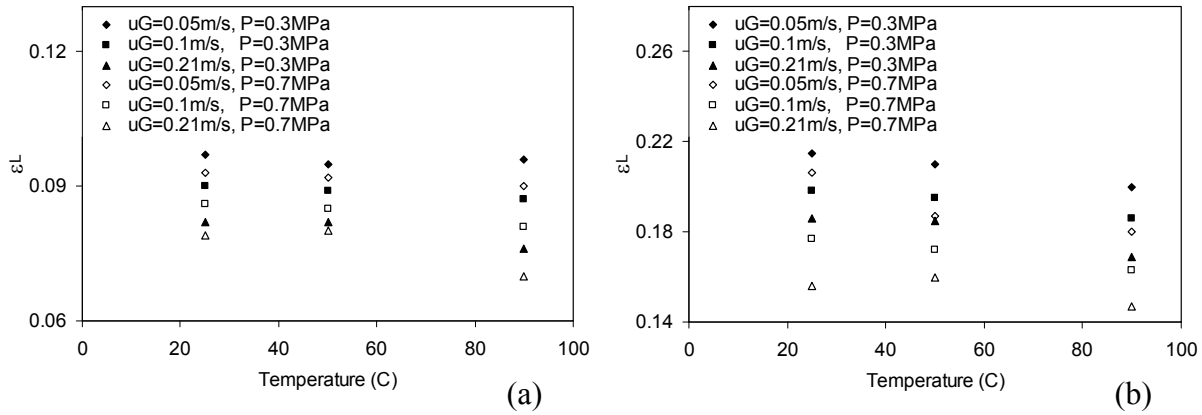


**Figure 6-2** Effect of temperature, pressure and superficial gas velocity on liquid holdup at trickle-to-foaming-pulsing transition points. (a) air-CTAB/water (b) air-CTAB-CMC/water

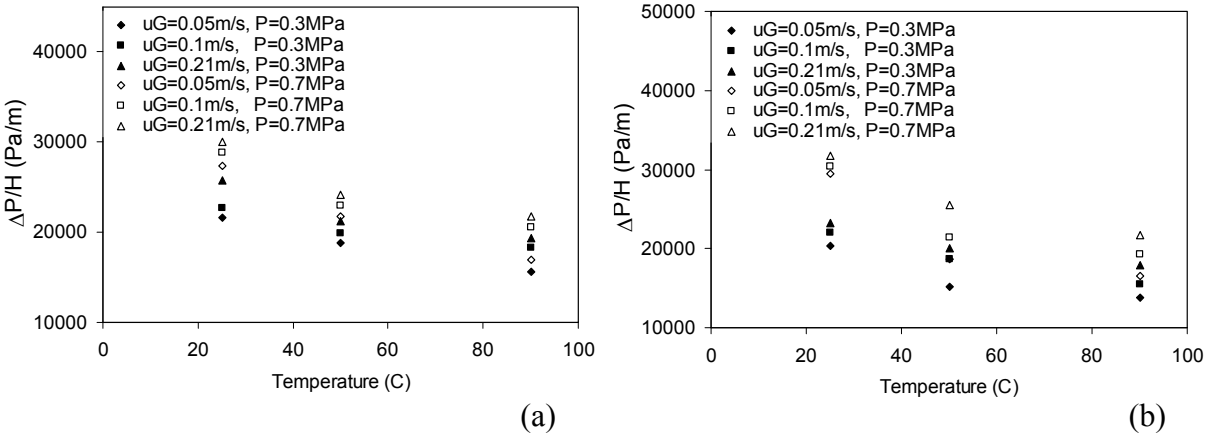


**Figure 6-3** Effect of temperature, pressure and superficial gas velocity on pressure drop at trickle-to-foaming-pulsing transition points. (a) air-CTAB/water (b) air-CTAB-CMC/water**.**

At constant temperature, the transition liquid holdup diminishes with increasing pressure and superficial gas velocity for both systems (Fig. 6-2). Such liquid holdup reduction is mirrored by the simultaneous increase of the transition pressure drops with increasing gas superficial velocity and/or pressure (Fig. 6-3). For these experiments, it was observed that the amount of foam produced with increasing pressure is more pronounced for air-CTAB-CMC/water system than that for air-CTAB/water system. This could be intuited from Fig. 6-2b where a more pronounced fall off of transition liquid holdup with increasing pressure and/or superficial gas velocity take place. However, the transition pressure drop rise is more sensitive to increasing pressure than to increasing gas superficial velocity (Fig. 6-3b).

### 6.3.2 Liquid Holdup & Two-phase Pressure Drop

The effect of reactor temperature, pressure and superficial gas and liquid velocities on liquid holdup for air-CTAB/water and air-water systems is illustrated in Figs. 6-4a,b and Figs. 6-4c,d, respectively. These plots include the holdup variations extending from trickle flow to foaming-pulsing flow regime. Similar to the air-water system, liquid holdup increases with superficial liquid velocity for the air-CTAB/water system. As expected, liquid holdup values for the foaming system are much lower than for the non-foaming system for equal fluid volumetric fluxes, and temperature and pressure. Furthermore, liquid holdup increases only slightly for the foaming system (Fig. 6-4a) in comparison with the non-foaming system (Fig. 6-4c) over a comparable liquid velocity range. Increasing reactor pressure and superficial gas velocity causes lower liquid holdups. The effect of superficial gas velocity and pressure is drastic for all superficial liquid velocities for the air-CTAB/water system, whereas it is more pronounced for the air-water system only at the higher superficial liquid velocities.

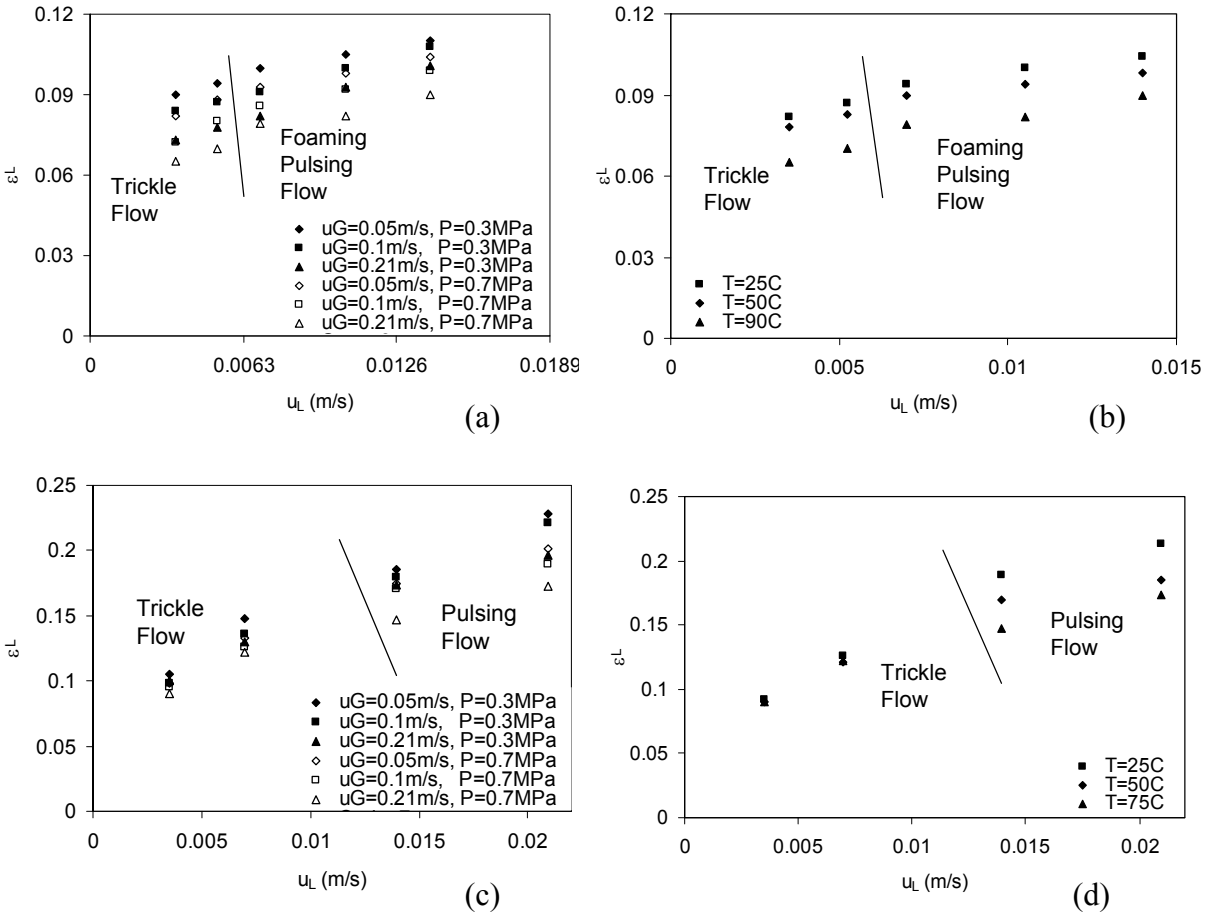


**Figure 6-4** Influence of pressure and superficial gas velocity (a,c) and temperature (b,d) on liquid holdup for air-CTAB/water and air-water systems

Liquid holdup decreases with increasing temperature for given pressure, and superficial liquid and gas velocities. For the same reasons outlined earlier, the dependence of liquid holdup to temperature is in qualitative agreement with that highlighted on the transition liquid holdup data. The air-CTAB/water system exhibits a remarkable knock-down effect by temperature over the whole superficial liquid velocities (Fig. 6-4c) whereas the air-water system is sensitive to temperature only in the high liquid throughput region (Fig. 6-4d).

Figs. 6-5a-d show the effect of temperature, pressure, and superficial liquid and gas velocities on liquid holdup for air-CTAB-CMC/water and air-CMC/water systems. At constant gas and liquid velocities and temperature, liquid holdup decreases with increasing pressures for the air-CTAB-CMC/water system similarly to the air-CTAB/water system. However, the effect of pressure for the non-Newtonian system is more visible at high superficial liquid velocity. As expected, the liquid holdup values are larger (Fig. 6-5a) than those of the air-CTAB/water system (Fig. 6-4a) due to the viscosity factor. There is a

remarkable difference between the effect of pressure and temperature on the liquid holdup for air-CTAB-CMC/water (Figs. 6-5a,b) and air-CMC/water (Figs. 6-5c,d) systems. The effect of pressure is more pronounced for the former (Figs. 6-5a,c) whereas the effect of temperature is more significant for the latter (Figs. 6-5b,d).

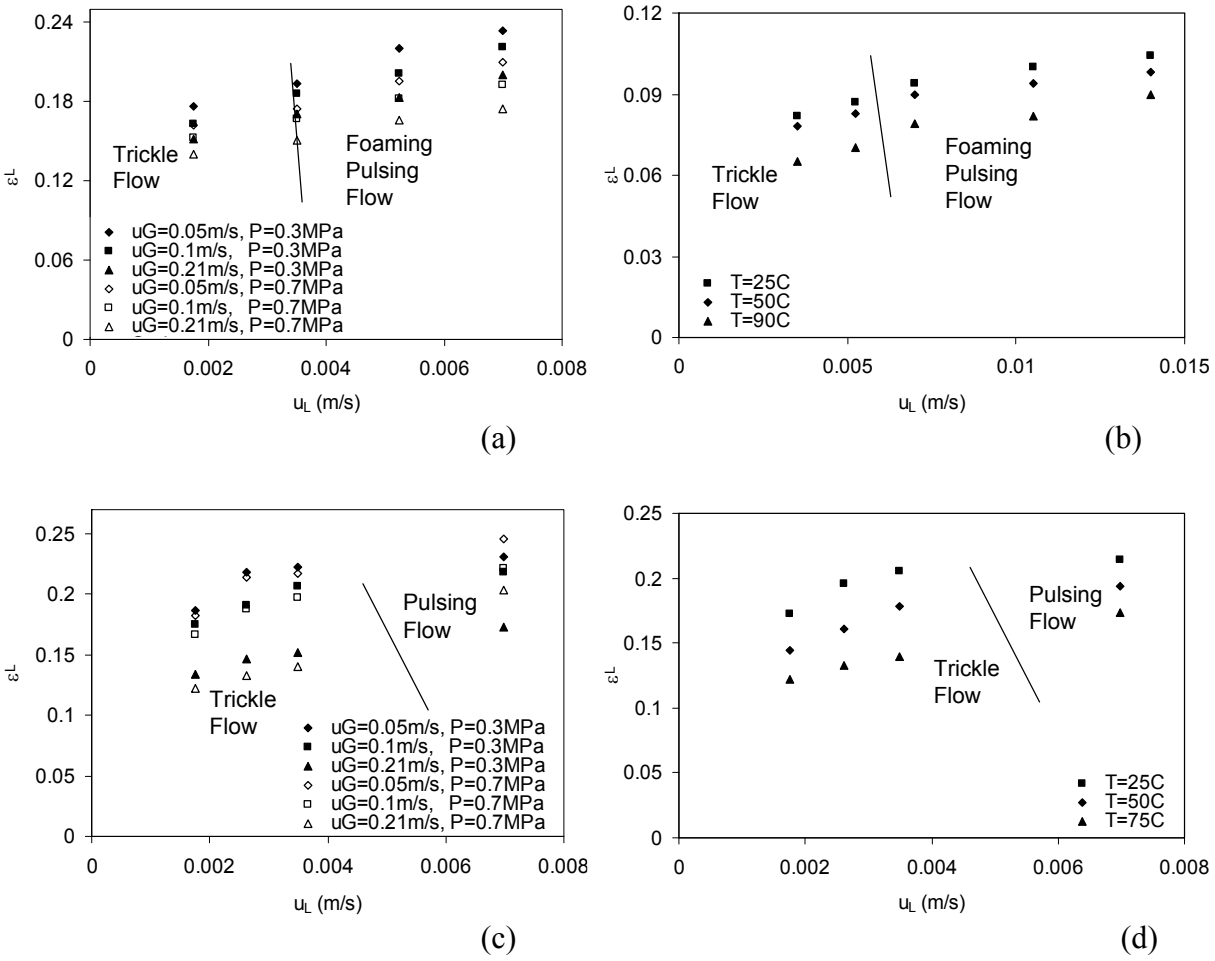


**Figure 6-5** Influence of pressure and superficial gas velocity (a,c) and temperature (b,d) on liquid holdup for air-CTAB-CMC/water and air-CMC/water systems

Figs. 6-6,7 show the effect of temperature and pressure on two-phase pressure drop at various superficial liquid and gas velocities for the Newtonian and the non-Newtonian foaming liquids, respectively. At constant superficial liquid and gas velocities, pressure drop decreases with increasing temperature and with decreasing pressure for the same reasons as the pressure drop behavior at the transition point discussed in Fig. 6-3. As seen in Fig. 6-6b, the effect of superficial liquid velocity on the pressure drop is very significant.

The onset of foaming which is characterized by the interaction between gas and liquid phases is more favorable at higher liquid throughputs occasioning higher pressure drops.

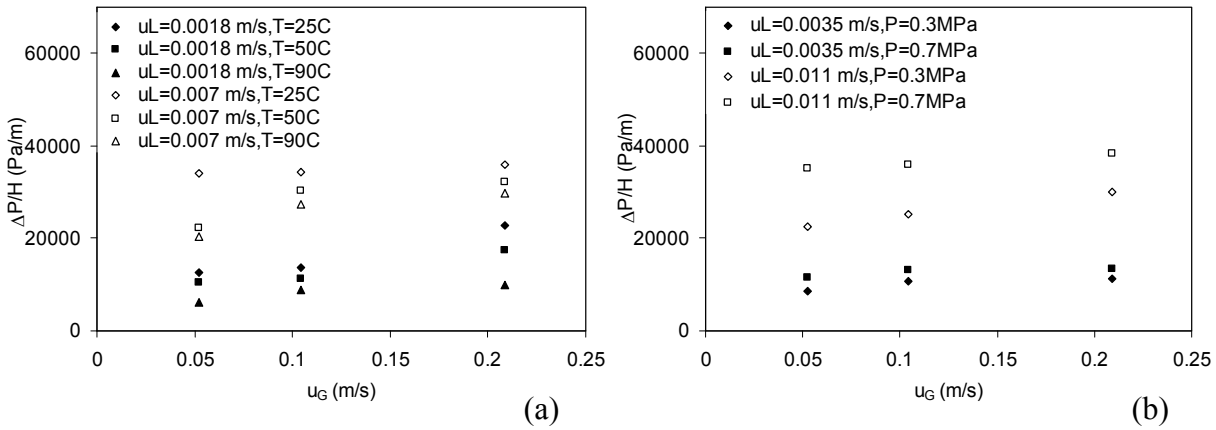


**Figure 6-6** Influence of temperature (a), and pressure and superficial gas velocity (b) on pressure drop for air-CTAB/water system.

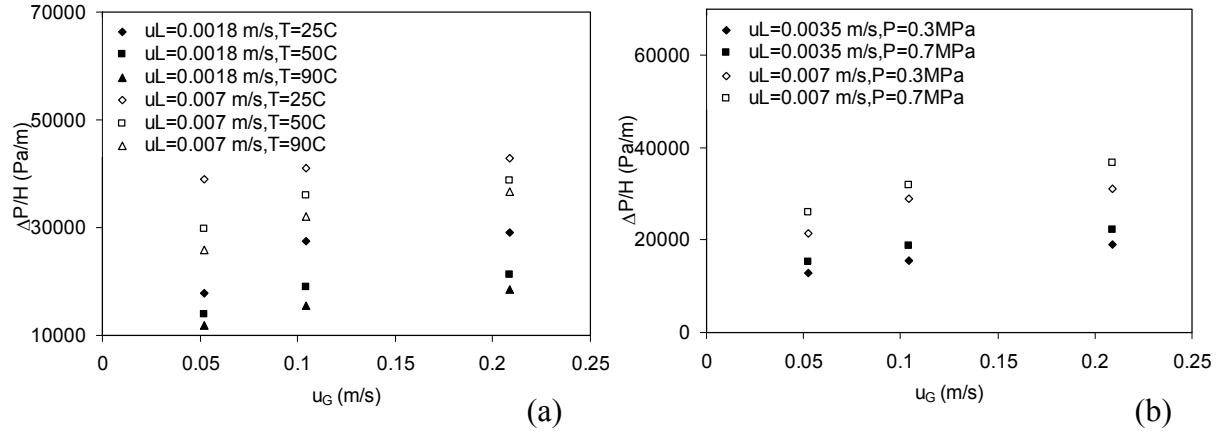


**Figure 6-7** Influence of temperature (a), and pressure and superficial gas velocity (b) on pressure drop for air-CTAB-CMC/water system.

### 6.3.3 Pulse Frequency and Velocity

Figs. 6-8a,b show the effect of temperature, pressure and superficial liquid velocity on the pulse frequency for the Newtonian and the non-Newtonian foaming systems, respectively. At the same operating conditions, the pulse frequency for the air-CTAB-CMC/water system is higher in comparison to the air-CTAB/water system. This could ascribe to the weaker foaming behavior observed for the Newtonian liquid. The pulse frequency increases with temperature and pressure with a more noticeable incidence from the pressure factor for

both systems. At constant temperature and pressure, the pulse frequency also increases abruptly with the superficial liquid velocity.

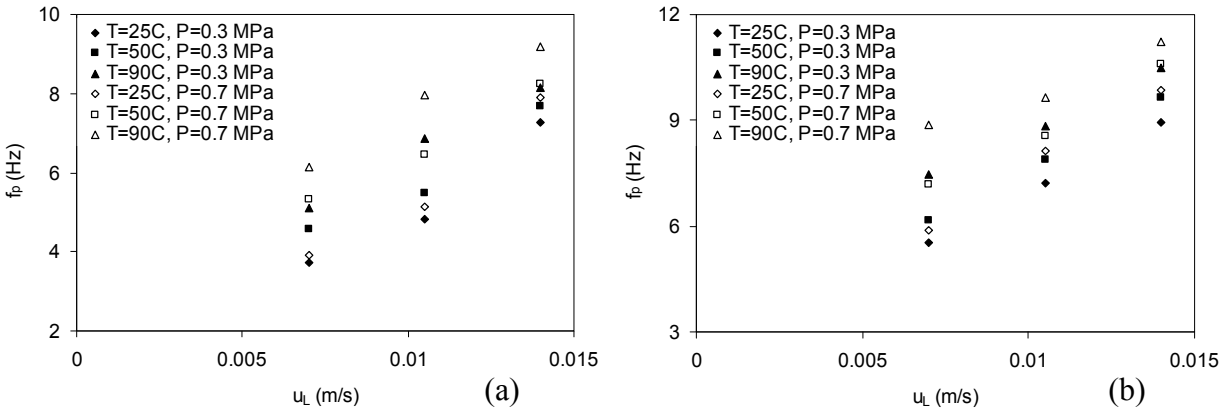


**Figure 6-8** Effect of temperature, pressure and superficial liquid velocity on pulse frequency for (a) air-CTAB/water (b) air-CTAB-CMC/water systems. $u_G$ = 0.21 m/s.

A second basic characteristic of foaming pulsing flow regime is the pulse velocity which was determined at elevated pressure and temperature as explained in the Experimental section. Figs. 6-9a,b illustrate that the pulse velocity increases with temperature at constant superficial liquid velocity and pressure due to a decrease in dynamic liquid viscosity and an increase in interstitial liquid velocity. The gradual increase of the pulse velocity with temperature is similar for Newtonian or non-Newtonian foaming systems. The pulse velocity decreases with the increasingly pressure for both systems in accordance with Burghardt et al. (2004) and Aydin and Larachi (2005) experimental findings for the coalescing systems. For the air-CTAB/water system (Fig. 6-9a), larger values of pulse velocities were reached in comparison to the air-CTAB-CMC/water system (Fig. 6-9b).

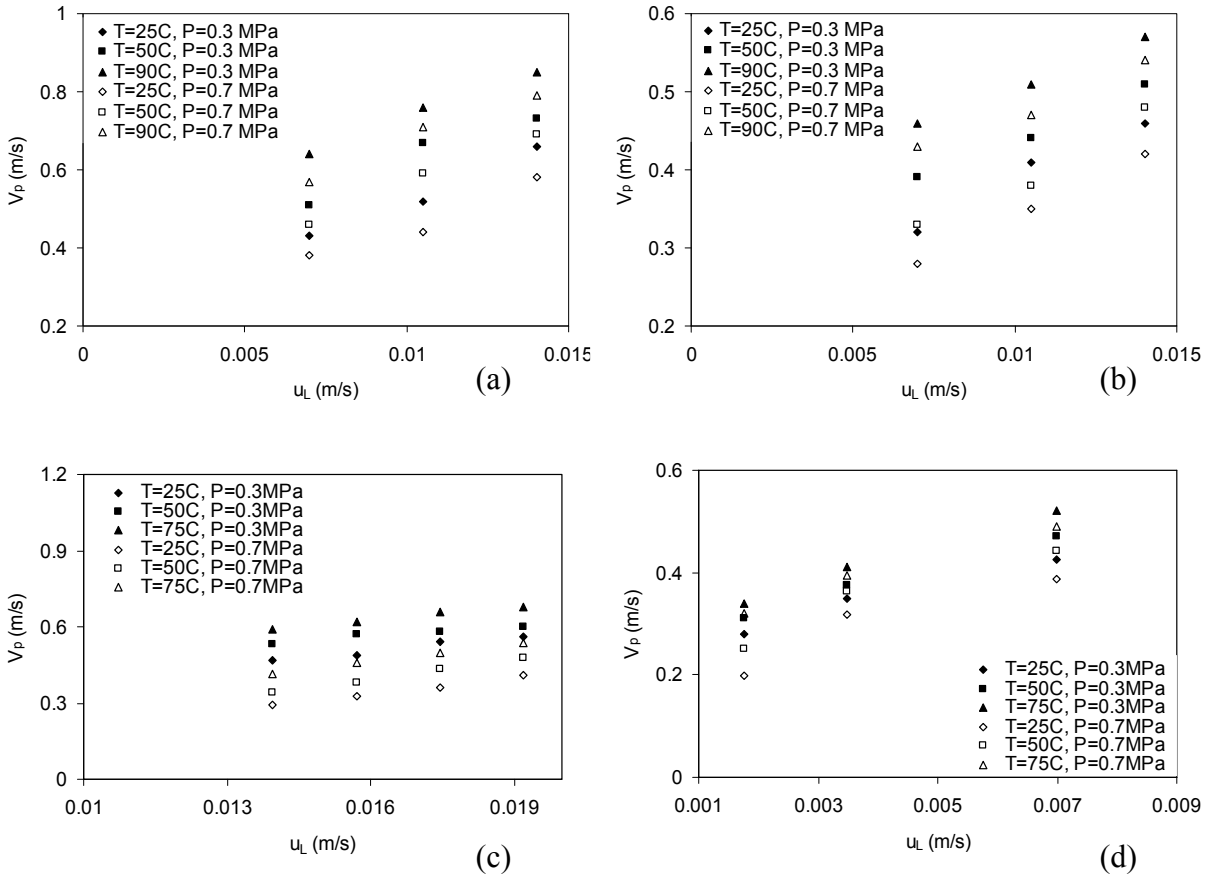


**Figure 6-9** Influence of temperature, pressure and superficial liquid velocity on pulse velocity for (a) air-CTAB/water (b) air-CTAB-CMC/water (c) air-water (d) air-CMC/water systems. $u_G$ = 0.21 m/s.

Figs. 6-9c,d show the effect of temperature and pressure on the pulse velocity for Newtonian and non-Newtonian coalescing systems without CTAB addition. The pulse velocities for the coalescing systems are lower than their foaming counterparts. This could be rationalized with higher liquid holdup, and thus lower interstitial velocity, for the former. As seen in Fig. 6-9, the effect of temperature and pressure is more pronounced for the foaming system.

## 6.4 Conclusion

In this study, the effects of elevated temperature and moderate pressure on the hydrodynamics of trickle-bed reactors were discussed for Newtonian and non-Newtonian foaming systems. The experimental observations were compared with Newtonian and non-Newtonian coalescing systems. The following conclusions were drawn:

* At constant elevated temperature, pressure and superficial gas velocity, the trickle-to-foaming pulsing flow transition boundary was observed at lower superficial liquid velocity for foaming systems. The transition boundary shifted towards higher gas and liquid superficial velocities with increasingly temperatures and pressures.

* At non-ambient conditions, the liquid holdup for foaming systems was lower than for coalescing systems and pressure drop was higher for foaming systems as known to be the case in room temperature and atmospheric pressure.

* Pulse frequency was an increasing function of temperature and pressure.

* Pulse velocity for foaming systems was larger as compared to coalescing systems and it increased with temperature and decreased with pressure.

## 6.5 Nomenclature

| | | |
|---|---|---|
| $f_p$ | pulse frequency | Hz |
| $P$ | pressure | Pa |
| $\Delta P/H$ | two-phase pressure drop | Pa/m |
| $T$ | temperature | °C |
| $u$ | superficial velocity | m/s |
| $V_p$ | pulse velocity | m/s |

**Greek letters**

| | |
|---|---|
| $\varepsilon_L$ | liquid holdup |
| $\sigma$ | surface tension |

**Subscripts**

| | |
|---|---|
| G | gas phase |
| L | liquid phase |
| p | pulse |

## 6.6 References

Aydin, B., Larachi, F., 2005. Trickle bed hydrodynamics and flow regime transition at elevated temperature for a Newtonian and a non-Newtonian liquid. Chemical Engineering Science 60, 6687-6701.

Aydin, B., Fries, D., Lange, R., Larachi, F., 2007. Slow-mode induced pulsing in trickle beds at elevated temperature for (non)Newtonian liquids, Chem. Eng. Sci. 62, 5554-5557.

Bartelmus, G., Janecki, D., 2003. Hydrodynamics of a cocurrent downflow of gas and foaming liquid through the packed bed. Part II. Liquid holdup and gas pressure drop. Chemical Engineering & Processing 42, 993-1005.

Bartelmus, G., Janecki, D., 2004. Hydrodynamics of the cocurrent downflow of a gas and a foaming liquid through a packed bed. Part I. Estimation of the transition boundary between the hydrodynamic regimes from the gas continuous flow to the pulsing flow. Chemical Engineering & Processing 43, 169-179.

Burghardt, A., Bartelmus, G., Janecki, D., 2003a. Parameters characterising the pulsing flow of gas and foaming liquid through the packed bed. Part I. Pulse velocity. Inzynieria Chemiczna I Procesowa 24, 151-164.

Burghardt, A., Bartelmus, G., Janecki, D., 2003b. Parameters characterising the pulsing flow of gas and foaming liquid through the packed bed. Part II. The frequency of pulsation and the structure of pulses. Inzynieria Chemiczna I Procesowa 24, 165-182.

Burghardt, A., Bartelmus, G., Szlemp, A., 2004. Hydrodynamics of pulsing flow in three-phase fixed-bed reactor operating at an elevated pressure, Ind. Eng. Chem. Res. 43, 4511-4521.

Charpentier, J.C., Favier, M., 1975. Some liquid holdup experimental data in trickle-bed reactors for foaming and nonfoaming hydrocarbons. AIChE Journal 21, 1213-1218.

Evans, D.F., Allen, M., Ninham, B.W., Fouda, A., 1984. Critical micelle concentrations for alkyltrimethylammonium bromides in water from 25 to 160ºC. J. Sol. Chem. 13, 87-101.

Janecki, D., Bartelmus, G., Krótki, T., 2005. The hydrodynamics of the pressure trickle-bed reactor with packed bed for foaming system. Proc. 7th World Congress Chemical Engineering, Glasgow, United Kingdom.

Larachi, F., Laurent, A., Midoux, N., Wild, G., 1991. Experimental study of a trickle bed reactor operating at high pressure: Two-phase pressure drop and liquid saturation. Chemical Engineering Science 46, 1233-1246.

Larkins, R.P., White, R.R., Jeffrey, D.W., 1961. Two-phase cocurrent flow in packed beds. AIChE Journal 7, 231-239.

Midoux, N., Favier, M., Charpentier, J.C., 1976. Flow pattern, pressure loss and liquid holdup data in gas-liquid downflow packed beds with foaming and nonfoaming hydrocarbons. Journal of Chemical Engineering of Japan 9, 350-356.

Morsi, B.I., Midoux, N., Charpentier, J.C., 1978. Flow patterns and some holdup experimental data in trickle-bed reactors for foaming, nonfoaming and viscous organic liquids. AIChE Journal 24, 357-360.

Morsi, B.I., Midoux, N., Laurent, A., Charpentier, J.C., 1982. Hydrodynamics and interfacial areas in downward cocurrent gas-liquid flow through fixed beds. Influence of the nature of the liquid. International Chemical Engineering 22, 142-151.

Prud'homme, R.K., Khan, S.A., 1996. Foams: Theory, Measurements, and Applications, CRC Press.

Rode, S., 1992. Analyse Spatio-Temporelle des Phénomènes Hydrodynamiques et de Transfert de Matière au Sein d'un Réacteur à Lit Fixe Opérant en Écoulement Monophasique de Liquide ou en Co-Courant vers le Bas de Gaz et de Liquide; Mise en Oeuvre de la Technique des Microsondes Électrochimiques. PhD Dissertation, Institut National Polytechnique de Lorraine, Nancy, France.

Sai, P.S.T., Varma, Y.B.G., 1987. Pressure drop in gas-liquid downflow through packed beds. AIChE Journal 33, 2027-2036.

Sai, P.S.T., 1997. Liquid saturation in concurrent gas-liquid downflow through packed beds. Bioprocess Engineering 16, 283-287.

Schramm, L.L., 1994. Foams: Fundamentals and Applications in the Petroleum Industry, American Chemical Society, Washington, USA.

Talmor, E., 1977. Two-phase downflow through catalyst beds. AIChE J. 23, 868-878.

Weekman, V.W., Myers, J.E., 1964. Fluid-flow characteristics of cocurrent gas-liquid flow in packed beds. AIChE Journal 10, 951-957.

Wild, G., Larachi, F., Laurent, A., 1991. The hydrodynamic characteristics of cocurrent downflow and cocurrent upflow gas-liquid-solid catalytic fixed-bed reactors: The effect of pressure, Rev. Inst. Franç. Pétr. 46, 467-490.

# Chapter 7 Fast-mode alternating cyclic operation in trickle beds at elevated temperature for foaming systems*

## Résumé

Le fonctionnement intermittent cyclique gaz-liquide, en mode rapide, a été exploré pour réduire l'apparition du régime d'écoulement moussant dans les réacteurs trickle bed opérés à température élevée et en surpression. Les effets de la température et le rapport de division temporelle sur les séries chronologiques de la conductivité électrique et de la perte de charge ont été analysés pour les systèmes air-bromure de cétyltriméthylammonium (CTAB) moussant en phase aqueuse et air-eau. Pour les rapports de division temporelle étudiés, on a constaté que le fonctionnement intermittent cyclique en mode rapide pourrait étendre le domaine de fonctionnement à température élevée du régime à faible interaction,. Par conséquent, l'augmentation de la température du réacteur a été proposée afin d'accélérer le drainage de la mousse et sa rupture qui s'est traduite par une diminution des niveaux de perte de charge, ainsi que par une chute brutale de la perte de charge lorsque l'alimentation passe du gaz au liquide. En outre, en ajustant les rapports de division, il a été possible de diminuer les pertes de charge des deux phases en fonctionnement cyclique en-deçà des niveaux correspondant au rendement barycentrique équivalent.

## Abstract

An alternating gas/liquid fast-mode cyclic operation procedure was explored for reducing the occurrence of foaming flow regime in trickle-bed reactors at elevated temperature and moderate pressure. The effect of temperature and split ratio on the electrical conductance and pressure drop time series was analyzed for the air-aqueous cetyltrimethylammoniumbromide (CTAB) foaming and air-water systems. For the split ratios studied, it was found that fast-mode alternating cyclic operation could enlarge the operational domain of the low interaction regime at elevated temperature. Hence, increased

* Aydin, B.; Hamidipour, M.; Larachi, F. Chemical Engineering Science, 62, 7539-7547, 2007

reactor temperature was suggested to allow faster foam drainage and breakdown which was reflected in the lower pressure drop levels as well as in the faster collapse in pressure drop when the flow was switched from gas to liquid feed. Also, by adjusting the split ratios it was possible to reduce the two-phase pressure drops in cyclic operation below the levels corresponding to the equivalent barycentric constant-throughput operation.

**Keywords** Trickle bed; cyclic operation; elevated temperature; foaming liquids

## 7.1 Introduction

Trickle bed reactors are randomly packed vessels in which reactant-carrying gas and liquid phases flow co-currently downwards. They are widely used in the petroleum industry such as in hydrotreating and hydrocracking processes (Meyers, 1996). As explained by Schramm (1994), foams in the petroleum industry play an important role in productivity and petroleum recovery and processing. Some of the foams could favor these processes but on the other hand occurrence of foams with impurities and corrosion products can also represent major problems in downstream processing of recovered crude oil (Kanicky et al., 2001). Often, foam formation is dealt with by adding antifoaming agents or defoamers. In addition to these chemically-mediated methods, alternative chemical-free concepts based on periodic operation of trickle bed reactors seem, to the best of the authors' knowledge, to have escaped the attention of researchers.

The hydrodynamics of foaming systems in trickle bed reactors were first reported in the early 1960's (Larkins et al., 1961; Weekman and Myers, 1964). A little afterwards, Charpentier and Favier (1975) developed a flow map for correlating the transitions between trickling and foaming and foaming-pulsing flow regimes. Till the late 1990s, the experimental work on pressure drop and liquid holdup were performed for a variety of similar foaming gas-liquid systems (Midoux et al., 1976; Talmor, 1977; Morsi et al. 1978, 1982; Sai and Varma, 1987; Sai, 1997). Most of these studies were concerned with ambient temperature and atmospheric pressure. Recently, Bartelmus and coworkers (Bartelmus and Janecki, 2003, 2004; Burghardt et al., 2003a,b; Janecki et al., 2005) investigated the trickle bed hydrodynamics for weakly and strongly foaming systems and characterized the trickle-to-pulsing flow regime transition, the pressure drop and liquid holdup up to 2 MPa, and the

pulse velocity and frequency at atmospheric pressure. At elevated pressure up to 8.1 MPa, Larachi et al. (1991) reported some pressure drop and liquid holdup data using as a foaming system nitrogen-1%w/w ethanol/water.

Numerous benefits of periodically operated trickle beds were underlined in the literature (Boelhouwer et al., 2002; Dudukovic et al., 2002). These studies comprise advantages of periodic operation such as induced pulsing on chemical reaction as well as on trickle bed hydrodynamics. Except the study by Xiao et al. (2001), the vast majority of periodic flow modulation experiments concerned liquid cyclic operation so it is crucial to search for alternative periodic modes aiming at the improvement of reactor performance via hydrodynamics stimulation of trickle beds especially at elevated temperature and pressure.

The present study is therefore designed with an aim to investigate the trickle bed hydrodynamics by testing a new type of fast-mode alternating cyclic operation on foaming systems. Alternating passages of gas- and liquid-rich phases through the packed bed is studied as a potential approach for impeding the persistence of foams, in particular, under elevated temperature and moderate pressure conditions. The goal pursued concerns maximizing the occurrence of trickle flow regime at the expense of foaming flow regime by studying the split parameters of the fast-mode alternating cyclic operation.

### 7.1.1 Rationale behind cyclic operation for mitigating foaming flow regime

The fast-mode alternating cyclic operation merely consists in superimposing ON/OFF gas flow with OFF/ON liquid flow feeds, as sketched in Fig. 7-1. Hence, when the liquid flow is switched ON, during the $\tau_L$ portion, the gas already nearby within the bed from the preceding $\tau_G$ time lapse quickly slows down and the flowing liquid mainly encounters a quasi-stagnant gas phase in trickle flow with $u_G \approx 0$. This has the advantage of reducing the ability of the liquid to foam by lowering the gas-liquid interfacial interactions thus forcing the trickle flow regime to prevail instead of foaming flow regime. Resuming gas flow during the subsequent $\tau_G$ portion while interrupting liquid irrigation induces the formation of *wet* foams specifically in the liquid-rich portions of the bed as soon as these are caught up by the gas flow. For not too short $\tau_G$ intervals, the foam structures may be pushed downwards by the flowing gas until they eventually get swept away from the bed. Because of liquid shortages characterizing the $\tau_G$ intervals, foam drainage and foam breakdown may

also take place *in situ* as the foam structures are being pushed towards the exit by the gas flow. Foam drainage, reminiscent of a liquid shower throughout the wet foam structures, thins the foam films progressively to the point they become unstable and foams start collapsing, in all likelihood, from their driest trailing end (Barigou et al., 2001). Because the surfactant levels used in the study were much less than the critical micelle concentrations (Table 7-1), the foam structures would not be able to build up thick liquid films during their formation, especially at the higher temperatures. This presumably would cause foam drainage and foam collapse to set in concomitantly while the foam structures migrate downstream (Barigou et al., 2001). Clearing the bed from the incipient foam structures has the advantage of restoring back a low interaction trickle flow regime as during the previous $\tau_L$ interval which is obviously less penalizing in terms of reactor operability than the foaming flow regime. Resumption of liquid flow for a subsequent duration $\tau_L$ preserves the formerly observed trickle flow regime, and so forth. It is clear from this analysis of the flow patterns in fast-mode alternating cyclic operation involving foaming systems that the unstable foaming flow regime operation of trickle-bed reactors could be significantly reduced by maximizing the occurrence of trickle flow regime at the expense of foaming flow regime.

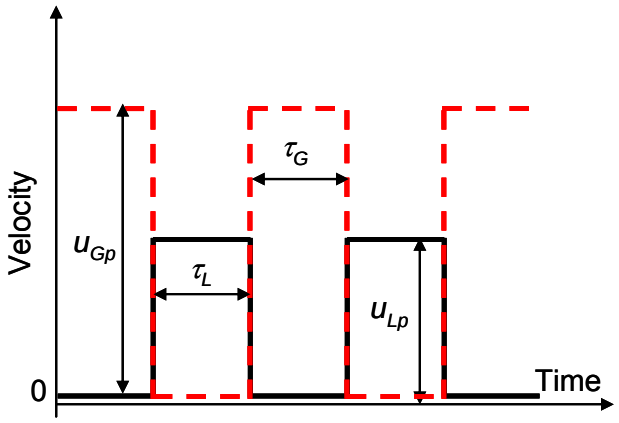


**Figure 7-1** Parameters characterizing the morphology of fast-mode alternating cyclic operation: ON-OFF cycled gas feed: $\tau_G$ = pulse gas feed period, $u_G$ = pulse superficial gas velocity ON-OFF cycled liquid feed: $\tau_L$ = pulse liquid feed period, $u_L$ = pulse superficial liquid velocity.

## 7.2 Experimental Setup and Procedure

The experiments were carried out in a 4.8 cm I.D. and 107 cm high stainless steel column rated to withstand temperatures and pressures as high as 100ºC and 5 MPa, respectively. The bed was packed with nonporous 3 mm glass spheres and had a porosity of 0.39. As a foaming system, the air-aqueous cetyltrimethylammoniumbromide (CTAB, 6.25 ppmw or $0.17 \times 10^{-4}$ mol/L) solution was used and its behavior was compared to the air-water base case. To prevent fading of foaminess during the high temperature tests, CTAB was chosen as it is a non-volatile surfactant in the studied temperature range. The CTAB critical micelle concentration, cmc, and the surfactant concentration, expressed as a percentage of cmc are given in Table 7-1 as a function temperature. Fractional surfactant concentrations between 0.6 and 1.8% cmc were already high enough to turn the system into a foaming one and to dramatically alter the reactor hydrodynamics with respect to the air-water base case. The fluid velocity ranges coincided with the foaming and trickle flow regimes (Charpentier and Favier, 1975) for air-CTAB/water system and with trickle flow regime for air-water system.

**Table 7-1** CTAB critical micelle concentration (cmc) as a function of temperature (Evans et al., 1984)

| Temperature, ºC | cmc, mol/L $\times 10^3$ | %cmc |
|---|---|---|
| 25 | 0.95 | 1.8 |
| 65 | 1.52 | 1.1 |
| 90 | 2.35 | 0.7 |

The cyclic operation feed policy we propose to study consists in *alternating* the gas (ON/OFF) and liquid (OFF/ON) feeds so as to yield fully segmented gas and liquid feed flow rates at the bed entrance: while the gas flow is ON, the liquid flow is OFF and *vice versa* as sketched in Fig. 7-1. Therefore, the time interval each phase is being fed must be brief enough to maintain sufficient gas-liquid contacting along the bed as well as to minimize gas and liquid phase segregation in the bed axial direction. Hence, only the ability of the fast-mode alternating cyclic operation was evaluated as a means to quickly sweep out of the bed the foam structures susceptible to form in the foaming flow regime.

Using two computer-controlled programmable solenoid valves, the line used for gas feed was allowed to deliver periodically the binary sequence ($u_G$,0), whilst simultaneously, the liquid feed line was required to discharge following the (0, $u_L$) binary sequence. The lapse during $u_G$ injection (respectively, $u_L$) lasted $\tau_G$ (respectively, $\tau_L$), with a split ratio defined as $S = \tau_L/(\tau_L + \tau_G)$. The values of $u_L$ and $u_G$ were adjusted using separate needle valves and were measured using calibrated rotameters. Both gas and liquid traversed, respectively, gas and liquid preheaters before entering the reactor. At the reactor outlet, both phases were funneled into a separator where gas was vented to the atmosphere and liquid was drained. The experiments were performed after temperature and pressure reached steady-state and the bed was preventively fully wetted by momentarily bringing the reactor into the pulsing flow regime.

An electrical conductance technique using two ring electrodes embedded 40 cm and 64.5 cm downstream in the bed was implemented for the measurement of the liquid electrical conductance during the fast-mode alternating cyclic operation. The conductance technique was described in detail elsewhere (Aydin and Larachi, 2005). As the foam structures being formed caused drastic rises in the amplitude of two-phase pressure drop regardless of the temperature and pressure levels in the reactor, pressure drop traces were also recorded at a sampling frequency of 10 Hz during cyclic operation with a differential pressure transducer connected to the top and bottom of the packed bed.

Experiments at ambient temperature and pressure were also carried out on a transparent Plexiglas column (5.7 cm I.D. and 80 cm high) to visualize the foam structures by means of a high-speed camera (100 frames/s) and to understand their behavior during the fast-mode alternating cyclic operation. Visual observation in the transparent column corresponded to the fluid throughputs and split ratios as those conducted in the opaque high temperature and pressure column. A borescope (Hawkeye Proslim 22” from Gradient Lens Corp.) was inserted downstream in the bed *ca*. 50 cm from the top to scrutinize the passages of foams during cyclic operation at the pore level. The field of view was 4 mm and the pixel resolution was 640×480.

## 7.3 Results and Discussion

During cyclic operation, two split ratios, S, of 50% and 80% were used, respectively. $S$ = 50% represents periodic operation of 5 s liquid flow at a given $u_L$ without gas flow ($u_G = 0$) followed by 5 s gas flow at a given $u_G$ without liquid flow ($u_L = 0$). In the same manner, a split ratio of 80% signifies 8 s of liquid flow at $u_L$ and $u_G = 0$, followed by 2 s gas flow at $u_G$ without liquid flow ($u_L = 0$).

Image post-processing after visualization of foaming flow in the Plexiglas column was carried out frame by frame to establish a 640x480 light-intensity map over 4x4 $mm^2$ field of views from which average light intensities and corresponding light-intensity standard deviations were computed. A per-frame coefficient of variation, i.e., ratio of standard deviation to average light intensity, was computed and plotted as a function of time.

Fig. 7-2 illustrates the coefficient-of-variation time series obtained for the foaming system (air-CTAB/water) under cyclic operation and, equivalently, under constant-throughput (or isoflow) conditions corresponding to barycentric gas and liquid superficial velocities, $(1-S)u_G$ and $Su_L$, respectively. The coefficient of variation for the air-water system under the same barycentric velocities is illustrated for comparison. Hence, for equivalent constant-throughput conditions, the foaming system is recognizable by the larger fluctuations exhibited by the coefficient of variation in comparison with the non-foaming system. The behavior of the foaming system during cyclic operation is also inferred from the evolution of the coefficient-of-variation time series in Fig. 7-2. For $S$ = 80%, when the time lapse $\tau_L$ is nearly completed, only a sparse amount of sub-millimeter bubbles is left at the expense of a liquid film accumulating between the packing particles (A1 frame). It is worthy of notice that the number of such bubbles is even scantier for $S$ = 50% (B1 frame) when $\tau_L$ is about to end. Foaming flow is activated in the bed when the flow is switched from liquid to gas (A2 & B2 frames) as is easily recognizable by the large fluctuations of the coefficient of variation shown in Fig. 7-2. For $S$ = 50%, foaming flow is less pronounced than for $S$ = 80%, due plausibly to the lesser accumulation of liquid allowed during the time lapse $\tau_L$ (B2 frame). When the flow is switched back to liquid and gas is cut off, stagnant sub-millimeter bubbles remain in the bed for both split ratios (A3 & B3 frames).

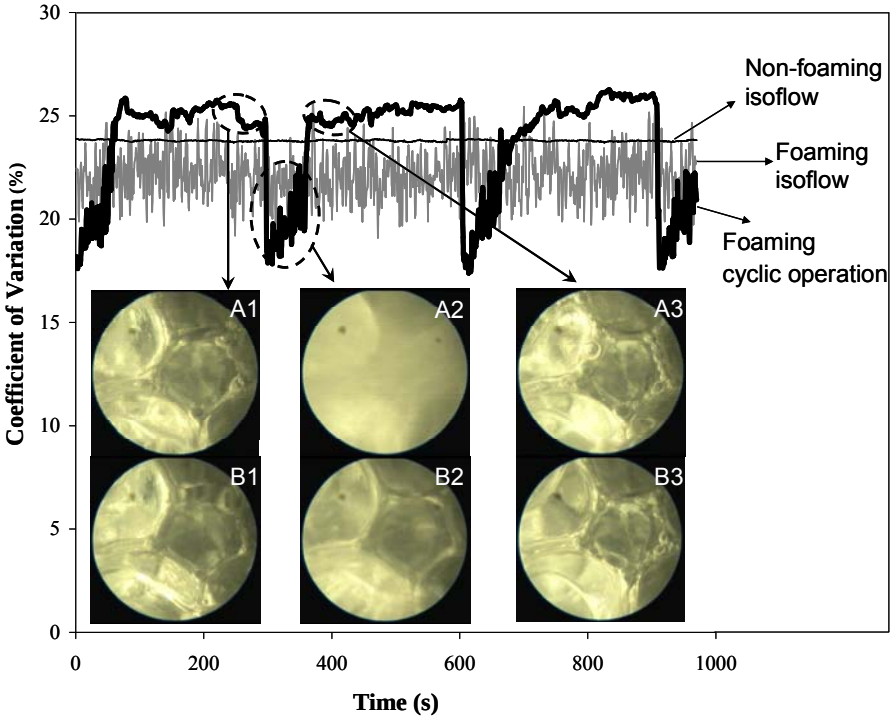


**Figure 7-2** Coefficient of variation vs. time for foaming and non-foaming isoflow as well as foaming cyclic operation. Images obtained for cyclic operation of air-CTAB/water system at $S$ = 80% (A1-A3) and $S$ = 50% (B1-B3).

Figs. 7-3a-d show the pressure drop traces obtained during cyclic operation at two split ratios for air-CTAB/water and air-water systems at varying temperatures and pressures. The isoflow pressure drops recorded for both systems are also shown for runs at gas and liquid barycentric velocities. Recall that cyclic operation is being tested in this work to evaluate its potential for mitigating foam formation in comparison to isoflow conditions. At ambient temperature, it is found that the pressure drop during cyclic operation for $S$ = 80% (Fig. 7-3b) is lower than in isoflow conditions.

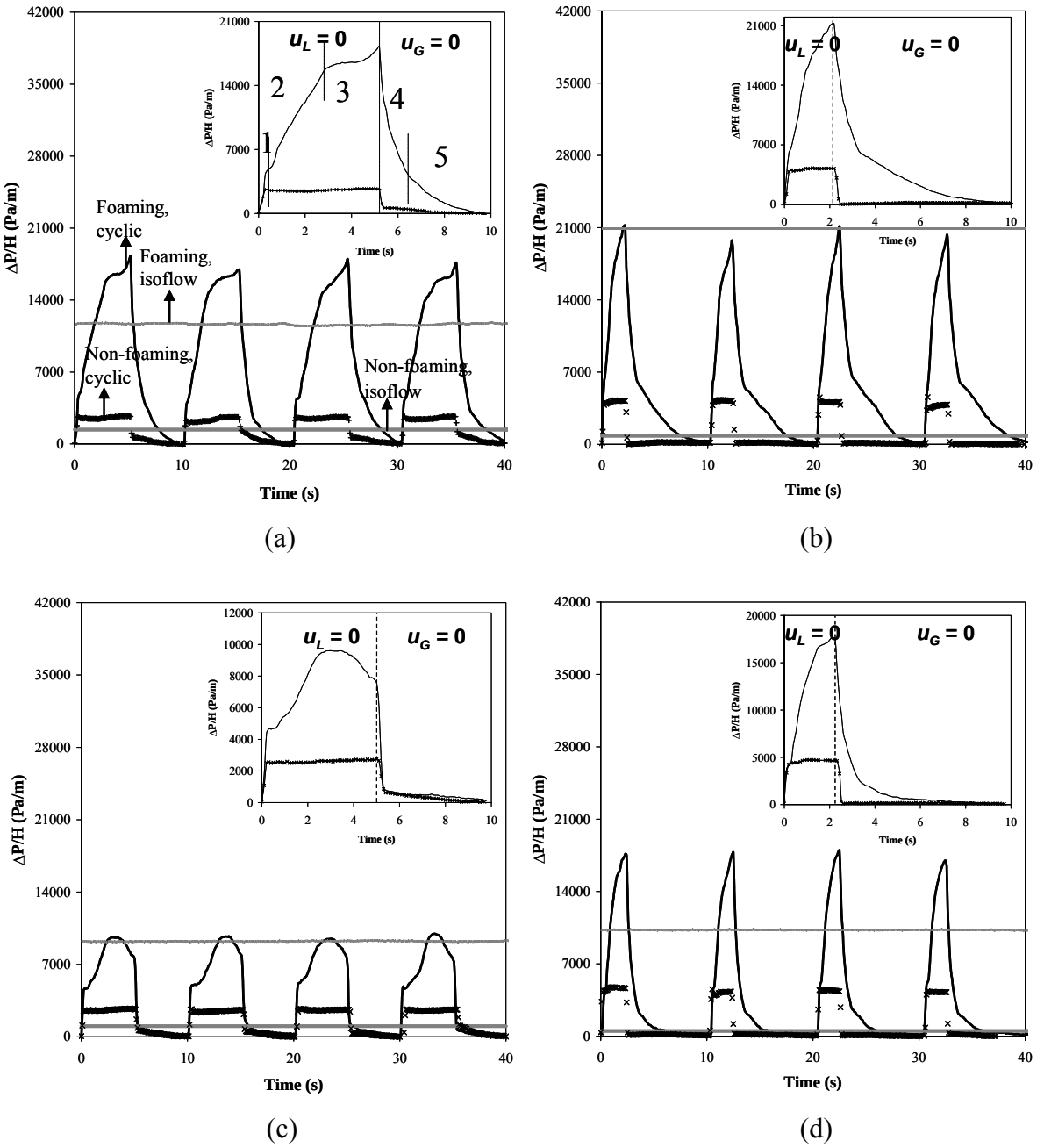


**Figure 7-3** Effect of temperature and split ratio, *S*, on two-phase pressure drop for air-CTAB/water and air-water in fast-mode alternating cyclic operation [$u_L$ = 7 mm/s, $u_G$ = 20 cm/s]: (a) $S$ = 50%, $T_r$ = 25ºC; (b) $S$ = 80%, $T_r$ = 25ºC; (c) $S$ = 50%, $T_r$ = 90ºC; (d) $S$ = 80%, $T_r$ = 90ºC. Comparison with corresponding pressure drops in barycentric isoflows: $S$ $u_L$ = 3.5 mm/s & (1-$S$)$u_G$ = 10 cm/s @ $S$ = 50%; $S$ $u_L$ = 5.6 mm/s & (1- $S$) $u_G$ = 4 cm/s @ S = 80%; $P_r$ = 0.3 MPa.

As seen in Fig. 7-3a inset, the pressure drop dynamics ($T_r$ = 25°C, $P_r$ = 0.3MPa) highlights five regions, each of which reflects different phenomena during the fast-mode alternating cyclic operation. At a given $u_L$, liquid holdup in the bed increases with extending the time lapse $\tau_L$. Switching to gas from liquid, the gas flow encounters a resistance across the bed that is dependent on the amount of liquid collected within during the previous $\tau_L$ portion. This causes an abrupt increase in pressure drop as in region 1. Foaming emerges along the bed as a result of dispersion and penetration of the gas phase through the liquid films. This foam-inception step is characterized by higher pressure drop as portrayed in region 2. This region is followed by region 3 with a slight increase of pressure drop when the foam flow reaches the bed bottom. A sudden and sharp collapse of pressure drop is observed when the gas flow is cut off and liquid flow is resumed (region 4). The subsequent long tail, corresponding to region 5, is ascribed to the slow migration of foam structures out of the bed. For the air-water system, the increase of pressure drop during the $\tau_G$ portion ($u_L$ = 0) is lower in comparison with the air-CTAB/water system. Moreover, a time-independent pressure drop is maintained during this period and could be explained by the segregated nature of trickle flow regime where gas and liquid try to define their relative permeabilities as much as possible apart from one another. When the gas flow is supplanted by liquid flow, pressure quickly equilibrates across the bed length as is known for gas-free flow trickle flow regime and non-foaming systems.

The pressure drop traces at $S$ = 80% ($T_r$ = 25°C, $P_r$ = 0.3MPa) for both systems are shown in Fig. 7-3b. Higher amount of liquid has accumulated in the bed during $\tau_L$ because of an extra 3 s liquid flow with respect to the case with $S$ = 50% (Fig. 7-3a). The incoming gas phase faces a stronger resistance before to establish gas flow which causes a sharper increase of pressure drop (region 1, Fig. 7-3b). Also, the tail corresponding to region 5 is longer in comparison with $S$ = 50% and could be explained by the presence of more small bubbles before resumption of gas flow, see A1 frame in Fig. 7-2.

Figs. 7-3c,d show the effect of reactor temperature ($T_r$ = 90°C, $P_r$ = 0.3MPa) on the pressure drop traces obtained during cyclic operation of air-water and air-CTAB/water systems at two split ratios. As seen in Fig. 7-3c and $S$ = 50%, the sudden increase of pressure drop and foam formation during the $\tau_G$ portion is similar to the regions 1 and 2 observed at ambient temperature. However, this increase is noticeably lower and the fall off

of pressure drop during the time lapse $\tau_L$ is faster presumably because of lower foam stability at the higher the temperature.

In order to reckon the effect of temperature on foam stability, foam drainage and breakdown, simple foam collapse tests were performed in a glass tube at 25°C and 90°C with aqueous CTAB solution. Foams were allowed to rise up to an equal height and the time needed for foam breakage was recorded. Foams persist a longer period of time at 25°C (Fig. 7-4, A1-4) than at 90°C (Fig. 7-4, B1-3) where no foam was left after 15 s. The viscosity decrease of liquid with increasing temperature causes the liquid on the bubble surface to drain faster thus reaching dry and unstable bubbles at an earlier moment. This would explain why pressure drop in the bed at $T_r$ = 90°C in regions 1 or 2 could not surpass that at $T_r$ = 25°C.

Fig. 7-3d shows the effect of temperature on the pressure drop traces for $S$ = 80%. The behavior of the pressure drop traces is similar to the one at 25°C. Short $\tau_G$ portions do not allow gas to exert pronounced influence on the system hydrodynamics. The tail region for 90°C is shorter in comparison with the ambient temperature one due presumably to a combination between short-lived foams and faster expulsion of foam structures out of the bed. At elevated temperature, pressure drop during cyclic operation for $S$ = 50% is lower than in isoflow conditions similarly to the case at 25°C and $S$ = 80%. This could signify that a lower foam load accumulated in the reactor in these two cases as could be asserted from the lower pressure drops.

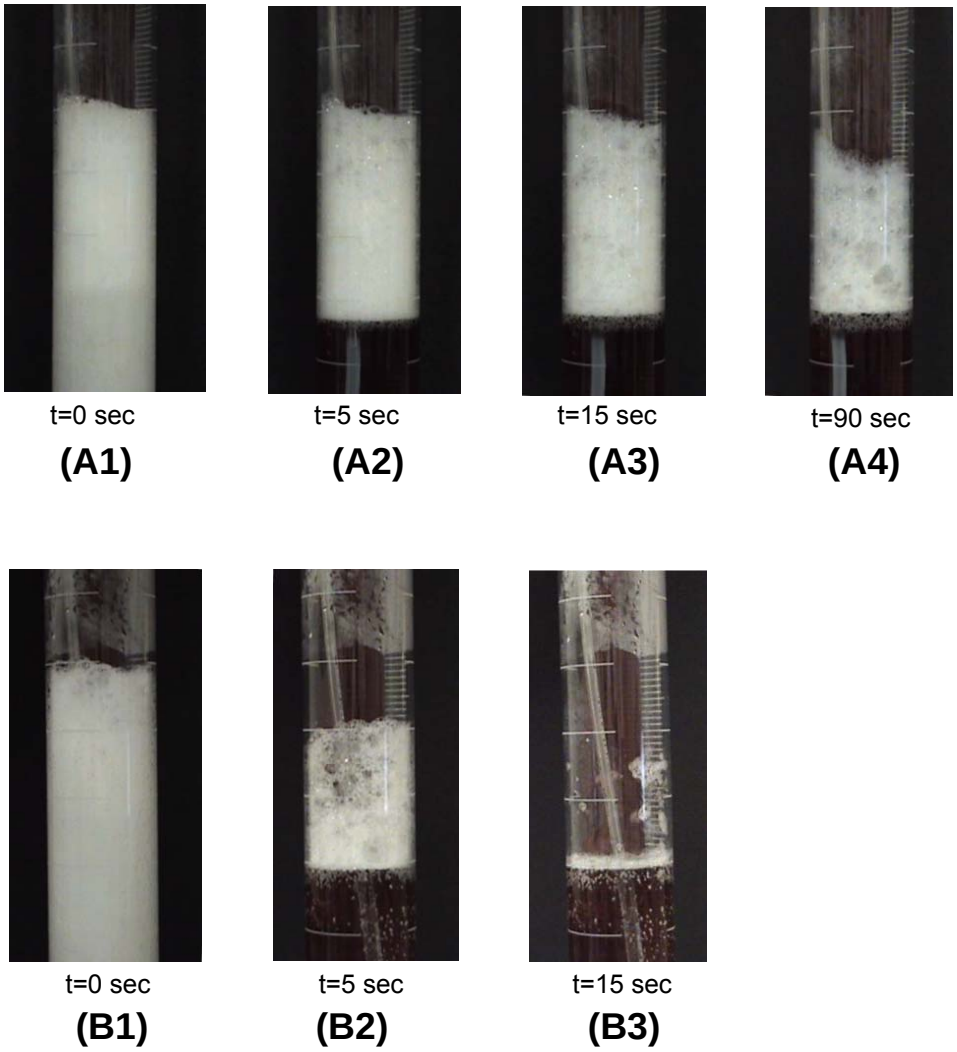


**Figure 7-4** Effect of temperature on foam stability. $T$ = 25°C (A1-A4), $T$ = 90°C (B1-B3).

To demonstrate the effect of reactor pressure ($T_r$ = 90°C, $P_r$ = 0.7MPa) on the pressure drop traces during cyclic operation of the foaming system, measurements are performed at both split ratios (Figs. 7-5a,b). As indicated in Fig. 7-5a, the system's behavior could be segmented in the five regions as previously for the case at 0.3 MPa. The effect of pressure is more pronounced after foam formation (region 3) where the denser gas partly overcomes the resistance to flow while traveling across the foam structures. For $S$ = 80% after switching from gas to liquid flow no tail is observed which could be explained by a complete sweep out of the bed of the foam structures because of higher drag force.

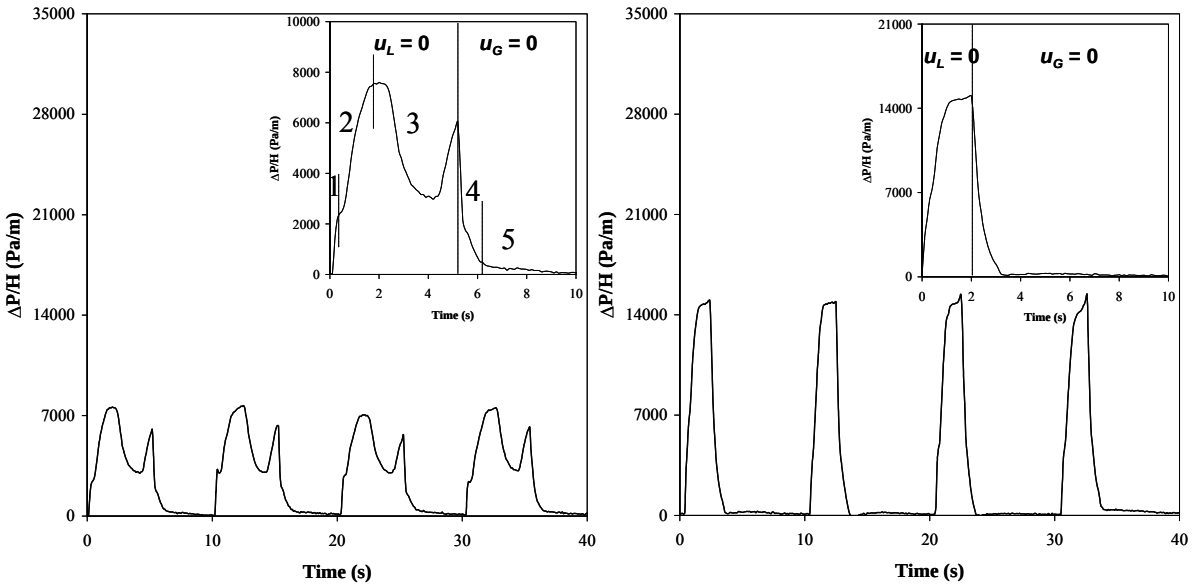


**Figure 7-5** Effect of pressure on pressure drop traces obtained along the bed during fast-mode alternating cyclic operation for air-CTAB/water system, $T_r$ = 90°C, $P_r$ = 0.7 MPa, $u_L$ = 7 mm/s, $u_G$ = 20 cm/s. (a) $S$ = 50%, (b) $S$ = 80%

Figs. 7-6a-d show the effect of the split ratio on the electrical conductance traces obtained at elevated temperature and moderate pressure ($T_r$ = 90°C, $P_r$ = 0.7MPa) for air-water and air-CTAB/water systems. The signals are registered at two bed depths: 40 cm (upper signal) and 64.5 cm (lower signal). As seen in Fig. 7-6a for the air-water system, when the gas enters the reactor ($u_L$ = 0), liquid is pushed downwards causing the appearance of a relatively sharp peak in the electrical conductance registered at 40 cm depth. This peak is followed by a slowly diminishing tail ascribed to trickling of the residual liquid left upstream of the ring probe during the remaining time left from $\tau_G$. It is unlikely that the tail is contributed by the liquid flow after $\tau_L$ sequence is resumed as no clear change is brought to the slope of the tail. Fig. 7-6b illustrates the conductance traces obtained at $S$ = 80% for the air-water system. As shown in Fig. 7-6b inset, a broader conductance peak forms due to the longer $\tau_L$ interval representing a higher accumulation of liquid for $S$ = 80% as compared to $S$ = 50%. At the end of each 10 s cycle, the electrical conductance dip in the time series

exhibits higher values for $S$ = 80% in comparison with $S$ = 50% suggesting that the amount of liquid held in the bed is very sensitive to the split ratio at the verge of the new cycle.

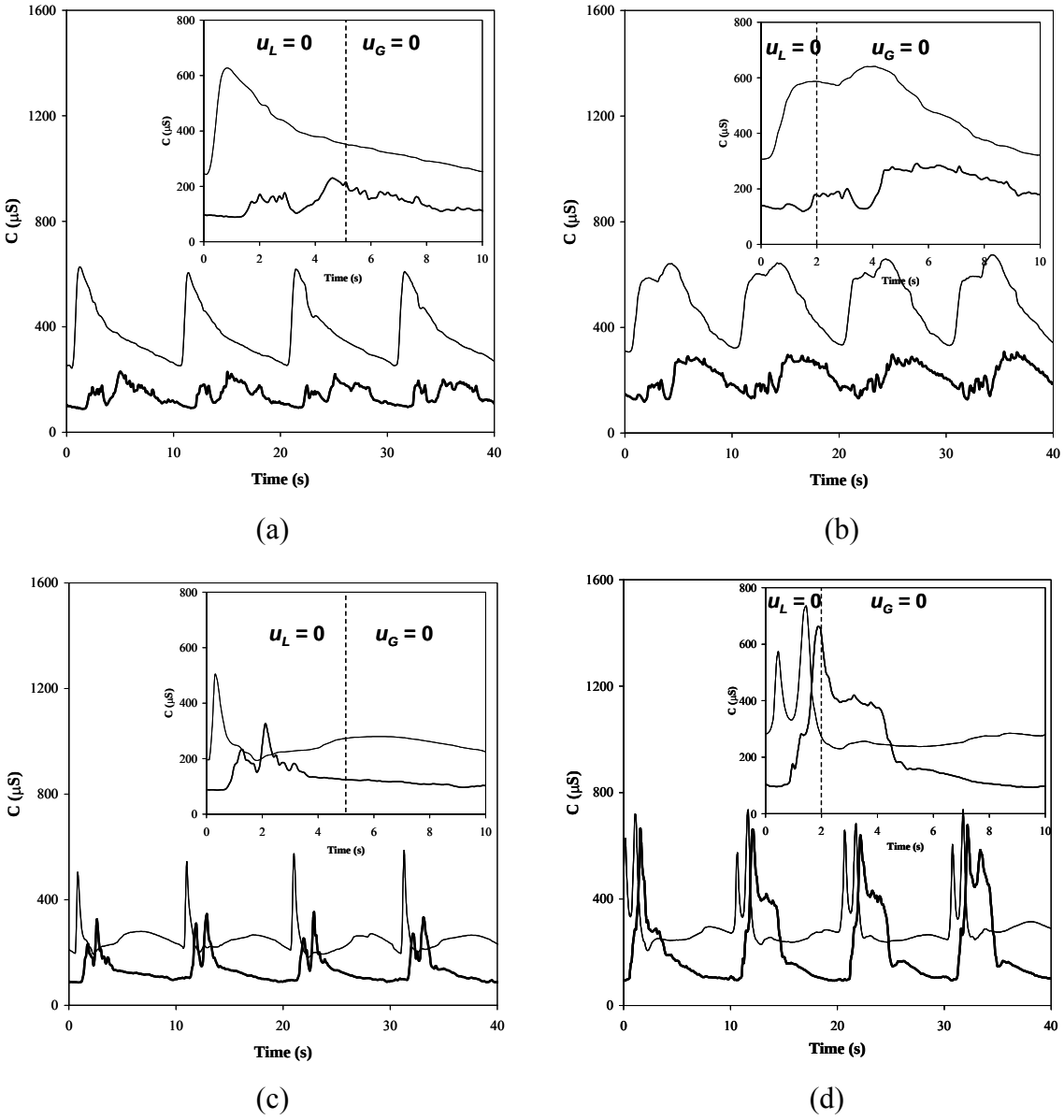


**Figure 7-6** Influence of split ratio on liquid electrical conductance during fast-mode alternating cyclic operation, $T_r$ = 90°C, $P_r$ = 0.7 MPa, $u_L$ = 7 mm/s, $u_G$ = 20 cm/s. (a) $S$ = 50%, air-water; (b) $S$ = 80%, air-water; (c) $S$ = 50%, air-CTAB/water; (d) $S$ = 80%, air-CTAB/water. Upper signal = upper probe, lower signal = lower probe

For air-CTAB/water system, steeper breakthrough rise and narrower electrical conductance peaks form in the early instances of the $\tau_G$ portion as compared to the air-water system for a given split ratio (Figs. 7-6c,d). Immediately after gas is introduced in the reactor, foam formation is induced resulting in a thorough interpenetration between liquid and fast flowing gas thus explaining the steeper breakthrough rise. The foam structures thus formed traverse the ring probe field of view rapidly leaving behind a relatively trickling flow regime region. The gas flows through the bed together with the nascent foams and liquid giving rise to shorter liquid residence times in the bed. This is in accordance with visual observations reported from the Plexiglas column. For $S$ = 50%, the time needed for the liquid to reach the axial position where the borescope is located in the bed when the gas flow is turned on amounts to 3.7 s and 0.5 s for the air-water and air-CTAB/water systems, respectively. After gas flow is switched to liquid flow, the time lapse $\tau_L$ is not sufficiently long for the liquid to reach the first probe when $S$ = 50% resulting in a decrease of electrical conductance (Fig. 7-6c). However this decrease in conductance is not observed for the first probe for $S$ = 80% suggesting sufficient time for liquid flow to attain the probe (Fig. 7-6d) to oppose reduction in the conductance signal. For $S$ = 80%, as explained for the air-water system, larger conductance values and broader conductance peaks obtained for both probes refer to more liquid accumulation during time lapse $\tau_L$ , as expected.

## 7.4 Conclusion

In this work alternating gas/liquid fast-mode cyclic operation was studied for foaming and non-foaming systems using image processing, pressure drop transient traces and electrical conductance traces at different split ratios, and two temperature and pressure levels. Alternating passage of gas- and liquid-rich phases through the packed bed can play a crucial role for controlling foam formation and stability at elevated temperature and pressure. Adjusting properly the split ratios yielded pressure drops in cyclic operation lesser than in isoflows conditions conducted under barycentric feed flow rates for the foaming system. Increased temperature was speculated to allow faster foam drainage and breakdown which was reflected in the lower pressure drop levels as well as in the faster collapse of region 5 identified in the pressure drop curves the higher the temperature.

## 7.5 Nomenclature

$C$ conductance, μSiemens (μS)

$u$ superficial velocity, m/s

$P_r$ pressure, MPa

$\Delta P/H$ two-phase pressure drop, Pa/m

$S$ split ratio

$T_r$ temperature, °C

τ time, s

**Subscripts**

G gas phase

L liquid phase

r reactor

## 7.6 References

Aydin, B., Larachi, F., 2005. Trickle bed hydrodynamics and flow regime transition at elevated temperature for a Newtonian and a non-Newtonian liquid. Chemical Engineering Science 60, 6687-6701.

Barigou, M., Deshpande, N.S., Wiggers, F.N., 2001. An enhanced electrical resistance technique for foam drainage measurement. Colloids and Surfaces A: Physicochemical and Engineering Aspects 189, 237-246.

Bartelmus, G., Janecki, D., 2003. Hydrodynamics of a cocurrent downflow of gas and foaming liquid through the packed bed. Part II. Liquid holdup and gas pressure drop. Chemical Engineering & Processing 42, 993-1005.

Bartelmus, G., Janecki, D., 2004. Hydrodynamics of the cocurrent downflow of a gas and a foaming liquid through a packed bed. Part I. Estimation of the transition boundary between the hydrodynamic regimes from the gas continuous flow to the pulsing flow. Chemical Engineering & Processing 43, 169-179.

Boelhouwer, J.G., Piepers, H.W., Drinkenburg, A.A.H. 2002. Advantages of forced non-steady operated trickle-bed reactors. Chemical Engineering & Technology 25, 647-650.

Burghardt, A., Bartelmus, G., Janecki, D., 2003a. Parameters characterising the pulsing flow of gas and foaming liquid through the packed bed. Part I. Pulse velocity. Inzynieria Chemiczna I Procesowa 24, 151-164.

Burghardt, A., Bartelmus, G., Janecki, D., 2003b. Parameters characterising the pulsing flow of gas and foaming liquid through the packed bed. Part II. The frequency of pulsation and the structure of pulses. Inzynieria Chemiczna I Procesowa 24, 165-182.

Charpentier, J.C., Favier, M., 1975. Some liquid holdup experimental data in trickle-bed reactors for foaming and nonfoaming hydrocarbons. AIChE Journal 21, 1213-1218.

Dudukovic, M.P., Larachi, F., Mills, P.L. 2002. Multiphase catalytic reactors: A perspective on current knowledge and future trends. Catalysis Reviews-Science & Engineering 44, 123-246.

Evans, D.F., Allen, M., Ninham, B.W., Fouda, A., 1984. Critical micelle concentrations for alkyltrimethylammonium bromides in water from 25 to 160ºC. Journal of Solution Chemistry 13, 87-101.

Janecki, D., Bartelmus, G., Krótki, T., 2005. The hydrodynamics of the pressure trickle-bed reactor with packed bed for foaming system. Proc. 7th World Congress Chemical Engineering, Glasgow, United Kingdom.

Kanicky, J.R., Lopez-Montilla, J.C., Pandey, S., Shah, D.O., 2001. Surface Chemistry in the Petroleum Industry, in: Holmberg, K. (Ed.), Handbook of Applied Surface and Colloid Chemistry, John Wiley & Sons, USA.

Larachi, F., Laurent, A., Midoux, N., Wild, G., 1991. Experimental study of a trickle bed reactor operating at high pressure: Two-phase pressure drop and liquid saturation. Chemical Engineering Science 46, 1233-1246.

Larkins, R.P., White, R.R., Jeffrey, D.W., 1961. Two-phase cocurrent flow in packed beds. AIChE Journal 7, 231-239.

Meyers, R.A., 1996. Handbook of petroleum refining processes. McGraw-Hill, 2nd ed., New York, USA.

Midoux, N., Favier, M., Charpentier, J.C., 1976. Flow pattern, pressure loss and liquid holdup data in gas-liquid downflow packed beds with foaming and nonfoaming hydrocarbons. Journal of Chemical Engineering of Japan 9, 350-356.

Morsi, B.I., Midoux, N., Charpentier, J.C., 1978. Flow patterns and some holdup experimental data in trickle-bed reactors for foaming, nonfoaming and viscous organic liquids. AIChE Journal 24, 357-360.

Morsi, B.I., Midoux, N., Laurent, A., Charpentier, J.C., 1982. Hydrodynamics and interfacial areas in downward cocurrent gas-liquid flow through fixed beds. Influence of the nature of the liquid. International Chemical Engineering 22, 142-151.

Sai, P.S.T., Varma, Y.B.G., 1987. Pressure drop in gas-liquid downflow through packed beds. AIChE Journal 33, 2027-2036.

Sai, P.S.T., 1997. Liquid saturation in concurrent gas-liquid downflow through packed beds. Bioprocess Engineering 16, 283-287.

Schramm, L.L., 1994. Foams: Fundamentals and Applications in the Petroleum Industry, American Chemical Society, Washington, USA.

Talmor, E., 1977. Two-phase downflow through catalyst beds. AIChE Journal 23, 868-878.

Weekman, V.W., Myers, J.E., 1964. Fluid-flow characteristics of cocurrent gas-liquid flow in packed beds. AIChE Journal 10, 951-957.

Xiao, Q., Cheng, Z.M., Jiang, Z.X., Anter, A.M., Yuan, W.K., 2001. Hydrodynamic behavior of a trickle bed reactor under forced pulsing flow. Chemical Engineering Science 56, 1189-1195.

# Chapter 8

# Polymer-filled composite porous catalytic particles for hydrodynamic studies in trickle bed reactors*

## Resumé

Une méthode simple est proposée pour la réduction de la porosité interne dans différentes particules poreuses trouvant une large utilisation dans les systèmes catalytiques à lit fixe. La méthode est basée sur un remplissage complet des pores par un polymère organique réticulé. Les particules ont été chargées en premier lieu avec le volume requis d'un monomère organique et réticulant pour la réalisation d'un blocage complet de la porosité interne et, par la suite, la polymérisation radicalaire in situ a été provoquée par chauffage sous atmosphère réduite. La méthode est facilement adaptable pour des particules de formes, de tailles et de structures poreuses diverses. Le remplissage sélectif et complet des pores a été confirmé par des mesures de physisorption d'azote, l'analyse thermogravimétrique et la microscopie électronique à balayage. Les différentes analyses confirment un blocage uniforme des pores. La différence d'angles de contact, avant et après imprégnation de polymères a été jugée négligeable. Le système est particulièrement adapté pour les études hydrodynamiques de traçage dans les réacteurs à lit fixe permettant la distinction entre des effets hydrodynamiques extra-granulaires (tels que la dispersion axiale) et des effets de transfert de matière intra-particulaire dont la connaissance est essentielle pour le dimensionnement de ces réacteurs. La rétention liquide et le nombre de Péclet ont été comparés pour un réacteur trickle bed empilé successivement avec des particules sphériques imprégnées et des billes de verre pour la vérification de la compatibilité de la méthode. Pour des vitesses superficielles de liquide et de gaz données correspondant au régime d'écoulement pulsé, la rétention liquide externe et le nombre de Péclet ont présenté des valeurs proches pour les deux types de particules.

---

* Aydin, B.; Bilodeau, S.; Hamidipour, M.; Larachi, F.; Kleitz, F. Industrial and Engineering Chemistry Research, submitted

# Abstract

A simple and scaleable method is proposed for suppressing internal porosity in various porous particles that are widely applied in packed bed catalytic systems. The method is based on a complete filling of the pores by a cross-linked organic polymer. The particles were first loaded with the volume of organic monomer and cross-linker needed to achieve complete blockage of the porosity, and subsequently, *in situ* radical polymerization was performed with heating under reduced atmosphere. The method is shown to be adaptable for particles of various shapes, sizes and porous structures. Selective and complete pore filling has been confirmed by nitrogen physisorption measurements, thermogravimetric analysis and scanning electron microscopy. The different analyses confirm uniform pore blocking. The difference in contact angle before and after polymer impregnation was found to be negligible. The system is especially suitable for packed bed hydrodynamic studies to disentangle extra-granular hydrodynamic effects (such as axial dispersion) from intraparticle mass transfer effects which are key to scaling down/up trickle bed reactors. The liquid holdup and Péclet number for a trickle-bed reactor packed with impregnated spherical particles and glass beads respectively were compared for the compatibility of the method. For given superficial liquid and gas velocities corresponding to the pulsing flow regime, the external liquid holdup and Péclet number were found to be correspondingly close for both particles.


## 8.1 Introduction

Catalytic fixed/packed bed reactor is one of the simplest three-phase reactors that usher an overwhelming range of catalytic reactions in industry (Biardi and Baldi, 1999). Porous packed beds find numerous applications in petroleum, petrochemical and chemical industries, in waste treatment and in biochemical and electrochemical processing. As known from numerous literature studies, a practical packed-bed type, *i.e.*, trickle-bed reactor (TBR) is widely used in various processes, *e.g.*, hydrotreating, hydrocracking, Fischer-Tropsch process (Meyers, 1996; Speight, 2001; Wang et al., 2003). Hydrodynamic studies in such TBRs have been reported since the 1960's (Schiesser and Lapidus, 1961; Nallaperumal, 1962). In TBRs for a fluid-solid reaction, the (porous) solid catalyst is

present as a bed of relatively small individual particles, randomly oriented and fixed in position. The fluid moves by convective flow through the spaces between the particles (Missen et al., 1999). Particles with different shapes and sizes are used to ensure good inter-phase contacting (Dudukovic et al., 2002). Non-porous particles (*e.g.* fabricated from glass) are also widely used for cold-flow hydrodynamic studies of TBRs.

One of the key parameters for the wettability of a particle is its contact angle. Contact angle is a quantitative measure of the wetting of a solid by a liquid. It is defined geometrically as the angle formed by a liquid at the three phase boundary where liquid, gas and solid intersect. In order to keep the contact angle of a non-porous particle as close as possible to the one for its porous *alter ego*, it is vital to obtain a non-porous packing analogue from the latter. This approach will expand the hydrodynamic studies done in the trickle bed reactors by allowing to disentangle extra-granular hydrodynamic effects (such as axial dispersion) from intraparticle mass transfer effects. This separation between physical retardation phenomena would give access to confident estimations of individual contributions which are key to scaling down/up trickle bed reactors. A simple, practical *recipe* to obtain non-porous packing analogues is still needed, which could also be scaled-up to increase the perspective of packed bed research. This method is required not to have a pronounced effect on the particle characteristics (*e.g.* size, shape, surface properties). By taking into consideration the above mentioned objectives the pores of packing particles may be filled to obtain non-porous particles while preserving the *same* contact angle. Early investigations of this matter were performed by Cui et al. who carried out effective diffusivity measurements with a packed bed of porous alumina that was previously impregnated with glycerol in aqueous ethanol solution (Cui, 1989; Cui et al., 1990). These measurements were performed at ambient temperature and atmospheric pressure. However, the stability of the method at elevated temperature was not addressed by these authors.

The aim of the present work is to provide a simple and effective method to convert particles that are porous in nature into a non-porous system. The method needs to be highly reproducible, scaleable to industrial ranges, and stability at elevated temperature should be sufficient. In addition, surface properties must not be drastically affected. In the 1990's, it was demonstrated that the pore system of ordered mesoporous materials (*e.g.* MCM-41-

type silicas) could be completely filled with different hydrophilic or hydrophobic polymers, resulting in pore-blocked materials exhibiting no adsorption capacity (Moller et al., 1998). This method was based on radical polymerization of vinyl monomers confined inside the mesopores (pores with dimensions comprised between 2 and 50 nm (Sing et al., 1985)). More recently, other examples of efficient mesopore filling with polymers were reported (Molenkamp et al., 2004; Choi et al., 2005; Save et al., 2006). Inspired by the method based on uniform impregnation of organic monomers inside mesoporous materials (Choi et al., 2005), we now report a pore filling strategy adapted for different packed bed particles, namely trilobe, quadrulobe, cylindrical and spherical alumina packings. In the present cases, a mixture of a selected vinyl monomer (hydroxyethylmethacrylate), a cross-linking agent, and a radical initiator were selectively introduced in the pores of packed bed materials, and subsequently polymerized *in situ* under reduced atmosphere at elevated temperature. To verify the validity of this approach, the degree of pore-filling, the polymer location, and the pore structures were analyzed by nitrogen physisorption measurements performed at 77 K, thermogravimetric analyses (TGA-DTA) and scanning electron microscopy (SEM). Contact angle measurements were also carried out to determine changes in surface nature. The resulting polymer filling is proven to be uniformely distributed throughout the particle structure without modification of size and shape, and porosity has been suppressed as probed by nitrogen sorption. Furthermore, a TBR was constructed with spherical alumina, polymer-filled spherical alumina and glass beads equal in diameter to compare the key hydrodynamic parameters for the reactor design. A residence time distribution model incorporating axial dispersion coefficient, external liquid holdup and intraparticle diffusion of tracer was used for data interpretation for the three types of packings. From the multiphase reactor point of view, this method is applicable to porous particles different in shape, size and porous structure, opening up useful opportunities in the study of the hydrodynamics of trickle beds.

## 8.2 Experimental Setup and Procedure

### 8.2.1 Materials

Different series of packed bed alumina-based materials were chosen for the investigation. The particles are labeled as spherical, cylindrical, triblobe and quadrulobe. The packed bed particles were supplied by Grace (USA) and Chevron-Texaco (USA). The pore-filling method is based on the use of a cross-linked organic polymer serving as a filler to plug all the internal porosity of the particles. The different reagents used for the preparation of the polymer filling, i.e. 2-hydroxyethyl methacrylate (HEMA 97%) and ethylene glycol dimethacrylate (EDMA 98%), benzoyl peroxide (BPO 97%) or a,a'-azoisobutyronitrile (AIBN, 98%), were obtained from Aldrich. Dichloromethane and diethylether were used as solvants. The HEMA and EDMA monomers were purified on a commercial alumina column. BPO was re-crystallized in acetone.

### 8.2.2 Methodology

The experimental procedure was derived from a methodology suggested by Choi et al. (2005) that was utilized to prepare homogeneous polymer coatings in nanoporous materials. First, the particles of interest were washed with ethanol and acetone for 15 min to remove dust and then dried at 363 K overnight. Note that the acetone washing is optional as it is only done to facilitate drying of the particles. The dried particles were analyzed by nitrogen physisorption at 77 K (BET) to determine precisely the total pore volume. The amounts of reagants were fixed according to the total pore volume obtained from sorption analysis with an excess of 5%. Note that HEMA and EDMA need to be filtered on alumina (or alternatively on silica) column to remove the polymerization inhibitors. The molar ratio HEMA/EDMA/BPO was 4:1:0.1812. Typically, for the impregnation of 250g of washed spherical alumina particles with a measured pore volume of 0.69 $cm^3/g$, 131.61g of HEMA, 41.46g of EDMA, 10.24g of BPO and 60 mL of dichloromethane were used. Alternatively, AIBN may as well be used as the radical initiator in diethyl ether as a solvant. For the impregnation, the reagents were pre-mixed in the solvent (e.g. dichloromethane) in a glass flask. After complete dissolution of the radical iniator in the solution, the mixture was added in 3 steps into the designed impregnation column containing alumina particles. The

experimental setup used for the impregnation of packed bed particles in large batch is schematically represented in Figure 8-1. At each of the 3 additions, the mixture was vigorously stirred/ shaken in the column. When the total volume of solution was added, the particles were then mixed vigorously for 15 min. To remove the solvent, the impregnated particles were dried first at 313 K for 2 h and then at 308 K overnight. Afterwards, the particles were placed in a dewar and subjected to freeze-vacuum-thaw cycles using an acetone/dry ice bath to remove the excess of solvent and air. The freeze-vacuum-thaw sequence was the following: freezing of the material for 15 min, vacuum drying for 30 min, and 30 min for re-heating up to room temperature (the flask remained closed). This sequence was repeated 3 times. After leaving the particles at 308 K for 3 h in the closed vessel under vacuum, an additional freeze-vacuum-thaw cycle was performed with a liquid nitrogen bath (5 min of freezing followed by vacuum treatment for 30 min, and re-heating). Note that this additional step is highly recommended to remove traces of water that are produced if the polymerization has already been initiated (case of large batches). Subsequently, vacuum radical polymerization was conducted stepwise as follows: The particles were maintained at 308 K for 6 h, then heated at 333 K for 4-6 h, at 373 K for 1 h and finally at 393 K for 1 h. After cooling, the recovered materials were washed briefly with ethanol and dried at 353 K for 6-8 hours. The pore-filled particles were then sieved to collect the particles in 2 mm diameter for the hydrodynamic experiments. In addition, to test the stability of the pore-filling method, dried particles were placed in water and heated at 363 K for 48 hours.

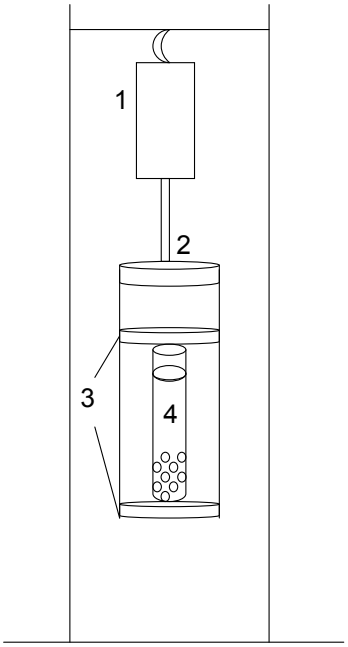


**Figure 8-1** Schematic representation of the experimental set up employed for the impregnation of the porous materials with the polymer precursor solution. After drying, the column is put under vacuum for the thermally induced radical polymerization.

### 8.2.3 Instrumentation

Nitrogen adsorption-desorption isotherms at 77 K were measured using a Micromeritics Tristar 3000 gas adsorption analyzer. Outgassing was done at 363 K for 3 h. The Brunauer-Emmett-Teller (BET) equation was used to calculate the surface area $S_{BET}$ from adsorption data obtained at $P/P_0$ between 0.01 and 0.2. The total pore volume ($V_t$) was obtained from the amount of nitrogen adsorbed at $P/P_0 = 0.97$. Pore size distributions were determined by applying the BJH (Barrett-Joyner-Halenda) algorithm. Thermogravimetric analysis was performed with a Jupiter STA 449C thermogravimetry-differential thermal analysis (Netzsch). Crushed polymer-filled samples were heated up to 973 K with a rate of 5 or 10 K/min. Scanning electron microscopy (SEM) images were obtained with a JEOL JSM-6360 microscope operating at 30 kV.

For the contact angle measurements a tensiometer (Kruss K14) was used. The contact angle for the trilobe, quadrulobe and cylindrical particles were measured by Wilhelmy technique (Wilhelmy, 1863). This technique measures the force resulting from the implementation of

a solid contact with the liquid (or removing liquid), similar to the surface tension measurement. The particles were hung up by a hook and by knowing the surface tension of the liquid, solid perimeter (thickness and width), the advancing or receding contact angle can be determined by moving the solid forward or backward in the liquid. The measure of the strength is carried out using a balance (Baussaron, 2005). It is linked to the contact angle according to:

$$\cos\theta = \frac{F_w}{\sigma \cdot L} \tag{8.1}$$

with $F_w$ = Wilhelmy force, $L$ = wetted length, $\theta$ = contact angle.

In addition, the spherical alumina particles were crushed into a powder and the contact angle was measured by applying the capillary penetration method and using the Washburn equation (Washburn, 1921):

$$m^2 = \frac{\rho \cdot \left[A^2.\kappa\right] \cdot \sigma \cdot \cos\theta}{2\mu} \cdot t \tag{8.2}$$

The term $A^2.\kappa$ is constant and it can be calculated when a liquid with a contact angle $\theta = 0°$ is used. The powder was placed in a closed tube containing a frit on the bottom. The liquid rises through the glass frit into the powder. The contact angle could be calculated by measuring the increase in weight as a function of time and applying the Washburn equation (eq 8.2).

### 8.2.4 Hydrodynamic Measurements

The Aris's tracer response method (Aris, 1956) with a downstream double-detection was implemented to compare three types of particles with same diameter: non-impregnated porous alumina, impregnated porous alumina and glass beads. Experiments at ambient temperature and pressure were carried out in a transparent Plexiglas column (5.7 cm I.D. and 40 cm high) at constant superficial liquid and gas velocities (0.006 m/s and 0.2 m/s respectively) corresponding to the pulsing flow to ensure complete external wetting. Two electrical conductance probes placed at the top and the bottom of the bed were used to

register the conductance signals for the inlet and the outlet during tracer injection. 0.2 mol/L NaCl was used as a tracer. The tracer was injected to the reactor via a 3-way pneumatic valve controlled by computer. This valve lets the tracer be introduced to the system from a separate reservoir for a given period (4s in this case). In order to provide an objective estimation of the merit of the polymer-filling method, we strived to assess the variability on the residence time distribution (RTD) due to imperfections in packing arrangement after each bed filling as well as tracer injection and flow fluctuations. Hence, to obtain representative averages, for each type of packing the bed was repacked 4 times with as many RTD determinations. Additionally, tracer injection was repeated 4 to 5 times to account for experimental errors and to determinate accurate hydrodynamic parameters. Overall, for each packing 18 repeat tests were carried out for the same gas and liquid superficial velocities, and average RTD curves were estimated thereof.

#### 8.2.4.1 RTD Models for Data Reduction

For non-porous packing bed (glass beads and impregnated alumina particles), the plug flow with axial dispersion (PD) model was used to describe the liquid back mixing state in the extragranular space. The liquid holdup ($\varepsilon_L$) and Péclet number ($Pe$) were determined using a non-linear least-squares fitting where the convolution method was used for a time-domain analysis of the non-ideal pulse tracer response data. The model consists of the axial-dispersion model (ADM) where the mass exchange between dynamic and static part of the flow has been neglected. Our previous work confirms satisfying results by implementing this method for the determination of these hydrodynamic parameters (Aydin and Larachi, 2005).

In the case of the bed filled with porous packing, intraparticle diffusion of the tracer inside the packing affects the residence time distribution of the liquid. This diffusion is known to be responsible from the observed long tailing of the outlet signal. Therefore a transient diffusion model of the tracer in the porous particle coupled with ADM has been used in the literature to describe the liquid flow (Iliuta et al., 1996). The ADIM (axial dispersion with intra-particle mass exchange) model proposed assumes that the liquid stream is divided into two zones: a dynamic zone in which the liquid flows through the bed as a piston flow with axial dispersion and a stagnant zone inside the pellet in direct contact with the dynamic

zone and assuming full pellet external wetting. The dynamic evolution of the tracer concentration in the particles is described in terms of a Fick's diffusion equation. The interpretation of the data requires the following parameters: Péclet number, the actual value of external liquid holdup in two-phase flow, the effective diffusion coefficient of the tracer ($D^{eff}$) in the pores of the particle and the liquid-solid mass transfer coefficient. It should be noted that the mass exchange between the dynamic and static liquid zones was neglected in the case of glass beads; which should also be applied for the porous particles. It is possible to determine these parameters by fitting the normalized experimental output response with the model predicted response. However, more reliable data could be extracted from the model if the determination of the parameters is done in a stepwise manner. Generally, for two beds (either porous or non-porous) of same height, packing diameter and porosity, working under same operating conditions, axial dispersion and liquid holdup are postulated to be equal provided full wetting is achieved and the contact angles are close. In our case, these parameters have been calculated for the glass beads to reduce the number of parameters extracted from the model for the porous particles. The ADIM transient mass balance equations in dimensionless spatial form are given as follows:

$$\varepsilon_L \frac{\partial C}{\partial t} + \frac{v_{SL}}{H}\frac{\partial C}{\partial x} = \frac{1}{Pe}\frac{v_{SL}}{H}\frac{\partial^2 C}{\partial x^2} - D^{eff}\frac{a_s}{r_p}\frac{\partial C_p}{\partial \zeta}\Big|_{\zeta=1} \tag{8.3}$$

$$\varepsilon_{L,\text{int}} \frac{\partial C_p}{\partial t} = \frac{D^{eff}}{r_p^2 \zeta^2}\frac{\partial}{\partial \zeta}\left(\zeta^2 \frac{\partial C_p}{\partial \zeta}\right) \tag{8.4}$$

where the boundary and initial conditions are:

$$x = 0, C\Big|_{x=0^-} = C\Big|_{x=0^+} - \frac{1}{Pe}\frac{\partial C}{\partial x} \tag{8.5}$$

$$x = 1, \frac{\partial C}{\partial x} = 0 \tag{8.6}$$

$$\zeta = 0, \frac{\partial C_p}{\partial \zeta} = 0 \tag{8.7}$$

$$\zeta = 1, C_p = C \tag{8.8}$$

$$t = 0, C_p = C = 0 \tag{8.9}$$

It should be pointed out that by neglecting the diffusion inside the particles; eq. 8-4 will be eliminated, thus retrieving the ADM form for non-porous particles.

The precision of the hydrodynamic parameters determination for the porous particles depends on the correctness of the evaluation of the liquid-solid mass transfer coefficient and effective tracer diffusivity. However, the dominant resistance is due to the intra-particle diffusion and therefore the sensitivity of the experimental response to the liquid-solid mass transfer coefficient is too low for the accurate estimation. Thus, as a boundary condition on the surface of the particle the concentration of tracer in the liquid bulk ($C$) was considered to be equal to the concentration in the particle ($C_p$), eq 8-8. Based on this assumption, it is not required to estimate or calculate the liquid-solid mass transfer coefficient.

An imperfect pulse method for time-domain analysis of non-ideal pulse tracer response data was used to estimate the effective diffusivity and internal porosity of the alumina beads as model parameters. The method used for the calculation of the model parameters is based on the least-squares fit of the normalized experimental output response with the model predicted response to minimize the relative square error function given below (Sicardi et al., 1980; Skomorokov et al., 1986):

$$F = \sqrt{\frac{\sum_{i}^{m}\left[\frac{C(t_i)\big|_{x=1} - C_{\exp}(t_i)\big|_{x=1}}{C_{\exp}(t_i)\big|_{x=1}}\right]^2}{m}} \tag{8.10}$$

This function assigns an equal importance to the entire output signal meaning that it also takes into account the tail. Literature works done on the calculation of the output response used a numerical procedure based on the orthogonal collocation method (Iliuta et al., 1996; Kulkarni et al., 2005). In this study, an existing MATLAB (version 7.4.0.287) code (*pdepe*) constructed on finite differences was used to solve each partial differential equation (PDE). Whenever, eq 8-3 needs the concentration derivative on the particle surface, eq 8-4 is

solved (using a coupled code) for the corresponding time and axial position. The *pdepe* solves initial-boundary value problems for systems of parabolic and elliptic PDEs in the one space variable and time. The ordinary differential equations (ODEs) resulting from discretization in space are integrated to obtain approximate solutions at specified times. The time integration is done with *ode15s*. The *ode15s* uses the backward differentiation formulas (also known as Gear's method) (Shampine and Reichelt, 1997). It is usually employed when Runge-Kutta algorithm (Shampine et al., 1999) fails or is very inefficient, and the problem is stiff. Considering the stiffness of the boundary condition when the tracer is injected, the solver will be able to solve the equations.

## 8.3 Results and Discussion

Series of nitrogen physisorption measurements were performed before and after polymer loading in order to determine the effect of the polymer filling on the surface area and pore volume of the particles. Thermogravimetric analyses were also carried out to establish the total organic polymer content for each modified material. The measured mass losses allow a precise estimate of the polymerization yields.

The nitrogen physisorption and TGA data obtained with the different materials under investigation are compiled in Table 8-1. Figure 8-2 shows the $N_2$ adsorption-desorption isotherms obtained for particles of different shape, size and porosity, before and after the impregnation and polymerization processes. Before polymer-filling, the materials usually exhibit typical type IV isotherms with a pronounced capillary condensation step at high relative pressures being characteristic of large mesopores (Sing et al., 1985; Thommes, 2004). Specific BET surface areas and total pore volumes of the particles (after solvant washing) are comprised between 95 to 151 $m^2/g$ and 0.275 to 0.69 $cm^3/g$, respectively, depending on the nature of packed bed material. The pore filling process was performed for each type of particles by impregnation of a mixture a vinyl monomer (HEMA) and a cross-linking agent (EDMA) selectively inside the pores, followed by radical polymerization under reduced atmosphere as detailed in the experimental section. As evidenced by the physisorption results, the adsorbed capacity has decreased close to zero for all porous materials filled with the cross-linking polymer. This is a clear indication that our method

may be suitable to fill totally the pores of various types of porous packed bed particles even exhibiting marked differences in porosity. The total filling of the pores is reflected by the very low specific surface areas and pore volumes measured by nitrogen sorption for the different materials (Table 8-1). Polymer-filled materials have very low BET surface area (about 3-10 $m^2/g$) and pore volumes decreased as low as 0.01-0.02 $cm^3/g$. Noteworthy is that the surface areas and pore volumes are maintained as low after the prolonged water treatment of the filled particles, as illustrated by the isotherms in Figure 8-2. Moreover, it should be noted that it was found favorable for a proper polymer-filling that the particles were first washed with ethanol and acetone, respectively for 15 min and then dried at 363 K, before evaluating the pore volume. This washing treatment usually causes only minor changes in the porosity of the materials. In the case of the trilobe particles for instance, we observed that the surface area was initially 159 $m^2/g$ and the pore volume was 0.44 $cm^3/g$, while after the washing step the surface area and the pore volume decreased to 151 $m^2/g$ and 0.42 $cm^3/g$, respectively. However, some differences in the material surface topology are observed.

**Table 8-1** BET surface areas and total pore volumes obtained from nitrogen physisorption at 77K of different packed bed particles, before and after the pore-filling treatment. Total weigth loss measured by thermogravimetry for the different polymer-filled composite samples.

| | Packed Ped Partices [a] | Spherical 1 | Spherical 2[b] | Cylinder | Trilobe | Quadrilobe |
|---|---|---|---|---|---|---|
| Before polymer loading | BET surf. area ($m^2/g$) | 95 | 132 | 125 | 151 | 120 |
| | TPV[c] ($cm^3/g$) | 0.402 (*0.48*) | 0.69 *(0.67)* | 0.405 *(-)* | 0.42 *(0.44)* | 0.275 *(0.29)* |
| After polymer loading | BET surf. area | -/8.6[b]/5.6[d] | - | 3.5 | 6.6 | 2.6 |
| | Crushed | 9.9 | - | - | 5.5 | 5.3 |
| | Water treated | 9.5 | 3.0 | 13 | 16 | 5.9 |
| | TPV | -/0.029[b]/0.019[d] | - | 0.009 | 0.019 | - |
| | Crushed | 0.027 | - | - | 0.015 | 0.012 |
| | Water treated | 0.047 | 0.009 | 0.023 | 0.034 | 0.009 |
| | weight lost (%) | - 32.8/- 34.2[b] | - 43.1 | - 28.3 | - 35.1 | - 29.6 |
| | Polymer yield | 98.5% | 102% | 98 % | 111% | 114% |

[a] The particles are washed with ethanol and acetone, filtered and dried.

[b] Polymer filling prepared with BPO as the radical initiator in $CH_2Cl_2$. Others were obtained with using AIBN in diethylether.

[c] TPV = total pore volume obtained at $P/P_0 = 0.97$. Values in parantheses are obtained with the raw materials before solvant washing.

[d] Polymer filling prepared with BPO in $CH_2Cl_2$ with an excess loading of polymer of 10 wt% vs the pore volume.

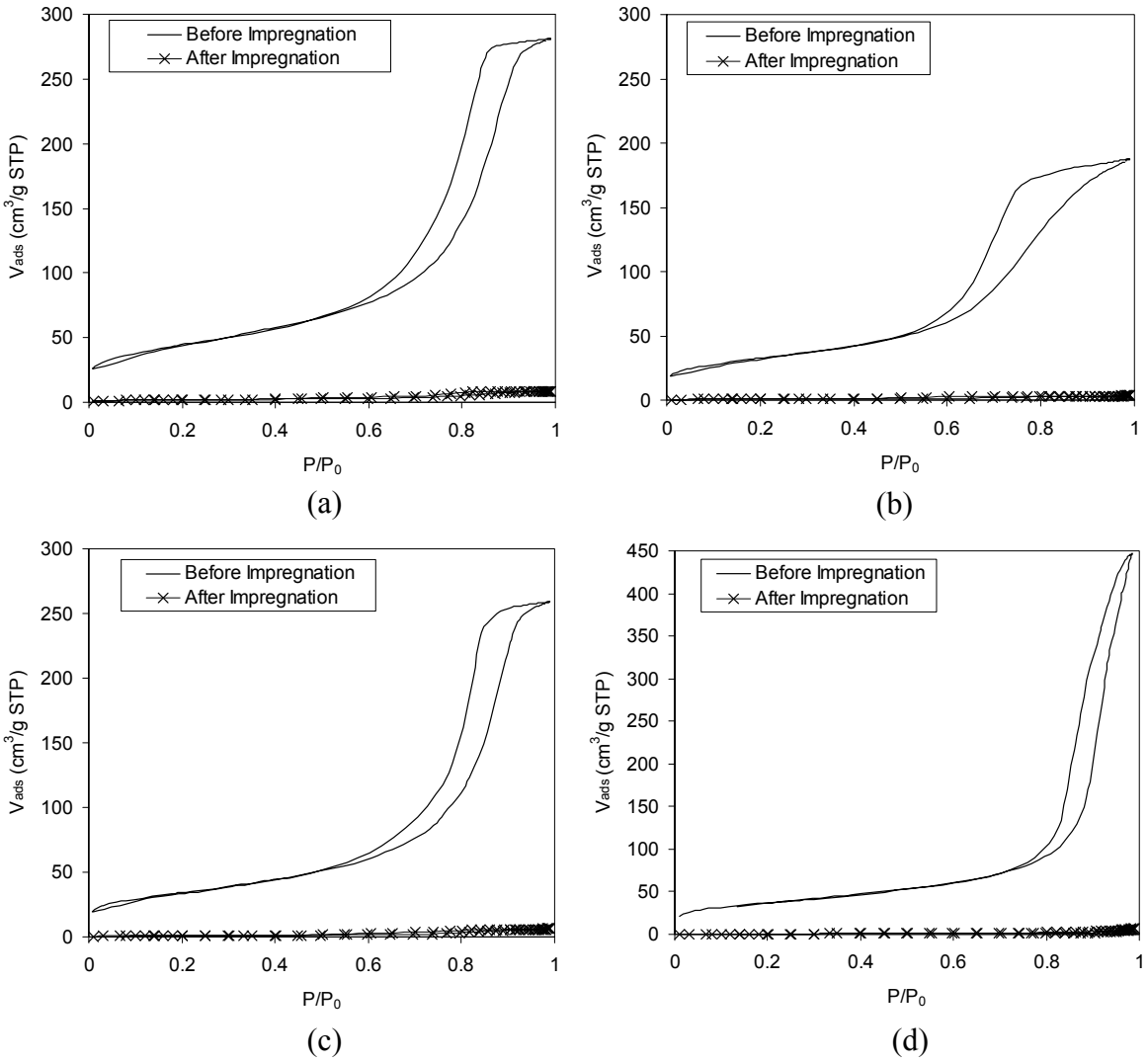


**Figure 8-2** Nitrogen physisorption isotherms measured at 77K of selected porous packed bed materials, before and after the filling with poly-HEMA: a) Trilobe, b) Quadrulobe c) Cylindrical, and d) Spherical materials.

Figures 8-3a and 8-3b show representative scanning electron microscopy images obtained for unwashed and washed trilobe, respectively, emphasizing slightly different surface morphology. Similar effects are visible for quadrulobe, cylindrical and spherical particles.

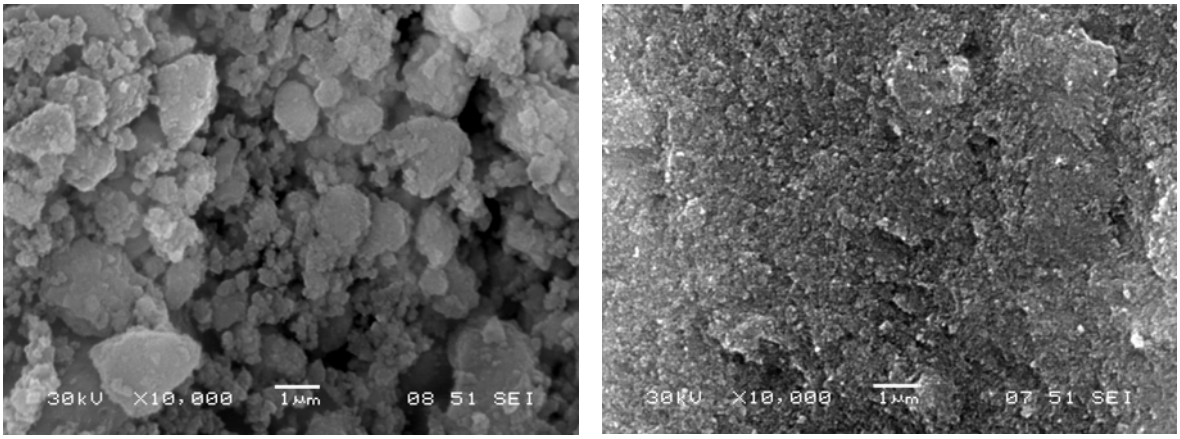


(a) (b)

**Figure 8-3** Typical SEM images of a trilobe material: a) Before particle washing, and b) After washing with ethanol.

The TGA plots of four different packed bed particles filled with polyhydroethylmethacrylate (poly-HEMA) are depicted in Figures 8-4a and 8-4b. The polymer content evaluated from the thermogravimetric analysis ranges from 28 to 43 wt% depending on the porosity of the initial material (Table 8-1). In all cases, high yields in cross-linked polymer are obtained (quantitative in monomer/cross linker conversion). The values of polymer yields above 100%, as quantified from TG analyses for some of the samples, might be attributed to the presence of small amount of residual solvent and/or the release water present in the particle structures. Also shown on the plots are the differential thermal analysis curves, indicative of exothermic nature of the effects occurring during thermal treatment of the polymer-filled particles. The pore-filling method remain valid irrespective the nature of the radical initiator (BPO or AIBN), and different volatile solvents may be used for the impregnation. For example, spherical particles were successfully filled with poly-HEMA, both with AIBN in diethyl ether or with BPO in dichloromethane, as viewed from the dramatically decreased specific surface area and pore volume values for the filled composites. Yields in polymer filling are almost identical in both cases (see Figure S1 for comparison). SEM imaging was also used for the verification of the polymerization restricted to the inside of the pore system without polymer formation on the outer surface of the material.

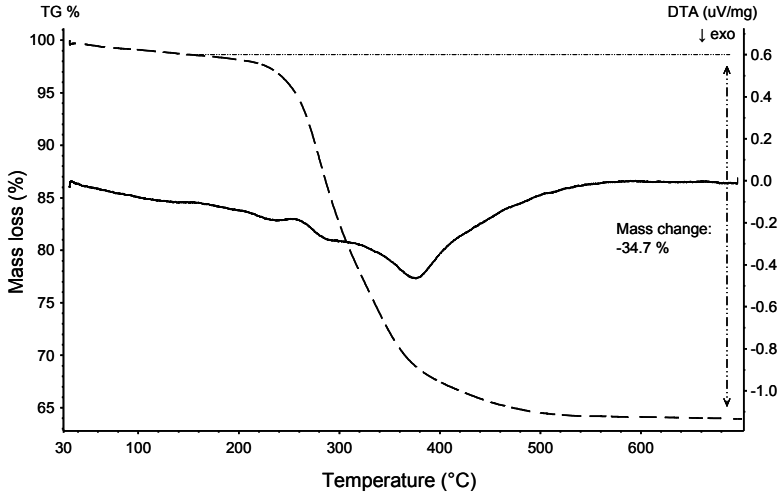
TG %
DTA (uV/mg)
↓ exo
Mass loss (%)
Mass change:
-34.7 %
Temperature (°C)

(a)

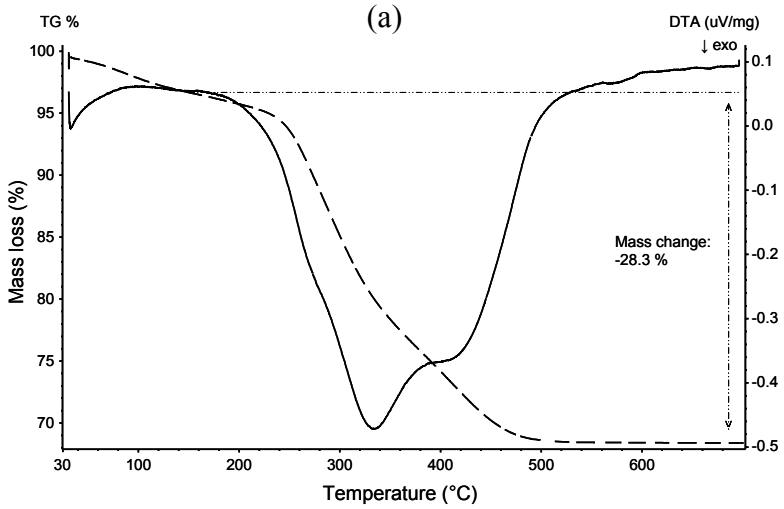
TG %
DTA (uV/mg)
↓ exo
Mass loss (%)
Mass change:
-28.3 %
Temperature (°C)

(b)

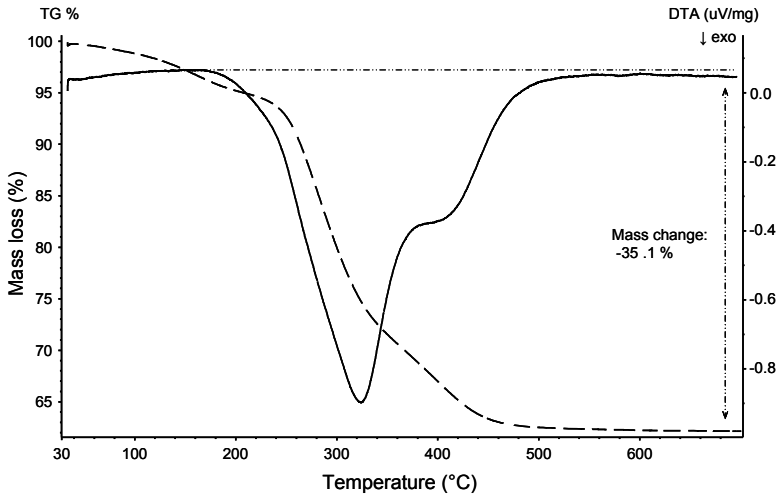
TG %
DTA (uV/mg)
↓ exo
Mass loss (%)
Mass change:
-35 .1 %
Temperature (°C)

(c)

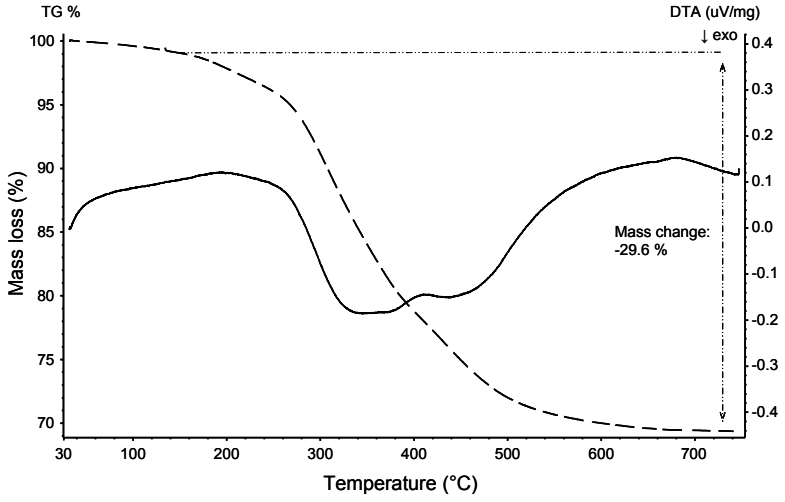


(d)

**Figure 8-4** Thermogravimetric analysis plots and DTA curves corresponding to the different polymer-filled packed bed materials: a) Polymer-spherical composite prepared with BPO in dichloromethane), b) Polymer-cylindrical composite obtained with AIBN/diethylether, c) Polymer-trilobe composite obtained with AIBN/diethylether, and d) Polymer-quadrilobe composite obtained with AIBN/diethylether. The heating rate was 5 K/min under air flow.

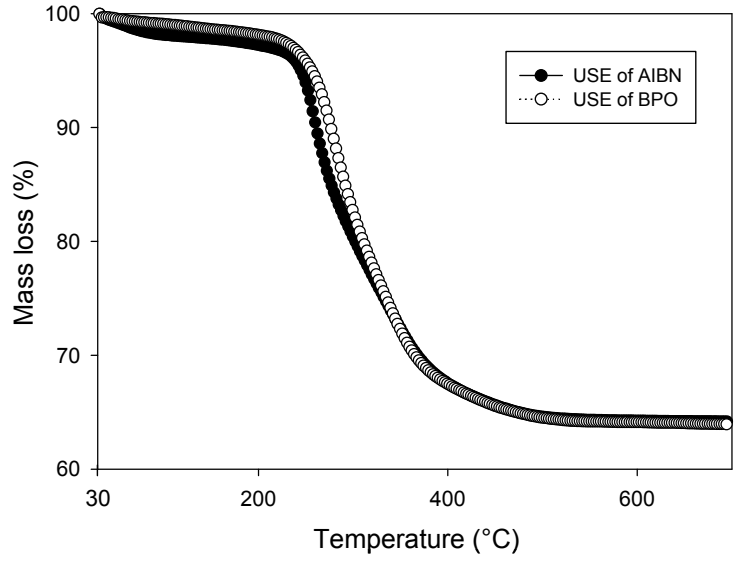


**Figure S1** Comparative TGA plots of polymer-filled spherical alumina particles prepared either with BPO as the radical initiator in dichloromethane or with AIBN in diethylether, as indicated. The heating rate was 5 K/min under air flow.

Figures 8-5a and 8-5b show no noticeable difference between the surface topology of the materials before or after the polymer introduction. The absence of polymer observed on the external surface of the particles, together with the large organic weight loss and the suppressed internal porosity, tend to confirm the location of the polymer species specifically inside the pores, hence acting as an efficient pore-filling material.

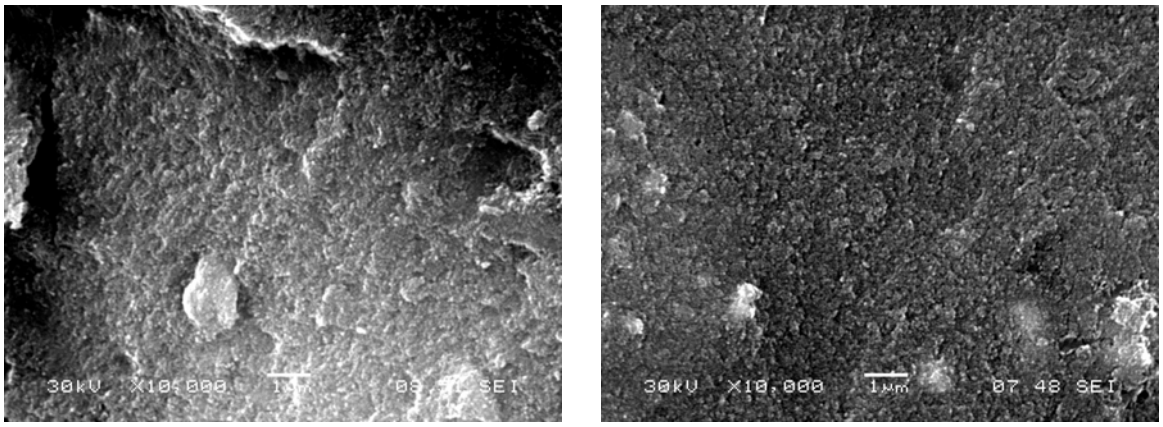


(a) (b)

**Figure 8-5** Representative SEM images of packed bed materials before and after polymer loading: a) Cylindrical material before polymer filling, and b) Cylindrical composite material after polymer filling.

Spherical particles supplied by Grace (sample *Spherical* 2, Table 8-1) were chosen for detailed hydrodynamics studies. In this latter case, the method for the pore filling was scaled up to reach the necessary amount of particles. Hence, 250 g of spherical particles of 2 mm in diameter were washed and dried, as done previously. This step was repeated 3 times to obtain the desired amount for a packed bed of 40 cm in height. The $N_2$ sorption analysis done for a small quantity of these particles (approx. 0.75 g) indicated us that the surface area was 132 $m^2/g$ and the pore volume was 0.69 $cm^3/g$. Similarly as before for other particles, polymer-filling resulted in an almost total loss of porosity with surface area and pore volume reduced at values of 3 $m^2/g$ and 0.009 $cm^3/g$, respectively. These values were obtained after leaving the particles in water at 363 K for 48h. Figures 8-6a and 8-6b show the pore size distributions obtained for these spherical particles before and after the impregnation and polymerization steps. The pore size distributions are obtained as the

derivative curves of the cumulative pore volumes measured by nitrogen sorption. As seen, the pore size distributions after polymer loading reached to zero, which confirms the complete filling of the pores.

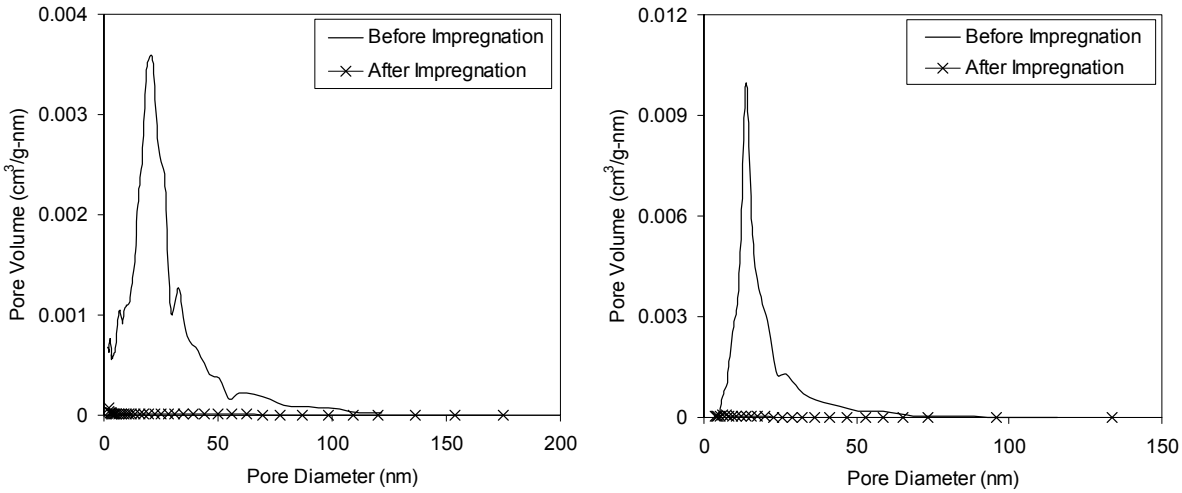


(a) (b)

**Figure 8-6** Nitrogen sorption pore size distribution curves (at 77K) of large batch of spherical packed bed alumina materials before and after polymer loading: a) Applying the BJH model to the adsorption branch of the isotherms, and b) Applying the BJH model to the desorption branch of the isotherms. The isotherms of the polymer-filled materials are measured after the treatment with water for 48h.

The reproducibility of method was additionally verified by TG analyses performed on several spherical particles originating from a same large batch and alumina particles issued from different batches. The results are shown in Figure 8-7. As can be seen, the TGA profiles are almost identical in all cases, suggesting excellent reproducibility and homogeneous distribution of the polymer-filling in the packed bed particles. The homogeneous location of the pore filling was further confirmed by SEM analysis.

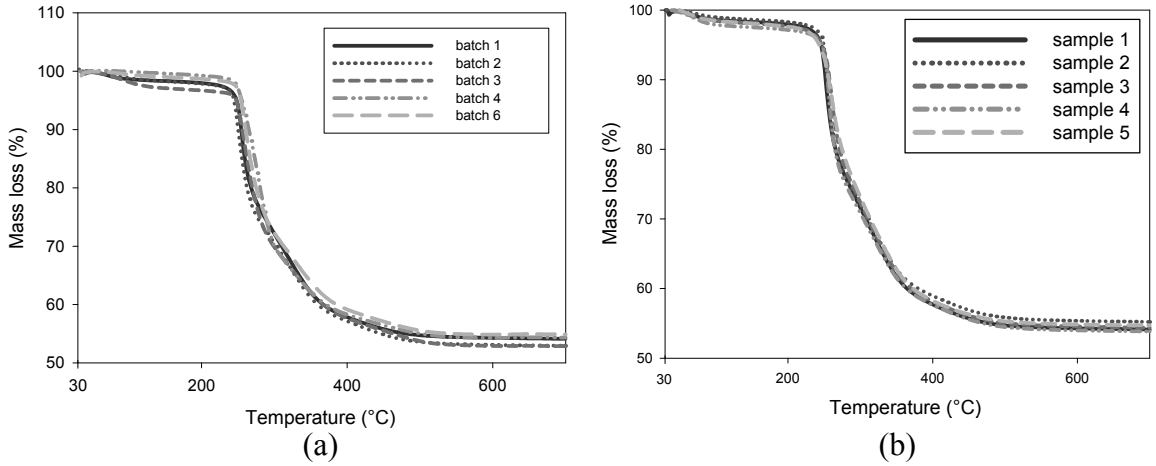


**Figure 8-7** Repeated TGA curves obtained with large batches of polymer-filled spherical particles: a) The thermogravimetric analyses were performed with 5 different samples issued from a single large batch to prove homogeneous distribution of the polymer filling; b) The thermogravimetric analyses were performed with 5 different samples issued out of 5 different large batches for evaluating the reproducibility of the loading method. The heating rate was 10 K/min under air flow.

Figures 8-8a and 8-8b are shown to illustrate that the external surface of the polymer containing alumina particle is akin to the surface of the pristine porous particle. Elemental analyses investigations (EDX) of the cross-section of single spherical particle performed in combination with the SEM (not shown) confirmed homogeneous distribution of carbonaceous species in the entire volume of the particle. The location of the polymer in the entire volume of the particles, including the core, is also supported by sorption analysis of crushed particles giving identical results as those of non-crushed particles. From these observations, the occurrence of a coating of polymer onto the sphere surface or polymer species located preferentially at the outer edge of the materials could be excluded. These results support that the polymer incorporation took place inside the internal pores (mesopores) of the packed bed materials. As also seen in Figures 8-8a and 8-8b the spheres are stable in terms of keeping their shape; thus there is no destruction during stirring/shaking in the column. The measured contact angle values for 4 particles were given in Table 8-2. As can be seen from Table 8-2, the difference in the contact angle before and after the polymer filling is almost negligible, indicating that the polymer filling has no major influence on the surface wettability properties.

**Table 8-2** Contact angles obtained for the original and polymer-filled particles.

| Samples | Trilobe | Quadrilobe | Cylindrical | Spherical 1 |
|---|---|---|---|---|
| Before polymer loading | 40° | 50° | 63° | 80° |
| After polymer loading | 47° | 56° | 70° | 88° |

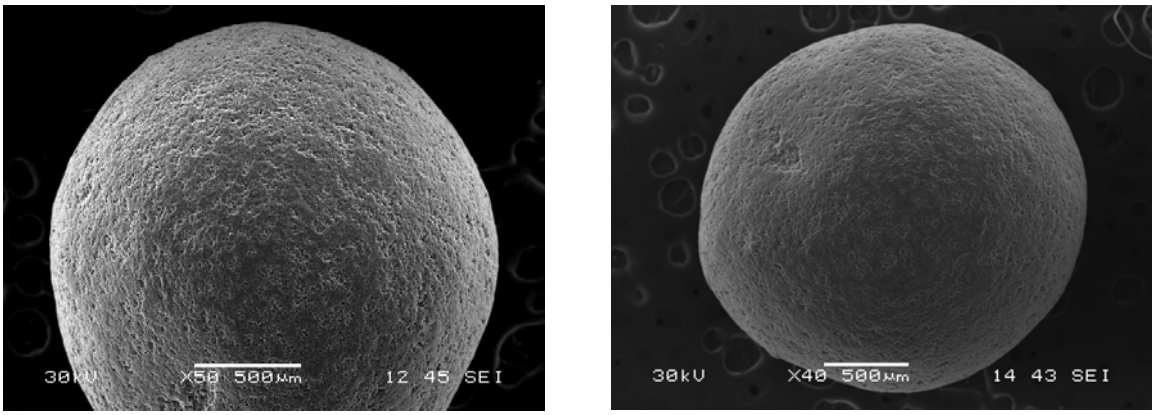


(a) (b)

**Figure 8-8** SEM overview images of the packed bed spherical alumina material: a) Before and b) After polymer introduction (in a large batch experiment).

The following section will discuss the hydrodynamic studies performed with the thus-treated particles and other reference materials. Figures 8-9a-c show the measured inlet and outlet responses together with the predicted outlet for glass beads, impregnated porous alumina (ADM model) and porous alumina particles (ADIM model) respectively. The liquid holdup and Péclet number calculated for two non-porous particles was found to be close. This may be given as a proof for the confirmation of obtaining non-porous particles via impregnation method. For given superficial liquid and gas velocities ADM model was

successful to predict an outlet response closed to the experimental outlet signal (Figures 8-9a,b). For glass beads, the liquid holdup and Péclet number were calculated as 0.12±0.0025 and 36±3.5 respectively where these values for the impregnated porous particles were 0.13±0.0021 and 30±2.3 respectively. Figure 8-9b shows that there is no tailing in the outlet response for the impregnated porous particles which is similar to that for the glass beads (Figure 8-9a). As seen in Figure 8-9c, ADIM model was used for the calculation of $D^{eff}$ (4e-9±0.032e-9) and $\varepsilon_{int}$ (0.2±0.005). Liquid holdup and Péclet number calculated for the glass beads were used to predict these parameters. We can observe a long tail in the outlet response of porous particles resulting from the diffusion into the pores of the particles. This above pronounced difference between impregnated porous and porous particles indicates qualitatively the filling of internal mesopores. Figure 8-9d shows the average residence time distribution function ($E$) for 18 experiments done at equal superficial liquid and gas velocities. The curve representative for porous particles indicates the distinct difference between porous and impregnated particles. As observed from the two curves for the glass beads and the impregnated particles, it could be pointed out that the behavior of the system for both particles is very close. The small difference at the peak of the residence time distribution curve might be attributed to the presence of residual large macropore (micrometer size) structure.

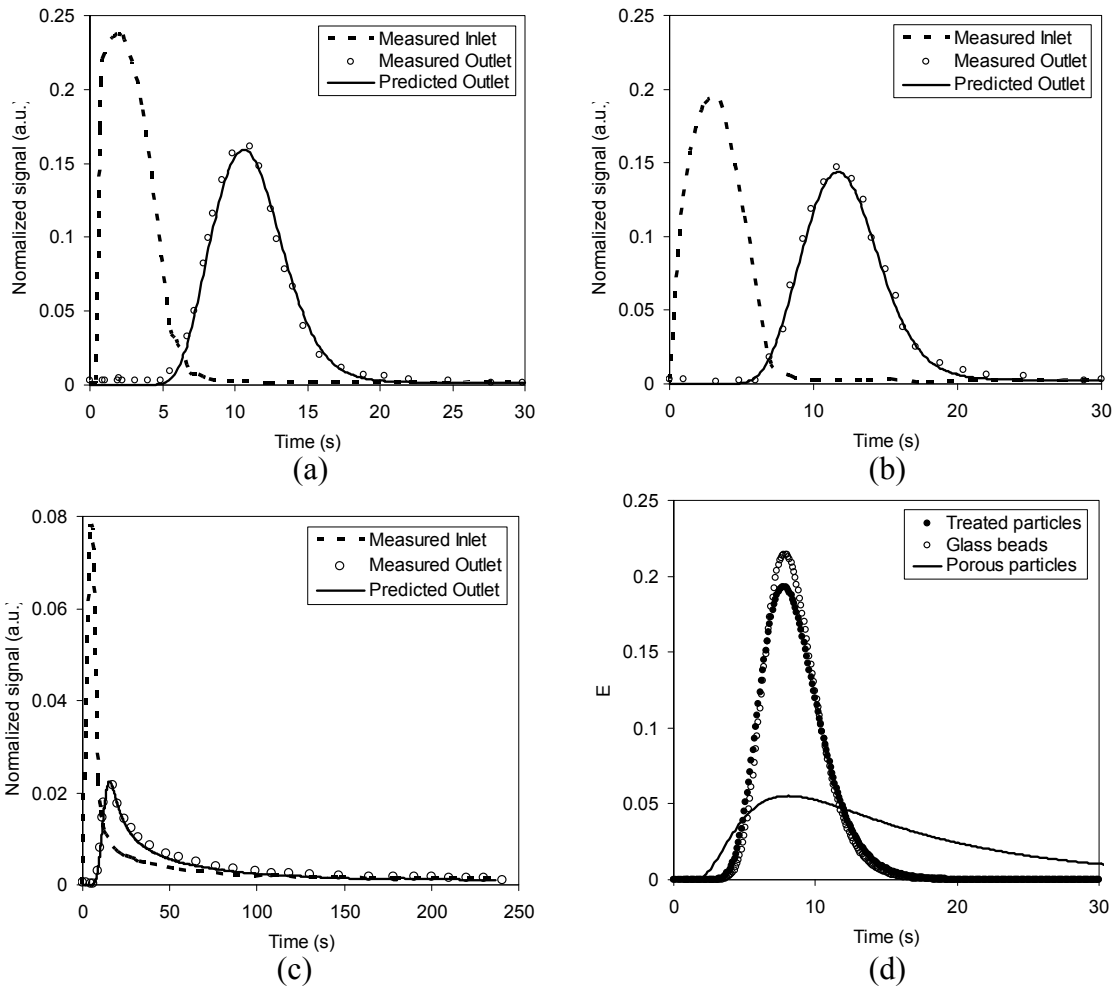


**Figure 8-9** Measured inlet and outlet responses, and predicted outlet responses shown for (a) glass beads reference materials, (b) the polymer-impregnated composite alumina particles and (c) the porous alumina particles. (d) The average residence time distribution function (E) for 3 particles, $u_G$ = 0.2 m/s, $u_L$ = 0.006 m/s.

As given in eq. 8-11 internal porosity of the impregnated particle is related to the pore and particle volumes:

$$\varepsilon_{\text{int}} = \frac{V_{\text{pores}}}{V_{\text{particle}}} \tag{8.11}$$

Multiplying the nominator and denominator of eq. 8-11 by the mass of particle, the resulting mathematical expression for the internal porosity could be given as follows:

$$\varepsilon_{int} = \frac{V_{pores}}{V_{particle}} \times \frac{m_{particle}}{m_{particle}} = \frac{V_{pores}}{m_{particle}} \times \rho_{particle} \qquad (8.12)$$

The first term in eq. 8-12 could be obtained from $N_2$ adsorption isotherms (0.0107 $cm^3/g$) and the particle density (1.5 $g/cm^3$) was measured experimentally. According to the calculations based on the experimentally found parameters the internal porosity of the impregnated particle was found to be 0.01. This value is in accordance with the explanation given for the small difference in the residence time distribution curves of glass beads and impregnated particles.

## 8.4 Conclusion

A simple method was developed for the filling of micro- and mesopores of porous particles by adsorption and polymerization of hydrophilic polymers into catalytic particles in use in trickle bed reactors. The method is especially suitable for packed bed hydrodynamic studies to disentangle extra-granular hydrodynamic effects (such as axial dispersion) from intraparticle mass transfer effects of catalytic particles which are key to scaling down/up trickle bed reactors. It was found that the method could be employed for large quantity of particles which favors the applicability of this method in industrial ranges. With an easy and reproducible approach, the internal porosity was completely filled. This method could be generalized by applying to various porous particles different in shape and size (e.g., spheres, extrudates, trilobes, quadrulobes) and using different solvents (e.g. diethyl ether or dichloromethane). The polymer-filling was found to be stable after leaving the particles in hot water (363K) for a certain period (48h in this case). After performing series of systematic experiments, it was found that the difference in the contact angle of the porous and the polymer impregnated-particles is negligible. Additionally hydrodynamic experiments performed in a TBR at ambient conditions show that the liquid holdup and Péclet number are close for glass beads and impregnated particles. These above mentioned results demonstrate the convenience of impregnated porous particles to study TBR hydrodynamics.

## 8.5 Nomenclature

$a_s$ specific area of the packing (surface of the particles/volume of the bed), $m^2/m^3$

C dimensionless tracer concentration in the dynamic zone of the liquid

$C_p$ dimensionless tracer concentration in the solid particle

$D^{eff}$ effective diffusion coefficient, $m^2/s$

$D_{ax}$ axial dispersion coefficient, $m^2/s$

H bed height, m

Pe Péclet number $Pe = \frac{Hv_{SL}}{D_{ax}\varepsilon_L}$

r radial position within solid particle, m

$r_p$ particle radius, m

t time, s

$v_{SL}$ superficial liquid velocity, m/s

x dimensionless axial coordinate

**Greek letters**

$\varepsilon_L$ liquid holdup

$\varepsilon_{L,int}$ internal liquid holdup

$\varepsilon_{int}$ internal particle porosity

$\zeta$ dimensionless radial coordinate $\zeta = \frac{r}{r_p}$

$\rho_L$ density, $g/cm^3$

## 8.6 References

Aris, R. On the dispersion of a solute in a fluid flowing through a tube. *Proc. Royal Soc. London. A-Math. Phys. Sci.* **1956**, *235*, 67.

Aydin, B.; Larachi, F. Trickle bed hydrodynamics and flow regime transition at elevated temperature for a Newtonian and a non-Newtonian liquid. *Chem. Eng. Sci.* **2005**, *60*, 6687.

Baussaron, L. Etude du mouillage partiel et du transfert de matiere liquide-solide en reacteur a lit fix arrose. PhD Thesis, Institut National Polytechnique de Toulouse, France, **2005**.

Biardi, G.; Baldi, G. Three-phase catalytic reactors. *Catal. Today* **1999**, *52*, 223.

Choi, M.; Kleitz, F.; Liu, D.; Lee, H.Y.; Ahn, W.-S.; Ryoo, R. Controlled polymerization in mesoporous silica toward the design of organic-inorganic composite nanoporous materials. *J. Am. Chem. Soc.* **2005**, *127*, 1924.

Cui, L.C. Diffusivité effective en chromatographie et en catalyse : Signification, mesure et intérpretation. PhD Thesis, Institut National Polytechnique de Lorraine, Nancy, France, **1989**.

Cui, L. C.; Schweich, D.; Villermaux, J. Consequence of flow nonuniformity on the measurement of effective diffusivity. *AIChE J.* **1990**, *36*, 86.

Dudukovic, M.P.; Larachi, F.; Mills, P.L. Multiphase catalytic reactors: A perspective on current knowledge and future trends. *Catal. Rev. – Sci. Eng.* **2002**, *44*, 123.

Iliuta, I.; Thyrion, F.C.; Muntean, O. Residence time distribution of the liquid in two-phase cocurrent downflow in packed beds: Air-Newtonian and non-Newtonian liquid systems. *Can. J. Chem. Eng.* **1996**, *74*, 783.

Kulkarni, R.R.; Wood, J.; Winterbottom, J.M.; Stitt, E.H. Effect of fines and porous catalyst on hydrodynamics of trickle bed reactors. *Ind. Eng. Chem. Res.* **2005**, *44*, 9497.

Missen, R.W.; Mims, C.A.; Saville, B.A. Introduction to chemical reaction engineering and kinetics. John Wiley&Sons Inc, New York, USA, **1999**.

Meyers, R.A. Handbook of petroleum refining processes. McGraw-Hill, 2ed ed., New York, **1996**.

Molenkamp, W.C.; Watanabe, M.; Miyata, H; Tolbert, S.H. Highly polarized luminescence from optical quality films of a semiconducting polymer aligned within oriented mesoporous silica. *J. Am. Chem. Soc.* **2004**, *126*, 4476.

Moller, K.; Bein, T.; Fischer, R.X. Entrapment of PMMA polymer strands in micro- and mesoporous materials. *Chem. Mater.* **1998**, *10*, 1841.

Nallaperumal, O. Trickle bed reactors-Kinetic study of gas-liquid reactions. *J. Sci. Ind. Res. A*. **1962**, *21*, 91.

Save, M; Granvorka, G.; Bernard, J.; Charleux, B.; Boissiere, C.; Grosso, D.; Sanchez, C. Atom transfer radical polymerization of styrene and methyl methacrylate from mesoporous ordered silica particles. *Macromol. Rapid Comm.* **2006**, *27*, 393.

Schiesser, W.E.; Lapidus, L. Further studies of fluid flow and mass transfer in trickle beds. *AIChE J.* **1961**, *7*, 163.

Shampine, L.F.; Reichelt, M.W. The Matlab ode suite. *SIAM J. Sci. Comp.* **1997**, *18*, 1.

Shampine, L.F.; Reichelt, M.W.; Kierzenka, J.A. Solving index-1 DAEs in Matlab and Simulink. *SIAM Rev.* **1999**, *41*, 538.

Sicardi, S.; Baldi, G. Specchia, V. Hydrodynamic models for the interpretation of the liquid flow in trickle-bed reactors. *Chem. Eng. Sci.* **1980**, *35*, 1775.

Sing, K.S.W.; Everett, D.H.; Haul, R.A.W.; Moscou, L.; Pierotti, R.A.; Rouquerol, J.; Siemieniewska, T. Reporting physisorption data for gas solid systems with special reference to the determination of surface area and porosity (recommendations 1984). *Pure Appl. Chem.* **1985**, *57*, 603.

Skomorokov, V.B.; Kirillov, V.A.; Baldi, G. Simulation of the liquid hydrodynamics in cocurrent two-phase upward flow through a packed bed. *Chem. Eng. J.* **1986**, *33*, 169.

Speight, J.G. Handbook of petroleum analysis, John Wiley & Sons Inc., New York, **2001**.

Thommes, M. in Nanoporous Materials; Science and Engineering; Lu G.Q., Zhao X.S., Eds.; Imperial College Press: London, U.K., 2004, pp 317-364

Wang, Y.-N.; Xu, Y.-Y.; Li, Y.-W.; Zhao, Y.-L.; Zhang, B.-J. Heterogeneous modeling for fixed-bed Fischer–Tropsch synthesis: Reactor model and its applications. *Chem. Eng. Sci.* **2003**, *58*, 867.

Washburn, E.W. The dynamics of capillary flow. *Phys. Rev.* **1921**, *17*, 273.

Wilhelmy, L. *Ann. Phys.* **1863**, *119*, 177.

# Conclusion

The studies on TBRs continue swiftly to better understand the hydrodynamics or to suggest new methods for the increase in the operation efficiency. A small progress could result in a major contribution for these reactors' output in industrial applications where high temperature and pressure is required. Therefore it is essential firstly to understand the physical phenomena and the feasibility of the alternative operation modes near to these conditions.

According to the author's knowledge, all the systematic studies, e.g., cyclic operation steady state experiments done in TBR were performed either at ambient temperature/ atmospheric pressure or ambient temperature/high pressure conditions. As industrial TBRs operate at high temperature and pressure, a systematic study was needed to explore the hydrodynamics of TBR operating at increased temperature. The comparison of the obtained experimental data with the suggested TBR models could show the applicability of these models under above mentioned conditions.

One of the definitions for the process intensification could be given as finding an operational method for boosting TBR performance. Unsteady, e.g., cyclic operation of TBR could be suggested as one of the methods for TBR process intensification. Therefore, it is inevitable to study the hydrodynamics of periodically operated TBR at increased temperature and/or pressure to understand and to investigate the benefits of this operation mode for different systems.

The main contributions of this research work could be summarized for two main operation modes. During constant throughput operation at constant increased temperature, pressure and superficial gas velocity, the trickle-to-foaming pulsing flow transition boundary was observed at lower superficial liquid velocity in comparison to trickle-to-pulsing flow transition. The transition boundary shifted towards higher velocities with increasingly temperature and pressure. At non-ambient conditions, the liquid holdup for foaming systems was lower than for coalescing systems and pressure drop was higher for foaming systems.

For the cyclic operation it was found that fast-mode cyclic operation outperforms slow mode for the same split ratio, pressure, temperature and fluid throughputs. Alternating passages of gas- and liquid-rich phases through the packed bed can play a crucial role for controlling foam formation and stability at elevated temperature and pressure.

TBR hydrodynamic studies could be expanded by different contributions. In this work a simple method was developed for the filling of micro- and mesopores of porous particles in use in trickle bed reactors. This method could be generalized by applying it to various porous particles different in shape and size used in industrial applications. Thus the extra-granular hydrodynamic effects could be distinguished from intraparticle mass transfer effects of catalytic particles which is noteworthy in scaling up/down of TBR.

In order to fill the gap in the steady state TBR hydrodynamic studies, a systematic experimental work was done on the temperature effect on flow regime transition, pulse velocity, two-phase pressure drop, liquid holdup and liquid axial dispersion coefficient for Newtonian (air-water) and non-Newtonian (air-0.25% Carboxymethylcellulose (CMC)) liquids (Chapter 1). For the two systems, the trickle-to-pulse flow regime transition boundary was found to shift to higher gas and liquid superficial velocities with increasingly temperatures. Under constant operating conditions, both two-phase pressure drop and liquid holdup decreased with temperature; whereas pulse velocity was observed to increase with temperature.

The hydrodynamics of trickle bed periodic operation at increased temperature/pressure came subsequently in regard to slow-mode induced pulsing (shock-wave breakthrough, plateau and decay times, shock wave breakthrough amplitude, shock wave velocity and the pulse frequency) which were studied for Newtonian and non-Newtonian power-law liquids (Chapter 2). For both systems, it was observed that the shock wave breakthrough and decay times and breakthrough amplitude decreased with increasing temperature and pressure. On the contrary, the shock wave plateau time increased with temperature and pressure. As the analysis was done for the liquid holdup traces and the liquid holdup decreased with temperature especially at the high liquid feed rates (Chapter 1); this phenomenon could be viewed as an obstacle for enhancement of reactor performance with cyclic operation at high

temperature and pressure operations. Additionally, the shock wave velocity and the pulse frequency were found to increase with temperature and pressure.

The flow regime transition at steady state was observed to be different than that at unsteady state operation. For the systematic analysis of this phenomenon the trickle-to-pulsing transition in cyclic operation was compared to spontaneous transition in constant-throughput flow for Newtonian and non-Newtonian systems (Chapter 3). It was found that at constant temperature and superficial gas velocity, higher superficial liquid velocity was required at cyclic operation with respect to constant-throughput mode for the trickle-to-pulsing transition for both systems. Liquid holdup at trickle-to-pulsing transition in cyclic operation was higher than that in constant-throughput mode. Pulse velocity and frequency increased with temperature and superficial gas velocity for cyclic operation and constant-throughput modes. Pulse velocity in cyclic operation was larger than in constant-throughput mode while the opposite was observed for the pulse frequency.

This study was extended by investigating the effects of temperature and pressure, superficial gas and (base and pulse) liquid velocities, and bed depth on the structure of the trickle-to-pulsing transition in cyclic operation and spontaneous pulsing conditions, on the pulse characteristics in the pulsing flow regime both in cyclic operation and spontaneous pulsing and on the evolution of the shock wave topological features (Chapter 4). In slow-mode cycling, the liquid holdups at the trickle-to-pulsing transition in the cyclic operation and spontaneous pulsing decreased with the temperature and pressure. For both operation modes, pulse velocities decreased with increasing pressure due to either larger-amplitude liquid holdup fluctuations or larger pulse frequencies. The shock wave breakthrough, decay and plateau times decreased with bed depth regardless of pressure and temperature.

Fast-mode liquid cyclic operation is another periodic operation needed to be investigated at increased temperature and/or pressure. The effect of temperature and pressure on the liquid holdup and pressure drop time series in terms of pulse breakthrough and decay times, pulse intensity, and pulse velocity was examined for the air-water system (Chapter 5). It was observed that fast-mode cyclic operation outperforms slow mode for the same split ratio, pressure, temperature and fluid throughputs in terms of pulse holdup. For holdup and pressure drop time series, the pulse breakthrough and decay times are decreasing functions

of temperature and pressure. Pulse intensity increased with the temperature and decreased with the pressure whereas the pulse velocity increased both with temperature and pressure.

A systematic experimental work on the steady state hydrodynamics of a trickle bed reactor was conducted at increased temperature for foaming liquids. The effects of temperature and pressure on the shift of the transition from trickle to foaming-pulsing flow regimes, on the two-phase pressure drop, the liquid holdup, and the pulse frequency and velocity were studied for Newtonian (air-cetyltrimethylammoniumbromide (CTAB)) foaming and non-Newtonian (air-0.25% CTAB-carboxymethylcellulose (CMC)) foaming systems (Chapter 6). The transition boundary shifted towards higher gas and liquid superficial velocities with increasingly temperatures and pressures. The pulse frequency increased with temperature and/or pressure whereas the pulse velocity increased with temperature but it decreased with increasing pressure.

As fast-mode outperforms the slow-mode operation in terms of liquid holdup traces an alternating gas/liquid fast mode cyclic operation was explored to reduce or retard the occurrence of foaming flow at increased temperature and pressure (Chapter 7). The effect of temperature and split ratio on the electrical conductance and pressure drop time series was analyzed for the air-aqueous cetyltrimethylammoniumbromide (CTAB) foaming and air-water systems. Alternating passage of gas- and liquid-rich phases through the packed bed was found to play an important role for controlling foam formation and stability at increased temperature and pressure. At optimized split ratio the pressure drop in cyclic operation was lower than in isoflow condition conducted under barycentric feed flow rates for the foaming system. Additionally increased reactor temperature was suggested to allow faster foam drainage and breakdown for the lower pressure drop as well as faster collapse in pressure drop when the flow was switched from gas to liquid feed.

The work was finalized with a simple method developed for the filling of micro- and mesopores of porous particles by adsorption and polymerization of hydrophilic organic monomers into catalytic particles. These particles were used to distinguish the extra-granular hydrodynamic effects (such as axial dispersion) from intraparticle mass transfer effects of catalytic particles in a TBR operating at ambient conditions (Chapter 8). It was found that the method could be employed for large quantity of particles which favors the

applicability of this method to lab- and pilot-scale ranges. The applicability of the method to various porous particles different in shape and size was confirmed by completely filling the internal porosity of spheres, extrudates, trilobes, and quadrulobes. Additionally the difference in the contact angle of the porous and the polymer impregnated-particles was negligible. TBR hydrodynamic experiments show that the liquid holdup and Péclet number are close for glass beads and polymer-impregnated particles for the air-water system.

## Recommendations and Future Work

The hydrodynamic studies of TBR are updated in terms of novel experimental and/or modeling efforts. As known from numerous published works industrial TBR operations require high temperature and high pressure. Taking these major points into consideration different research topics could be suggested among various ideas.

Many chemical processes are determined by the rate of mass transfer between phases. Mass transfer is one of the complicated interactions take place between the phases in a trickle bed reactor. As explained in detail cyclic operation of TBR could be suggested as a remarkable step in the process intensification of industrial reactors. Systematic gas-side and liquid-side mass transfer studies is needed in a periodically operated TBR at high pressure high temperature to investigate the influence of cyclic operation on the mass transfer. The effects of temperature and pressure on the mass transfer fluctuations should be deduced to perceive the advantages and/or disadvantages of cyclic operation.

Another strategy for the process intensification is the dramatic reduction in size. The very high heat transfer rates allow the microreactors to operate highly exothermic processes isothermally. Thus in parallel to ongoing kinetic studies in microreactors, hydrodynamic studies should be performed at high temperature and high pressure for constant throughput mode and the cyclic operation. The observed phenomena could be compared with a TBR larger in size operating at the same conditions.

Monitoring the identification of flow regimes, characteristics of pulses, shock waves is mandatory to consolidate the previous investigations done with different methods.

Therefore visualization of multiphase flow in cyclic operation as well as in constant throughput flow at elevated temperature and pressure is challenging. Visualization could be done for micro- and lab-scale reactors to identify the differences during scale up/down of TBRs.

The experimental observations reported in this work will be consolidated with the visualization of the above mentioned phenomena. A phenomenological model will lead to the application of various reliable computational techniques based on experimental cyclic operation efforts. Modeling of the cyclic operation of TBRs is difficult and scarce because of the complexity of the system. Further study is mandatory for the modeling of periodically operated TBR based on high temperature high pressure experiments.